

AN INVESTIGATION OF HEAT TRANSFER
IN SPRAY COOLING

by

BALASUBRAMANIAM PRABHAKAR

B.Sc., Osmania University, India, 1967
B.E.(Metallurgy), Indian Institute of Science, 1970
M.A.Sc., The University of British Columbia, 1973

A THESIS SUBMITTED IN PARTIAL FULFILMENT OF
THE REQUIREMENTS FOR THE DEGREE OF
DOCTOR OF PHILOSOPHY

in

THE FACULTY OF GRADUATE STUDIES
Department of Metallurgical Engineering

We accept this thesis as conforming
to the required standard

THE UNIVERSITY OF BRITISH COLUMBIA

November 1980

© B. Prabhakar, 1980

In presenting this thesis in partial fulfilment of the requirements for an advanced degree at the University of British Columbia, I agree that the Library shall make it freely available for reference and study. I further agree that permission for extensive copying of this thesis for scholarly purposes may be granted by the head of my department or by his or her representatives. It is understood that copying or publication of this thesis for financial gain shall not be allowed without my written permission.

Department of METALLURGICAL ENGINEERING

The University of British Columbia
2075 Wesbrook Place
Vancouver, Canada
V6T 1W5

Date 22 Jan '87

ABSTRACT

Spray water fluxes and heat-transfer coefficients have been measured for some commercial spray nozzles, with a view to generating reliable and accurate data for the design of spray chambers of continuous casting machines. Sprays produced by both full cone and vee-jet nozzles have been investigated.

The distribution of water in the sprays has been measured for different spray pressures and distances from the nozzle, by measuring the amount of water arriving at collector tubes inserted in the sprays. Thermocouples embedded in a heated stainless 'heat transfer probe' allowed the temperature transients within the probe to be measured during the spray cooling of these probes. Analysis of these transients by a solution to the 'Inverse Boundary Value Problem' allowed the calculation of the heat-transfer coefficients and surface heat fluxes as a function of the surface temperature of the cooled surface of the probe.

The results of this investigation indicate that the most important variable affecting the heat-transfer coefficient is the local water flux at the cooled surface. The coefficients have also been determined to be temperature sensitive even at surface temperatures in excess of

800 °C. For the same value of water flux, neither the nozzle type nor the spray pressure has a strong influence on the heat-transfer coefficients. Correlations of the form

$$h = P(1) \dot{m}^{P(2)}$$

have been obtained between the heat-transfer coefficients and spray water fluxes for different surface temperatures.

The form of the correlation obtained when the effect of surface temperature between 800 and 1000°C was included is

$$h = P(1) \dot{m}^{P(2)} \left(\frac{T_s}{1000} \right)^{P(3)}$$

where $p(3)$ is negative. This showed that the operating boiling process in the present spray cooling experiments was unstable film boiling, causing scatter in the data.

TABLE OF CONTENTS

	<u>Page</u>
Abstract	ii
Table of Contents	iv
List of Tables	ix
List of Figures	xii
List of Symbols	xxi
Acknowledgements	xxii
<u>Chapter</u>	
1 INTRODUCTION	1
1.1 Secondary Cooling and Crack Formation	5
1.1.1 Spray Related Defects in Billets	8
1.1.2 Spray Related Defects in Slabs	11
1.2 Spray Chamber Design and Control	16
1.3 Scope of the Present Work	18
2 REVIEW OF THE LITERATURE	20
2.1 Introduction	20
2.2 Single Droplet Studies	25
2.2.1 Dynamics of Droplet Impact	25
2.2.2 Heat Transfer to Sessile Drops	26
2.2.3 Heat Transfer to Impinging Drops	28
2.2.4 Extension of Single Drop Experiments to Characterization of Spray Heat-Transfer	33
2.3 Heat Transfer in Sprays	34
2.3.1 Transient Methods	35
2.3.2 Steady-State Methods	51
2.3.3 In-plant Measurements	55
2.4 Summary	56

<u>Chapter</u>		<u>Page</u>
3	EXPERIMENTAL	62
	3.1 Introduction	62
	3.2 Spray Nozzles	63
	3.3 Water Supply System	65
	3.4 Spray Nozzle Mounting	68
	3.5 Measurement of Spray Water Fluxes	68
	3.5.1 Factors Affecting Spray Flux Measurements ...	70
	3.5.2 Apparatus	70
	3.5.3 Experimental Procedure	72
	3.6 Spray Heat-Transfer Measurements	74
	3.6.1 Requirements for the Measurement of Temperature Transients	74
	3.6.2 Selection of Steel for the Probe Material ...	82
	3.6.3 Probe Fabrication	83
	3.6.4 Selection of the Thermocouple Material	85
	3.6.5 Thermocouple Installation	86
	3.6.6 Lead Wires and Connections	90
	3.6.7 The High Speed Recorder	92
	3.6.8 Mounting of the Heat Transfer Probe for Heating	93
	3.6.8.1 Type I Experiments	93
	3.6.8.2 Type II Experiments	96
4	ANALYSIS OF THE MEASURED TRANSIENTS	102
	4.1 Digitising and Smoothing of the Transients	102
	4.2 Analysis of the Temperature Transients	103

<u>Chapter</u>		<u>Page</u>
4.2.1	Previous Solutions to the Inverse Boundary Value Problem	105
4.2.1.1	Analytical and Analog Methods	105
4.2.1.2	Numerical Methods	108
4.2.1.3	Other Related Solutions	109
4.2.2	Method Employed in the Present Work	110
4.2.2.1	The Direct Problem	113
4.2.2.2	The Inverse Problem	117
4.3	Validation of the Mathematical Formulation Used	119
5	RESULTS AND DISCUSSION	126
5.1	Spray Flux Measurements	126
5.1.1	Spray Fluxes for a 1/4 GG 10 Nozzle	127
5.1.1.1	Horizontal Centreline Spray Profiles - Type A Collectors	127
5.1.1.1.1	Differences Between Similar Spray Nozzles	129
5.1.1.1.2	Effect of Vibrating the Collectors	132
5.1.1.1.3	Effect of Different Pressurizing Gases	132
5.1.1.1.4	Effect of Spray Pressure at Constant Distance	133
5.1.1.1.5	Effect of Spray Distance at Constant Pressure	133
5.1.1.2	Spray Flux Map for the 1/4 GG 10 Nozzle	137
5.1.1.2.1	Water Fluxes Obtained with Type A Collectors	143
5.1.1.2.2	Water Fluxes Obtained with Type B Collectors	148

<u>Chapter</u>	<u>Page</u>
5.1.2 Other Full Cone Nozzles - Spray Fluxes with Type A Collectors	151
5.1.3 Vee ² jet or Flat-jet Nozzles; Measurements Made with Type A Collectors	158
5.2 Measurements of Heat-Transfer Coefficients	163
5.2.1 General Observations of the Cooling Process..	163
5.2.2 Validation of the Experimental Technique Used	166
5.2.3 Determination of the Initial Temperature Profiles	170
5.2.4 Results of Type I Experiments	171
5.2.5 Results of Type II Experiments	176
5.2.5.1 Average of Spray Fluxes Over the Area of the Probe Face	186
5.2.5.2 Comparison of Data for Peak and Average Fluxes	188
5.2.5.3 Results from Experiments Performed with Other Nozzles	196
5.3 Efficiency of Spray Cooling	198
5.4 Calculation of Droplet Velocities and Droplet Momenta Within the Sprays	213
5.5 The Nature of the Boiling Process	216
5.6 Temperature Dependence of the Heat- Transfer Coefficient	221
5.7 Comparison with the Results of Other Workers	221
5.8 Problems Limiting the Measurements.....	236
5.9 Application of the Data for Spray Chamber Design	238
6.0 SUMMARY AND CONCLUSIONS	240
BIBLIOGRAPHY	24

Appendices

Page

I	Measured Spray Fluxes for the Various Nozzles Used in this Investigation	255
II	Horizontal Centreline Spray Flux Profiles, Spray Flux Contour Maps and Three Dimensional Representations of Spray Fluxes	276

LIST OF TABLES

<u>Tables</u>	<u>Page</u>
I Spray related defects	15
IIa Summary of studies on heat extraction in sprays - transient measurements	59
IIb Summary of Studies on heat extraction in sprays - steady state measurements	60
IIc Summary of studies on heat extraction in sprays - in-plant measurements	61
III Capacities and spray angles for the nozzles investigated in this work ⁹⁰	64
IV Coefficients of the fitted power curves correlating the heat-transfer coefficients to the peak values of spray water flux at different surface temperatures.	187
V Coefficients of the fitted power curves correlating the heat-transfer coefficients to water fluxes averaged over the area of the probe face, for different surface temperatures	195
VI List of nozzles other than 1/4 GG 10 and operating spray pressures used in the measurement of spray heat-transfer coefficients	197
VII Coefficients of the curves fitted to correlate spray efficiency to the peak value of the spray water fluxes for different surface temperatures	211
VIII Coefficients of the curves fitted to correlate the spray efficiency to the value of spray water flux averaged over the area of the probe face, for different surface temperatures	212
IX Calculated droplet velocities and droplet momenta in the sprays produced by the nozzles studied in this investigation	215
X Multiple regression coefficients for the water flux and temperature dependence of the heat-transfer coefficients.....	222
XI Basis for the method used for the determination of water fluxes by different investigators of spray heat extraction	224
XII Coefficients of power curves fitted to the variation of heat-transfer coefficients with water fluxes averaged over the whole sprayed area, for different surface temperatures	234

Appendix I

<u>Tables</u>	<u>Page</u>
I-1 Spray flux map for the 1/4 GG 10 nozzle at a spray pressure of 0.13 MPa for a nozzle distance of 10.16 cm (Type A collectors)	256
I-2 Spray flux map for the 1/4 GG 10 nozzle at a spray pressure of 0.13 MPa for a nozzle distance of 15.24 cm (Type A collectors)	257
I-3 Spray flux map for the 1/4 GG 10 nozzle at a spray pressure of 0.13 MPa for a nozzle distance of 20.32 cm (Type A collectors)	258
I-4 Spray flux map for the 1/4 GG 10 nozzle at a spray pressure of 0.13 MPa for a nozzle distance of 10.16 cm (Type B collectors)	259
I-5 Spray flux map for the 1/4 GG 10 nozzle at a spray pressure of 0.27 MPa for a nozzle distance of 10.16 cm (Type A collectors)	260
I-6 Spray flux map for the 1/4 GG 10 nozzle at a spray pressure of 0.27 MPa for a nozzle distance of 15.24 cm (Type A collectors)	261
I-7 Spray flux map for the 1/4 GG 10 nozzle at a spray pressure of 0.27 MPa for a nozzle distance of 20.32 cm (Type A collectors)	262
I-8 Spray flux map for the 1/4 GG 10 nozzle at a spray pressure of 0.27 MPa for a nozzle distance of 10.16 cm (Type B collectors)	263
I-9 Spray flux map for the 1/4 GG 10 nozzle at a spray pressure of 0.41 MPa for a nozzle distance of 10.16 cm (Type A collectors)	264
I-10 Spray flux map for the 1/4 GG 10 nozzle at a spray pressure of 0.41 MPa for a nozzle distance of 15.24 cm (Type A collectors)	265
I-11 Spray flux map for the 1/4 GG 10 nozzle at a spray pressure of 0.41 MPa for a nozzle distance of 20.32 cm (Type A collectors)	266
I-12 Spray flux map for the 1/4 GG 10 nozzle at a spray pressure of 0.41 MPa for a nozzle distance of 10.16 cm (Type B collectors)	267

Appendix I

<u>Tables</u>	<u>Page</u>
I-13 Horizontal centreline spray water flux distribution for the 1/8 GG 5 nozzle	268
I-14 Horizontal centreline spray water flux distribution for the 1/8 GG 6 SQ nozzle	269
I-15 Horizontal centreline spray water flux distribution for the 1/4 GG 6.5 SQ nozzle	270
I-16 Horizontal centreline spray water flux distribution for the 1/4 GG 12 SQ nozzle	271
I-17 Horizontal centreline spray water flux distribution for the 1/4 GG 14.5 nozzle	272
I-18 Horizontal centreline spray water flux distribution for the 1/4 GG 14 W nozzle.....	273
I-19 Horizontal centreline spray water flux distribution for the 1/4 U8020 nozzle	274
I-20 Horizontal centreline spray water flux distribution for the 3/8 U5060 nozzle	275

LIST OF FIGURES

<u>Figures</u>	<u>Page</u>
1 Schematic diagram of a billet caster showing the different heat extraction zones	3
2 Spray related cracks in continuously cast billets and slabs	6
3 Typical boiling curves for a wire, tube, or horizontal surface in a pool of water at atmospheric pressure ⁵² ..	21
4 Variation of heat flux with surface temperature in spray cooling ⁵³	24
5 Effect of droplet velocity on the heat transferred to the droplet ⁶⁵	31
6 Non wetting droplet heat transfer efficiency ⁶⁵	32
7 Dependence of spray efficiency on water flux ⁵³	37
8 Variation of spray heat-transfer coefficients with surface temperature	38
9 Dependence of the heat-transfer coefficients on water flux and surface temperature ⁷⁰	41
10 Effect of water temperature on spray heat-transfer coefficients	43
11 Variation of spray heat-transfer coefficient with water flux as reported in various studies on spray heat extraction	45
12 Variation of heat-transfer coefficients with surface temperature, from various studies on spray heat extraction	46
13 Variation of heat-transfer coefficients with water flux for different droplet velocities ⁸¹	53
14 Schematic diagram of the water supply system	66
15 Schematic diagram of the mount for the spray nozzle ...	69
16 Schematic diagram of the apparatus used for the measurement of spray water fluxes	71

<u>Figure</u>		<u>Page</u>
17	Dependence of the mean error in calculated heat-transfer coefficients on the distance of the point of measurement below the cooled surface ⁹⁷	78
18	Three alternative configurations for thermocouple placement in the heat transfer probe	81
19	Schematic diagram of the heat-transfer probe with installed thermocouples	84
20	Schematic diagram of the capacitor discharge welding apparatus	88
21	Electrical connections to the recording equipment	91
22	Schematic diagram of the probe installation for the Type I heat transfer experiments	94
23	Schematic diagram of the probe installation for the Type IIa heat transfer experiments	97
24	Photograph of the heating plate mounted on the tiltable mount	99
25	Schematic diagram of the probe installation for the Type IIb heat transfer experiments	102
26	Division of the heat transfer probe into nodes	113
27	Comparison of back-calculated values of heat-transfer coefficients and surface temperatures with expected values, for $h = 2.094 \text{ kW/m}^2\text{h}$	122
28	Comparison of back-calculated values of the heat-transfer coefficient and surface temperatures with expected values, for $h = 4.19 \text{ kW/m}^2\text{h}$	123
29	Comparison of back-calculated values of the heat-transfer coefficient with expected values, for h varying with surface temperature	125
30	Comparison of back-calculated values of the heat-transfer coefficient, using transients obtained at different distances from the cooled face	125

<u>Figure</u>		<u>Page</u>
31	Typical horizontal centreline profile obtained with the 1/4 GG 10 nozzle, for a spray distance of 15.24 cm and a spray pressure of .41 MPa	128
32	Variation in the measured spray water fluxes for four different 1/4 GG 10 nozzles	130
33	Reproducibility of the spray flux measurements for a 1/4 GG 10 nozzle (Number 9)	130
34	Reproducibility of the spray flux measurements for a 1/4 GG 10 nozzle (Number 4)	131
35	Effect of vibrating the collectors on the spray water flux measurements	131
36	Effect of spray pressure at constant distance for a 1/4 GG 10 nozzle at a distance of 15.24 cm	134
37	Effect of spray pressure at constant distance for a 1/4 GG 10 nozzle, at a distance of 10.16 cm	135
38	Effect of spray pressure at constant distance for a 1/4 GG 10 nozzle, at a distance of 20.32 cm	136
39	Effect of distance at constant pressure for a 1/4 GG 10 nozzle, for a spray pressure of 0.27 MPa	138
40	Effect of distance at constant pressure for a 1/4 GG 10 nozzle, for a spray pressure of 0.13 MPa	139
41	Effect of distance at constant pressure for a 1/4 GG 10 nozzle, for a spray pressure of 0.41 MPa	140
42	Variation of spray water flux with pressure and distance at the centre of the spray produced by a 1/4 GG 10 nozzle	141
43	Variation of spray water flux with pressure and distance 5.08 cm from the centre of the spray produced by a 1/4 Gg 10 nozzle	142
44	Spray flux contour maps for a 1/4 GG 10 nozzle for a nozzle distance of 10.16 cm and spray pressure of 0.41 MPa (Type A collectors)	144

<u>Figure</u>		<u>Page</u>
45	Spray flux contour maps for a 1/4 GG 10 nozzle for a nozzle distance of 15.24 cm and spray pressure of 0.41 MPa (Type A collectors)	145
46	Spray flux contour maps for a 1/4 GG 10 nozzle for a nozzle distance of 20.32 cm and spray pressure of 0.41 MPa (Type A collectors)	146
47	Three dimensional representation of the spray fluxes for the 1/4 GG 10 nozzle for a nozzle distance of 15.24 cm and spray pressure of 0.27 MPa	147
48	Spray flux contour map for a 1/4 GG 10 nozzle for a spray pressure of 0.41 MPa and nozzle distance of 10.16 cm (Type B collectors)	149
49	Three dimensional representation of the spray fluxes for a 1/4 GG 10 nozzle, for a spray pressure of 0.13 MPa and a nozzle distance of 10.16 cm (Type B collectors)	150
50	Horizontal centreline spray flux profiles for a 1/8 GG 5 nozzle, at a nozzle distance of 10.16 cm	152
51	Horizontal centreline spray flux profiles for a 1/8 GG 5 nozzle, at a nozzle distance of 15.24 cm	153
52	Horizontal centreline spray flux profiles for a 1/4 GG 6.5 nozzle, at a nozzle distance of 10.16 cm ...	155
53	Horizontal centreline spray flux profiles for a 1/4 GG 6.5 nozzle, at a nozzle distance of 15.24 cm ...	156
54	Horizontal centreline spray flux profiles for a 1/8 GG 6 SQ nozzle, at a nozzle distance of 10.16 cm ..	157
55	Horizontal centreline spray flux profiles for a 1/4 HH 14.5 SQ nozzle at a nozzle distance of 10.16 cm .	159
56	Horizontal centreline spray flux profiles for a 1/4 HH 14.5 SQ nozzle at a nozzle distance of 15.24 cm .	160
57	Horizontal centreline spray flux profiles for a 1/4 GG 14 W nozzle, at a nozzle distance of 10.16 cm ..	161
58	Horizontal centreline spray flux profiles for a 1/4 U8020 nozzle, at a nozzle distance of 15.24 cm ...	162

<u>Figure</u>		<u>Page</u>
59	Comparison of calculated and measured temperatures, for an average heat-transfer coefficient of $1.05 \text{ kW/m}^2\text{K}$	168
60	Comparison of calculated and measured temperatures, for an average heat-transfer coefficient of $1.88 \text{ kW/m}^2\text{K}$	169
61	Variation of heat-transfer coefficients with water flux for a surface temperature of 850°C (Type I experiments)	172
62	Variation of heat-transfer coefficients with water flux for a surface temperature of 1000°C (Type I and Type IIa experiments)	174
63	Variation of heat-transfer coefficients with surface temperature (Type I experiments)	175
64	Variation of heat-transfer coefficients with surface temperature (Type IIa experiments)	178
65	Variation of the measured heat-transfer coefficients with peak values water flux for a surface temperature of 1000°C	180
66	Variation of the measured heat-transfer coefficients with peak values water flux for a surface temperature of 800°C	181
67	Variation of the measured heat-transfer coefficients with peak values water flux for a surface temperature of 850°C	182
68	Variation of the measured heat-transfer coefficients with peak values water flux for a surface temperature of 900°C	183
69	Variation of the measured heat-transfer coefficients with peak values water flux for a surface temperature of 950°C	184
70	Variation of the measured heat-transfer coefficients with peak values water flux for a surface temperature of 1050°C	185
71	Variation of the measured heat-transfer coefficients with values of water flux averaged over the probe face, for a surface temperature of 800°C	189

<u>Figure</u>		<u>Page</u>
85	Variation of spray cooling efficiency with values of water flux averaged over the probe face, for a surface temperature of 900°C	207
86	Variation of spray cooling efficiency with values of water flux averaged over the probe face, for a surface temperature of 950°C	208
87	Variation of spray cooling efficiency with values of water flux averaged over the probe face, for a surface temperature of 1000°C	209
88	Variation of spray cooling efficiency with values of water flux averaged over the probe face, for a surface temperature of 1050°C	210
89	Variation of critical temperature with water flux.....	217
90	Variation of the heat flux with surface temperature ofr different water fluxes.....	219
91	Curves fitted to the measured vatiation of heat-transfer coefficients with peak values of water fluxes.	226
92	Curves fitted to the measured variation of heat transfer coefficients with values of water flux averaged over the probe face.....	227
93	Curves fitted to the measured variation of heat-transfer coefficients with values of water flux averaged over the whole sprayed area.....	235

Appendix II

Figure

II-I	Spray flux contour map for a 1/4 GG 10 nozzle, for a spray pressure of 0.13 MPa at a nozzle distance of 10.16 cm (Type A collectors).....	277
------	---	-----

Appendix II

<u>Figure</u>	<u>Page</u>
II-2 Spray flux contour map for a 1/4 GG 10 nozzle, for a spray pressure of 0.13 MPa at a nozzle distance of 15.24 cm (Type A collectors)	278
II-3 Spray flux contour map for a 1/4 GG 10 nozzle, for a spray pressure of 0.27 MPa at a nozzle distance of 10.16 cm (Type A collectors)	279
II-4 Spray flux contour map for a 1/4 GG 10 nozzle, for a spray pressure of 0.27 MPa at a nozzle distance of 15.24 cm (Type A collectors)	280
II-5 Spray flux contour map for a 1/4 GG 10 nozzle, for a spray pressure of 0.13 MPa at a nozzle distance of 20.32 cm (Type A collectors)	281
II-6 Spray flux contour map for a 1/4 GG 10 nozzle, for a spray pressure of 0.27 MPa at a nozzle distance of 20.32 cm (Type A collectors)	282
II-7 Spray flux contour map for a 1/4 GG 10 nozzle, for a spray pressure of 0.13 MPa at a nozzle distance of 10.16 cm and Type B collectors	283
II-8 Spray flux contour map for a 1/4 GG 10 nozzle, for a spray pressure of 0.27 MPa at a nozzle distance of 10.16 cm Type B collectors	284
II-9 Three dimensional representation of the spray flux distribution for a 1/4 GG 10 nozzle, for a spray pressure of 0.13 MPa and a nozzle distance of 10.16 cm (Type A collectors)	285
II-10 Three dimensional representation of the spray flux distribution for a 1/4 GG 10 nozzle, for a spray pressure of 0.27 MPa and a nozzle distance of 10.16 cm (Type A collectors)	286
II-11 Three dimensional representation of the spray flux distribution for a 1/4 GG 10 nozzle, for a spray pressure of 0.13 MPa and a nozzle distance of 15.32 cm (Type A collectors)	287
II-12 Three dimensional representation of the spray flux distribution for a 1/4 GG 10 nozzle, for a spray pressure of 0.27 MPa and a nozzle distance of 20.32 cm (Type A collectors)	288

Appendix II

<u>Figure</u>	<u>Page</u>
II-13 Horizontal centreline spray flux profiles for a 1/4 GG 10 SQ nozzle at a nozzle distance of 10.16 cm	289
II-14 Horizontal centreline spray flux profiles for a 1/4 GG 10 SQ nozzle at a nozzle distance of 15.24 cm	290
II-15 Horizontal centreline spray flux profiles for a 1/4 GG 10 SQ nozzle at a nozzle distance of 20.32 cm	291
II-16 Horizontal centreline spray flux profiles for a 1/4 GG 12 SQ nozzle at a nozzle distance of 10.16 cm	292
II-17 Horizontal centreline spray flux profiles for a 1/4 GG 12 SQ nozzle at a nozzle distance of 15.24 cm	293
II-18 Horizontal centreline spray flux profiles for a 1/4 GG 12 SQ nozzle at a nozzle distance of 20.32 cm	294
II-19 Horizontal centreline spray flux profiles for a 3/8 HH 18 SQ nozzle at a nozzle distance of 10.16 cm	295
II-20 Horizontal centreline spray flux profiles for a 3/8 HH 18 SQ nozzle at a nozzle distance of 15.24 cm	296
II-21 Horizontal centreline spray flux profiles for a 3/8 HH 18 SQ nozzle at a nozzle distance of 20.32 cm	297
II-22 Horizontal centreline spray flux profiles for a 1/4 U8020 nozzle at a nozzle distance of 20.32 cm	298
II-23 Horizontal centreline spray flux profiles for a 3/8 U5060 nozzle at a nozzle distance of 17.78 cm	299

LIST OF SYMBOLS

Q	Heat flux	kW/m^2
h	Heat-transfer coefficient	$\text{kW/m}^2\text{K}$
\dot{m}	Water flux	$\text{g/m}^2\text{s}$
T_s	Surface temperature	$^{\circ}\text{C}$
T_w	Water temperature	$^{\circ}\text{C}$
T_a	Ambient temperature	$^{\circ}\text{C}$
r_o	Droplet radius	cm
d	Droplet diameter	m
η	Spray cooling efficiency	
v	Droplet velocity	m/s
V_1, V_2	Velocity	m/s
k	Thermal conductivity	W/mK
ρ	Density	kg/m^3
C_p	Heat capacity	Ws/kg
Δh_v	Heat of vaporization	Ws
σ	Surface tension	N/m
P_1, P_2	Pressure	Pa
Δx	Node spacing	m
Δt	Time increment	s
T_i	Temperature at the i th node	$^{\circ}\text{C}$
T_i^*	Temperature at the i th node, at time $t + 0.5 \Delta t$	$^{\circ}\text{C}$
$P(1), P(2), P(3)$	Coefficients of fitted curves	
We	Weber Number	

ACKNOWLEDGEMENTS

The author wishes to express his sincere gratitude to his research supervisors, Dr. J.K. Brimacombe and Dr. F. Weinberg, for their help and guidance through the course of this work. The discussions and assistance of fellow graduate students, faculty members and technicians have been invaluable. Financial assistance in the form of a Killam Predoctoral Fellowship, and a research grant from the American Iron and Steel Institute (Grant No. 36-337) is gratefully acknowledged.

Chapter 1

INTRODUCTION

Continuous casting is gaining a position of ever increasing importance in the steel industry with its capability of being able to produce blooms, billets and slabs of different cross sections and a wide variety of steel grades. Compared to conventional ingot casting, continuous casting of steel results in a significant reduction in processing costs by:¹

- i) Increasing the yield of blooms and slabs by about 10%
- ii) Reduction in the energy consumption by a substantial amount
- iii) Improving product quality and homogeneity
- iv) Reducing operating costs
- v) Reducing capital investment by eliminating ingot teeming, soaking pits, and primary rolling mills.

Higher productivity has also been enhanced, especially with the introduction of BOF converter facilities, the use of sequential casting, and the use of higher casting speeds.

Moreover, cost reductions are effected by the strand casting of many semifinished shapes, including beam blanks and rounds.

Since quality requirements are continually being upgraded, the production technology of a process like continuous casting must also be improved, at least at the same pace, in order to produce an acceptable and marketable product. The influence of the production parameters on the quality of the cast product has therefore been the object of much scrutiny. The results of a large number of investigations, both theoretical and experimental, have clarified, to a reasonable extent, the effect of the major production parameters on the quality of the steel produced.² However, many factors, such as spray cooling, require attention, since it has been shown that improper spray cooling leads to a large number of casting defects as described in a following section.

The location of the spray heat extraction zones in relation to the other heat extraction zones in a continuous billet casting machine can be seen from an observation of Figure 1. Three main stages for the heat extraction from the strand can be observed from this Figure:

- i) the mould region
- ii) the spray zones below the mould

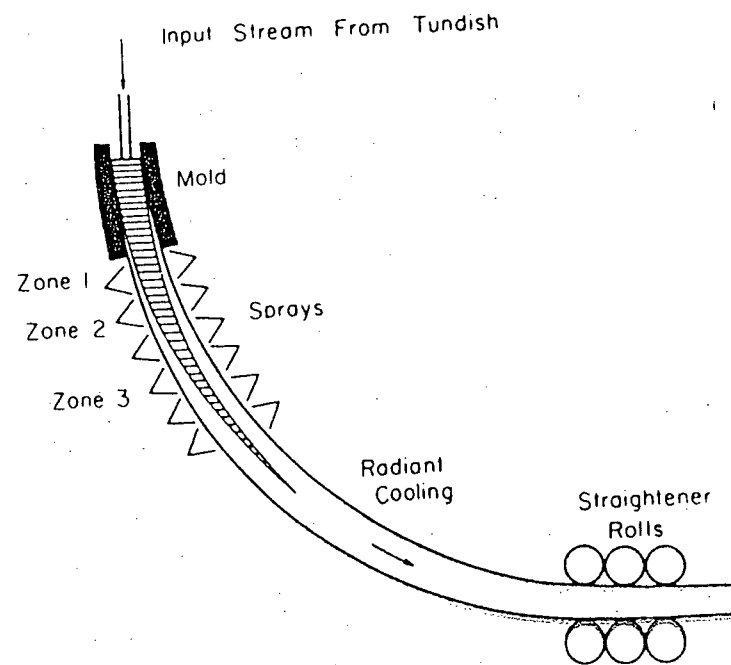


Figure 1 Schematic diagram of a billet caster showing the different heat extraction zones.

- iii) the radiative cooling zone after the strand emerges from the spray zones.

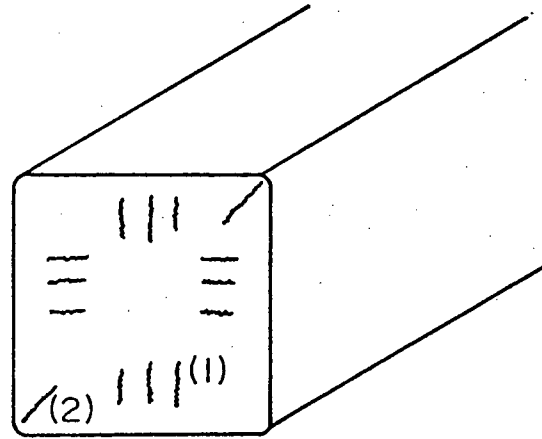
The water cooled copper mould serves to form a thin skin of solidified steel, which supports the core of liquid metal. Much of the heat removed in the strand (50 to 65% in the case of slabs) is extracted by the water sprays in the spray cooling zones, also referred to as the secondary cooling zone. In this zone, the cooling of the strand surface not only promotes solidification, but also provides the solidified shell with enough strength to support the liquid core, and also serves to avoid remelting of the shell. In the third cooling region, heat is lost by the strand to the surroundings by the process of radiative heat transfer. Slab casters are similar, except that a number of support and driving rolls are present through the length of the machine, from just below the mould to the cut-off section.

In the early days of continuous casting, the design of the spray cooling system was based primarily on two requirements: high heat extraction rates for maximum productivity, and simplicity for ease of operation as well as maintenance. The use of high heat extraction rates in the spray regions must be tempered by the fact that, as mentioned before, many of the types of cracks in the cast product are spray related, and as such, careful consideration must be

given to the design of the secondary cooling zone in order to minimize crack formation.

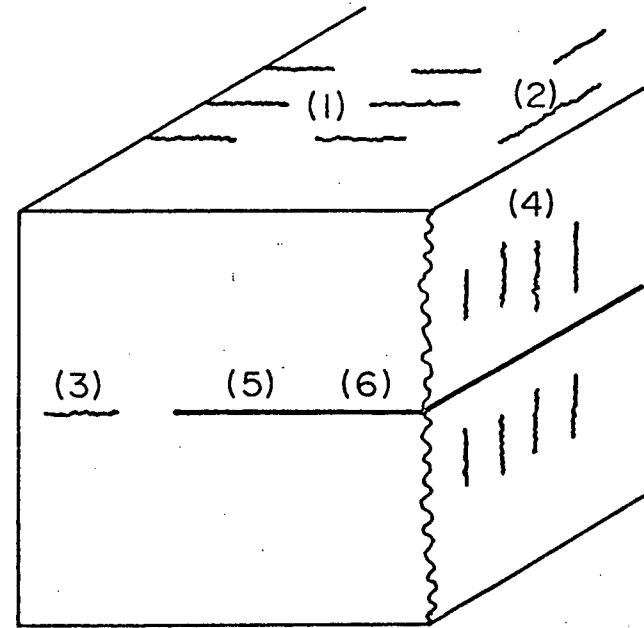
1.1 Secondary Cooling and Crack Formation

Defects have been linked to spray practice in the continuous casting of billets and slabs and are shown schematically in Figure 2. Cracks form during the casting process when sufficiently high tensile strains are generated in those portions of the strand that possess low ductility. The origin of these strains can be traced back both to thermal and mechanical factors. When the strand surface is being cooled, steep temperature gradients are set up in the solidifying shell. When there is a change in the rate of heat extraction at the surface, these temperature gradients change rapidly, generating differential thermal expansion and thermal strains in the shell. Crack formation then occurs when the magnitude of the strains is greater than the ductility of the material. In some cases, temperature excursions of the solid shell due to variations in the cooling rate of the surface promote the formation of phases like AlN, which can reduce the high temperature ductility and lead to crack formation. Mechanical strains can be generated by one or a combination of the following: ferrostatic pressure of the liquid pool, mould friction, machine misalignment, and bending and straightening operations. Many reviews³⁻⁹ deal comprehensively with the types and morphologies of defects, their causes, and



Billet

- (1) Midway cracks
- (2) Rhomboidity / diagonal cracks



Slab

- (1) Transverse surface cracks
- (2) Longitudinal, mid-face cracks
- (3) Triple-point cracks
- (4) Midway cracks (radial streaks)
- (5) Centre-line cracks
- (6) Centre segregation

Figure 2 Spray related cracks in continuously cast billets and slabs.

methods for their prevention in strand cast products.

From the literature, the fact emerges that spray related cracks (with the exception of transverse cracks in slabs) form close to the solidification front, in a temperature range within roughly 50 to 75°C of the solidus. Investigation of the high temperature mechanical properties of steel¹⁰⁻¹⁵ have shown that the ductility of the steel at temperatures close to the solidus temperature is very low - of the order of 0.2 to 0.3%. This low ductility results from the presence of low melting-point liquid films enriched with positively segregated elements like sulphur and phosphorus, separating adjacent dendrites. From the foregoing statements, it can be generalized, that most types of cracking in continuously cast products can be prevented if the magnitude of the tensile strains, imposed either thermally or mechanically, can be reduced to less than about 0.2%.

From Figure 2, it can be seen that slabs have a larger number of spray related defects, as compared to billets. This is because slabs are prone to bulging of the broad face due to ferrostatic pressure exerted by the liquid core. Spray cooling affects bulging, because it changes the temperature gradients in the solid shell, and thus the resistance of the shell to deformation under the influence of the ferrostatic pressure. Bulging is also affected by roll pitch, distance below the

meniscus, and the casting speed.⁹

1.1.1 Spray Related Defects in Billets

The most common defect linked to improper spray cooling practice in billets is the midway or halfway crack. These have also been referred to as radial streak, or ghost lines. These cracks can be seen in transverse sections, and lie normal to the faces of the billet. Their position in the transverse section is approximately halfway between the surfaces and the centre of the section. This type of crack is caused by reheating of the billet surface when the rate of heat extraction at the surface is suddenly reduced. This may occur when the billet passes from one spray cooling zone to another or from the spray cooling zone to the radiation cooling zone below the sprays.¹⁶⁻²⁰ The sudden reduction of the surface heat extraction rates can be caused by excessive spray cooling in some spray cooling zones, or by a spray cooling zone of insufficient length. The surface reheating results in the generation of compressive strains on the outside of the strand, and tensile strains near the solidification front. Cracking then occurs if the strains exceed the critical strains of 0.2 to 0.3% in the regions of low ductility. Thus, to prevent the formation of midway cracks the surface reheating must be minimized by proper spray cooling design. A maximum limit on the surface reheating of 100°C has been

proposed²¹ to prevent the occurrence of these cracks. This criterion has been used by Agarwal²² in his redesign of the spray system in an operating billet caster, and he has demonstrated that proper spray cooling can alleviate the formation of such cracks.

In an indirect way, a high casting temperature also has been linked to the formation of midway cracks because high casting temperatures lead to the formation of long, columnar zones during solidification. Midway cracks are able to form more easily between the dendrites in the columnar zone which runs perpendicular to the tensile stress, as compared to the equiaxed zone. Therefore, it is advantageous to have a predominantly equiaxed structure in the casting to reduce cracking. However, this is not often a practicable solution, since the steel may become too cold toward the end of the casting, such that skulls form in the tundish and ladle, and nozzles become blocked. Therefore it is advantageous to control the formation of midway cracks by proper design of the spray cooling zones. A final measure is the reduction of sulphur and phosphorus levels (to below 0.02%), which improves the high temperature mechanical properties of the steel.

The other spray related defects - diagonal cracking and rhomboidity, are associated with unsymmetrical cooling

of the billet faces. Though in some cases these defects have their origin in the mould, they can also arise in the upper spray regions if the water pressure in all the spray risers is not equal, or if some of the nozzles are plugged. Thus, if two adjacent faces are cooled more rapidly than other faces^{3,23} in the mould or in the secondary cooling zone, the billet contracts to generate a diagonal tensile strain between the colder faces. If the strain is large, the billet distorts and takes on a rhomboid shape with an acute angle between the colder faces. A crack may then form near the solidification front along the diagonal joining the obtuse corners, that is, perpendicular to the tensile strain. Uniform cooling on all faces minimizes the formation of such cracks.

The occurrence of centreline cracking in billets has been attributed to the sudden drop in the centreline temperature at the completion of solidification,¹⁷ since there is no more latent heat being released. Thus, the cooling rate at the centre becomes higher than the rate at the surface. This causes a rapid rearrangement of the temperature gradients in the billet, and imposes a tensile strain at the centre, contributing to centreline cracking. By applying water sprays to the point corresponding to the bottom of the liquid pool, the surface can also be made to cool rapidly so that the difference in the cooling rates between the centre and the

surface is decreased. As a consequence, the tensile strains are reduced, and centreline cracking avoided.²⁴

1.1.2 Spray Related Defects in Slabs

Bulging caused by ferrostatic pressure, as mentioned earlier, is the cause of most types of cracks in slabs. These include triple point cracks, centreline cracks,²⁵ radial streaks²⁶ and centreline segregation.²⁷⁻³¹ The tendency for bulging can be reduced by increasing the secondary cooling in the upper spray zones, which provides a stronger shell.^{27,28} In addition, proper adjustment of roll gaps and roll forces also reduces bulging.

Though spray cooling is not the primary cause for the formation of longitudinal, mid-face cracks, spraying conditions in the upper spray zones are known to exacerbate the cracking problem. These cracks initiate in the mould, and can break through to the surface depending on the secondary cooling and the strand support system.^{4,7,32,33} Reduction in the cooling provided in the upper spray zones has been found to have a beneficial influence on the surface quality, and to reduce the incidence of this type of crack. However, it should be noted that if the spray cooling in the top zone is inadequate, the surface of the slab may become too hot and lead to large strains due to bulging. On the other hand, excessive water cooling

in the spray zones results in rapid cooling of the surface, generating large transverse tensile strains, which can open up small cracks formed in the mould. Thus, an optimum value of spray cooling must be chosen, to compromise between overcooling and bulging.

Transverse surface cracks resulting from improper spray practice can be a serious problem in slabs cast from steel containing $>.02\%$ Al, $>1\%$ Mn, or Nb and V. These cracks occur almost exclusively on the inner radius surface of strands produced in arc type continuous casting machines. Since these cracks lie at the base of oscillation marks, and are quite fine, they are difficult to detect except with the aid of a control-pass scarf. The formation of these cracks has been attributed largely to straightening of the slabs,^{4,16,34} when the temperature of the top surface, which is under axial tension, is between 700 and 900°C. In this temperature range, the steel is shown to have a low ductility as the result of the precipitation of AlN (or presumably, the nitrides and carbides of Nb and V, if present) at grain boundaries. AlN precipitation has been found to be enhanced by cooling - reheating cycles in the same temperature range.^{24,35} Reduction of spray cooling in the upper spray zones has been used to alter the cooling - reheating cycles, thus reducing the AlN precipitation and improving the ductility of the

steel at the straightener.^{35,36} The brittle zone has been avoided during straightening by one of two spray practices: by keeping the surface temperature of the slab above the 700 to 900° C region,^{24,36,37} or by keeping it below this temperature range.^{35,38}

All remaining defects shown in Figure 2 are the result of bulging of the broad face of the slab. Triple point cracks, running perpendicular to the narrow face, lie within the V shaped region formed by the meeting of the three solidification fronts. Bulging of the broad face results in an outward rotation of the cold corners, causing a slight concavity of the narrow face. Thus, tensile stresses are generated near the solidification front in a direction parallel to the narrow face. If the resulting tensile strains exceed the ductility of the material in this area, triple point cracks arise.

Midway cracks or radial streaks in slabs are seen running normal to the broad face in longitudinal sections, as can be seen from Figure 2. Insufficient spray water and high casting speed are the most important factors contributing to the formation of this type of crack.³⁹ The cracks are caused by the squeezing action of support rolls on a bulged region of slab, generating tensile strains at the solidification front.

Centreline cracks are the result of bulging close to the bottom of the liquid pool. Cracking can be reduced by regapping the rolls correctly, reducing casting speed, or increasing spray cooling to reduce bulging.

Centre segregation is affected primarily by bulging and superheat,^{27,28,29,40} Bulging near the bottom of the pool causes the remaining liquid, enriched in solutes such as Mn, C, S and P, to be drawn down into the bulged area. Spray cooling and casting speed are factors affecting centre segregation insofar as they affect the slab surface temperature, and consequently, the resistance to bulging.

In the control of bulging of the broad faces of the slab, the roll pitch and roll gaps in the support assembly are of primary importance. Spray practice plays a smaller part, by increasing the bulging resistance if the slab surface temperature is maintained at a low enough temperature. However, since sprays play an important role in the prevention of defects such as transverse cracks, a degree of freedom is lost if the sprays must be tied to bulging control. It should be emphasized that, within reasonable limits, the use of sprays solely to limit bulging is an indication of defects in the machine design or poor maintenance.⁹

The causes for the defects discussed in this section

TABLE I Spray Related Defects

Crack Type	Spray Related Cause	Other Factors	Corrective Action
BILLETS			
Midway Cracks	Reheating of surface below spray chamber	High casting temperature S and P >.02%	Adjust sprays to minimize reheating, lower pouring temperature, S and P levels.
Rhomboidity/Diagonal Cracks	Asymmetrical cooling	See Ref. 4	Ensure uniform spray cooling on all four faces.
Centreline Cracking	Rapid cooling of centre region below pool	Severe secondary cooling and high pouring temperature	Adjust secondary cooling near the bottom of the pool.
SLABS			
Transverse, Surface Cracks	Precipitation of AlN and straightening with surface between 700 and 900°C.	Steel composition >0.02% Al >1% Mn, Nb, V	Adjust sprays to prevent reheating from below 700°C or maintain slab surface outside 700-900°C range at straightener.
Longitudinal, Midface Cracks	Overcooling in upper spray zones - Bulging	See Ref. 4	Reduce cooling in upper spray zones. Check for bulging.
Triple Point Cracks	Bulging	See Ref. 4	Regap rolls.
Midway Cracks	Bulging	High casting speed Increasing S, C	Check roll gaps. Increase spray cooling. Reduce casting speed.
Centreline Cracks	Bulging	High casting speed	As above.
Centreline Segregation	Bulging	High casting speed High superheat	As above. Reduce superheat.

and methods for alleviating the cracking problems are summarized in Table I.

1.2 Spray Chamber Design and Control

From the foregoing discussion, it is clear that cooling in the secondary cooling zones must be properly designed and controlled in order to avoid defects in the cast products. The design of spray chambers from the standpoint of reduction of thermal strains in the strand has been dealt with in the recent literature^{9,21,41} for the case of billets. The variation of spray cooling in various zones of a slab caster to minimize formation of transverse cracks has also been discussed.^{9,35} These designs are arrived at from a knowledge of the heat transfer coefficients at various points in the spray chamber that would be necessary to maintain the strand surface temperatures at levels that would minimize the factors leading to crack formation. These heat transfer coefficients are then used in conjunction with data regarding their variation with spraying parameters in order to arrive at the final design of the spray chamber - the nozzle types to be used, nozzle-to-nozzle spacing, nozzle-to-strand distance and water pressure in the risers feeding the nozzles.

It is assumed in these designs that the caster is

operating at steady state. In reality, however, changes occur during the casting of a single heat or a sequence of heats such that true steady state is rarely achieved. Variations in casting speed in particular are unavoidable as a result of normal operating procedures such as start-up, capping off, tundish or shroud changes, or due to unplanned events such as nozzle blockage. The problem then arises of adjusting the sprays to minimize deleterious effects on product quality and machine operation. It has been common practice to vary the spray water throughout the secondary cooling zone in direct proportion to the change in casting speed (within predetermined limits) such that the specific water flow (l/kg) remains the same. However, since it is desirable to keep the thermal history of any given slice of material passing through the casting machine similar to that which would be obtained under steady state conditions, such a method is unsatisfactory. The spray cooling must be altered, not in proportion to the casting speed, but according to the time that the slice has spent in the machine prior to reaching any given location, i.e., according to the age at each location in the strand. The adjustment of the sprays according to the principle of cooling-with-time requires three types of information:

- i) The age or residence times of slices passing selected points at any time.

- ii) The desired relationship between spray heat-transfer coefficients and time.
- iii) The relationships between the spray heat-transfer coefficients and the spray parameters.

Baptista⁴² has determined spray adjustments to be made to a slab caster during transients in the casting procedure caused by speed changes, based on such residence time calculations.

There are disadvantages to the manual adjustment of sprays, and thus automatic control has been developed.⁴³⁻⁵¹ This can be achieved through the application of automatic control theory and mathematical models of the continuous casting process. Control is performed by a real-time process control computer, which constantly monitors the various operating conditions of the casting machine, and which automatically controls the water flows in the secondary cooling zone to adjust for changes in the operating conditions.

1.3 Scope of the Present Work

It becomes obvious from the foregoing discussion that for designing the spray chambers in continuous casting machines, adequate and reliable data is required linking

the various spray parameters (for instance spray pressure, spray water flux) to heat-transfer coefficients. The purpose of this work therefore was to generate such data, and to investigate the relationships between the spray parameters and heat-transfer coefficients at the high surface temperatures that prevail in the spray chambers of continuous casting machines. Laboratory studies were performed to determine the distribution of the water in the sprays produced by several commercial nozzles under various operating conditions, and heat-transfer coefficients were measured for these sprays under corresponding conditions.

Chapter 2

HEAT FLOW IN SPRAY COOLING

REVIEW OF THE LITERATURE

2.1 Introduction

In the continuous casting process, the strand emerges from the mould at temperatures exceeding 1250° C. The cooling applied below this point must not only extract heat from the casting to promote solidification at reasonable rates, but should do so at a rate that maintains the surface temperatures of the strand within close limits. Water jets can be used to provide high heat extraction rates, but controlling the surface temperatures within the limits desired would be a difficult task. Spray cooling with atomized water sprays provides a better solution, not only by providing controllable cooling of the strand, but also by providing acceptable heat extraction rates for economical production of continuously cast products.

The physics of spray cooling involves a combination of boiling heat transfer and droplet dynamics. A short description of the boiling process follows, to clarify the role of the different boiling regimes in the cooling of hot surfaces.

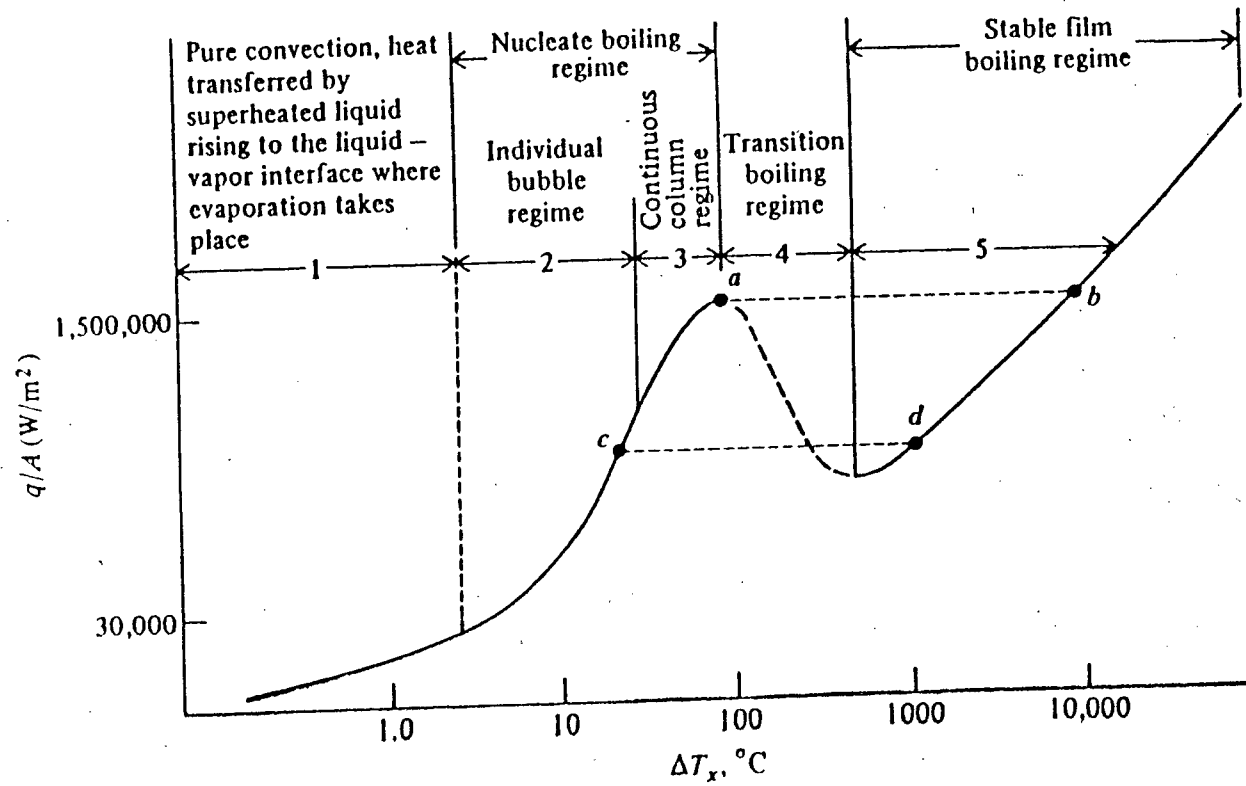


Figure 3 Typical boiling curves for a wire, tube, or horizontal surface in a pool of water at atmospheric pressure.⁵²

A typical example of the heat flux obtained during the cooling of a hot surface immersed in a pool of water at saturation temperature is illustrated in Figure 3.⁵² Thus, when the temperature difference between the surface and the water is within a few degrees, the process of free convection transfers heat to the liquid surrounding the surface. Convection currents then circulate the superheated fluid, and evaporation occurs at the surface of the fluid. As the temperature difference increases, vapour bubbles are formed at various nucleation sites on the hot surface, and as the temperature of the hot surface increases further, these bubbles become larger and more numerous and rise up to the surface. This region of temperature in which the formation of rising vapour bubbles is the mechanism of heat transfer, is known as the "nucleate boiling regime", and the heat flux increases rapidly as the surface temperature increases. A further increase of the surface temperature causes the appearance of continuous columns of bubbles. The "transient boiling region" with corresponding lowering of the heat flux then appears at higher surface temperatures, since there is a limit to the number of vapour columns that can be generated at the surface. This is because the space between the columns becomes too small to accommodate the streams of liquid which must move toward the hot surface to replace the liquid evaporated to form the vapour columns.

A further increase of surface temperature beyond this region leads to a phenomenon known as "stable film boiling". In this form of boiling, a vapour film completely blankets the heated surface, and heat is then transferred across the vapour film by the process of conduction and radiation. As can be seen from Figure 3, the heat flux in this regime is low, and increases at higher temperatures due to the increased role of radiation in the heat transfer process. The temperature above which stable film boiling occurs is known as the "Liedenfrost point", and is also referred to as the "critical point" in the heat transfer literature.

Similar regimes are also observed in the spray cooling of hot surfaces as can be seen from Figure 4.⁵³ Spray cooling can be used to augment cooling in the region corresponding to surface temperatures above the Liedenfrost, or critical, point. This is possible because the momentum of the droplets in the spray allows them to penetrate the vapour layer and aid in the heat extraction from the surface.

Many studies have been undertaken to clarify the role of the different variables associated with the heat transfer between a hot surface and liquid droplets impinging on the surface. The following discussion deals with the various aspects of the interactions of the impinging droplets with the hot surface.

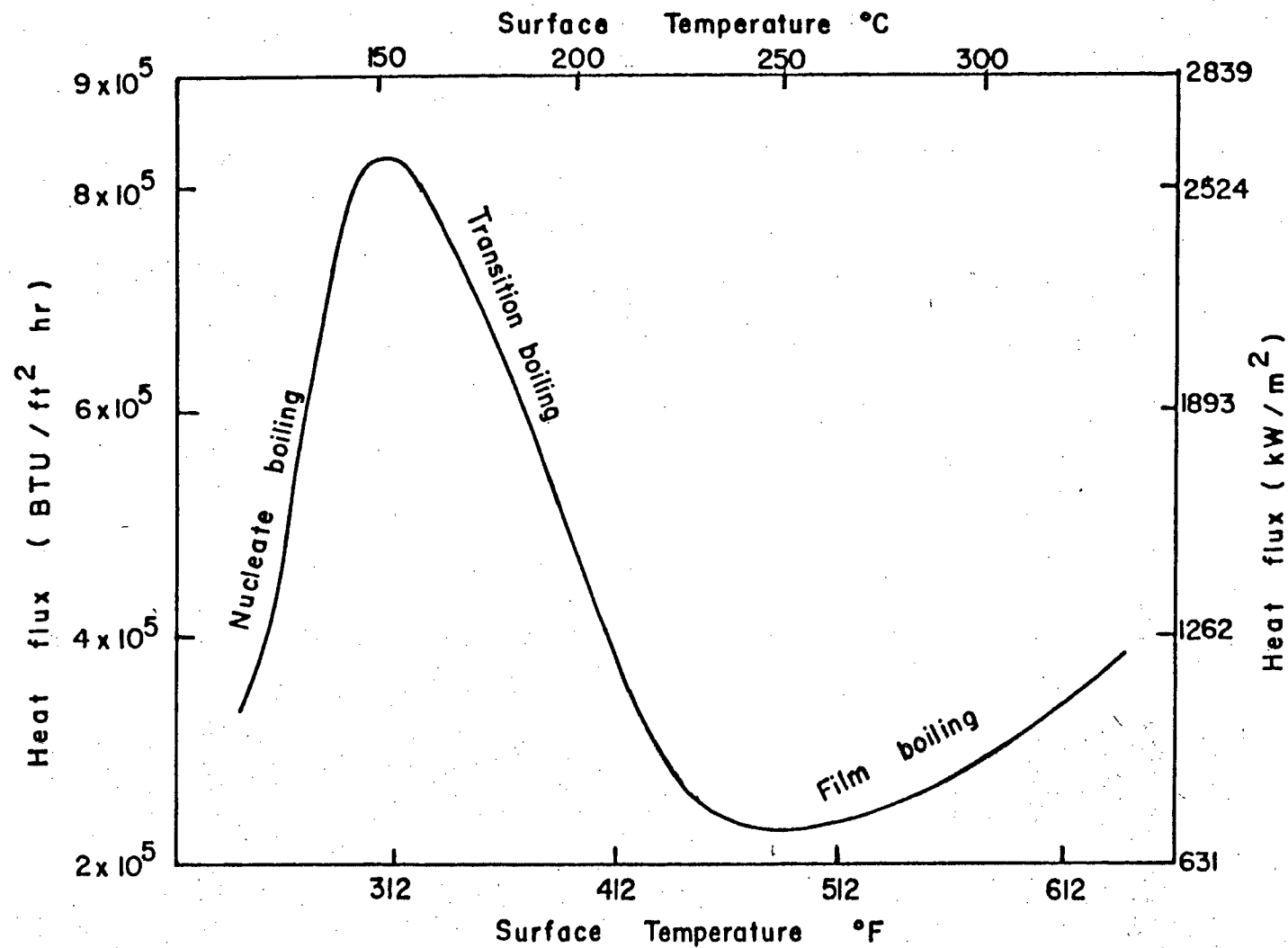


Figure 4 Variation of heat flux with surface temperature in spray cooling.

2.2 Single Droplet Studies

Because of the complex nature of sprays and spray cooling, some investigators have taken the approach of studying the effect of single droplets impinging on a hot surface, with a view to building up a picture of spray cooling by summing the effects of all the drops in the spray. Two different situations have been considered - a sessile drop resting on a hot surface, and a single drop impinging on a hot surface.

2.2.1 Dynamics of Droplet Impact

Heymann^{54,55} has presented an analytical model of the collision process between a liquid drop and a solid surface, and obtained quantitative results for the impact pressure generated at the surface by the impinging droplets. This analysis was developed for the case of high speed impact between the drop and the solid surface, and specifically, was undertaken to clarify the effect of the collisions on the erosion process on the surface. As such, the analysis dealt with cold surfaces in the absence of heat transfer.

Savic and Boulton⁵⁶ have also investigated the fluid flow associated with the impact of liquid droplets on a

solid surface. In addition to the calculation of the distribution of pressure in the area of impact, they have calculated the shape of the drop as it spreads on impact. High speed photography was used to confirm the results of their calculations for the case of droplets of water of .476 cm (3/16") diameter impinging on a cold surface. When the surface temperature was increased to 700° C, spreading of the drop on the surface was observed, after which vapour bubbles caused by the boiling process caused disintegration of the drops. No quantitative heat transfer results were presented, but the interaction of fluid flow and heat flow was shown.

2.2.2 Heat Transfer to Sessile Drops

Gottfried⁵⁷ and Wachters et al.⁵⁸ have studied theoretically the heat transfer to sessile water droplets on a hot surface (300° C to 400° C). The assumptions used in their work include the following:

- i) The drops are nearly spherical except for the lower part near the hot surface (spheroidal)
- ii) The drops are nearly sessile until complete evaporation takes place
- iii) A thin film of vapour insulates the drop from the surface
- iv) Radiation heat transfer between the surface and the drops is negligible.

The aim was to calculate the vapour film thickness below the sessile drop, and the shape of the drop as it evaporated due to heat flow into the drop from the hot surface. From photographs of the sessile drops during evaporation, Wachters et al.⁵⁸ determined the evaporation rates of the drops. Assuming that heat is transferred to the drop through the vapour cushion and also due to vapour flow around the drop, the evaporation rates of the drops were theoretically calculated. The experimental results indicated that the bottom of the drops assumed a flat shape parallel to the hot surface. Water drops on heated gold surfaces were used in the experiments. Drop diameters were varied between 0.25 mm to 2.7 mm, and surface temperatures from 100° to 400° C.

From observations of evaporation times, Moriyama^{59,60} obtained heat-transfer rates between a hot low carbon steel surface (surface temperatures between 300° to 800° C) and water drops (2.45 mm to 5.29 mm in diameter) and has proposed a correlation of the form.

$$Q = 849.92 \exp (0.00216 T_s + 8.821 r_o) \quad \dots 2.1$$

for the heat transfer to a single drop of radius r_o cms. The heat transferred to the droplet is seen to rise as the surface temperature and the drop radius increase. This correlation fits Gottfried's data well.

2.2.3 Heat Transfer to Impinging Drops

Wachters and his co-workers^{61,62} have compared the heat transfer between hot surfaces (up to 400° C) and impinging droplets (diameters between 60 μ and 2 mm). With predictions made from their earlier work⁵⁸ for sessile drops, they found a large discrepancy existed between the observed values and the theoretical predictions. This has been attributed to two factors:

- i) The drop stays in the vicinity of the hot surface for a relatively short time before rebounding
- ii) The spheroidal state was not attained in their experiments until the surface temperature exceeded 400° C.

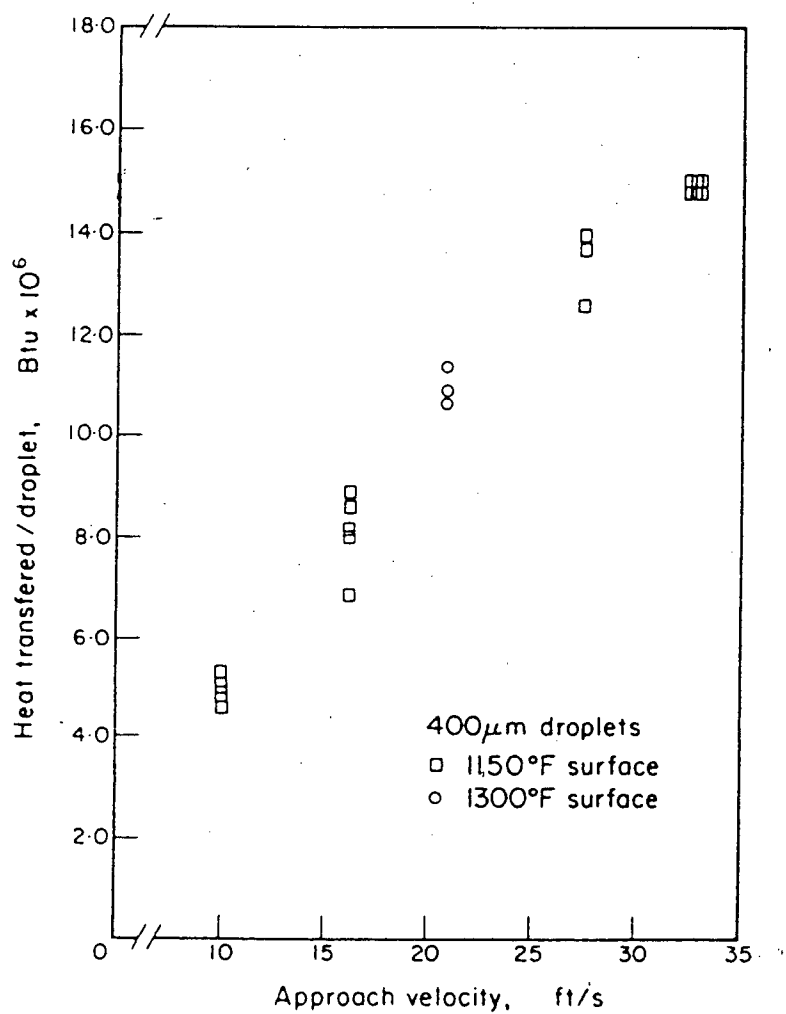
With the use of high speed photography, they found that the large (2 mm dia.) drops disintegrated above a critical Weber Number of 80. For Weber numbers below 30, no drop disintegration was observed. From photographic observations, the volume reduction of the drops due to evaporation was found to decrease as the surface temperature increased. The volume loss was less than 0.5% of the original drop volume when the surface temperature increased beyond 200° C.

Heat-transfer rates for a series of impinging droplets

were obtained by McGinnis and Holman⁶³ and Holman et al.⁶⁴ The experimental technique used was to have the droplets falling vertically on a polished nickel plated copper plate, maintained at constant temperature, and inclined at 27° to the horizontal. A peak in the heat-transfer rates was found for various liquids, at a surface temperature of approximately 150°C . The maximum heat flux at these temperatures was attributed to the opposing effects of the thermal gradient in the vapour film below the drop and the decreasing droplet contact time as the surface temperature increased. The experiments were carried out for surface temperatures below 300°C .

Pedersen^{65,66} has performed experiments with moving drops of water propelled horizontally toward a vertical heated target. The target material was a small stainless steel cylinder 6 mm in length with a diameter of 6 mm, heated by radiation in a resistance heated furnace. The heat flux caused by the impinging droplets was determined from the measured temperature transient experienced by the target when the droplets were allowed to impinge on it. Photographic observations were also made of the collision of the droplets with the plate, to determine the droplet velocity. The droplet sizes used in this study were 200, 300 and 400 microns in diameter, with drop velocities up to 9 metres per second. Target temperatures up to 700°C were used.

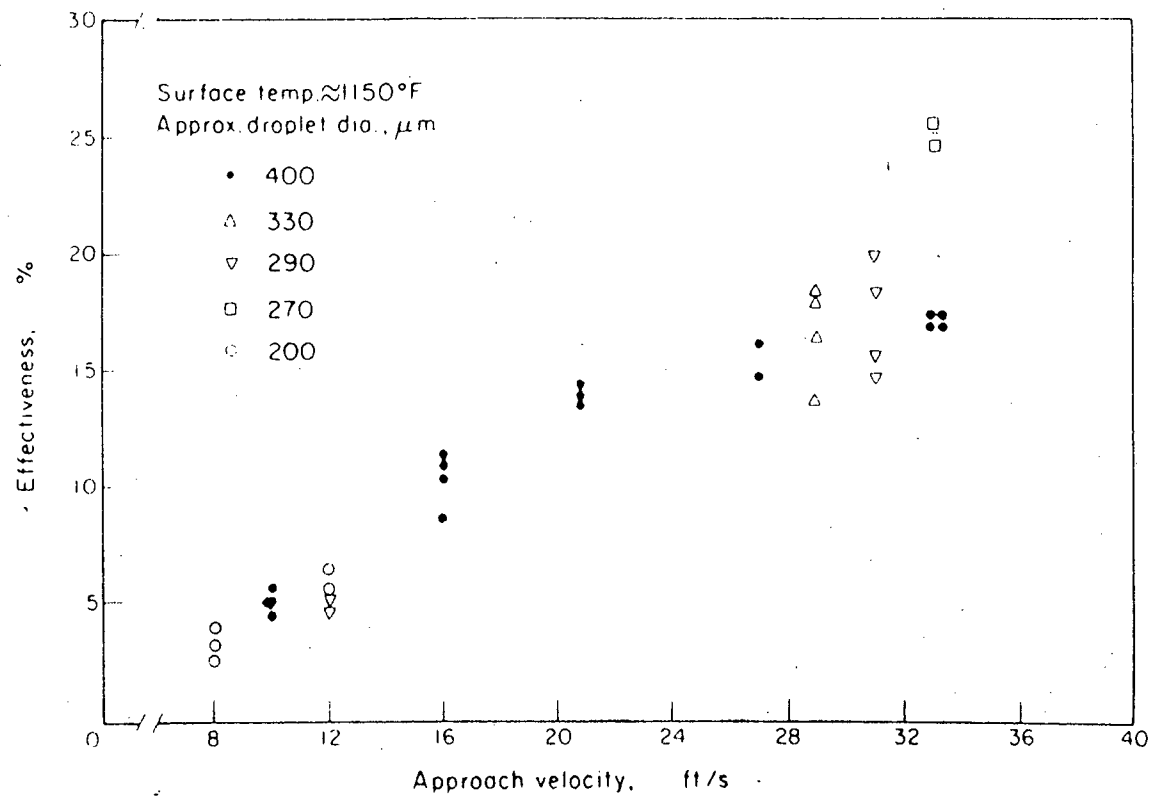
As can be seen from the results of his experiments presented in Figure 5, an increase in the droplet velocity increases the heat transferred to each droplet. Defining the heat-transfer efficiency as the ratio of the heat transferred to the droplet to the total heat required for the evaporation of the droplet, his results show an efficiency that increases with increasing approach velocity as shown in Figure 6. The use of heat-transfer efficiency serves to eliminate the effect of droplet size. Photographic studies of the droplet impingement show that the difference in the behaviour of the droplet during collision with the target depends on the target surface temperature. The different heat-transfer regimes encountered have been labelled as "wetting", "transition" and "nonwetting", corresponding to the droplet behaviour on impact. These regimes generally correspond to the nucleate boiling, transition and film boiling regions respectively, as noted in Figure 3. When the surface temperature is in the region corresponding to the nucleate boiling zone, it was found that the drops spread out on the surface on impact, and that evaporation takes place mainly by nucleate boiling within the drop. This has been termed the "wetting" regime. High heat fluxes and efficiencies have been found in this region. The efficiency decreases as the surface temperature increases and the drop behaviour on impact changes. In the "nonwetting" region, the droplets break up into smaller droplets after



$$1 \text{ B.T.U.} = 1055.56 \text{ Ws}$$

$$1 \text{ ft/s} = 0.3048 \text{ m/s}$$

Figure 5 Effect of droplet velocity on the heat transferred to the droplet.⁶⁵



1 ft/s = 0.3048 m/s

Figure 6 Non wetting droplet heat transfer efficiency.⁶⁵

initially spreading out on the surface on impact. The smaller droplets then rebound from the surface.

2.2.4 Extension of Single Drop Experiments to Characterization of Spray Heat Transfer

Using the assumptions noted below, Moriyama⁵⁹ has obtained a correlation for spray cooling based on the results of his single droplet experiments. The assumptions used in his analysis for droplets in the spray are:

- i) The droplets are spherical and of constant diameter
- ii) There is no interaction of droplets
- iii) The droplets behave in the same manner as quiescent droplets on a hot surface
- iv) There is no disintegration of droplets on the hot surface.

It is to be noted that in an actual physical situation of spray cooling, none of these assumptions would hold. Using a value of droplet retention time (proportional to drop radius) as proposed by Wachters and Westerling⁶² the correlation found for the spray cooling heat flux Q in the film boiling region was

$$Q = 586.15 \dot{m} r_o^{-1.5} \exp(0.00216 T_s + 8.821 r_o) \dots 2.2$$

This correlation however, predicts much lower heat-transfer coefficients in sprays when compared to the results of other workers which will be presented in the following section.

2.3 Heat Transfer in Sprays

Laboratory experiments using either steady state or transient measurement techniques have also been performed to characterize the heat transfer between commercial water sprays and hot surfaces.

Steady state experiments have been carried out by supplying a hot metal sample with an energy input equivalent to that extracted from the sample by the spray directed onto it. The measured value for the energy input and the sample temperature allow the calculation of the surface heat fluxes and the heat-transfer coefficients.

Transient methods used for the evaluation of the heat-transfer coefficients fall into two categories:

- i) In the first category, temperature transients within the hot metal sample are recorded during the spraying interval, and mathematical methods used to calculate the heat-transfer coefficients.

- ii) In the second category, pyrometers are used to monitor the surface temperature of the hot surface being sprayed. The measured variation of surface temperature and the known initial condition of temperature distribution in the sample, when used in the solution of the conduction equation in the solid, yield the required heat-transfer coefficients.

In-plant measurements on operating continuous casting machines have also been used to obtain heat-transfer coefficients in the secondary cooling zone. These coefficients can be obtained by performing heat balances on the strand using measured values of the strand surface temperatures at various positions.

The different techniques used and the experimental findings are dealt with in more detail below.

2.3.1 Transient Methods

For sprays produced by commercial full cone spray nozzles (Spraying Systems Co. 1/8 GG1 and 1/8 GG 3001.4), spraying downwards onto the face of a resistance heated chrome plated copper bar, Gaugler⁵³ calculated temperature dependent heat-transfer coefficients for various

spraying conditions from temperature transients measured inside the bar with Chromel-Alumel thermocouples. As mentioned in an earlier section, he observed three distinct regions in the heat flux vs. surface temperature relationship (Figure 4). The results of his experimental work are presented in Figures 7 and 8 (Curve 1). The experimental conditions used in his work were:

Initial surface temperature	400° C
Water fluxes	From 0.716 to 3.7 $\text{g}/\text{m}^2\text{s}$
Droplet velocities	From 16 to 26 m/s

The film boiling range in his work was found to exist at temperatures greater than 250° C, and a correlation of the form

$$\eta = 1.031 \times 10^{-2} (T_s - T_w) (\dot{m})^{-0.67} \pm 10\% \quad \dots 2.3$$

was found for the efficiency for all drop sizes and velocities. This relationship, presented in graphical form in Figure 7, shows the influence of the local water flux on the efficiency. The corresponding correlation of the heat flux to the spray is

$$Q = 3.6952 (T_s - T_w) \dot{m}^{0.33} \pm 10\% \quad \dots 2.4$$

The heat flux to the spray increased with an increase in the concentration of droplets in the spray (drops per unit volume) and also as the droplet momentum increased. However,

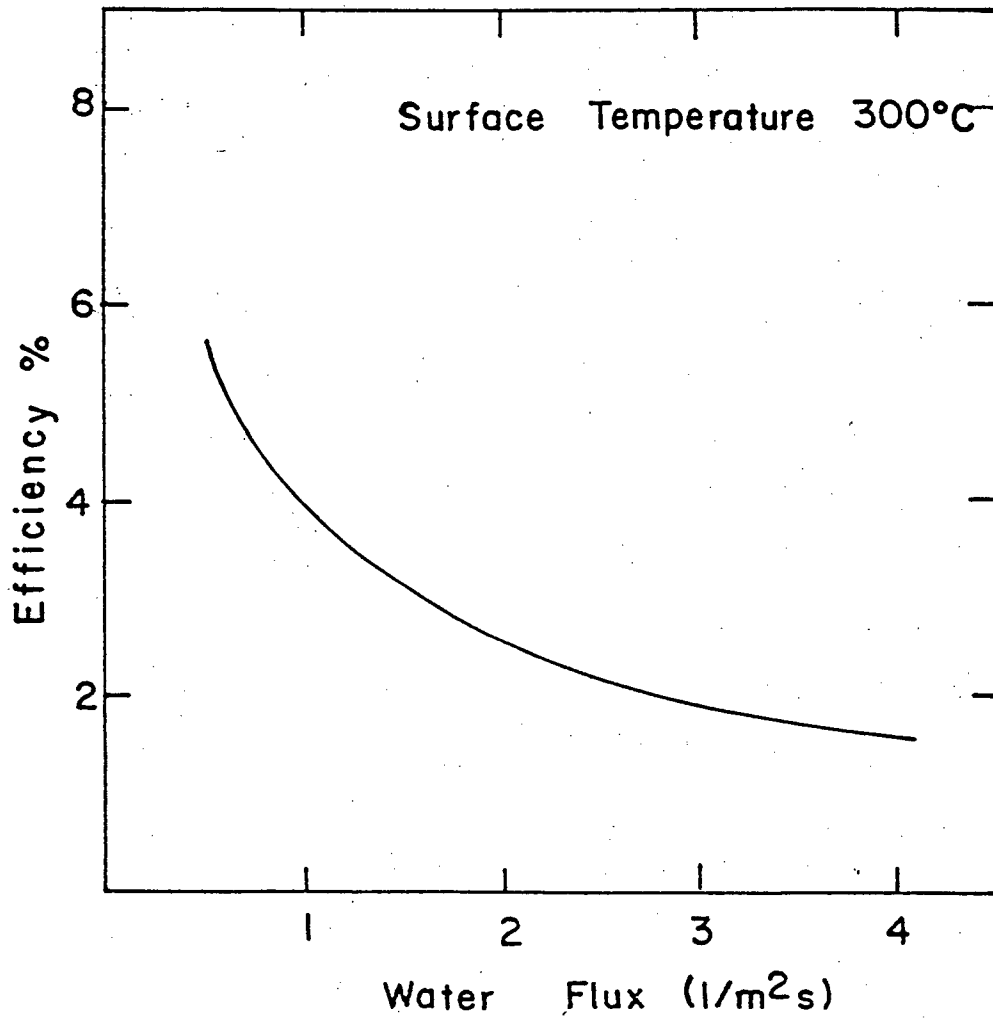


Figure 7 Variation of efficiency with water flux ⁵³.

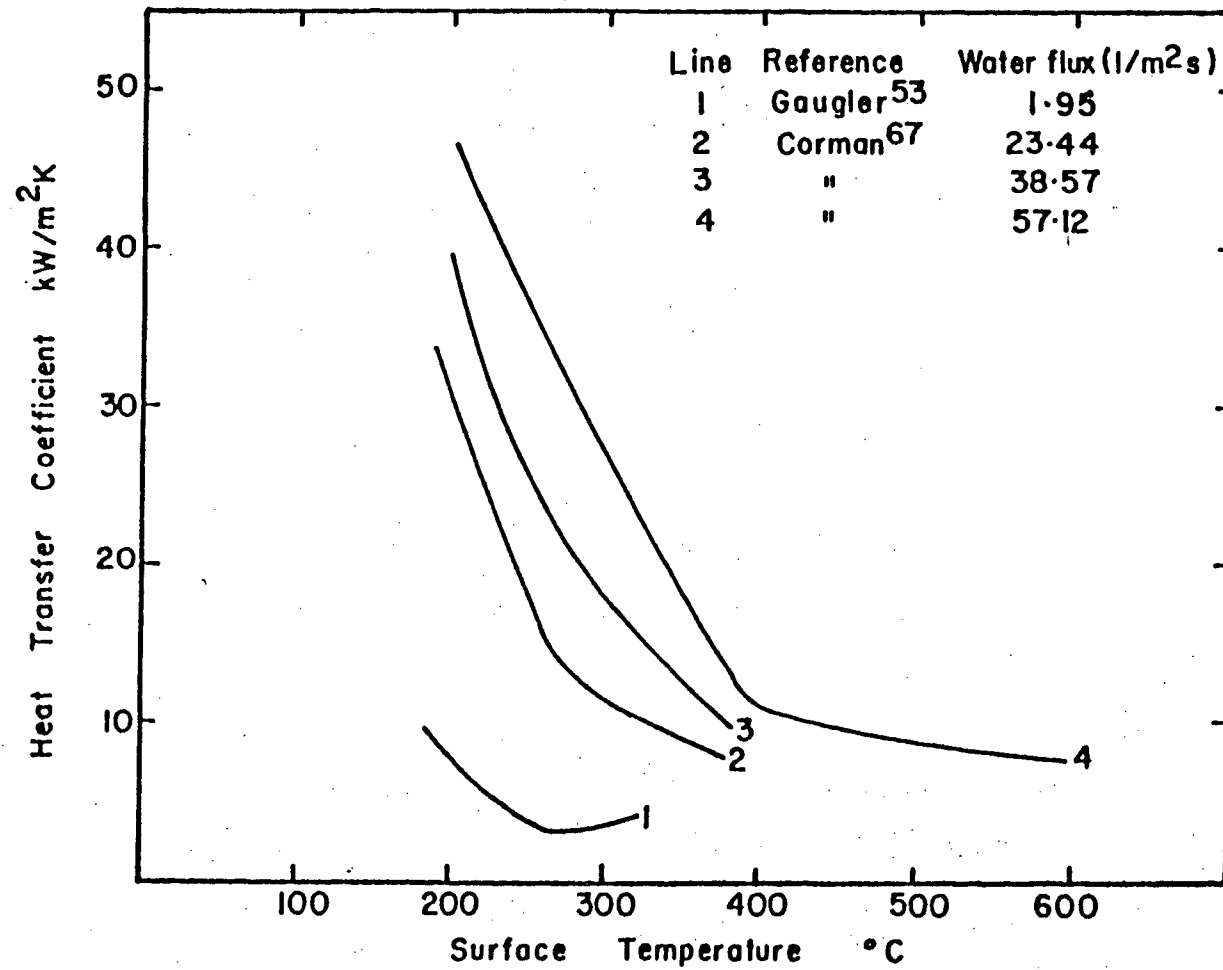


Figure 8 Variation of spray heat-transfer coefficients with surface temperature.

the heat transferred to each droplet decreased with increasing water flow.

Curves 2, 3 and 4 in Figure 8 are results obtained by Corman,⁶⁷ who used the same equipment as Gaugler⁵³ to extend the range of the measurements to higher temperatures and higher water fluxes. The results presented are for the Spraying Systems Co. 1/8 GSS nozzle. Increasing the water flux not only increased the heat-transfer coefficients, but also shifted the critical point to higher temperatures.

In their study of strip cooling on runout tables, Auman et al.⁶⁸ determined the quantity of heat removed from an instrumented stainless steel plate (AISI 304, 15 cm by 20 cm by 2 cm thick), which was heated to about 1100° C and passed through a spray of water directed vertically downward. Full cone sprays and fan sprays were used in their experiments, with spray water fluxes as high as 217 $\text{g}/\text{m}^2\text{s}$. In agreement with other investigators, the three regimes of heat transfer corresponding to different surface temperatures were observed. The heat flux to the sprays was found to increase as the water flux increased. However the rate of increase of heat flux was found to decrease with increasing water flux. The spray cooling efficiency was also found to decrease with increasing water flux.

Meaningful comparison of these observations with the results of other workers is not possible because the surface temperatures at which these heat fluxes were obtained are not reported.

Cylindrical nickel probes heated to 800°C and then spray cooled were used by Lambert and Economopoulos⁶⁹ in their spray heat-transfer studies. Their results show qualitative agreement with the work of Auman et al. In this case too, since only the spray pressure of 0.098 MPa (14.2 psi), and the nozzle to probe distances (10-20 cms) were reported, comparison with other results is not feasible.

The effect of spray variables on the Liedenfrost temperature was investigated by Hoogendoorn and DenHond⁷⁰ using full cone atomizer nozzles at pressures of up to 1.1 MPa (160 psi). Spray droplets of 0.2 to 1 mm diameter, with velocities of 10 to 30 m/s, were directed downward onto a heated (AISI 321) stainless steel plate instrumented with thermocouples. The spray water fluxes used in this study varied from 0.6 to $25 \text{ g/m}^2\text{s}$. Figure 9 shows some of the results obtained from this study. Curves 1 and 2 represent the variation of the heat-transfer coefficient as a function of the surface temperature for a water temperature of 20°C . It can be observed that the critical point is

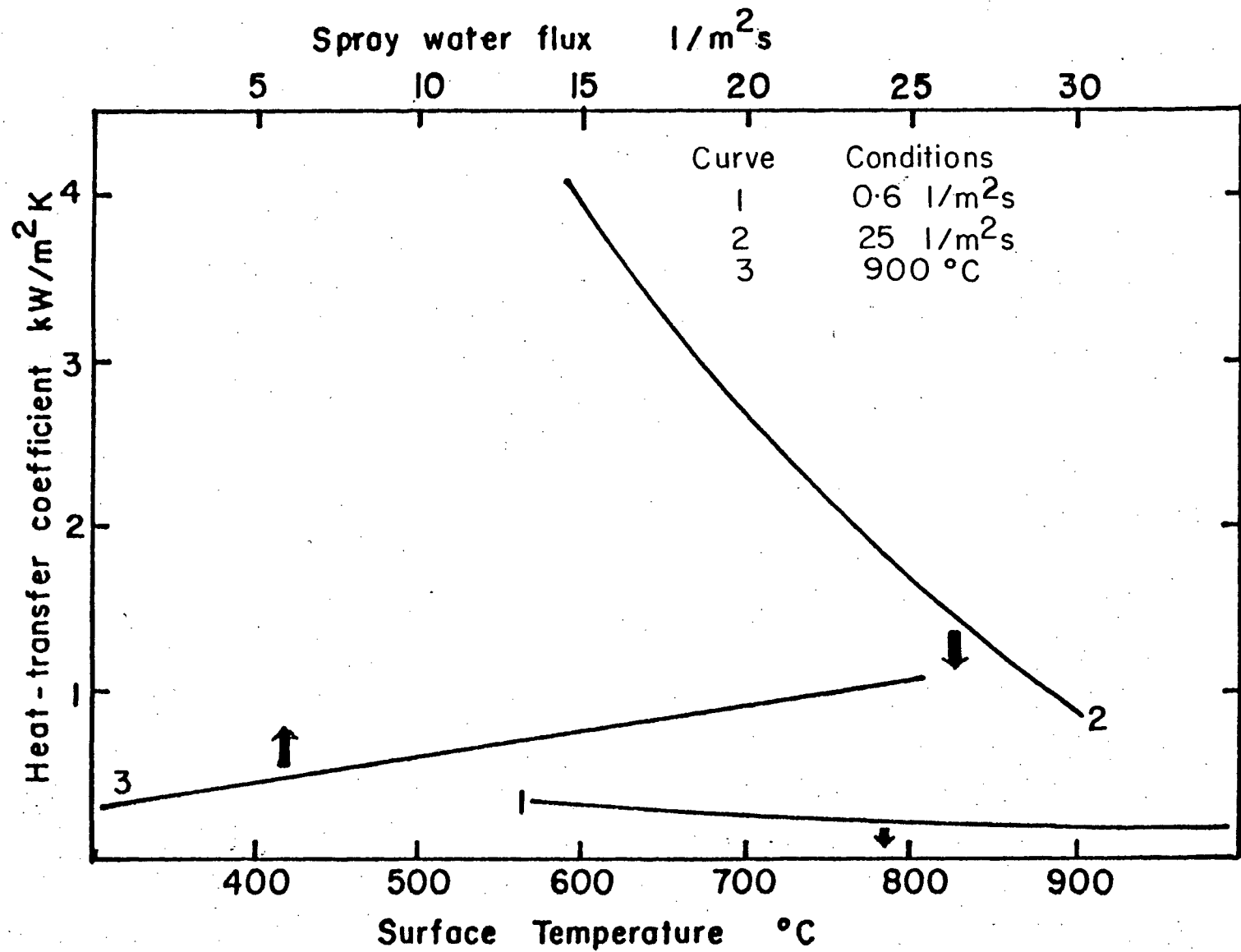


Figure 9 Dependence of the heat-transfer coefficients on water flux and surface temperature.⁷⁰

below 600° C for the case of a low water flux ($0.6 \text{ } \ell/\text{m}^2\text{s}$) as shown by Curve 1, whereas, for a much higher water flux of 25 ($\ell/\text{m}^2\text{s}$), this temperature lies above 900° C (Curve 2). The increase of the heat-transfer coefficients with increase of spray flux for a surface temperature of 900° C is illustrated by Curve 3 of this Figure. A fairly wide scatter of $\pm 20\%$ in their results has been reported. Comparison of the heat-transfer coefficients obtained by spraying downward on the hot surface with those from spraying onto a vertical plate showed no significant differences.

Mitsutsuka and his co-workers^{71,72} carried out experiments using a horizontal plate of low carbon steel, heated in a furnace to 930° C, and cooled by spraying both the top and the bottom simultaneously. The correlation fitting their results is of the form

$$h = A \dot{m}^n (1 - b T_w) \quad \dots 2.5$$

where A, b and n are constants. The exponent n varied from 0.3 to 0.8 for water fluxes greater than $0.08 \text{ } \ell/\text{m}^2\text{s}$. The value of b varied between 0.005 to 0.008 for \dot{m} of about $10 \text{ } \ell/\text{m}^2\text{s}$. The effect of the water temperature on the heat-transfer coefficient for a spray water flux of $10 \text{ } \ell/\text{m}^2\text{s}$ is shown in Figure 10, Curve 3. It can be observed from this curve that the water temperature exerts a large influence

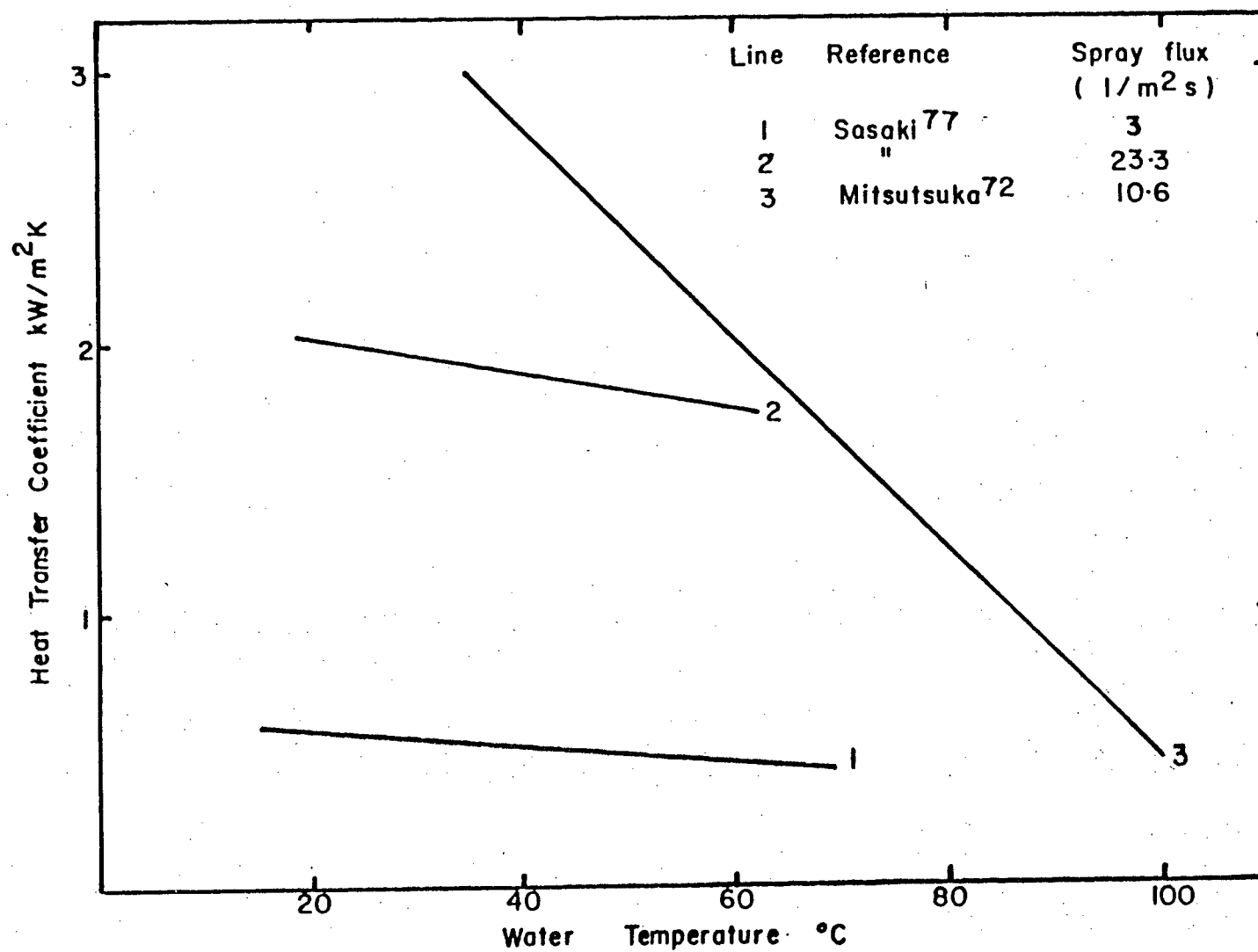


Figure 10 Effect of water temperature on spray heat-transfer coefficients.

on the heat-transfer coefficient, which decreases rapidly by approximately 1% for every 1°C rise in the water temperature. The heat-transfer coefficient correlation has been used with modification by other workers,^{35,73} and a value for b of 0.0075 has been adopted. Nozaki³⁵ for instance, has found that the heat-transfer coefficients obtained from Mitsutsuka's correlation were too high when applied to slab casters, in which there are a large number of rolls in the secondary cooling chamber. He has therefore incorporated an accommodation coefficient which was determined by measurements on an operating caster, and has proposed a correlation of the form

$$h = 1.57 \dot{m}^{0.55} (1 - 0.0075 T_w) / \alpha \quad \dots 2.6$$

where α is the accommodation coefficient with a value of 4. The heat-transfer coefficient vs. water flux relationships used by Ishiguro⁷³ and Nozaki corresponding to altered forms of Mitsutsuka's correlation are presented in Figure 11, Curves 1 and 2 respectively.

Using a vertical stainless steel plate, heated to 1100°C before spray cooling, Sugitani⁷⁴ determined that the heat-transfer coefficients dropped rapidly with increasing surface temperature, as shown in Figure 12, Curves 10 and 11. It must be observed, that for Curve 11 in this Figure, in

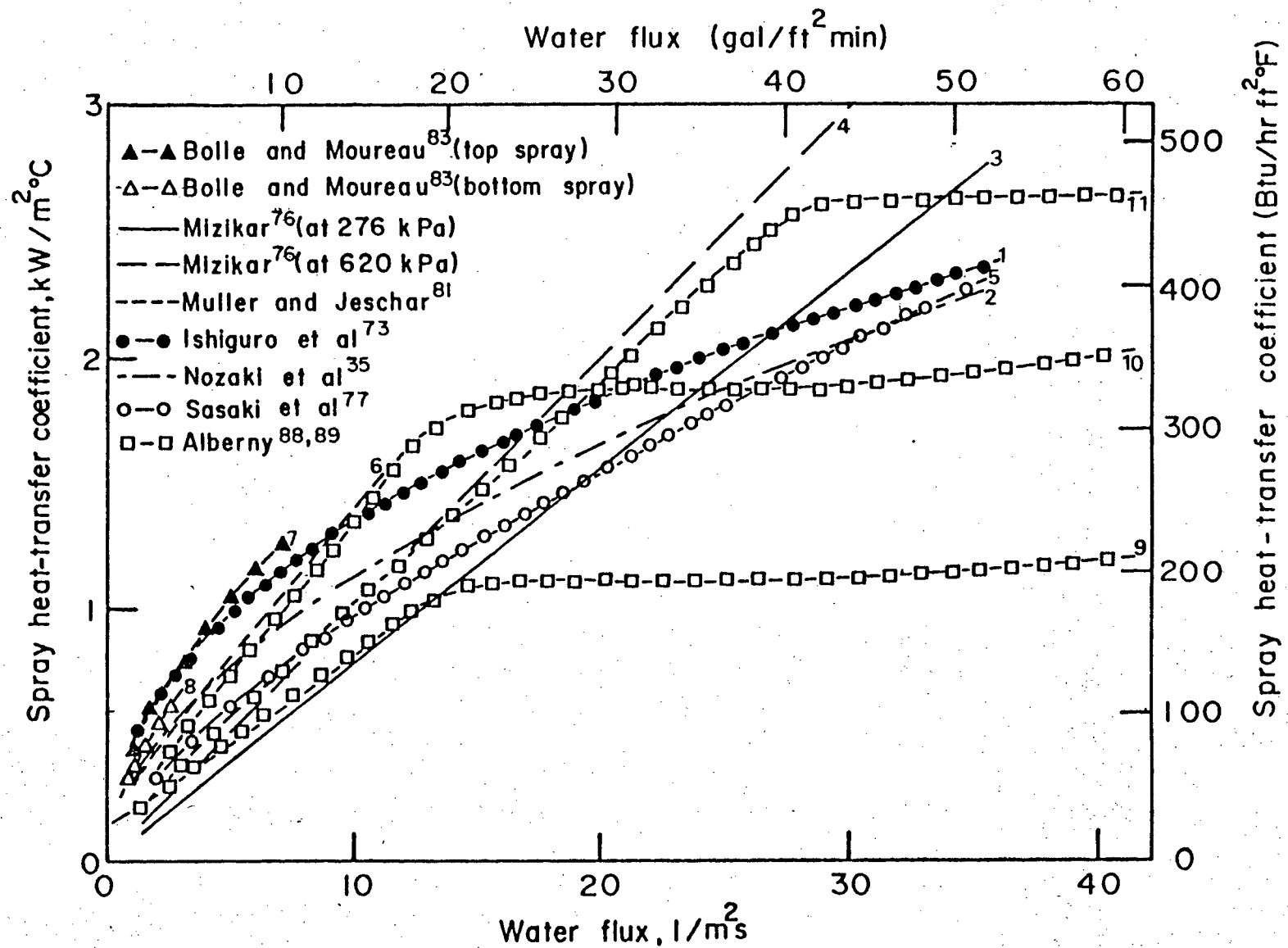


Figure 11 Variation of spray heat-transfer coefficient with water flux as reported in various studies on spray heat extraction.

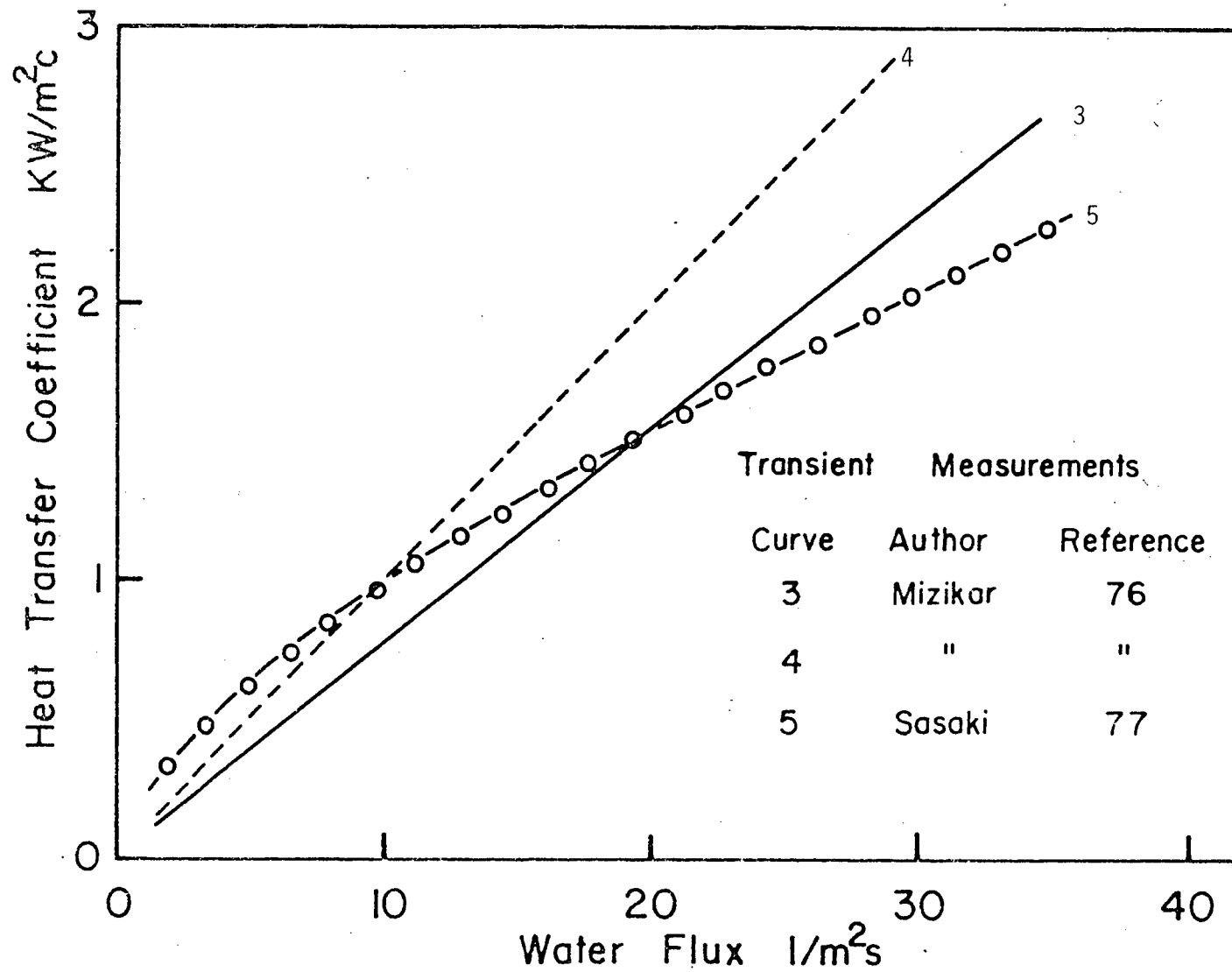


Figure 11a Variation of spray heat-transfer coefficient with water flux as reported in various studies on spray heat extraction -- Transient measurements

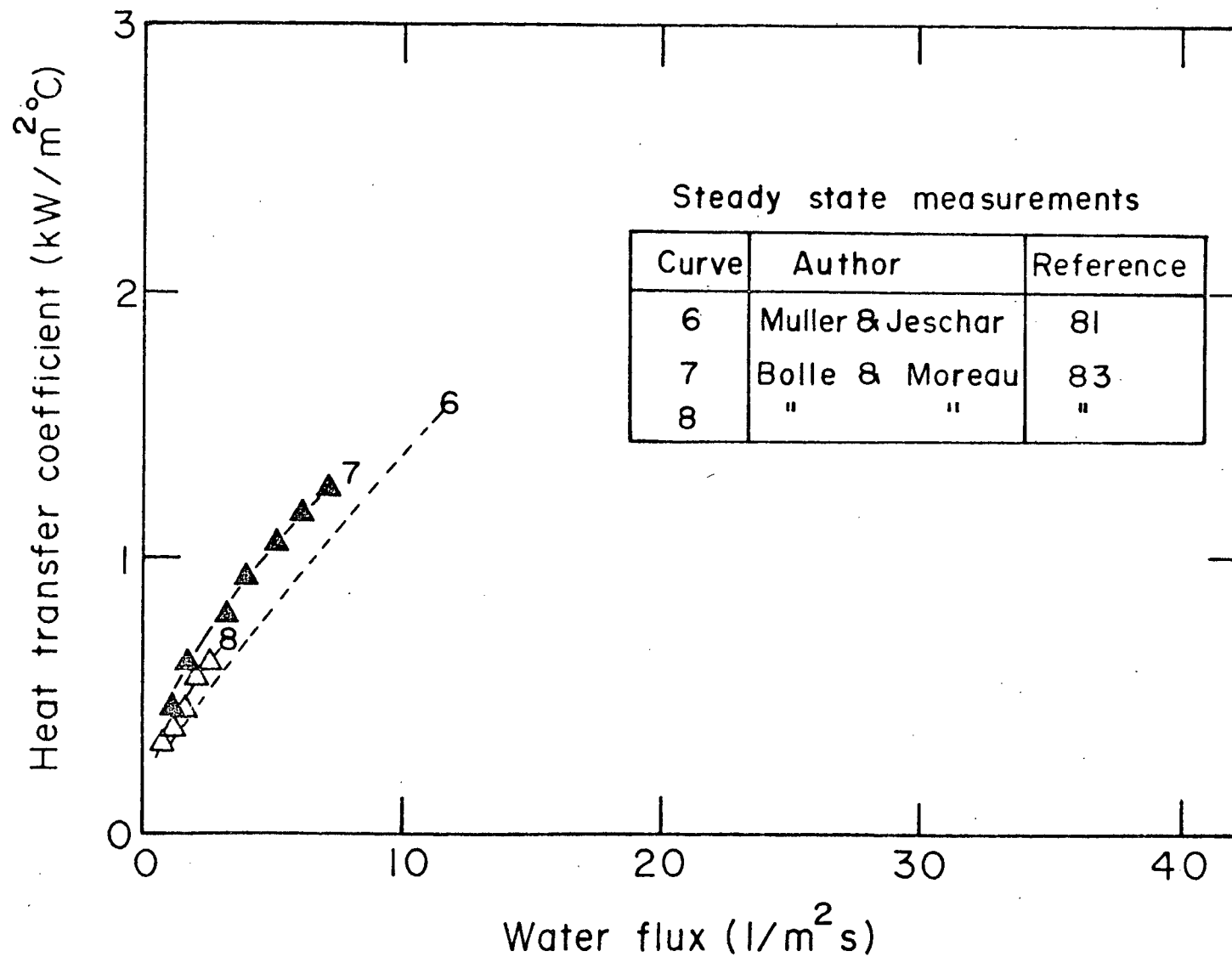


Figure 11b Variation of spray heat-transfer coefficient with water flux as reported in spray heat extraction studies -- Steady state measurements

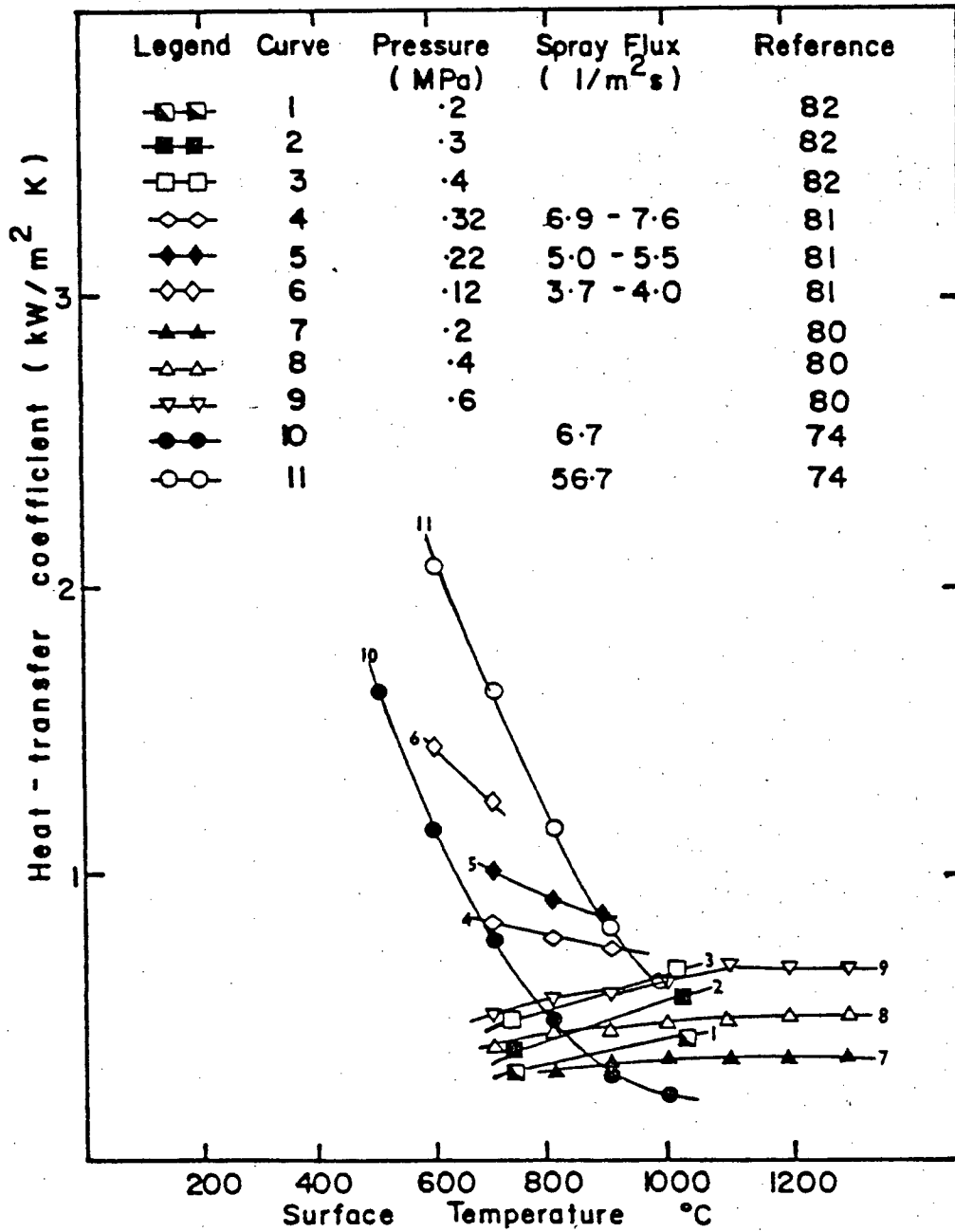


Figure 12 Variation of heat-transfer coefficients with surface temperature, from various studies on spray heat extraction.

which there is no reduction in the slope of the curve even at surface temperatures of 1000°C , the water flux is very high, with a value of $56.7 \text{ g/m}^2\text{s}$.

Spray heat-transfer coefficients were measured for full cone and flat jet spray nozzles by Nilles et al.¹⁴ and Etienne et al.⁷⁵ Sprays impinging vertically downward onto a polished face of a resistance heated, platinum rod of 1 cm diameter were used for the heat transfer measurements. They found that for sprays produced by full cone nozzles, there was no effect of surface temperature on the heat transfer coefficients, as long as the water fluxes at the surface were less than $5 \text{ g/m}^2\text{s}$. When higher water fluxes were used, surface temperature played a greater role in the variation of the heat-transfer coefficients: a decrease of the surface temperature from 900°C to 800°C caused an increase in the heat flux by 10 to 15%. Spray efficiency was found to decrease with increase in the water flux. The major parameter that was found to affect the heat-transfer coefficients, however, was found to be the water flux. No effect of the type of spray, or of the distance between the nozzle and the probe was found on the heat-transfer coefficient, so long as the water flux remained the same. A scatter in the results of 12% is reported for measurements at 900°C , and the scatter was observed to increase as the surface temperature decreased. At 700°C , the scatter in

the results was found to be 25%. The correlations obtained between heat fluxes and water fluxes for different temperatures are:

$$Q = -87.7 + 313.5 \dot{m}^{0.54} \quad (900^\circ \text{C}) \quad \dots 2.7$$

$$Q = -356.0 + 492.4 \dot{m}^{0.18} \quad (800^\circ \text{C}) \quad \dots 2.8$$

$$Q = -793.4 + 820.3 \dot{m}^{0.4} \quad (700^\circ \text{C}) \quad \dots 2.9$$

For sprays produced by flat jet nozzles, it was observed that the surface temperature had little effect on the heat flux when the water flux was less than $4 \text{ g/m}^2\text{s}$. On increasing the water flux beyond this limit, it was found that a lowering of the surface temperature again caused an increase in the heat flux - increasing it by 10 to 15% when the surface temperature was lowered from 900°C to 800°C . A law of the form

$$Q = \text{Constant } \dot{m}^n \quad \dots 2.10$$

was observed to correlate the heat fluxes to water fluxes at 900°C , with the exponent n decreasing from a value of 1 to 0.5 when the water flux increased from 2 to $20 \text{ g/m}^2\text{s}$. Decreasing the surface temperature was found to increase the scatter in the results obtained. For overlapping sprays from two flat jet nozzles, it is reported that a noticeable effect of the type of spray and of the distance between the spray and the cooled surface was observed. Heat flux

correlations observed from their experiments for flat jet sprays and a surface temperature of 900° C are:

$$Q = 182.4 + 77.2 \dot{m}^{0.93} \quad \text{nozzle-to-nozzle spacing 8 cm} \\ \text{probe to nozzle distance 11 cm} \quad \dots 2.11$$

$$Q = 80 + 218.8 \dot{m}^{0.81} \quad \text{nozzle-to-nozzle spacing 20 cm} \\ \text{probe to nozzle distance 35 cm} \quad \dots 2.12$$

Mizikar⁷⁶ employed a stainless steel plate, heated to about 1000° C and fixed vertically, in his laboratory experiments. He found that surface temperatures in excess of 600° C did not influence the heat-transfer coefficients. For a 1/4 GG10 Spraying Systems Co. nozzle, he obtained linear relationships between the heat-transfer coefficients and the water fluxes for two different water pressures. The relationships obtained were

$$h = 0.0776 \dot{m} + 0.22 \quad \text{for a pressure of 0.276 MPa} \quad \dots 2.13$$

$$h = 0.1 \dot{m} + 0.22 \quad \text{for a pressure of 0.620 MPa} \quad \dots 2.14$$

The constant of 0.22 represents the contribution due to radiation heat transfer. These relationships are shown graphically in Figure 11, Curves 3 and 4, respectively, after subtracting the radiation contribution. The angle of impingement of the drops did not affect the heat-transfer coefficients, but an increase in the droplet momentum caused

an increase in these coefficients.

Sasaki et al. and Sugitani^{77,78} used a novel approach in the determination of heat-transfer coefficients in spray cooling. A vertical stainless steel plate (Type 18-8) was heated to about 1200° C in a resistance furnace and was sprayed from both sides for short periods of time (0.3 to 1 sec) with full cone and flat jet nozzles. During the spray cooling interval, the surface temperature was monitored by optical pyrometers sighted on the surface. From the change in surface temperature with time, the heat-transfer coefficients were calculated. Water fluxes were varied from 2.67 to 41.8 $\text{g/m}^2\text{s}$ and spray pressures from 0.14 MPa to 0.35 MPa. The surface temperature of the plate was found to affect the heat-transfer coefficients, and a correlation of the form

$$h = 708 \dot{m}^{0.75} T_s^{-1.2} + 0.116 \quad \dots 2.15$$

was proposed for the range of surface temperatures between 700° and 1200° C. This equation, for a surface temperature of 1150° C, is shown in Figure 12, Curve 5. The effect of water temperature was not as great as that observed by Mitsutsuka, as can be observed from Figure 10, Curves 1 and 2.

Bamberger et al.⁷⁹ carried out unsteady-state heat-transfer studies to measure the heat-transfer coefficients for the spray cooling of non-ferrous materials (nickel, aluminium, and copper), with surface temperatures between 250 and 1000° C, and for water fluxes varying from 10 to 100 g/m²s. The measurements indicate a dependence of the heat-transfer coefficients on the thermophysical properties of the material. The most important parameter affecting the heat-transfer coefficients was found to be the spray water flux and the coefficients were also found to be a function of the surface temperature. The correlation obtained from the results of their work is

$$h = 0.1 \dot{m}^{0.55} (0.07 \sqrt{k_p C_p} (-0.0049 T_s + 28)) \dots 2.16 \\ + h_{\text{radiation}}$$

They have reported that they have obtained a large scatter in their results, especially when the surface temperatures were between 250 and 700° C.

2.3.2 Steady-State Methods

From the measured values of electrical energy required to maintain the temperature of the measuring section constant during spraying, Junk⁸⁰ evaluated the heat-transfer coefficients during spraying with oval nozzles. The

results of his experiments are shown in Figure 12, Curves 7, 8 and 9, for different spray pressures. Flattened pipes made of heat and scale resisting steels heated by electrical currents passing through them were used as the measuring section. The surface temperatures were calculated from a measured temperature within the pipe. Junk has proposed several functional relationships between the heat flux and certain parameters, e.g. the spray pressure, spray distance, the spray water flux, and the average impingement pressure. However, since the coefficients in the relationships are not given, the relative effects of these parameters cannot be evaluated.

From the results of their experiments using steel plates, Muller and Jeschar⁸¹ found that the heat-transfer coefficients are functions of both the water flux and the droplet velocity at the exit from the nozzle. The measurements, excluding the radiation component are described by the equation

$$h = 0.01 V + (0.107 + 6.8 \times 10^{-4} V) \dot{m} \quad \dots 2.17$$

The experimental results are shown in Figures 11 and 13. Fan jet nozzles, and full cone nozzles operated at pressures of up to 1 MPa were used to extract heat from vertical, resistance heated steel plates, with surface areas varying from 20 to 65 sq. cm. Water fluxes used in the experiments

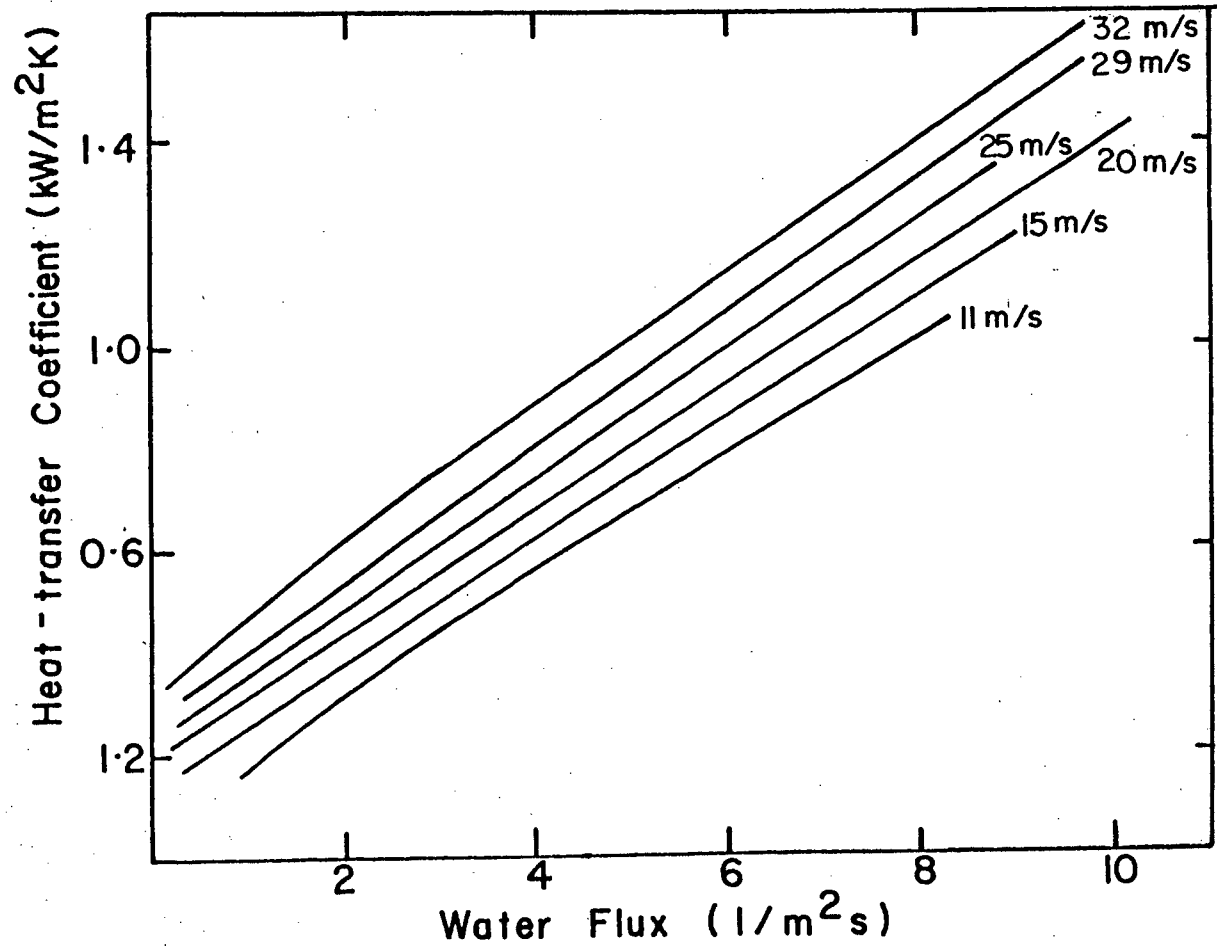


Figure 13 Variation of heat-transfer coefficients with water flux for different droplet velocities.⁸¹

varied from 3 to 9 $\text{kg/m}^2\text{s}$, with droplet velocities ranging between 10 and 35 m/s. Plate surface temperatures were varied between 700° and 1200° C. The errors in the heat-transfer coefficients are reported to be less than 15%. These coefficients were found to be insensitive to surface temperature in the range studied. The spray cooling efficiency was found to drop with an increase in the water flux.

Experiments by Bolle and Moreau⁸²⁻⁸⁴ were conducted with fan type sprays, similar to those used by Muller and Jeschar, spraying downwards onto a resistance heated, flat plate, containing imbedded thermocouples. Water pressures of 0.1 MPa to 0.5 MPa were used in their studies, and the water fluxes used ranged from 1 to 7 $\text{kg/m}^2\text{s}$. The heat fluxes obtained from this work were higher than those obtained by Muller and Jeschar in the surface temperature range studied (500° to 1000° C). In agreement with Muller and Jeschar, the spray heat extraction efficiency was found to drop as the water flux or spray pressure increased, and the heat-transfer coefficients increased with increasing water flux, as represented by the correlation

$$h = 0.423 (\dot{m})^{0.556} \pm 17\% \quad \dots 2.18$$

for surface temperatures between 600° and 900° C and water

fluxes between 1 and 7 $\text{L/m}^2\text{s}$. It was also found that cooling by spraying upwards from below the hot surface yielded heat-transfer coefficients that were about 15% lower than those obtained from the above correlation. The results from the two correlations are shown in Figure 11, Curves 7 and 8.

2.3.3 In-plant Measurements

Heat balances on an operating caster have been performed using either analytical methods⁸⁵⁻⁸⁷ or a numerical solution of the mathematical model of the process.^{14,88,89}

The measured surface temperatures at various positions in the caster were used as input in the calculations, which yield the average heat-transfer coefficients in different cooling zones.

Akimenko et al.⁸⁵⁻⁸⁷ determined that the heat-transfer coefficients increase as the water flux increases, until a water flux of 8.5 $\text{L/m}^2\text{s}$ was reached. Any further increase in the water flux did not affect the heat-transfer coefficients. A slight dependence of the heat-transfer coefficients on the water temperature has been reported, with the coefficients decreasing as the water temperature increases.

The results of the work of Alberny et al.^{88,89} are presented in Figure 11, Curves 9, 10 and 11. These were obtained for different spray configurations on a centrifugal continuous caster. The surface temperature for which these coefficients were obtained vary from 1050 to 1250° C. From this Figure, it is seen that there is a levelling off of the heat-transfer coefficient beyond a certain value of the water flux. It is interesting to note that the insensitivity of the heat-transfer coefficients to water flux beyond a limiting value has been observed only in the cases where these coefficients have been obtained from heat balances on operating casters.

2.4 Summary

From the preceding discussion of the various investigations of heat-transfer in water sprays, it can be seen that the main variables that have been studied are the following:

- i) Local water fluxes at the cooled surface
- ii) The surface temperature
- iii) Water pressures at the nozzle
- iv) Droplet size
- v) Droplet velocities in the spray
- vi) Water pressure at the spray nozzle
- vii) Temperature of the spray water

A wide range of results has been obtained, as reported in this chapter. In many cases, different investigations show conflicting results, and, in addition, in many cases, lack of data regarding the experimental conditions makes meaningful comparisons impossible. In general, however, some conclusions may be arrived at from the mass of data available regarding spray cooling.

- i) In strand casting, the temperature of the strand surface as it passes through the sprays is greater than 900°C and is higher than the "critical point" beyond which a phenomenon akin to film boiling takes place. A vapour cushion exists next to the strand surface, but the momentum of the water droplets in the spray allow them to penetrate this cushion increasing the heat flow from the surface. Nonwetting behaviour takes place on impact.
- ii) Increasing the droplet momentum in the spray, either by increasing the droplet size or the velocity, increases the heat-transfer coefficient.
- iii) At constant drop size and velocity, increasing the water flux to the surface increases the heat transfer coefficient.

- iv) Application of the results of single droplet experiments to gross sprays leads to incorrect heat transfer coefficient predictions, because of interactions in the sprays.
- v) The extent of the effect of the water temperature on the heat-transfer coefficients is unclear.
- vi) The efficiency of the spray is usually low, less than 10%, and this is decreased if the flow rate is increased.
- vii) Increasing the droplet velocity or the water flux shifts the "critical point" to higher temperatures.

A summary of the experimental methods and experimental conditions used, as well as the results of various investigations on spray heat transfer discussed in this chapter are presented in Table II.

TABLE IIa Summary of Studies on Heat Extraction in Sprays - Transient Measurements

Investigator & Reference No.	Nature of the Heated Surface	Direction of Spraying	Initial Temperature °C	Spray Nozzle Type	Spray Fluxes $\text{L/m}^2\text{s}$	Comments
Gaugler ⁵³	Horizontal upper face of chrome plated copper cylinder heated in a furnace. Surface area 1.2 sq. cm.	Downwards	400	Full cone 1/8 GG 1 1/8 GG 3001.4	.716 to 3.7	$\eta = 1.487 \times 10^{-3} (T_s - T_w) \dot{m}^{-0.66} \pm 10\%$ $h = 3.695 \dot{m}^{0.33} \pm 10\%$ Increasing droplet momentum increases h. Heat transfered to each drop decreases as \dot{m} increases.
Corman ⁶⁷	Same as Gaugler.	Downwards	900	Full cone 1/8 GSS	Up to 57	Increasing \dot{m} increases h and moves critical point to higher temperatures.
Auman et al. ⁶⁸	AISI 304 stainless steel, furnace heated. Area 300 sq cm.	Downwards	1100	Full cone and fan jet.	Up to 217	Increasing \dot{m} increases η and h.
Lambert and Economopoulos ⁶⁹	Cylindrical nickel probes. Area 3.1 sq cm.	Horizontal	800			Only spray pressure of 0.098 MPa reported. Results similar to that of Gaugler.
Hoogendoorn and den Hond ⁷⁰	Horizontal stainless steel plate (AISI 321), furnace heated. Area 269 sq cm.	Downwards	1000	Shick	0.6 to 25	Increasing \dot{m} and drop velocity increases critical temperature, to as much as 900°C scatter $\pm 20\%$. No difference in h when a vertical plate was used.
Mitsutsuka Shimada ^{71,72}	Horizontal low carbon steel plate, heated in a resistance furnace. Area 484 sq cm.	Upwards and downwards simultaneously.	930	Full cone	1 to 50	$h = A \dot{m}^n (1 - b T_w)$ $0.5 < n < 0.8$ $0.005 < b < .008$ for $\dot{m} = 10.3 \text{ L/m}^2\text{s}$. h decreases as T_w increases.
Sugitani et al. ⁷⁴	Vertical stainless steel plate heated in a resistance furnace. Surface area 500 sq cm.	Horizontal	1000 to 1200	Full cone and flat jet.	Up to 60	h is a strong function of T_s even above 700°C.
Nilles et al. ¹⁴ Etienne et al. ⁷⁵	Polished surface of a platinum rod, heated by a resistance wire wound around it. Surface area 0.79 sq. cm.	Downward	1050	Full cone and flat jet.	1.5 to 50	h is a function of T_s even above 700°C. h increases as T_s decreases. η decreases with increasing \dot{m} . Scatter increases as T_s decreases for full cone nozzles: $Q = -36.7 + 313.5 \dot{m}^{0.54} \text{ (900°C)}$ $Q = -356.0 + 492.4 \dot{m}^{0.18} \text{ (800°C)}$ $Q = -793.4 + 492.4 \dot{m}^{0.4} \text{ (700°C)}$
Mizikar ⁷⁶	Stainless steel plate (AISI 304) heated in a resistance furnace. Area 161 sq cm.	Horizontal	1000	Full cone 1/4 GG 10 1/4 GG 6.5 3/8 GG 15	0 to 20	h constant above T_s of 600°C. h increases as \dot{m} increases. Increasing spray pressure increases h for the same \dot{m} . $h = 0.0776 \dot{m} + 0.22$ at 0.276 MPa $h = 0.1 \dot{m} + 0.22$ at 0.620 MPa.
Sasaki et al. ⁷⁷ Sugitani ⁷⁸	18-8 stainless steel plate heated in a resistance furnace.	Horizontal sprayed on both sides	700 to 1200	Full cone and fan jet		h is a function of T_s . $h = 708 \dot{m}^{0.75} T_s^{-1.2} + 0.116$ for $700^\circ\text{C} < T_s < 1200^\circ\text{C}$
Bamberger et al. ⁷⁹	Nonferrous materials Ni, Al, Cu		Various, depending on material		10 to 100	$h = 0.1 \dot{m}^{0.55} (0.07 \text{ kPC}_p \exp(0.0049 T_s + 28)) + h_{\text{radiation}}$ Large scatter in results at lower surface temperatures.

Table IIb Summary of Studies on Heat Extraction in Sprays - Steady State Measurements

Investigator & Reference No.	Nature of the Heated Surface	Direction of Spraying	Initial Temperature °C	Spray Nozzle Type	Spray Fluxes \dot{m}/m^2s	Comments
Junk ⁸⁰	Resistance heated flattened steel pipes. Area 83 to 207 sq cm.	Horizontal		Oval		Correlations obtained between spray pressure, nozzle distance, \dot{m} values of the coefficients are not given.
Muller and Jeschar ⁸¹	Resistance heated steel plates. Area 20 to 65 sq cm.	Horizontal	700 to 1200	Full cone and fan jet.	0.3 to 9	Drop velocities 10 to 35 m/s. Scatter $\pm 15\%$. h is a function of droplet velocity. $h = 0.01v + (0.107 + 6.8 \times 10^{-4} v) \dot{m}$ h is independent of T_s η decreases as \dot{m} increases.
Bolle and Moreau ⁸²⁻⁸⁴	Resistance heated flat stainless steel plate (AISI 309) Area 128 sq cm.	Vertically downwards and upwards	500 to 1000	Fan type similar to Muller and Jeschar	1 to 7	Heat fluxes higher than those of Bolle and Moreau. η decreases as \dot{m} or spray pressure increases. When spraying vertically downwards. $h = 0.423 \dot{m}^{0.556} \pm 17\%$ Cooling by spraying vertically upwards decreased h by about 15% when compared with spraying vertically downwards.

Table 11c Summary of Studies on Heat Extraction in Sprays - In-plant Measurements

Investigator & Reference No.	Nature of the Heated Surface	Direction of Spraying	Initial Temperature °C	Spray Nozzle Type	Spray Fluxes $\text{kg/m}^2\text{s}$	Comments
Nozaki ³⁵						Measurements on slab casters. Altered form of Mitsutsuka's equation: $h = 1.57 \dot{m}^{0.55} (1 - 0.0075 T_w)/\alpha$ $d = 4$ (Nozaki)
Akimenko et al. ⁸⁵⁻⁸⁷					Up to 15	h increases with increasing \dot{m} , but remains constant if $\dot{m} > 8.5$ h decreases as T_w increases
Alberny et al. ^{88,89}					Up to 56	Measurements on centrifugal caster. h increases with increasing \dot{m} to a certain value of \dot{m} and then stays constant beyond this value.

Chapter 3

EXPERIMENTAL

3.1 Introduction

The measurements carried out in this investigation fall into two categories:

- i) Measurements of local water fluxes within the sprays
- ii) Measurements of heat-transfer coefficients.

i) For the measurements of local water fluxes, several industrial spray nozzles were used, and these were supplied with water at constant pressure (within a range from 70 kPa to 700 kPa). Local water fluxes were measured in various positions within the sprays at different distances (10 to 25 cm) from the spray nozzle, for the different spray pressures used. It was found that some water flowed downward through the spray cone adjacent to the vertical plate on which the spray impinged. This amount of water was also measured.

ii) Heat-transfer measurements were carried out for the conditions corresponding to those for which the water fluxes were measured. In the heat-transfer measurements, a

stainless steel "heat-transfer probe", with thermocouples embedded in it, was first heated to temperatures in the order of 1150° C. This was then sprayed with water, and the temperature-time transients during the cooling were recorded on an oscillographic recorder. Analysis of these transients then yielded the required heat-transfer coefficients, and their variation with the surface temperature of the heat-transfer probe.

3.2 Spray Nozzles

The following commercial spray nozzles, provided by Spraying Systems Co. (Mississauga, Ontario) were used in this investigation.

1/8 GG 5

1/8 GG 6 SQ

1/4 GG 6.5

1/4 GG 10

1/4 GG 10 SQ

1/4 GG 12 SQ

1/4 HH 14.5 SQ

3/8 HH 18 SQ

1/4 U 8020

3/8 U 5060

The first number in the designation represents the pipe

TABLE III Capacities and Spray Angles for the Nozzles Investigated in this work.⁹⁰

Nozzle Number 1	Pressure psi	Capacity litres/sec								Spray Angle(degrees)		
	MPa	5	10	20	30	40	60	80	100	7	20	80
		0.03	0.07	0.14	0.21	0.28	0.41	0.55	0.69	0.05	0.14	0.55
1/8 GG 5		0.023	0.032	0.045	0.053	0.061	0.077	0.084	0.097	52	65	69
1/8 GG 6 SQ		0.028	0.039	0.054	0.065	0.071	0.090	0.103	0.116	60	66	60
1/4 GG 6.5		0.030	0.042	0.057	0.071	0.084	0.097	0.110	0.123	45	50	46
1/4 GG 10		0.047	0.065	0.090	0.110	0.122	0.155	0.174	0.194	58	67	61
1/4 GG 10 SQ		0.047	0.065	0.090	0.110	0.122	0.149	0.168	0.187	62	67	61
1/4 GG 12 SQ		0.056	0.077	0.110	0.129	0.149	0.181	0.207	0.226	70	75	68
1/4 GG 14 W		0.046	0.090	0.123	0.149	0.168	0.200	0.226		114	120	103
1/4 HH 14.5 SQ		0.071	0.094	0.129	0.155	0.181	0.213	0.245	0.271	78	82	85
1/4 U 8020		0.046	0.065	0.090	0.110	0.129	0.161	0.181	0.207		74	83
3/8 U 5060		0.136	0.194	0.271	0.387	0.471	0.549	0.614	0.865		43	53

thread size of the nozzles. The second number is a measure of the nozzle capacity (flow rate through the nozzle). The letters GG and HH indicate nozzles producing full cone sprays. The nozzle numbers containing U indicate that these nozzles produce vee-jet sprays. The capacities and spray angles of the different nozzles are presented in Table III.⁹⁰

Full cone nozzles, as the name indicates, provide sprays which are conical in shape. Vee-jet nozzles produce a flat, wide spray, and in the cases of the nozzles used, the width of the sprays was between 2.5 to 5 cm.

3.3 Water Supply System

A stable source of pressurized water at the pressures and flow rates needed for the study was required. The range of pressures required was between 69.5 to 695 kPa (10 to 100 psi), to be constant within 3.5 kPa (0.5 psi).

Figure 14 shows a schematic diagram of the equipment constructed to meet this requirement. A 150 litre (33 gallon) domestic hot water tank rated for a pressure of 1048 kPa (150 psi) was used to provide the pressurized reservoir supply. The tank was filled with water from the mains supply, and was then pressurized with compressed

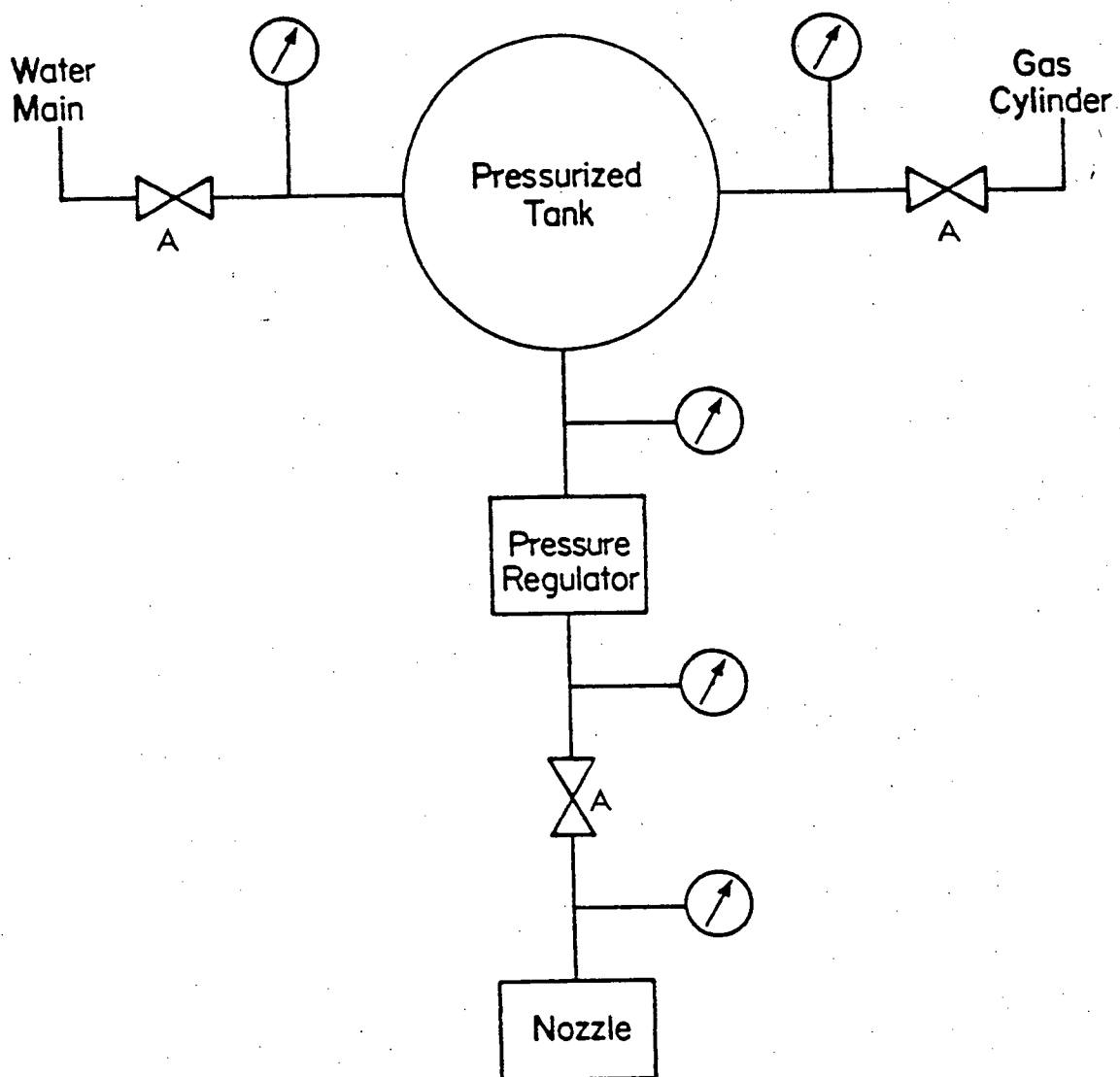


Figure 14 Schematic diagram of the water supply system.

nitrogen from a gas cylinder to a pressure of 820 kPa (125 psi). The pressurized water from the tank was passed through either of two water pressure regulators (CASHCO Type D 1/2) with 103 to 276 kPa (15 to 40 psi) or 276 kPa - 522 kPa (40 to 80 psi) ranges depending on the pressure required at the spray nozzle.

The water pressure immediately behind the spray nozzle was monitored by both a Marsh 15 cm (6 in) dia. Bourdon type pressure guage with a range of 0 to 1100 kPa (0 - 160 psi), and a CEC pressure transducer. The output from the transducer went to a Wheatstone Bridge circuit, and recorded on a Honeywell Elektronik 194 chart recorder. By monitoring the pressure trace on the recorder, it was established that the water pressure at the nozzle could be kept constant within the required range for a period of nearly 10 minutes, which was much longer than that used either for the water flux or heat-transfer measurements.

Referring to Figure 14, electrically switched solenoid valves (marked A) were installed in the flow system to turn the water or gas supplies on or off, and to initiate or stop the spray. In this way, a quick response of the spray system was ensured. Typically, the spray stabilized within 0.2 seconds of the start of spraying. This was

determined by monitoring the output of the CEC pressure transducer on a cathode ray oscilloscope.

3.4 Spray Nozzle Mounting

Each nozzle was mounted on a frame, such that the nozzle axis was horizontal. A schematic of the mounting set-up is shown in Figure 15. The mount had the capability of allowing the nozzle to be moved over a range of 15.24 cm (6 in) in the vertical direction and an equivalent amount in the horizontal direction. Larger movements in the horizontal direction were possible by unclamping and moving the mounting itself.

3.5 Measurement of Spray Water Fluxes

Data reported by Mizikar⁷⁶ for the 1/4 GG 10 full cone nozzle indicated that the spray water flux within the sprayed cone was nonuniform. This nonuniformity in the distribution of water fluxes in the spray led to the necessity of determining the local water fluxes in different positions within the spray. Only in this way could water fluxes be related to the heat-transfer coefficients at corresponding positions in the spray. Measurements were made by inserting collector tubes into the spray at fixed points and determining the amount of water arriving at the collectors in a fixed time.

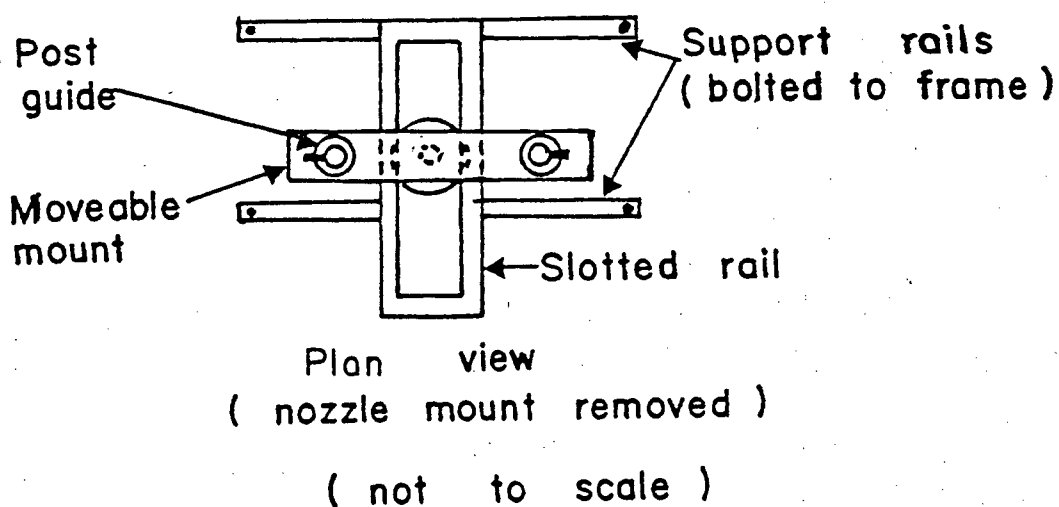
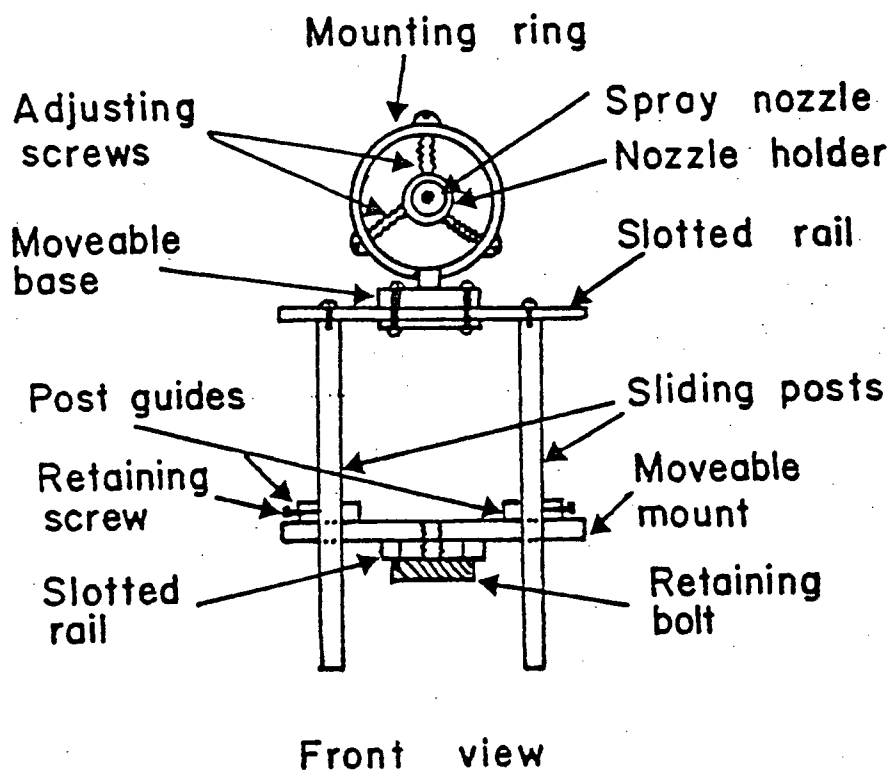


Figure 15 Schematic diagram of the mount for the spray nozzle.

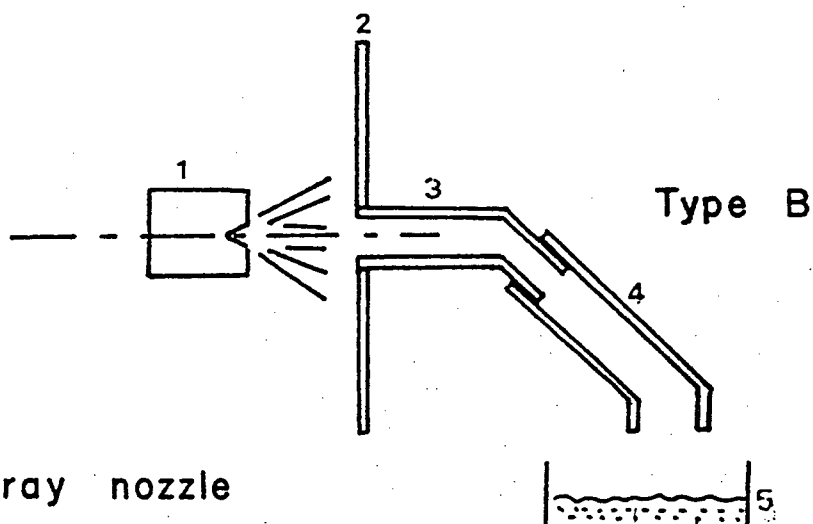
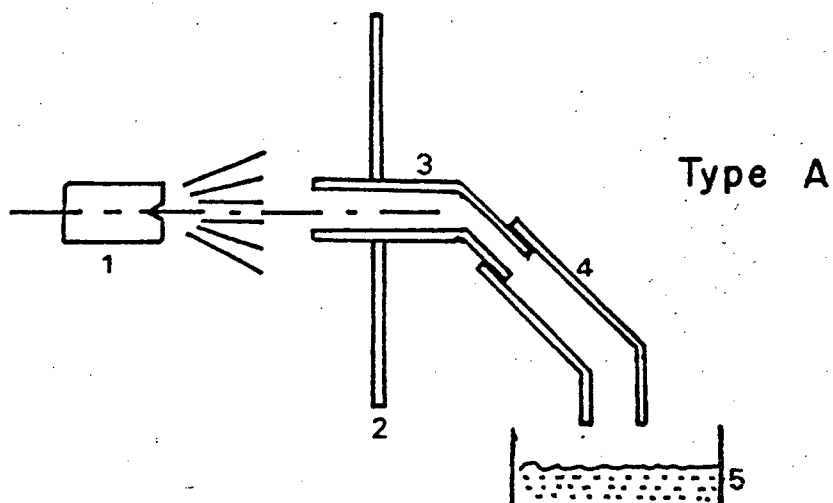
3.5.1 Factors Affecting Spray Flux Measurements

The following factors were considered to be important in the choice of the experimental method used for the measurements:

- i) Collection time: Short collection times could give rise to misleading values of fluxes due to the non-stabilized nature of the spray immediately after initiation or termination of spraying.
- ii) Collector tube size: Use of very small collector tubes, could cause the larger droplets in the spray to rebound from these tubes, and lead to the measurement of lower spray fluxes than would actually be present.
- iii) Spray axis alignment: Alignment of the spray axis in a vertical position such that the spray faced downward, might not indicate the distribution spray fluxes actually present during operation of the sprays in the casting process where the spray axis is normally horizontal.

3.5.2 Apparatus

The apparatus used to measure the spray water flux distribution is shown in Figure 16. It consisted of a



- 1 Spray nozzle
 - 2 Aluminum sheet
 - 3 Copper collector tube
 - 4 Plastic tube
 - 5 Water receptacle
- (not to scale)

Figure 16 Schematic diagram of the apparatus used for the measurement of spray water fluxes.

1.6 mm (1/16") thick aluminium sheet held in a vertical plane, in which 13 holes in a horizontal line were drilled on 25.4 mm (1 in) centres. Copper tubes with an O.D. of 12.8 mm (0.5 in) and I.D. of 10.6 mm (0.415 in) were inserted through the holes and anchored so that their axes were horizontal. Behind the sheet, the tubes were angled downward at about 45° to the horizontal. Plastic hoses connected to these tubes carried the water collected to a set of preweighed glass beakers with a capacity of 250 ml.

3.5.3 Experimental Procedure

The spray nozzle axis was aligned parallel to the axis of the collector tubes, and the nozzle was fixed at a known distance from the front of the tubes. Normally, the tubes were anchored so that they projected a distance of 6 mm (1/4 in) from the front of the aluminium sheet (Type A experiment, Figure 16a).

The spray was then turned on and the water intercepted by individual collector tubes flowed into the glass beakers. Depending on the spray pressure and the distance of the nozzle tip from the plate surface, the spray time was chosen such that at least 200 g. of water was collected in the beaker corresponding to the central collector tube. This experiment was repeated, starting with empty beakers, so that the cumulative spraying time for any set of spray conditions was

about 10 minutes. This procedure was followed to reduce the effect of random errors in the measurements.

While spraying on the plate surface, it was observed that a large quantity of water flowed downward along the surface of the vertical plate. This will be referred to as the "water curtain". For the evaluation of the effect of the "water curtain", the collector tubes were placed flush with the plate surface (Type B experiment, Figure 16b). Thus, when the measurements were performed, the measured water fluxes were the sum of the water arriving at the collector tips directly from the spray, and also the water arriving at the collectors as a consequence of the presence of the water curtain.

For most of the nozzles investigated, water fluxes were obtained only in a horizontal line perpendicular to and coinciding with the spray axis; however, in the case of the 1/4 GG 10 nozzle, more extensive measurements were performed. By moving the spray nozzle axis in 25.4 mm (1 in) increments in the vertical direction, with respect to the collector tubes, a "map" of the spray fluxes throughout the spray cone was obtained, with and without the water curtain i.e., both with collectors flush with the plate surface, and collectors protruding from the surface.

The water fluxes in specific portions of the spray were calculated from the weight of water collected at that position in the spray during the spraying period.

3.6 Spray Heat-Transfer Measurements

The estimation of the heat-transfer coefficients for different spraying conditions requires a knowledge of the surface temperature of the solid being sprayed and the temperature gradient at the surface. Since the direct measurement of surface temperatures poses many problems, subsurface temperature measurements were made during the spraying interval and used in the calculation of the heat-transfer coefficients.

This section deals with the requirements of the temperature measurement system, criteria for the selection of the technique used, and the experimental method employed.

3.6.1 Requirements for the Measurement of Temperature Transients

The measurement system should indicate faithfully and accurately, the change in the temperature with time as the point of measurement. The introduction of a temperature sensor, in this case, thermocouples, into the

solid, can affect the thermal field and the flow of heat that would be present in the absence of the sensor. Proper precautions are thus necessary to ensure that this disruption is as small as possible, and a compromise reached between the desired accuracy of measurement and the interaction of the measuring sensor with the heat flow.

The methods of minimizing the errors in measurements of the type under discussion include the following:

- i) Using small installation sizes - i.e. small diameter thermocouple wire, with associated small sizes of insulating tubes, and correspondingly small holes drilled for the insertion of the thermocouples.
- ii) Location of the sensor (thermocouple) as close as possible to the surface losing heat.
- iii) Reduction of the thermal resistance between the sensor and the point of temperature measurement to a minimum.
- iv) Locating the sensor wires in an isothermal region for at least 20 wire diameters.^{91,92}
- v) Using thermocouples with a fast response to changing temperatures.

These factors are dealt with in detail below.

As mentioned earlier, the interaction of the sensors with the heat flow must be minimized, and as such, the use of small diameter thermocouples, insulating tubes, and small holes becomes mandatory in measurements of the type under discussion. This however is offset by considerations of the ease of placement and the reduction of thermocouple life at high temperatures as the wire size is reduced.

Evaluation of the measurement errors resulting from the interaction of the thermocouples with the heat flow has been attempted, using both numerical and analytical techniques.⁹³⁻⁹⁶ These methods involve the solution of the conduction equation in the solid around an "idealized" thermocouple embedded in it, using appropriate boundary conditions. Since these boundary conditions can be defined only for certain idealized conditions not met with in practice, an uncertainty is introduced regarding the effective use of the solutions obtained by the schemes proposed for the estimation of the errors.

All the solutions proposed assume temperature independent thermophysical properties, both of the thermocouple, and of the material in which the temperature is measured. The thermocouple is considered to be a homogeneous cylindrical material, embedded in a semi-infinite

body with perfect thermal contact, and placed normal to a semi-infinite surface through which a time variable heat flux passes. The conditions investigated include both the cases where the thermocouple material either has a higher or lower thermal conductivity than the surrounding material. As pointed out by Sparrow,⁹³ the calculations of errors in the measurements of temperature transients is a formidable problem, even for relatively simple physical situations, because the mathematical formulation requires the solution of coupled partial differential equations. The methods recommended to reduce the errors introduced are to use small diameter thermocouple wire, and to use thermocouple materials whose thermophysical properties approximate closely those of the material in which the temperatures are to be measured.

When the surface temperature at the surface of a solid body is subjected to changes or perturbations, these changes are propagated into the solid, but are progressively damped as the distance from the surface increases. The problem becomes more acute as the thermal conductivity of the solid decreases. The effect of the point of measurement below the surface on the error in the calculated heat-transfer coefficients have been computed by Economopoulos⁹⁷ and presented in Figure 17. Examination of the Figure reveals that the error decreases as the thermocouple is placed closer to the surface whose temperature is changing.

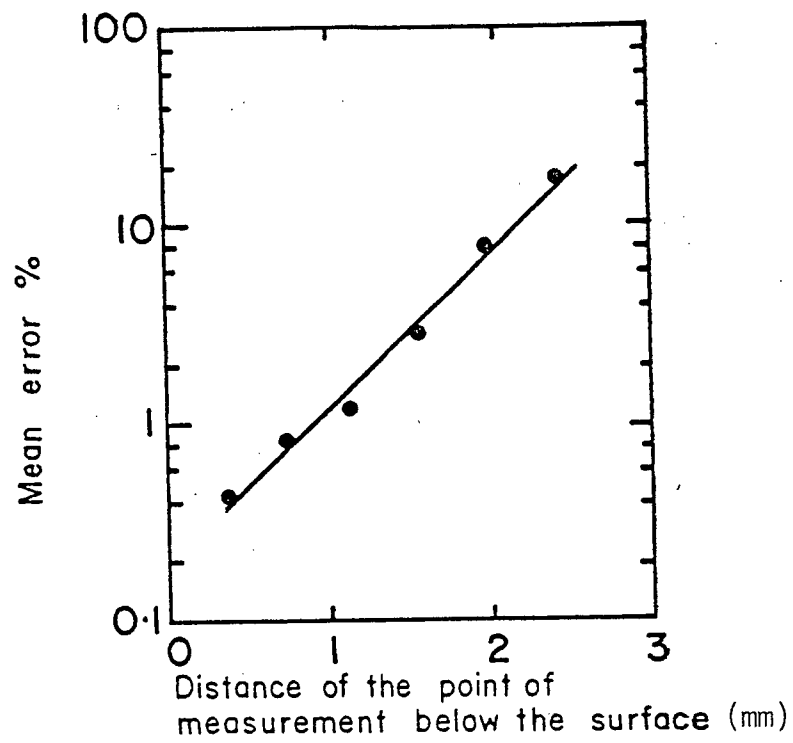


Figure 17 Dependence of the mean error in calculated heat-transfer coefficients on the distance of the point of measurement below the cooled surface.⁹⁷

Measured temperatures could be in error when there is a thermal resistance between the measuring junction and the point at which these measurements are made. This is illustrated in the case of spring loaded thermocouples by Otter,⁹¹ who shows that as the spring pressure on the thermocouple assembly is increased, bringing the thermocouple in more intimate contact with the point of measurement, the measurement error decreases. Elimination or reduction of this contact resistance can be effected by proper welding of the thermocouple junction to the material in which measurements are made.

An isothermal region in the thermocouple wire close to the measuring junction prevents the generation of any e.m.f. caused due to temperature gradients in the wire.

Thermocouple response time becomes a very important factor when fast temperature transients are being measured. As the mass of the thermocouple measuring junction increases, the thermal inertia of the thermocouple increases, resulting in an increase in the response time of the thermocouple to a changing temperature in its environment. Reduction of this response time can be effected either by reducing the thermal mass of the measuring junction (by using fine thermocouple wires with small welded junctions),

or by the use of "intrinsic" type thermocouples.^{98,99}

This is because the latter type of thermocouple has an instantaneous step output for a step input. In spite of the lowering of the response time, the use of small welded bead junctions is disadvantageous in that an uncertainty arises as to the exact point contributing to the production of the thermoelectric e.m.f.

Holes drilled for the insertion of the thermocouples could be placed in the cylindrical measuring probe in the three alternative configurations illustrated in Figure 18. In the experiments performed in this study, separate wires welded to the steel heat-transfer probe were used to obtain the temperature transients within the probe. When the thermocouple holes are placed parallel to the probe axis, the exact point where the thermocouples contact the steel probe can be determined. On the other hand, it has been reported⁹⁵ that this geometry is likely to cause the largest measurement error. Placing the thermocouples perpendicular to the probe axis, however, aids in obtaining an isothermal region in the thermocouple wire adjacent to the junction. Unfortunately, when this method is employed, the point at which the measured thermoelectric e.m.f. is being generated is uncertain. Referring to Figure 18, this point could be anywhere between x and $x + 2r$, where r is the radius of

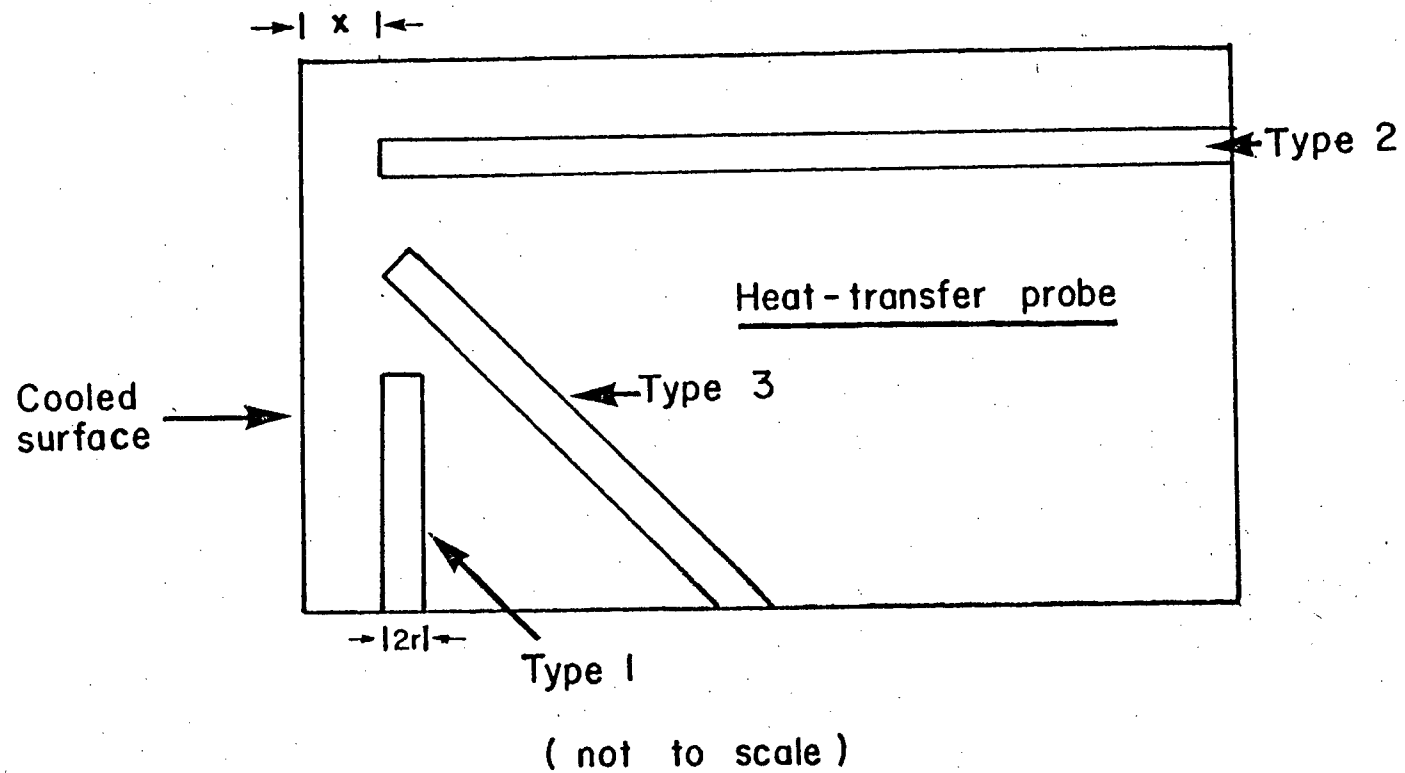


Figure 18 Three alternative configurations for thermocouple placement in the heat transfer probe.

the thermocouple wire. Angling the hole to the probe axis also has this disadvantage.

Since the exact location of the point of measurement is an input for the method used for the data analysis, this was the overriding criterion in the choice of locating the thermocouple holes parallel to the cylinder axis. In addition, the installation of the thermocouple wires and insulation, and subsequent welding of the thermocouple wire to the bottom of the blind hole was facilitated in this case. Experiments performed using this method for different heat-transfer conditions established the validity of the use of this technique for the range of heat-transfer coefficients obtained in this work. This will be discussed in a later section.

3.6.2 Selection of the Steel for the Probe Material

In selecting the most suitable steel for the probe, the following factors were considered:

- i) No solid-state transformations should occur in the steel between room temperature and 1100° C.
- ii) There should be minimal scaling during heating and spray cooling.

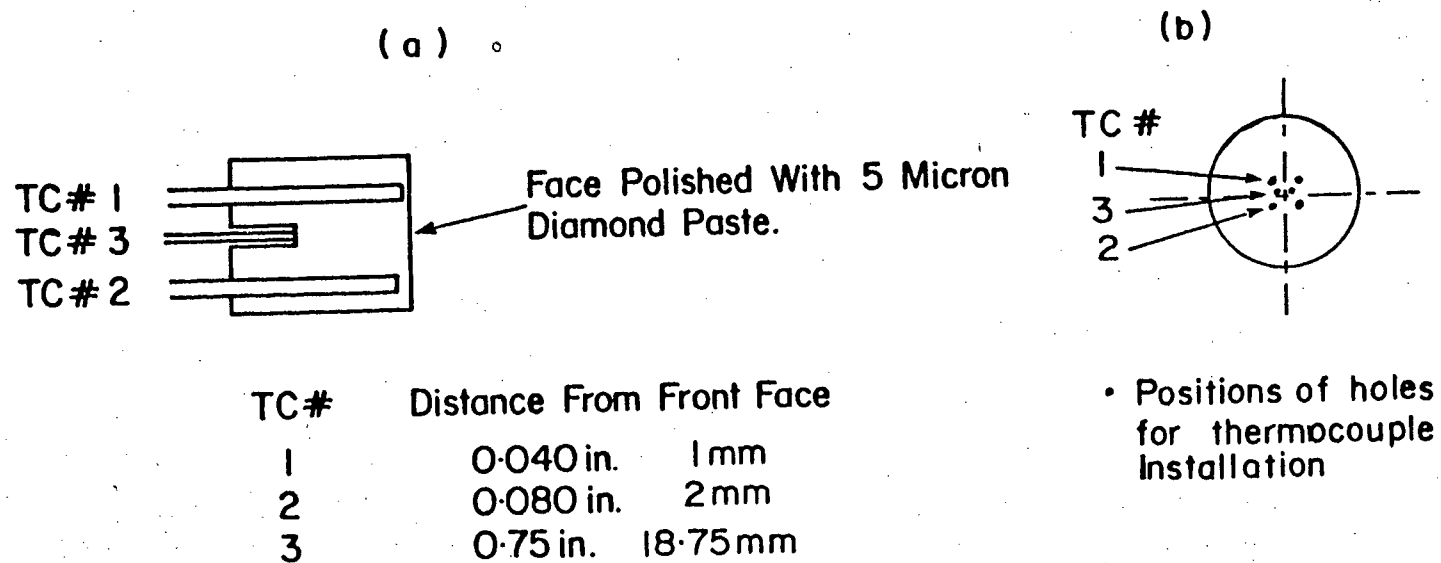
- iii) The steel should be similar to steels used in continuous casting.
- iv) The thermophysical property data for the steel should be available in the temperature region up to around 1100° C for the heat-transfer calculations.

On the basis of the factors listed above, AISI 304 stainless steel appeared to be most suitable. It is an austenitic stainless steel at all temperatures, shows an acceptable scaling resistance, has well documented thermophysical characteristics, and is cast continuously in billet and slab form.

3.6.3 Probe Fabrication

A 25.4 mm (1 in) diameter rod of the stainless steel material was used to make the probes, which were either 25.4 mm or 31 mm (1.25 in) in length. This length was cut from bar stock and the sectioned face to be sprayed was then polished to 4/0 emery grit. Fine polishing was subsequently performed with 5 micron diamond paste to give the sample a smooth, reproducible starting surface.

A schematic representation of the sample is shown in Figure 19. Three sets of two holes each were drilled from



m/1 304 Stainless Steel

Figure 19 Schematic diagram of the heat-transfer probe with installed thermocouples.

the rear of the probe (the face away from the sprayed face) so that the ends of each set of holes terminated at 1 mm, 2 mm, and 19 mm (0.040, 0.080 and 0.75 in) from the sprayed face. The diameter of the holes was 1.8 mm, and the bottom of the holes were made flat with a flat tipped drill of the same diameter. As shown in Figure 19b, the holes were placed within a radius of 4 mm of the axis of the cylinder.

The holes were then cleaned of cutting swarf and cutting fluid by injecting denatured alcohol with a hypodermic syringe. After etching the inside of the holes with a solution of Marble's etch (10 g. CuSO_4 , 50 ml. HCl , 50 ml. water), the holes were then cleaned again with alcohol. The probe, after being dried, was then ready for the insertion and welding of the thermocouple leads for the temperature measurements.

The careful cleaning described above was found to be absolutely necessary, as the presence of dirt or moisture inside the holes either prevented the thermocouple wire from fusing with the steel during welding, or produced welds that failed prematurely in service.

3.6.4 Selection of the Thermocouple Material

The following criteria were used in the selection of the thermocouple material:

- i) The upper operating range of the thermocouple required is to be greater than 1150°C .
- ii) The thermoelectric output of the thermocouple should be large to obtain maximum sensitivity in the temperature measurement.
- iii) The thermocouple material should have thermo-physical properties similar to those of the probe material.
- iv) The welding of the thermocouple wires to the steel probe should be effected easily.

Of the materials readily available and often used, Chromel - Alumel thermocouples satisfy the above criteria, and these were adopted in the present work. The upper operating temperature limit of this type of thermocouple is around 1250°C , and therefore care was taken not to exceed a temperature of 1175°C during the heating cycle of the probe. The thermocouple wire used had a nominal diameter of 0.6 mm (0.025 in).

3.6.5 Thermocouple installation

Single bore mullite tubes with an O.D. of 1.6 mm (1/16 in) and an I.D. of 0.76 mm (0.030 in) were cut to the required lengths, such that their edges were reasonably flat. These were then inserted into the drilled

holes; the thermocouple wires were inserted into these tubes and spark welded into place, using the capacitor discharge apparatus shown schematically in Figure 20.

Experiments were first carried out to establish the welding conditions and procedure which would yield satisfactory welds at the bottom of a hole. These tests consisted of spark welding 0.6 mm thermocouple wires of chromel and alumel onto cleaned and polished 304 stainless steel plates, such that the wire axis was perpendicular to the plate. The wire was then pulled along its axis, and then bent at an angle to the axis to see whether failure occurred at the weld. Though the welds withstood the tensile forces along the axis of the wire very well, any twisting or bending of the wire about its axis resulted in a greater susceptibility of the weld to fail. The procedure was repeated at different values of capacities and voltage, to establish optimum values. Optimum conditions were obtained with a total capacity of 6950 MFD in the capacitor bank, and voltages of 40 volts and 50 volts for alumel and chromel respectively.

The decay of voltage across the capacitor bank during the welding was found to be different for welds that failed easily and those that did not. This decay was therefore monitored with a Tektronix storage oscilloscope during welding. If the trace indicated that a poor weld had been

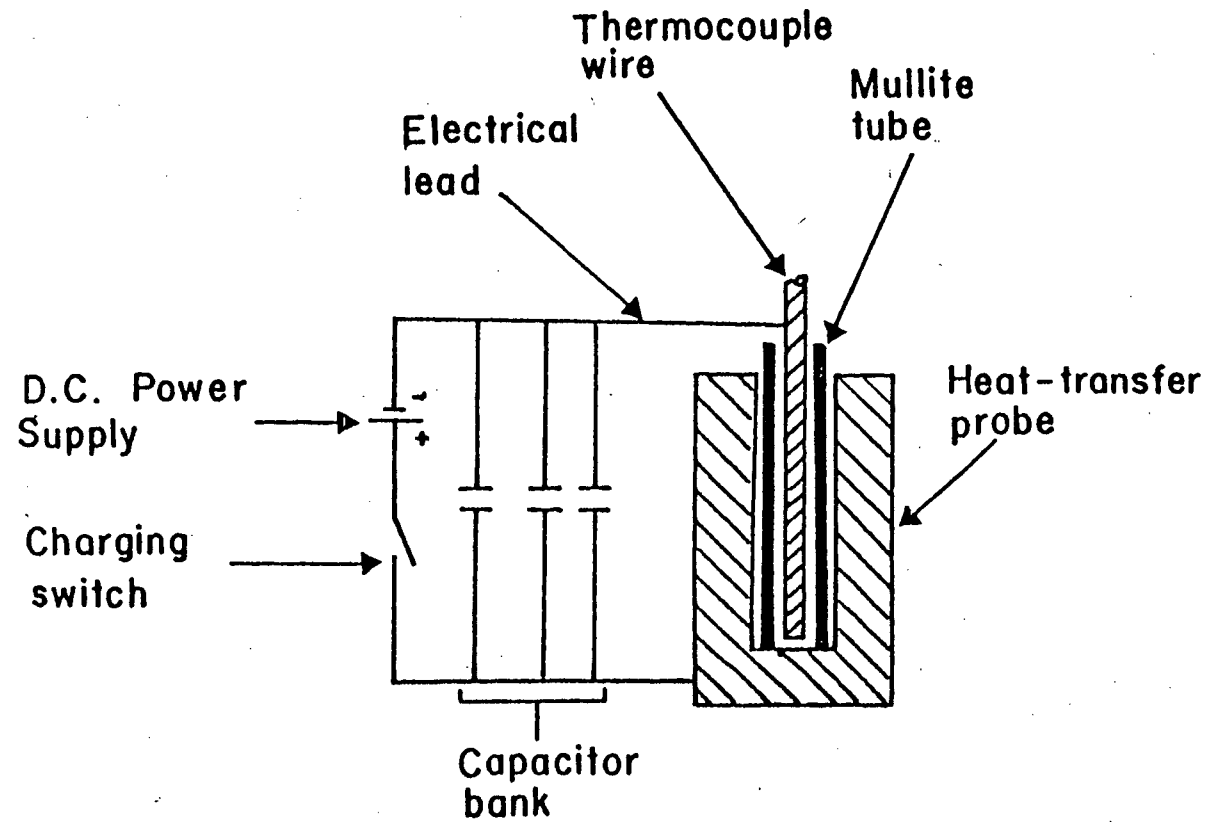


Figure 20 Schematic diagram of the capacitor discharge welding apparatus.

formed, then the sample was normally discarded, since rewelding was usually found to give inferior welds that failed quickly under service conditions.

In addition to setting up the voltages and capacitances in the welding circuit, care had to be taken that the ends of the thermocouple wires perpendicular to the wire axis were flat - this was done by filing off the end with a jewellers file. The thermocouple wires also had to be pushed into the holes in a reproducible manner. Welds of good quality were obtained when the negative terminal from the capacitor bank was connected to the thermocouple wire, with the positive lead attached to the stainless steel.

Since nondestructive post-weld examination was impossible, great care had to be exercised during the welding of the thermocouple wires to the bottom of the blind holes. During handling of the probes after the thermocouple wires had been welded in place, any twisting of the wire was avoided to reduce the chance of weld failure.

The thermocouple wires outside the probe were electrically insulated with 3 mm (1/8 in) mullite double bore tubing for a distance of 1.25 metres (about 3.75 ft).

The ends of the thermocouple wires were connected to a terminal block.

3.6.6 Lead Wires and Connections

The electrical connections made from the thermocouples are shown in Figure 21. From the end of the terminal block, which was assumed to be isothermal, 0.6 mm diameter fibreglass sheathed chromel - alumel thermocouple wires were used to make connections to the cold junction. This was an ice-water mixture maintained at 0° C in a Dewar flask. The cold junctions were made by welding copper wires to the ends of the thermocouple leads.

From the cold junction, all lead wires were made of copper, and three sets of connections were then made - to a multipoint switch, a digital voltmeter and a high speed recorder. Connections to the multipoint switch allowed the output from any thermocouple to be monitored continuously during the heating cycle on a Honeywell Elektronik 194 chart recorder. A special filter was used in these recorders when induction heating was employed, to filter out any e.m.f. picked up by the thermocouple due to induction from the coil. A multichannel digital voltmeter (HP 2070A Datalogger) with a visual digital display measured the millivolt output from the thermocouples.

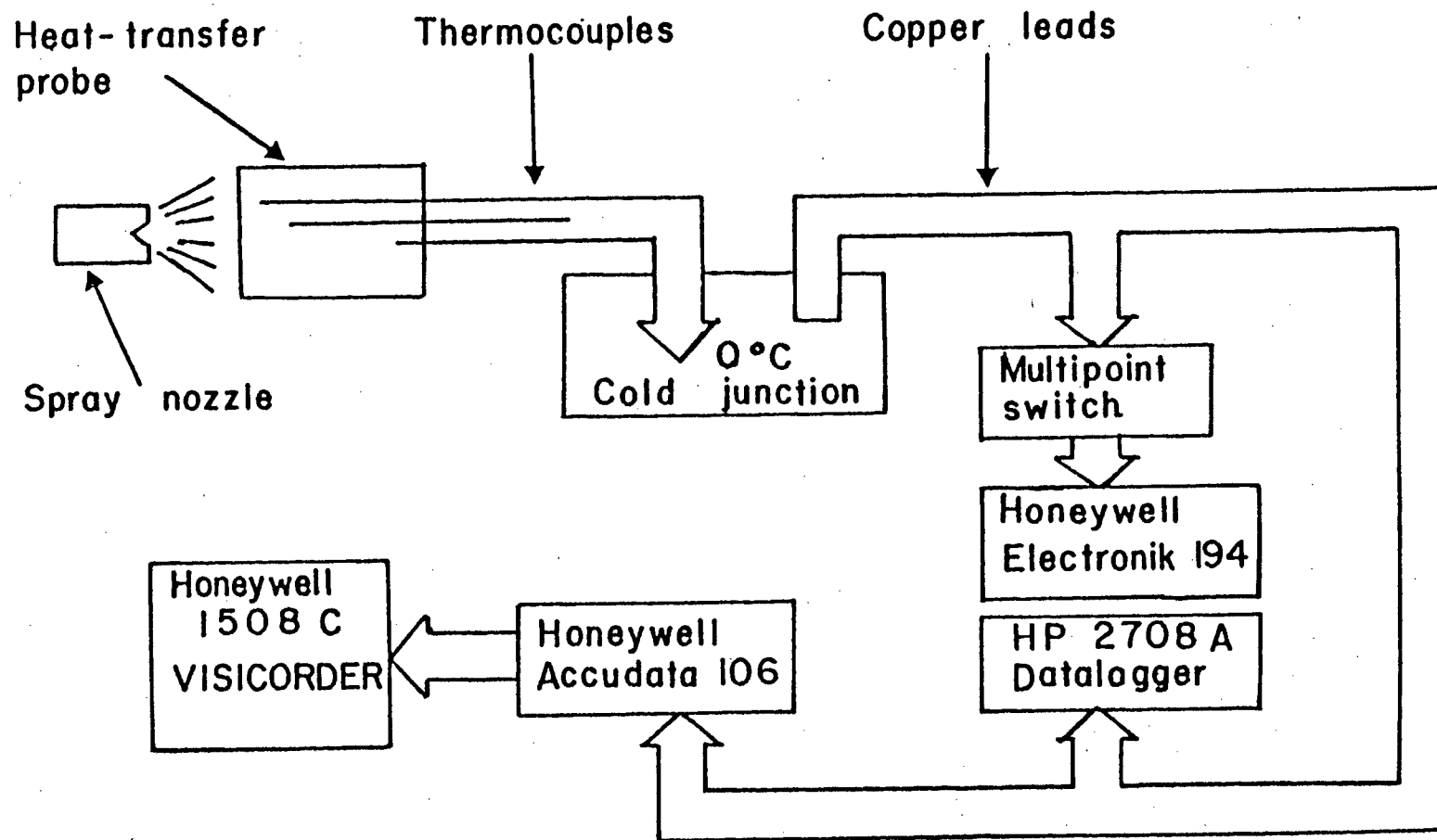


Figure 21 Electrical connections to the recording equipment.

Temperature transients during the cooling of the probe face by the spray were monitored on a high speed recorder to be described below.

3.6.7 The High Speed Recorder

A high speed recorder with a low inertia in the recording system was necessary in the experiments, because the thermocouple outputs could vary by as much as 10 mV/second. The equipment used was a five channel Honeywell 1508C "VISICORDER", which was an ultraviolet recorder.

The thermocouple outputs were fed into Honeywell "ACCUDATA 106" signal conditioners which then produced deflection signals to the galvanometers in the Visicorder.

It was necessary to calibrate the signal conditioners so that a change of 1 mV in the input corresponded to a 1 cm deflection on the chart. The output from the signal conditioners was dependent not only on the millivolt input, but also on the external resistance of the circuit. Therefore, the resistance of the thermocouples and lead wires (typically 25 ohms) were measured, using a Keithley Ohmmeter, accurate to 0.5 ohm. A precision resistance box, with corresponding resistances set on it was then connected

to the signal conditioners, and using an internally generated e.m.f. of 1 to 10 millivolts, the deflections of the galvanometers were adjusted to the required values with the help of a calibration potentiometer built into the signal conditioners.




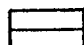


Since full scale deflection on the chart corresponded only to 16 millivolts, and the thermocouples produced outputs of about 45 millivolts at 1100° C, internally generated signals of 30 millivolts from the signal conditioners were used to offset the scale.

3.6.8 Mounting of the Heat-Transfer Probes for Heating

Either of two methods, induction heating or heating in a gas fired furnace, was used to heat the probes to 1100° C. The two sets of experiments corresponding to the two types of heating are labelled Type I and Type II experiments, respectively. Since the apparatus used for each type was different, these will be discussed separately.

3.6.8.1 Type I Experiments

A diagram of the probe installation used in this series of experiments is shown in Figure 22.

-  Fiberfrax Insulation
-  316 Stainless Steel Heater Block
-  304 Stainless Steel Heat Transfer Sample
-  Asbestos Sheet
-  Al_2O_3 Powder
-  Induction Coil

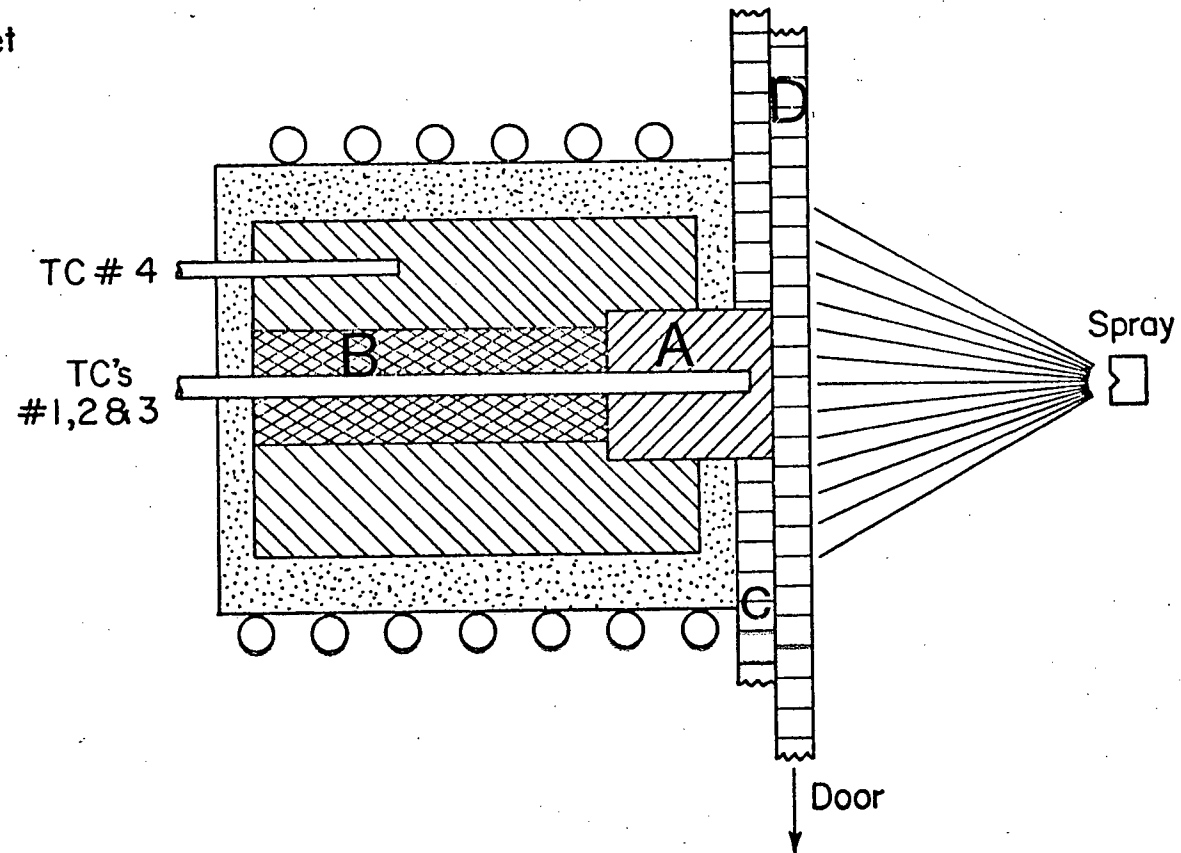


Figure 22 Schematic diagram of the probe installation for the Type I heat transfer experiments.

Referring to this Figure, the instrumented probe, A, was shrink fitted into a AISI 316 stainless steel hollow cylindrical heater block with 6 mm (1/4 in) of the length of the probe extending from the heater block. The cylindrical heater block was 75 mm (3 in) in diameter, 100 mm (4 in) in length and had an axial hole B of 20 mm dia. (3/4 in), except for a length of about 19 mm (3/4 in) in the region where the probe was installed. Here the diameter was about 25 mm (1 in). The axial hole served as a passage for the thermocouple wires. This hole was then filled with alumina powder for insulating purposes after the installation of the probe.

The portion of the heat transfer probe protruding from the heater block was then cemented with alumina cement into a 25.4 mm (1 in) hole in a vertical asbestos plate, C, which was 6 mm (1/4 in) thick, such that the polished face of the probe was flush with the surface of the asbestos sheet. An asbestos door, D, was then hung in front of the block. This door was suspended from a solenoid arrangement, which caused the door to fall when the solenoid was tripped.

An insulating layer of Fibrefrax was then wrapped around the heater block, and the assembly enclosed in an induction coil.

Power to the coil was provided from an Inductotherm motor generator unit. The temperature of the heater block was monitored with a thermocouple marked TC #4 in the Figure. The power input to the coil was between 1 and 2 KW, which heated the probe to 1000°C in about 40 to 60 min. Slow heating was used to minimize the temperature gradient along the axis of the probe. The thermal gradients existing in the probe at the instant of the initiation of spray cooling was less than 10°C per cm.

When the temperature of the probe reached the required starting temperature, the Visicorder was turned on, the spray was started and stabilized, and within 2 seconds, the solenoid holding up the door was tripped.

When the spray impinged on the sample, the probe cooled rapidly, and the transients measured by the thermocouples were recorded on the Visicorder.

3.6.8.2 Type II Experiments

In this case, the probe was mounted in a 304 stainless steel plate, and the whole assembly heated in a gas fired furnace before spraying water on the probe face. A diagram of the installation is shown in Figure 23. A 25.4 mm (1 in) diameter hole was drilled in

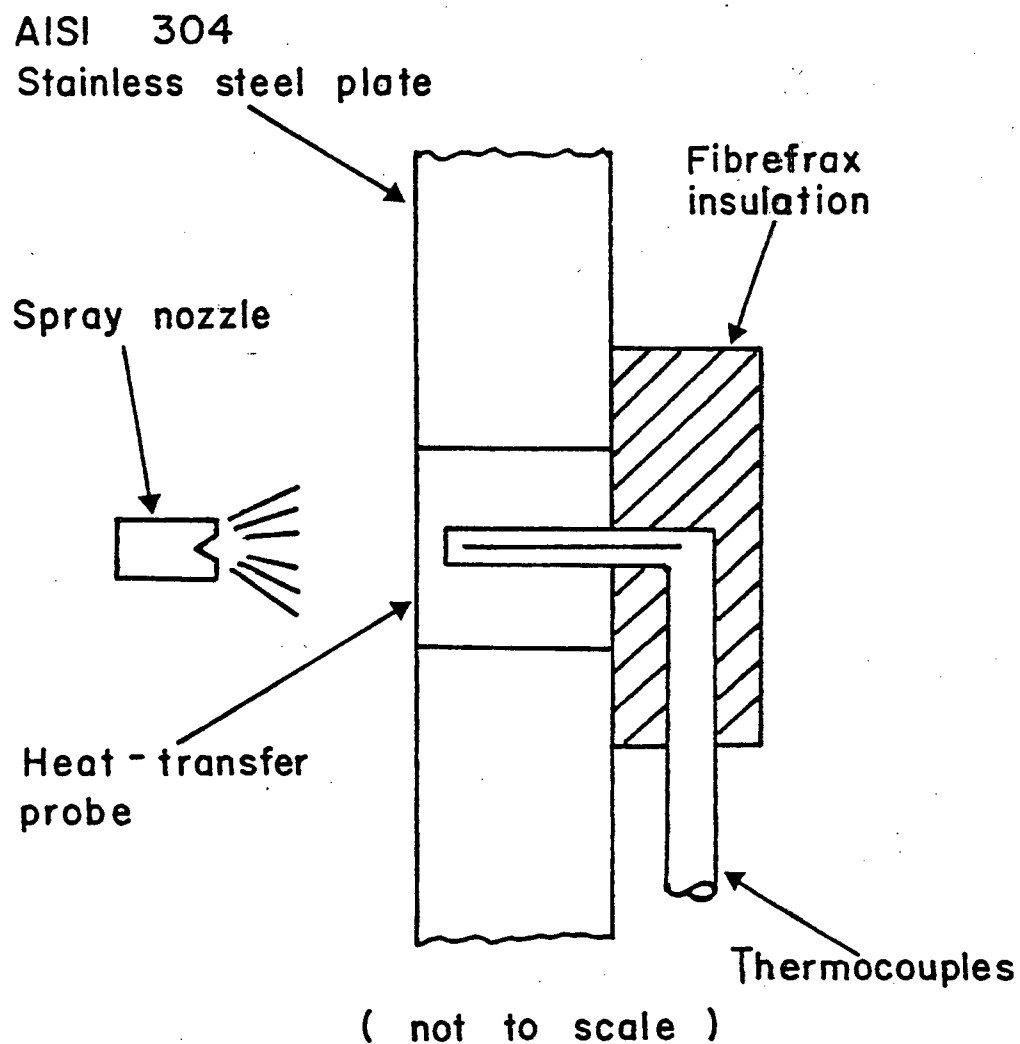


Figure 23 Schematic diagram of the probe installation for the Type IIa heat transfer experiments.

the middle of the AISI 304 stainless steel plate, of dimensions 406 mm x 203 mm x 25.4 mm (16 in x 8 in x 1 in). The probe was then pressfitted into the hole, with its polished surface flush with the plate face. The insulating tubes surrounding the thermocouples in the vicinity of the probe were anchored to the plate with screws and strapping. The end of the probe, at the thermocouple exit, and its surroundings were insulated with "Fibrefrac" insulating wool. (Type IIa experiments)

As shown in Figure 24, the plate was then attached by bolts to a tiltable mount B mounted on a movable trolley C. The spray holder was also mounted on the trolley, with the spray axis horizontal. The tiltable mount allowed the plate to be positioned in a horizontal position into a gas fired furnace D. When tilted 90° from this position, the plate was brought into a vertical position, with the polished probe surface facing the spray.

The plate was first heated up in the gas fired furnace in which the atmosphere was kept neutral or slightly reducing, in order to minimize the oxidation of the probe surface. In most of the experimental runs, a stainless steel cap, about 15 cm (6 in) square and 2.5 cm (1 in) deep was placed over the face of the probe, and nitrogen was passed into the cap, to further reduce the oxidation of the



Figure 24 Photograph of the heating plate mounted on the
tiltable mount.

probe face in the furnace.

When the plate reached the desired temperature, the cap was removed, the mount moved away from the furnace, and the plate tilted up into the vertical position. The Visicorder was activated, and after turning on the spray, the output of the thermocouples monitored on the high speed recorder.

In order to investigate the cooling effect of water flowing down the plate surface, experiments were carried out using 31 mm (1 1/4 in) long probes mounted into the plate. The first 6 mm (1/4 in) was then fitted with a stainless steel ring as shown in Figure 25. In this configuration, the end of the probe was cooled only by the drops of water impinging on it. (Type IIb Experiment)

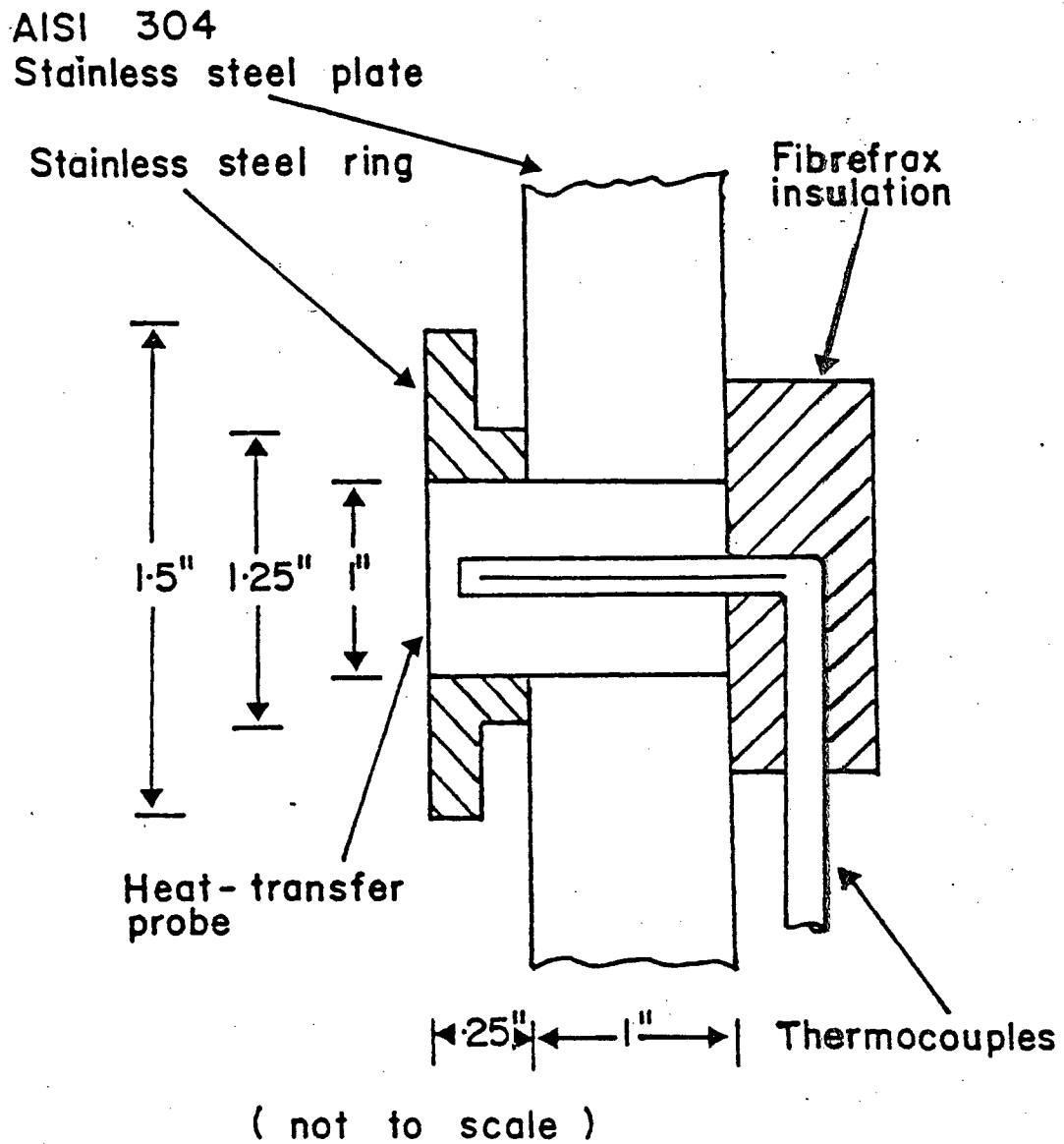


Figure 25 Schematic diagram of the probe installation for the Type IIb heat transfer experiments.

Chapter 4

ANALYSIS OF THE MEASURED TEMPERATURE TRANSIENTS

This chapter presents the conversion of the temperature-time curves obtained from the Visicorder into machine readable form, as well as the mathematical method employed to calculate the heat-transfer coefficient vs. surface temperature relationships from the measured transients.

4.1 Digitising and Smoothing of the Transients

The first step in the analysis of the measured data was digitising the time-millivolt traces obtained on the Visicorder. The chart traces were digitised either using either a "Gradicon" digitiser belonging to the Mechanical Engineering Dept., U.B.C., or a "Talos Cybergraph" digitiser located in the Computer Centre, U.B.C. The former digitiser provided punched computer cards with the x and y coordinates (with regard to a set origin) of the point being digitised. The latter machine directly entered these coordinates into a magnetic disc storage unit. Both digitisers had a resolution of 0.001 inch.

The digitised points were then read into a digital

computer (initially an IBM 370/168 and later an Amdahl V6) and the millivolt readings were converted to temperatures using a computer program written for the conversions. The time corresponding to each digitised value of voltage was obtained using a conversion factor depending on the chart speed in the recorder and the distance coordinate of the digitised point.

The temperature-time transients were then smoothed by fitting a polynomial of maximum degree 7, with temperature as the dependent and time as the independent variable. The necessity of smoothing the transients has been pointed out by Economopoulos.⁹⁷ The difference between the digitised and the fitted values was, in most cases, less than 1°C. The fitted values were then used as input to the computer program used to calculate the heat-transfer coefficients. This program will be described in a later section of this chapter.

4.2 Analysis of the Temperature Transients

This section describes the steps involved in the analysis of the temperature transients measured inside the heat-transfer probe during cooling by the water spray. Initially, a discussion of the solution of the conduction equation to calculate the variation of the temperature

within a body, undergoing heating or cooling under the influence of known boundary conditions is presented. The modification of this solution to the case where the boundary conditions are the unknowns, and are to be evaluated, is subsequently discussed.

In the case of a solid body which is losing heat to its environment, at a rate that is proportional to the difference in the temperature between the surface of the body and that of the environment, the continuity of heat flow at the surface requires that

$$-k \left. \frac{\partial T}{\partial x} \right|_s = h (T_s - T_a) \quad \dots 4.1$$

From this equation, it can be observed that a knowledge of the surface temperature and the temperature gradient at the surface is necessary in order to evaluate the heat-transfer coefficient.

Accurate measurements of the surface temperature, especially when the thermal evolution is rapid, and in the presence of an adverse environment, are extremely difficult, and in many cases, impossible. This difficulty is avoided by measuring subsurface temperatures within the solid and reconstructing the variation of the surface temperatures with time, by calculation.

As opposed to the "Direct Problem", in which the temperature variations in a body undergoing cooling or heating with known boundary conditions can be calculated using the laws of unsteady state heat conduction, the present problem requires the solution of the "Inverse Boundary Value Problem" in heat conduction to determine the surface temperatures and surface heat fluxes using measured values of temperature transients within the body. Both analytical and numerical methods have been proposed to attack this problem, as discussed below. It must be noted, that although in most cases, the treatment of this problem is with respect to the cooling of a body, it is equally applicable to the case of heating of solids.

4.2.1 Previous Solutions to the Inverse Boundary Value Problem

4.2.1.1 Analytical and Analog Methods

Shumakov¹⁰⁰ has presented a method of step-by-step calculation applicable to the heating of plane plates, based on the assumption that the boundary conditions remain constant for each time increment. In this method, the temperature dependence of the thermo-physical properties of the solid can be taken into account. However, it has been reported⁹⁷ that this method presents

a severe limitation when high cooling or heating rates are encountered, and in materials whose thermal diffusivities are rather low, as in the case of steels.

Paschkis and Stoltz^{101,102} have measured transient temperatures in quenched samples of silver and steel, and have used an analog computer for the determination of the boundary conditions.

Mirsepasi¹⁰³ has reported a graphical method for the solution of the inverse problem for semi-infinite bodies, but this relates to solids in which the thermophysical properties are temperature independent.

Stoltz¹⁰⁴ has used a numerical inversion of the analytical solution of the simplified 'direct problem', using the assumptions of constant thermophysical properties and no internal heat generation. Though developed for the case of spheres, it can be extended to slabs and cylinders. He points out that in the solution of the problem, calculations are based on the use of truncated data which have been damped, and that using too small a time step in the calculations leads to oscillations in the solution. An additional constraint, which also applies to some of the other methods is that the initial temperature through the

solid is assumed to be uniform.

Sparrow et al.¹⁰⁵ have presented a more general, computationally simple technique, which makes it possible to utilize, in some cases, the graphical method of Mirsepassi¹⁰³ to simplify major parts of the calculations. The equations have been developed for spheres, cylinders and slabs, including cases in which the initial temperatures may be non-uniform within the body. Basically, the solution involves obtaining a Laplace transform of the unsteady state conduction equation, and upon substitution of the measured temperatures at a point within the body, the surface temperature can be calculated as a combination of two terms -- an integral and the inverse Laplace transform of a function. The integration is easily performed using numerical techniques on a digital computer. Once the surface temperature is known, the application of the solution of the direct problem yields the temperature distribution in the body, and from this, the surface heat fluxes and the surface heat transfer coefficients are extracted. The method is reported to produce smooth, non-oscillating results, but is limited to the use of constant thermophysical properties.

The use of this technique is further elaborated upon

by Gaugler⁵³ and Corman⁶⁷ in the treatment of their heat transfer data. The latter author reports that the use of small time steps dictated by the rapid cooling transients obtained in his study, tended to cause stability problems in the solution.

Other treatments of the inverse problem are also available,¹⁰⁶⁻¹⁰⁹ but they are limited in that they cannot deal with variable thermophysical properties.

4.2.1.2. Numerical Methods

Unlike the previous investigations in which the calculations were done by either one or a combination of analog computers, analytical solutions, and numerical integrations of parts of the solution, a purely numerical method for the solution of the inverse problem has been proposed by Economopoulos, Lambert and Greday.^{69,97,110} This method involves the replacement of the partial derivatives in the unsteady state conduction equation with finite differences.

No assumption regarding the function expressing the variation of the surface temperature or heat flux is made, and this technique lends itself to the use of variable thermophysical properties. A set of algebraic equations which are obtained for the heat balances at different

portions of the solid is solved by the Gauss-Siedel iterative technique to yield the temperature distribution in the body at a given time, and from this, the surface heat fluxes and surface heat-transfer coefficients can be obtained. This method is useful even for the analysis of fast transients within the solid which would arise from the presence of high heat fluxes.

The effects of the influences of various parameters e.g. the distance of the point of temperature measurement below the surface, the values of the space and time increments used in the discretisation of the partial derivatives, the degree of accuracy of the iterations etc. on the computed results have been examined.

4.2.1.3 Other Related Solutions

A numerical solution of the inverse problem has been proposed for the determination of thermal conductivities of solids.¹¹¹ While all the above-mentioned methods for the solution of the inverse problem deal only with unidirectional conduction, Imber¹¹² has worked out a method for the solution of the problem in two dimensions.

Both the above methods involve the simultaneous determination of temperature transients at various positions in the body being heated or cooled.

4.2.2 Method Employed in the Present Work

A purely numerical technique is employed to analyze the measured temperature transients, since this method has the following capabilities:

- i) The presence of non-uniform temperatures in the heat-transfer probe as the initial condition could be taken into account.
- ii) The temperature dependent variation of the thermophysical properties can be accommodated.
- iii) The equations obtained are easily solved in a fairly simple manner on a digital computer.

The approach involves the division of the measuring section in a direction perpendicular to the heat-flow direction, performing heat balances on each slice, and the simultaneous solution of the set of equations obtained to yield the values of the required parameters.

The assumptions used in the formulation of the solution are:

- i) The existence of unidirectional conduction in the solid in a direction out of, and perpendicular to, the face of the probe being sprayed.
- ii) Absence of shape or volume changes in the

heat-transfer probe due to temperature changes.

- iii) The temperature of the spray water impinging on the probe is assumed to be constant, equal to the measured temperature of the water in the spray water delivery system.

Since the material of the probe used in the measurements was AISI 304 grade stainless steel, no heat evolution occurs due to phase transformations.

Figure 26 shows the division of the heat-transfer probe into nodes so that heat balances can be performed. Since only unidirectional conduction is being considered, the cross section of the nodes in the direction perpendicular to the paper is considered to be unity. Δx is taken as the spacing between the nodes in the direction of heat conduction. However, it can be noted that the surface node has only half this thickness. The same holds for the thickness of the node at the rear end of the sample away from the sprayed face, at which the temperature was also being monitored. To perform the heat balances, the discretised treatment of the conduction equation assumes that the node sizes are small enough that the point at the centre of each nodal volume has a temperature that is representative of that of the whole nodal volume. The

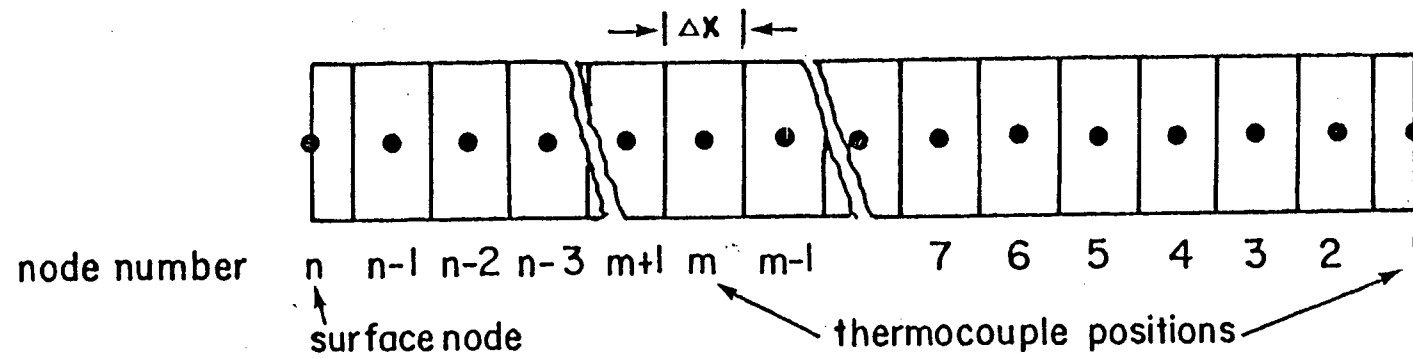


Figure 26 Division of the heat transfer probe into nodes.

time variable is also discretised into small increments, and the heat balances are performed for all nodes for each time increment.

4.2.2.1 The Direct Problem

In order to simplify the presentation of the equations used for the inverse problem, the formulation for the 'direct problem' is presented first and the changes subsequently made to this formulation to yield the solution to the 'reverse problem' are then discussed.

The total number of nodes is taken to be n , with the node number increasing from the interior to the surface losing heat. Assuming for the moment that the thermal conductivity remains constant, and that there is no internal heat generation or consumption within the solid, an implicit finite difference scheme can be used to perform the heat balances on each node. It is to be noted that the initial temperature at each node is a known quantity. Then after an interval of time Δt the heat balance for the i th interior node yields

$$\frac{k(T_{i-1}^* - T_i^*)}{\Delta x} - \frac{k(T_i^* - T_{i+1}^*)}{\Delta x} = \rho_i C_{p_i} \frac{\Delta x}{\Delta t} (T_i^* - T_i) \dots 4.2$$

The interfacial area between the nodes, as mentioned earlier, is unity.

Rearranging this equation and moving all the known values to the right hand side of the equation and the unknowns to the left, an equation of the form

$$a_i T_{i-1}^* + b_i T_i^* + c_i T_{i+1}^* = d_i \quad \dots 4.3$$

results, where the a , b , c represent the coefficients of the unknown temperatures. Similar equations are obtained for the other interior nodes.

If the temperature-time relationship for node 1 is known, then the equation for the second node will be of the form

$$a_2 T_3^* + b_2 T_2^* = d_2 \quad \dots 4.4$$

For the surface node numbered n , if the boundary condition is of the form shown in equation 4.1, then the heat balance yields

$$b_n T_{n-1}^* + c_n T_n^* = d_n \quad \dots 4.5$$

Thus, considering all the nodes, a set of $n-1$ algebraic expressions is obtained which are to be solved simultaneously in order to yield the $n-1$ unknown temperatures,

as shown below.

$$\begin{bmatrix}
 b_n & c_n & & & \\
 a_{n-1} & b_{n-1} & c_{n-1} & & \\
 & a_{n-2} & b_{n-2} & c_{n-2} & \\
 & & \cdot & & \\
 & & \cdot & & \\
 & & \cdot & & \\
 & & \cdot & & \\
 & & & a_3 & b_3 & c_3 \\
 & & & & a_2 & b_2
 \end{bmatrix}
 \begin{bmatrix}
 T_n^* \\
 T_{n-1}^* \\
 T_{n-2}^* \\
 \cdot \\
 \cdot \\
 \cdot \\
 T_3^* \\
 T_2^*
 \end{bmatrix}
 =
 \begin{bmatrix}
 d_n \\
 d_{n-1} \\
 d_{n-2} \\
 \cdot \\
 \cdot \\
 \cdot \\
 d_3 \\
 d_2
 \end{bmatrix}
 \dots 4.6$$

The right hand side matrix is completely defined, as is the coefficient matrix containing the a's, b's, and c's. It can be observed above, that the coefficient matrix on the left hand side, corresponds to the form of a 'tri-diagonal matrix'.

Because of the special nature of such a matrix, Gaussian elimination or complex iteration schemes (e.g. the Gauss-Siedel iterative technique) need not be utilized to solve this set of equations to obtain the unknown temperatures. Instead, a simple recursive method, sometimes referred to as the 'Thomas Method'⁵² can be used for the solution, at a saving of a considerable amount of computation. Using the temperature solution thus obtained, the

process is repeated for the next time step, progressively building up the change in the thermal field with time.

Other numerical methods are also available¹¹³ to perform such calculations for the direct problem, but the 'implicit finite difference method' just discussed has the advantage of yielding stable, non-oscillating solutions for a wide range of Δt and Δx . Detailed treatments of the numerical stability of this and other procedures are available elsewhere.¹¹³⁻¹¹⁶

The treatment of variable thermophysical properties is also simple in the above method. In performing the heat balances, average values of the thermal conductivities are used for the conduction term between any two adjacent nodes being considered. These are based on the value of the thermal conductivities calculated for each node at the time at which the temperature of the node is known. The value of the specific heat is also calculated for each individual node, depending on the temperature of the node. To refine the solution further, iterative techniques are used, which involves recalculating the thermophysical properties for the nodes using the temperatures computed at the end of the time step, and solving the set of simultaneous equations again. The process is repeated until the temperature solutions converge to specified limits.

4.2.2.2 The Inverse Problem

Moving on to the problem at hand, the surface temperature and the convective type boundary condition i.e. the heat-transfer coefficient, are unknown. However, the temperature history of an interior node, say the m th node, close to the surface, is the measured input. The equations discussed for the direct problems thus have to be restructured to provide the values of these unknowns.

At the surface node, the application of the heat balance yields a non linear equation of the form

$$a_n T_{n-1}^* + (b_n + h) T_n^* + h T_a = d_n \quad \dots 4.7$$

since both h and T_n^* are unknowns.

The three other equations that need changing involve the balances for node m and the nodes flanking node m i.e., nodes numbered $m-1$ and $m+1$. The reformed equations would be

$$a_m T_{m-1}^* + c_m T_{m+1}^* = d_m \quad \dots 4.8$$

$$a_{m-1} T_{m-2}^* + b_{m-1} T_{m-1}^* = d_{m-1} \quad \dots 4.9$$

$$b_{m+1} T_{m+1}^* + c_{m+1} T_{m+2}^* = d_{m+1} \quad \dots 4.10$$

The end result is that, once again, $n-1$ equations in

$n-1$ unknowns is obtained. However, the system of algebraic equations to be simultaneously solved includes one non-linear equation. The solution of such a set is complex, and is not possible with the use of the recursive formula mentioned earlier in connection with tridiagonal matrices.

Simplification of this system, however, is easily effected using the observation that for nodes 1 to m , the initial and boundary conditions are completely defined. As such, the thermal field for this section of the system can be obtained easily by the use of the solution to the direct problem.

From Equation 4.8, the value for T_{m+1}^* is obtained by substitution of the value of T_{m-1}^* , which has been previously calculated by solving the set of algebraic equations for nodes 1 to m . Similar substitutions made for the difference equations for nodes $m+2$ to n yield the temperatures at these nodes. Substitution of these known temperatures into Equation 4.7 yield the heat-transfer coefficients, and with a simple further calculation, the surface heat flux is obtained. The time is then incremented and the operation is repeated, yielding the surface temperatures and corresponding heat-transfer coefficients and surface heat fluxes as a function of time.

4.3 Validation of the Mathematical Formulation Used

As a first step, a computer program based on uni-directional conduction was written for the geometry used in the present experiments, assuming constant thermophysical properties. The thermal history within the solid was then calculated for known boundary conditions, chosen such that the analytical solutions available could be used to check the calculations. This step was necessary since analytical solutions for transient heat conduction are normally unable to handle variable thermophysical properties or complex boundary conditions. Once the computer program was debugged, so that the numerical calculations matched the analytical solution, it was modified to accept a varying initial temperature distribution in the solid, and to accommodate variable thermophysical properties. Calculations were then performed using this program with different heat-transfer coefficients as boundary conditions.

Another program, using the mathematical formulation discussed in Section 4.2.2.2 was then written, and the temperature transients obtained from the calculations involving the "direct problem" were supplied as input, in order to back-calculate the surface temperatures and heat-transfer coefficients. The temperature transients at a designated position was first smoothed using the polynomial fitting

routine mentioned in Section 4.1, so as to maintain similarity between the handling of the test data with that of the experimental data. Initial tests were carried out for the case of constant heat-transfer coefficients. A slightly different initial condition (temperature distribution in the solid) than that used to calculate the temperature transients using the solution to the 'direct problem' was then introduced into the solution for the 'inverse problem'. This was done to observe the sensitivity of the solution to the 'inverse problem'. The back-calculated heat-transfer coefficients were then compared with the values used to generate the temperature transients. The results, for two values of heat-transfer coefficients, 2.094 and $4.19 \text{ kW/m}^2\text{K}$ (0.05 and $0.1 \text{ cal/cm}^2 \text{ s } ^\circ\text{C}$) are shown in Figures 27 and 28 respectively. It can be observed from these Figures, that the back-calculated heat-transfer coefficients match the expected values to well within 5% after the first two or three time steps (of 0.1s duration), and that the calculated surface temperatures match the expected surface temperatures very well. Subsequently, the surface heat-transfer coefficient was allowed to vary from $1.675 \text{ kW/m}^2\text{K}$ at 800°C to $2.094 \text{ kW/m}^2\text{K}$ at 1000°C in the solutions to the 'direct problem'. The calculated temperature transients at 0.1 cm from the surface were then used to back-calculate these coefficients in the 'inverse problem'.

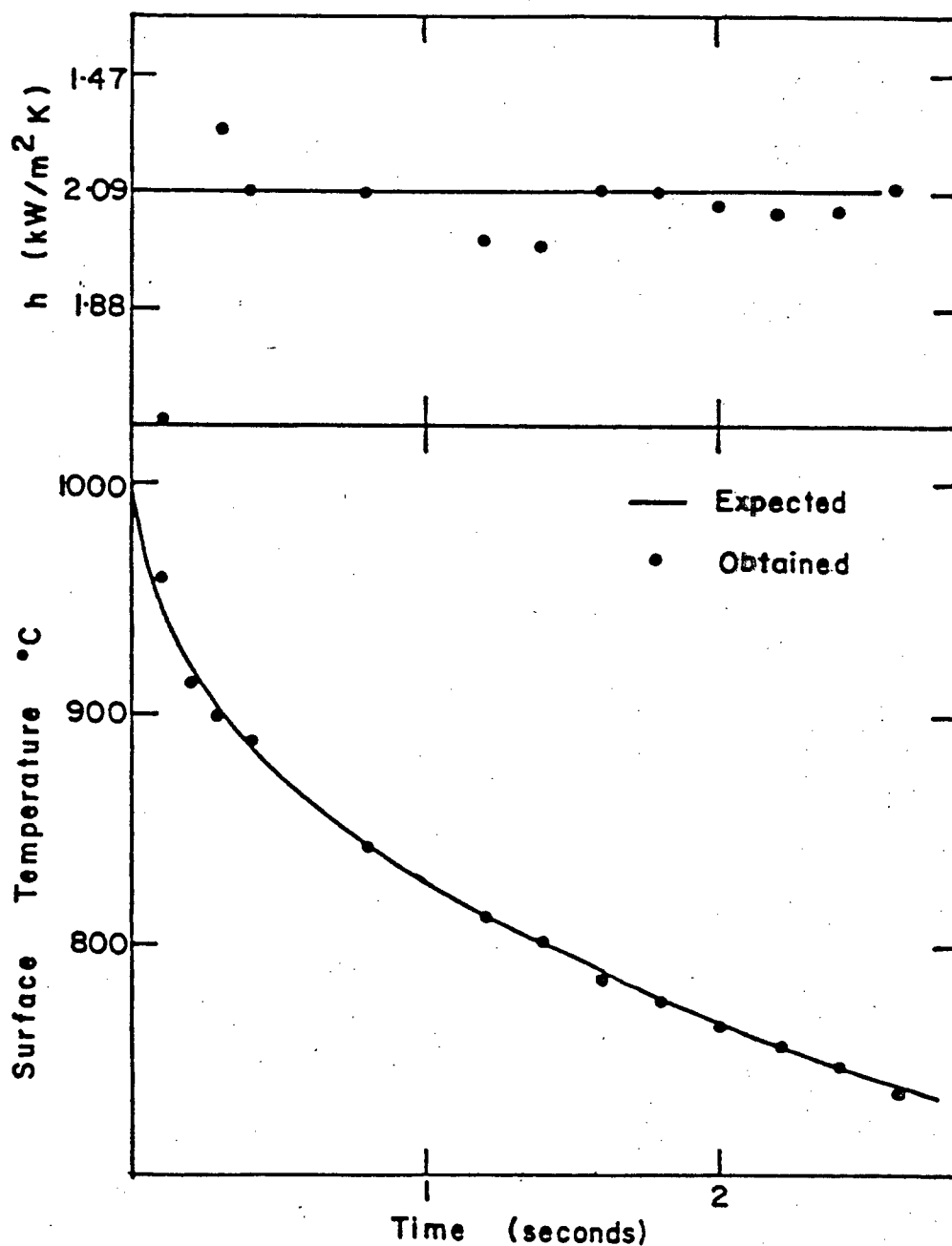


Figure 27 Comparison of back-calculated values of heat-transfer coefficients and surface temperatures with expected values, for $h = 2.094 \text{ kW/m}^2\text{h}$.

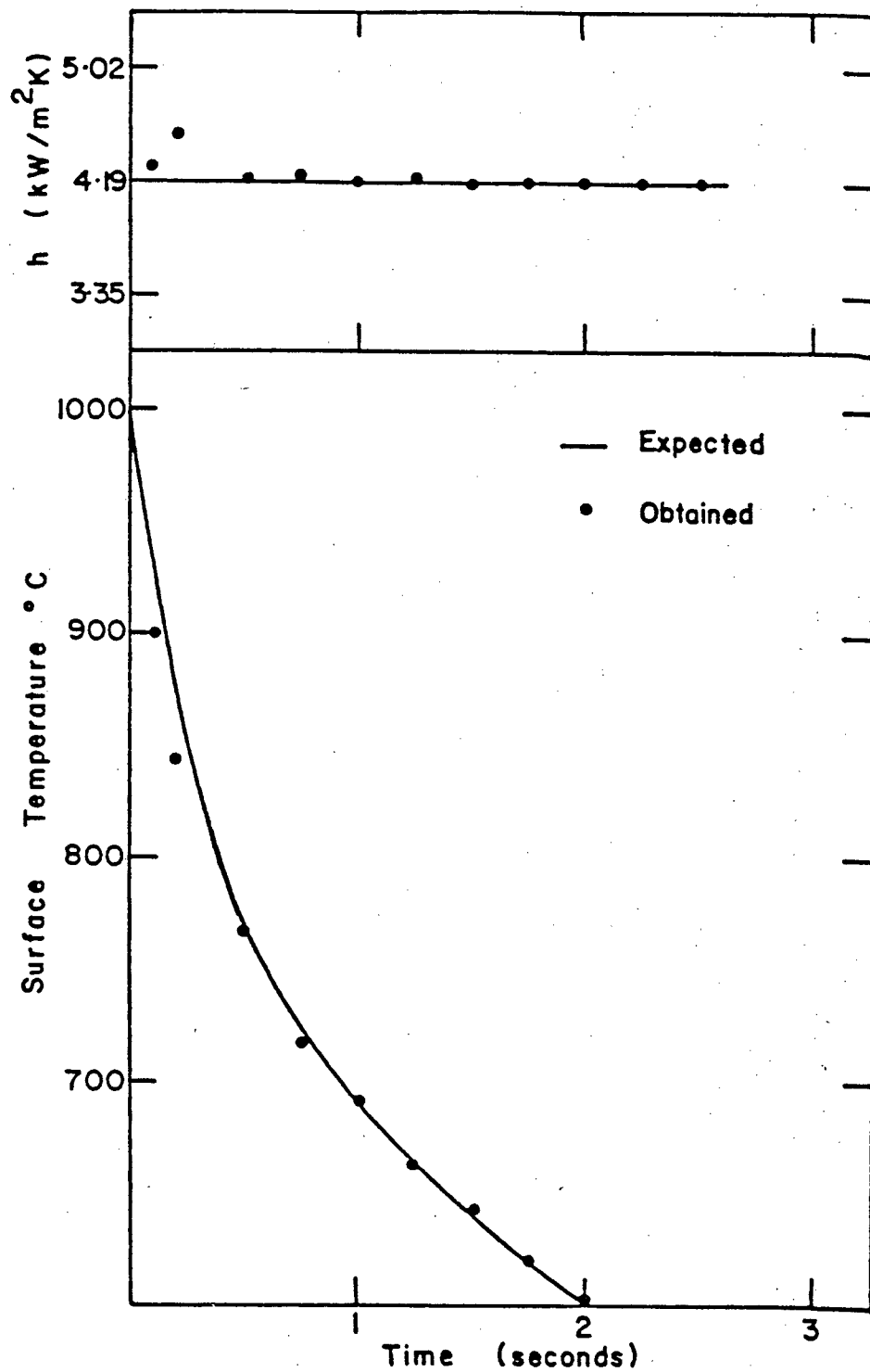


Figure 28 Comparison of back-calculated values of the heat-transfer coefficient and surface temperatures with expected values, for $h = 4.19 \text{ kW/m}^2\text{h}$.

The results plotted in Figure 29, show very good agreement between the expected and calculated values. The effect of using transients at larger distances from the cooled face is shown in Figure 30. Here, the distances used were 0.175 and 0.20 cm respectively. Again, very good agreement between the calculated and expected values is observed after the first two time steps.

Thus, it was established with the test data that the mathematical formulation of the 'Inverse' Boundary Value Problem' used in this work is valid, and predicts the expected heat-transfer coefficients with an accuracy of well within 5% when used with the test data.

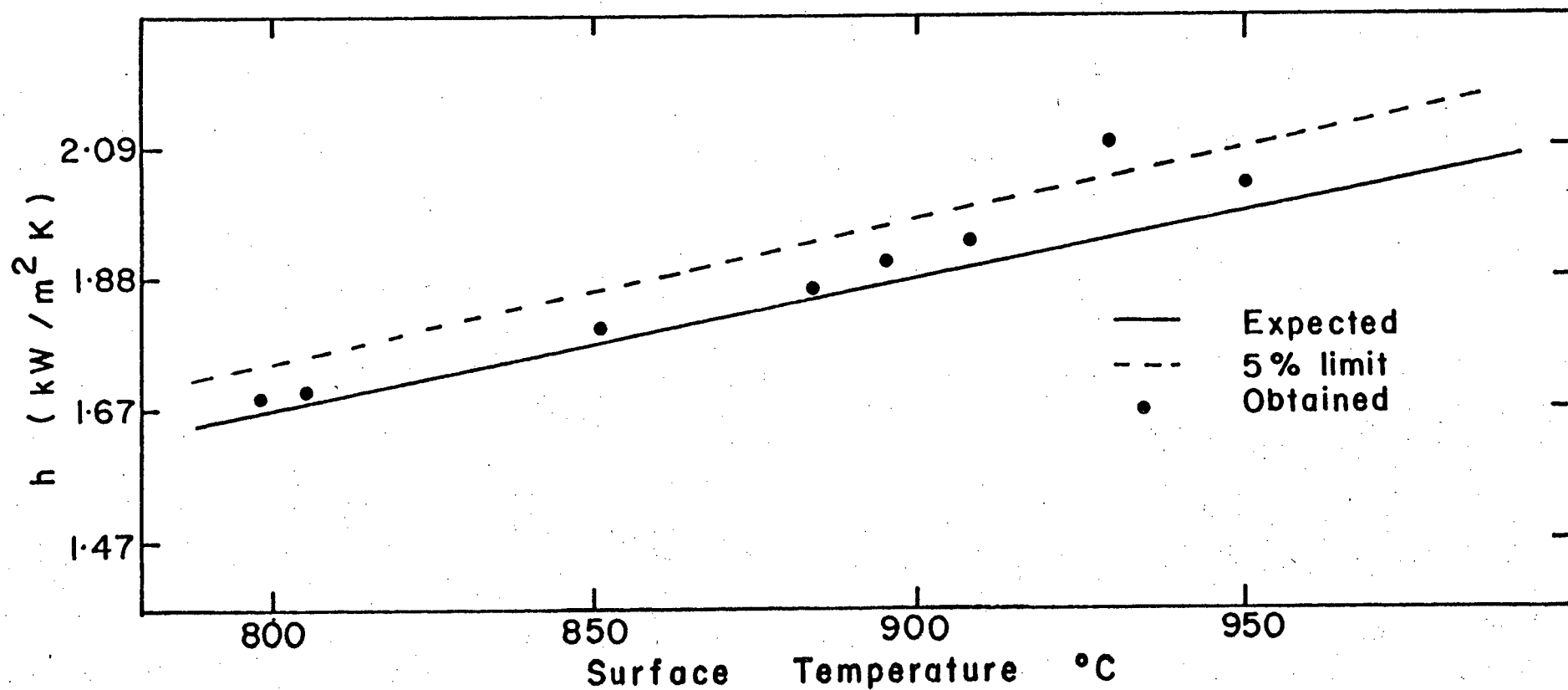


Figure 29 Comparison of back-calculated values of the heat-transfer coefficient with expected values, for h varying with surface temperature.

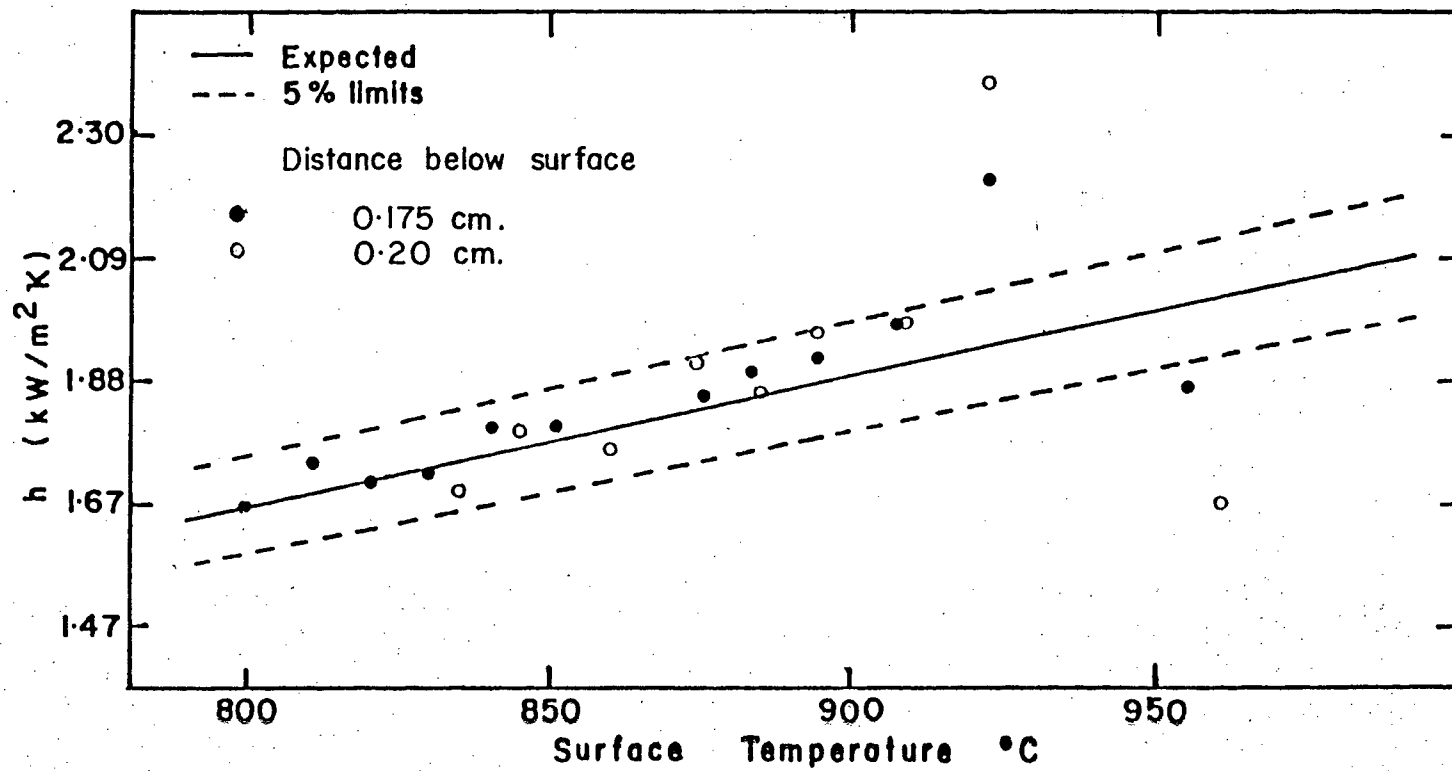


Figure 30 Comparison of back-calculated values of the heat-transfer coefficient, using transients obtained at different distances from the cooled face.

RESULTS AND DISCUSSION

The experimental findings reported in this chapter include measurements of spray water fluxes for various spray nozzles enumerated in Section 3.2, under a range of operating conditions, and measurements of corresponding heat-transfer coefficients.

5.1 Spray flux measurements

As described earlier in Chapter 3 on experimental methods, two types of spray collectors were used in the characterization of the spray water distribution. The Type A collecting system measured the spray flux arriving at the tips of the collectors directly from the spray nozzle, while measurements with the Type B collectors gave a measure of the combined volume of water arriving at the collectors directly from the spray, and that flowing downward adjacent to the sprayed face under the influence of gravity. In this section, spray profiles obtained with both collection systems are presented. These correspond to the spray fluxes obtained with the horizontal series of collector tubes, with the axis of the middle tube being aligned with that of the spray nozzle. Measurements of spray fluxes were carried out for most of the sprays at

distances of 10.16, 15.24 and 20.32 cm (4, 6 and 8 in) respectively from the tip of the nozzle, and at spray pressures of 0.13, 0.27 and 0.41 MPa (20, 40 and 60 psi) respectively.

5.1.1 Spray Fluxes for a 1/4 GG 10 Nozzle

The majority of the spray flux measurements were made with a 1/4 GG 10 nozzle. This nozzle provides a conical spray pattern, and is known as a "full cone" type nozzle, in which water entering the nozzle is imparted a swirling motion by a specially shaped vane within the nozzle.

5.1.1.1 Horizontal Centreline Spray Profiles - Type A Collectors

A typical horizontal centreline spray flux profile obtained for the 1/4 GG 10 nozzle, at a distance of 15.24 cm (6 in) and for a spray pressure of .41 MPa (60 psi) is shown in Figure 31. It is seen that the spray distribution is not uniform, and is characterized by a high water flux in the centre of the spray, and a rapidly decreasing flux towards the edges of the spray pattern. Although the published spray angle for this nozzle is between 60° and 70° for this spraying condition, it can be observed that the spray covers a larger area, corresponding to the included angle of the spray cone of about 80°.

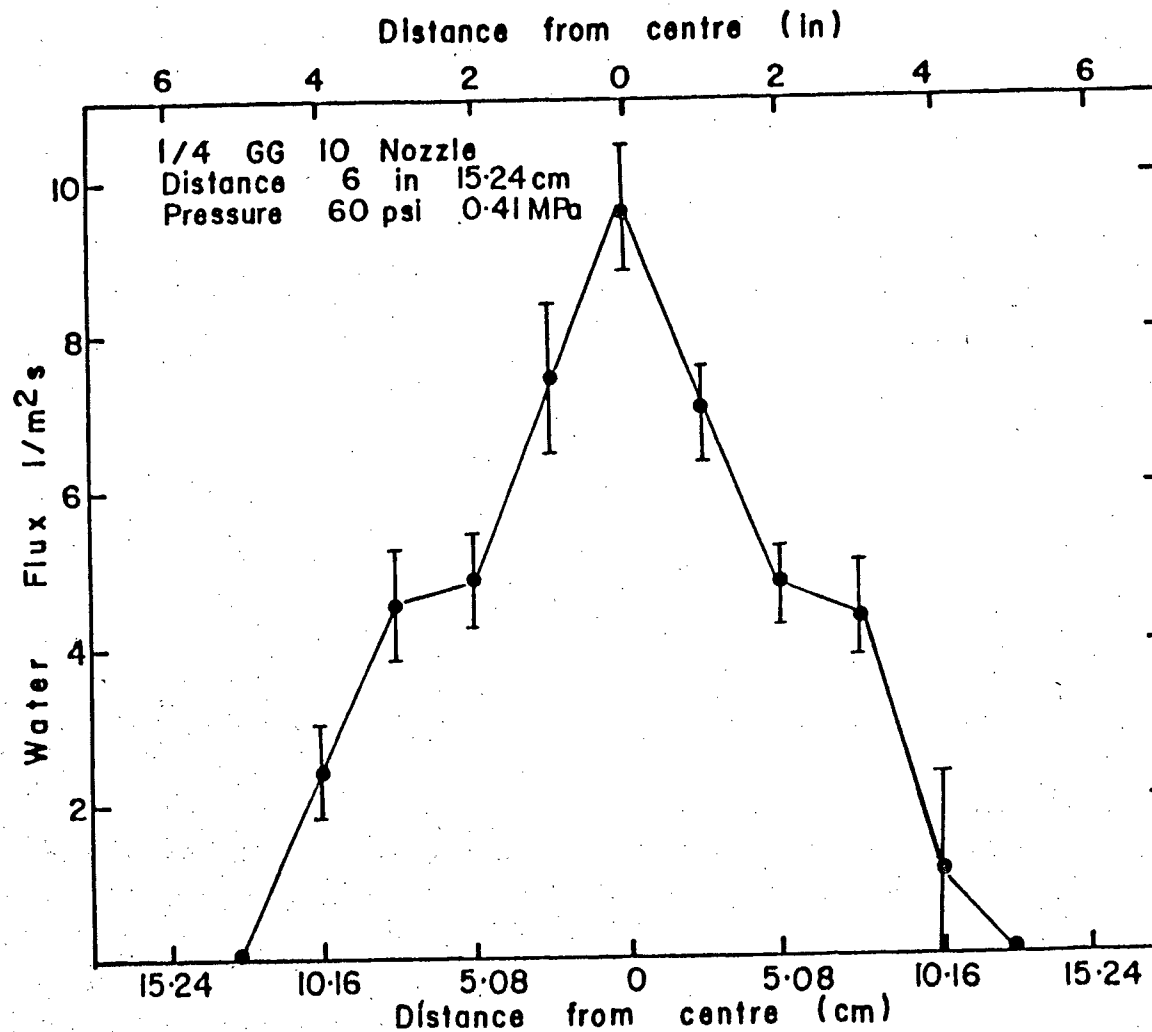


Figure 31 Typical horizontal centreline profile obtained with the 1/4 GG 10 nozzle, for a spray distance of 15.24 cm and a spray pressure of .41 MPa.

5.1.1.1.1 Differences Between Similar Spray Nozzles

Differences in the spray flux profiles were observed when different 1/4 GG 10 spray nozzles were used under the same spraying conditions. The spray flux profiles were not always symmetrical about the centreline, as can be seen from the spray flux profiles in Figure 32, for four 1/4 GG 10 nozzles. These non-symmetrical spray patterns were obtained with the spray nozzle axis accurately aligned with the axis of the central collector tube. Three sets of measurements of spray fluxes for one of the 1/4 GG 10 nozzles are shown in Figure 33. The reproducibility of the measurements is seen to be excellent from this Figure. This was typical of most of the nozzles, but in a few cases some scatter of the measurements was observed (Figure 34), in spite of great care to measure water fluxes under identical experimental conditions. In view of the variability between similar nozzles, spray flux profiles were obtained for eleven 1/4 GG 10 nozzles. The average of the eleven sets of measurements is plotted in Figure 31. The error bars plotted on this Figure correspond to 1σ limits on the average values. The results of this series of measurements demonstrates that there is a manufacturing variability in the nozzles, with relatively large variations, of the order of 30%, and as such, the measured spray fluxes from any nozzle correspond only to the sprays obtained for that particular nozzle. This is an

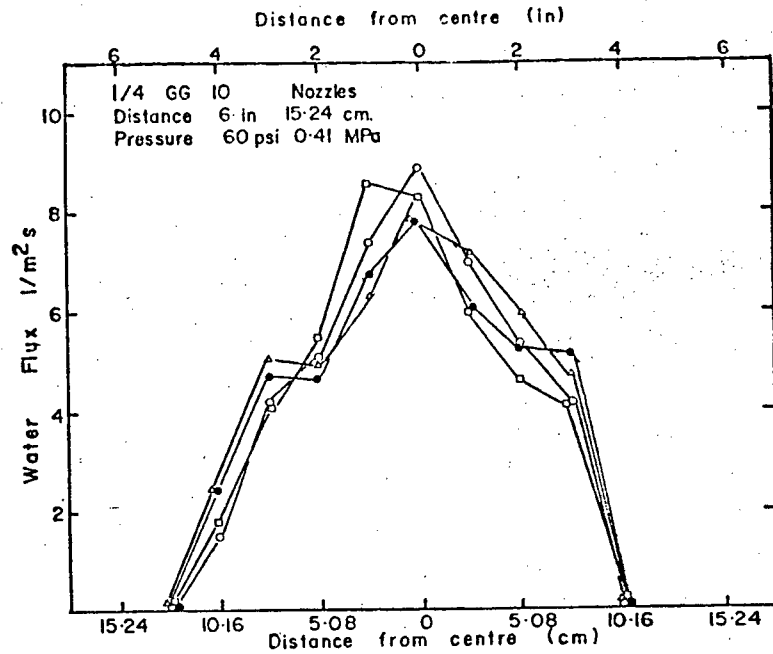


Figure 32 Variation in the measured spray water fluxes for four different 1/4 GG 10 nozzles.

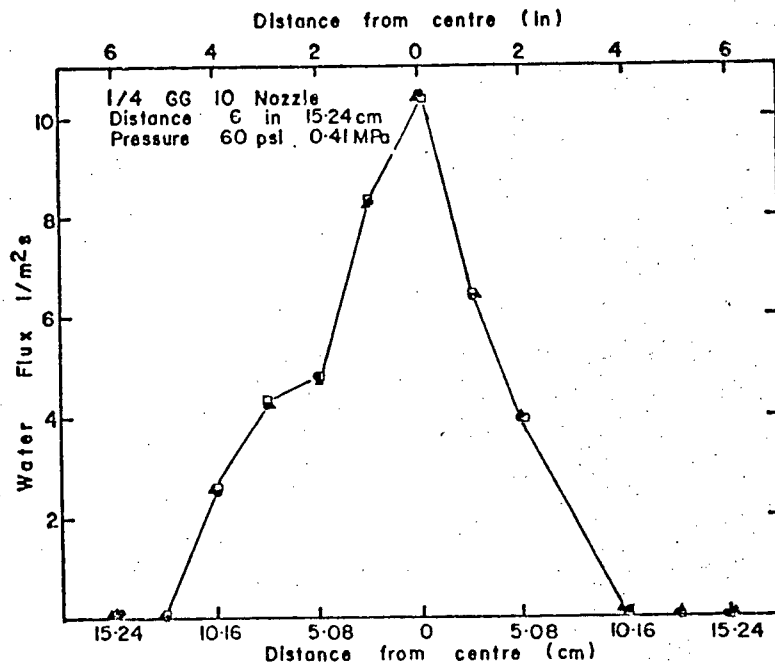


Figure 33 Reproducibility of the spray flux measurements for a 1/4 GG 10 nozzle (No. 9).

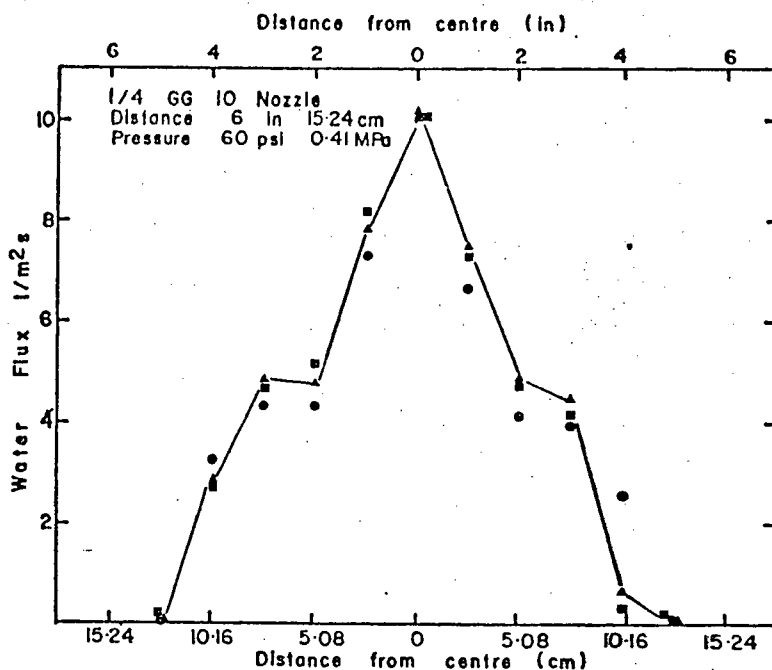


Figure 34 Reproducibility of the spray flux measurements for a 1/4 GG 10 nozzle (Number 4).

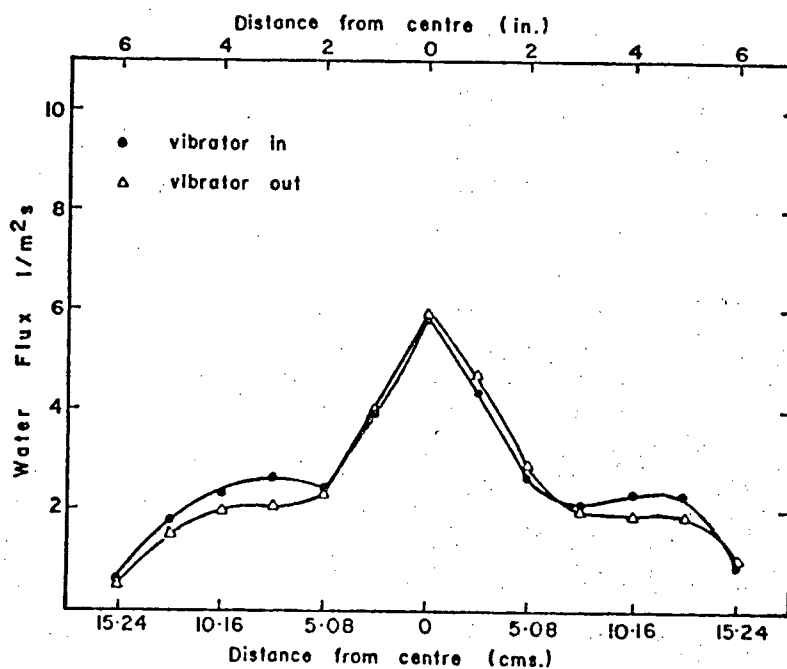


Figure 35 Effect of vibrating the collectors on the spray water flux measurements.

important point to note when attempts are made to correlate spray heat-transfer coefficients with the spray variables. Very little data has been reported in the literature regarding the variation of the spray fluxes within the sprayed area. The possibility of variability between similar spray nozzles has also never been reported. For the remainder of the measurements, a nozzle exhibiting the most symmetrical spray flux profile was used.

5.1.1.1.2 Effect of Vibrating the Collectors

A sixty hertz vibrator was connected to the plate holding the spray collectors in order to check whether there was any resistance to the flow of water through the collector tubes. The difference obtained with and without the vibrator was small, as shown in Figure 35, obtained for a nozzle operated at a spray pressure of 0.41 MPa (40 psi). In view of the small difference, vibration of the plate was discontinued for all further measurements.

5.1.1.1.3 Effect of Different Pressurizing Gases

Since there was a possibility that the gas used to pressurize the water system could dissolve in the water and subsequently be released

at atmospheric pressure at the nozzle orifice, affecting the sprays produced, three different gases (nitrogen, argon and air) were used in the pressurizing system. Spray flux profiles were then measured, but no significant differences in the spray profiles were obtained due to the different gases.

5.1.1.1.4 Effect of Spray Pressure at Constant Distance

Figure 36 shows the spray flux profiles obtained at a distance of 15.24 cm (6 in) from the spray nozzle, for three different spray pressures of 0.13, 0.27 and 0.41 MPa (20, 40 and 60 psi) respectively. An increase in the spray pressure increases the spray flux at any point in the spray, because of the increase in the flow-rate of water through the nozzle. The magnitude of the increase, however, is smallest in the central portion of the spray, and becomes larger towards the edge of the spray pattern. Similar results obtained for spray distances of 10.16 cm and 20.32 cm (4 and 8 in) are shown in Figures 37 and 38.

5.1.1.1.5 Effect of Spray Distance at Constant Pressure

The effect of increasing nozzle distance at constant pressure on the spray flux

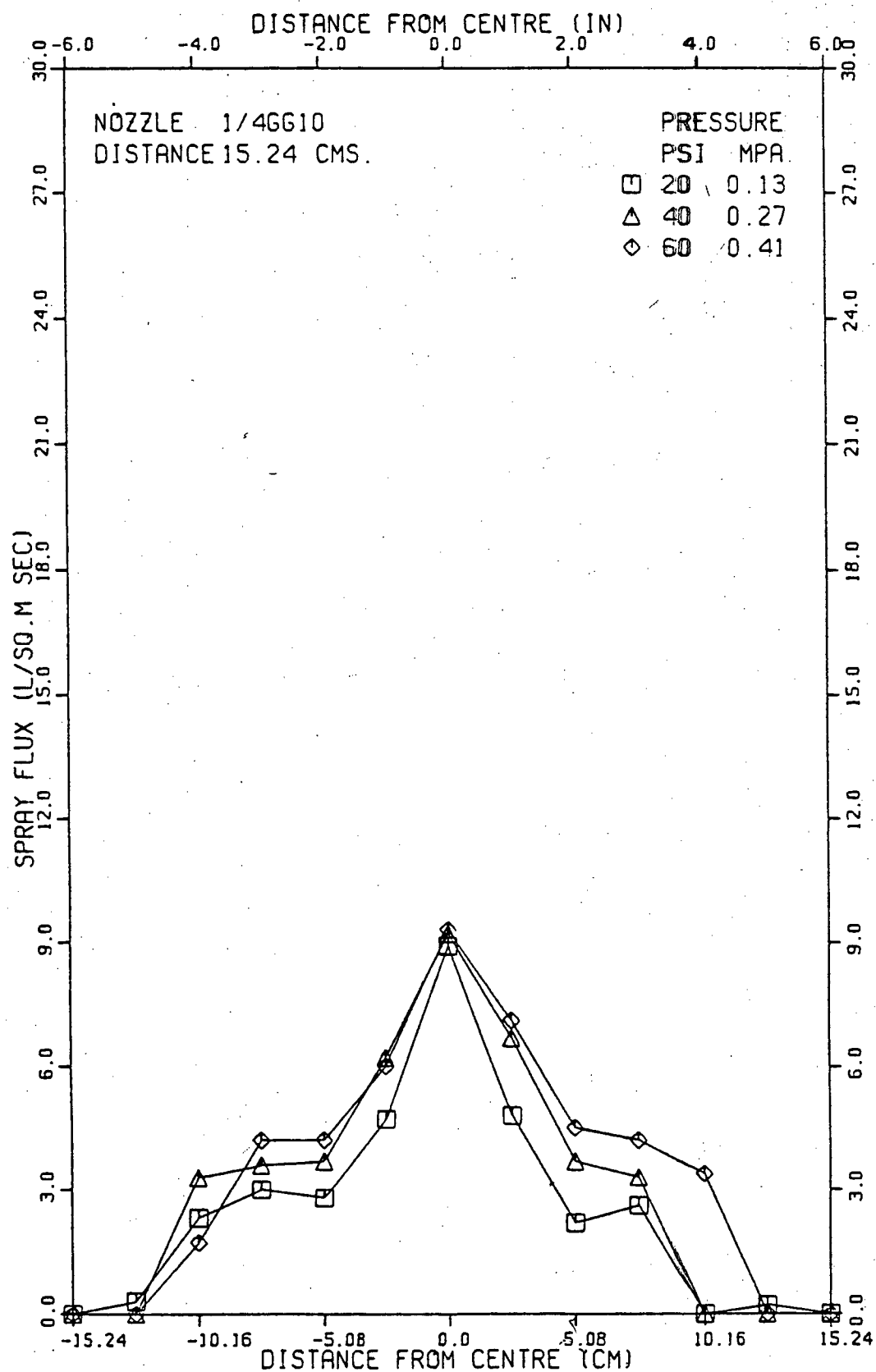


Figure 36 Effect of spray pressure at constant distance for a
1/4 GG 10 nozzle at a distance of 15.24 cm.

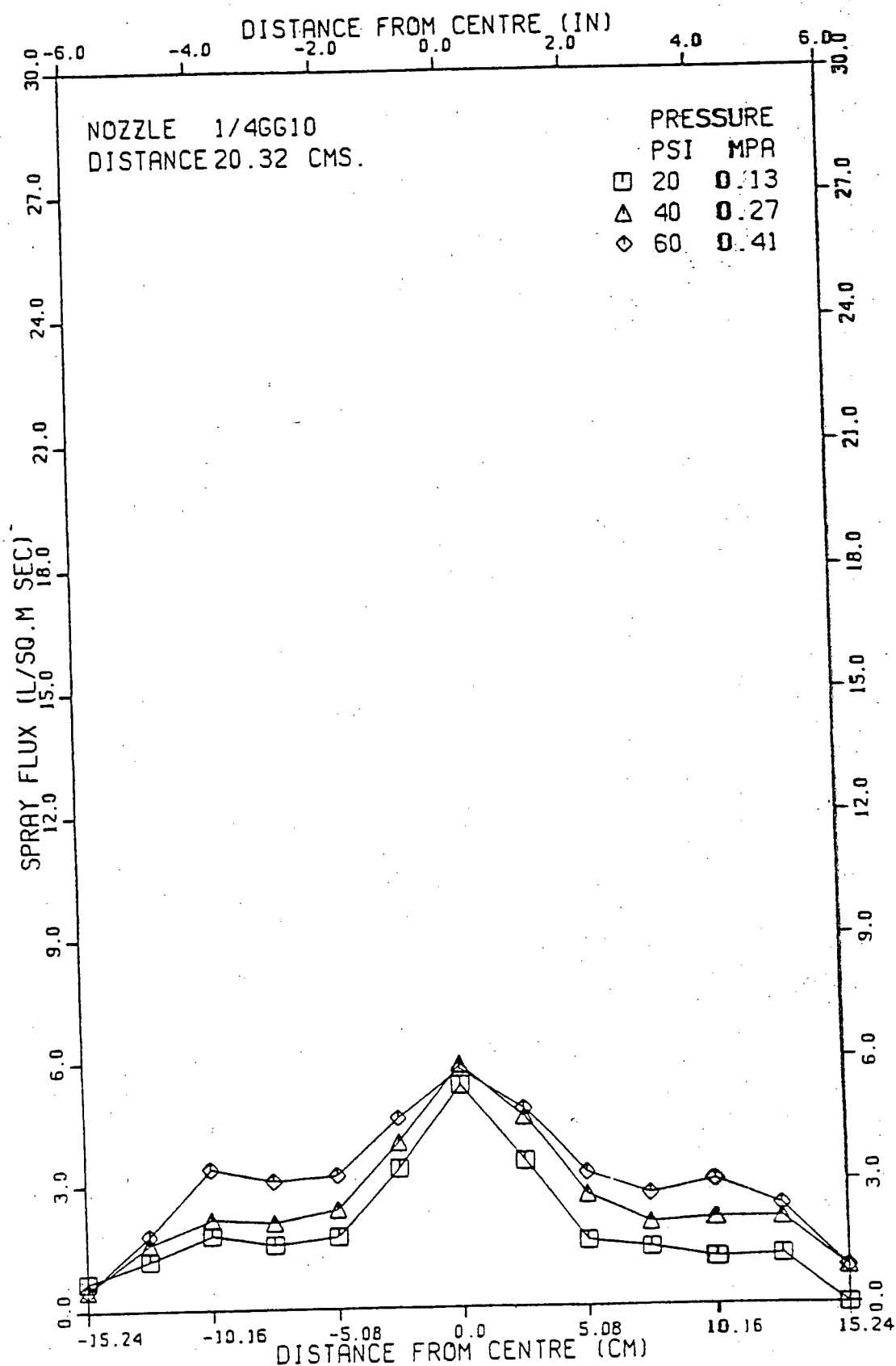


Figure 38 Effect of spray pressure at constant distance for a 1/4 GG 10 nozzle, at a distance of 20.32 cm.

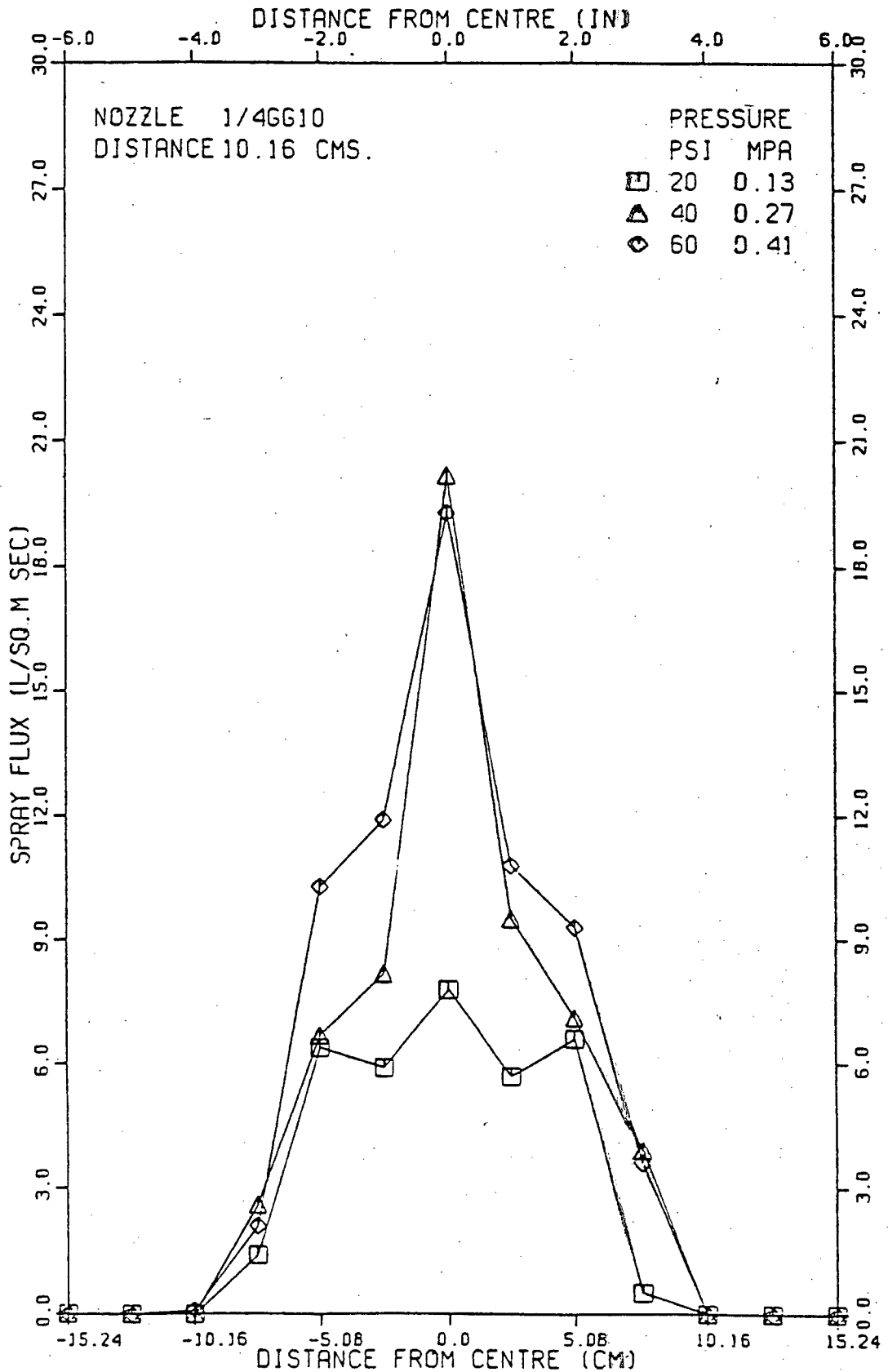


Figure 37 Effect of spray pressure at constant distance for a 1/4 GG 10 nozzle, at a distance of 10.16 cm.

profiles is shown in Figure 39 for a spray pressure of 0.27 MPa (40 psi). As the distance increases, it can be observed that, as expected, the area of the spray coverage increases. The largest effect, however is the marked drop in the spray flux in the centre of the spray as the spray distance increases. The spray profile also tends to become more uniform as larger distances, as seen from the profile obtained at a distance of 20.32 cm (8 in) from the nozzle. Results published by Mizikar⁷⁶ for nozzle distances of 20.32 cm (8 in) and 10.16 cm (4 in) are also plotted on this Figure, and are seen to be lower than those obtained in this investigation. Similar results obtained for spray pressures of 0.13 MPa and 0.41 MPa (20 and 60 psi) are given in Figures 40 and 41 respectively.

The variation of the spray water flux with pressure and distance at the axial centreline of the spray, and a position 5.08 cm (2 in) from the centreline are plotted in Figures 42 and 43 for spray pressures of 0.13, 0.27 and 0.41 MPa (20, 40 and 60 psi) respectively. It should be noted that the spray flux at the centre of the spray was always highest when the spray nozzle was operated at 0.27 MPa (40 psi).

5.1.1.2 Spray Flux Map for the 1/4 GG 10 Nozzle

Spray flux maps of the sprayed area were obtained by moving the nozzle in vertical increments

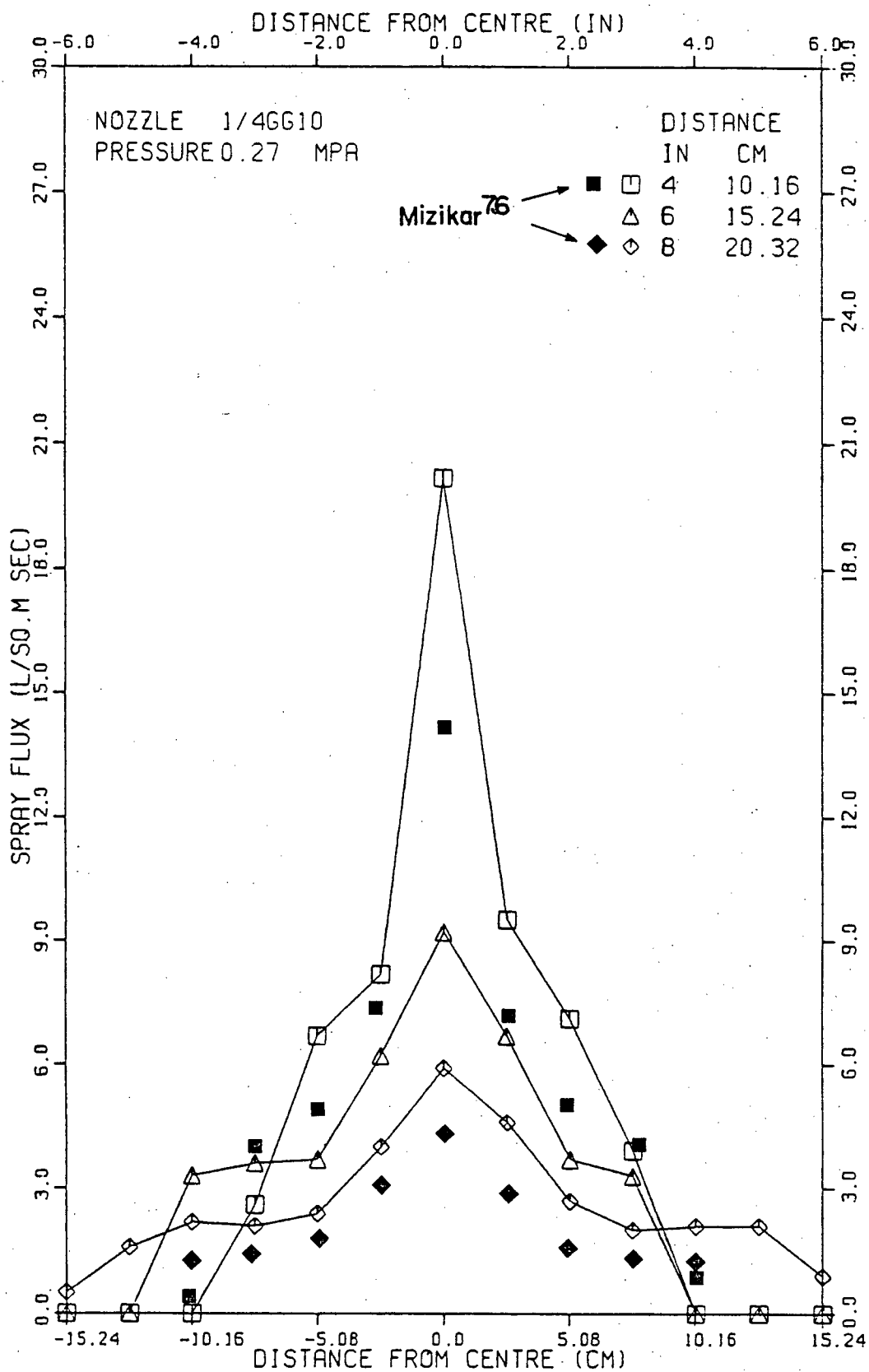


Figure 39 Effect of distance at constant pressure for a 1/4.GG 10 nozzle, for a spray pressure of 0.27 MPa.

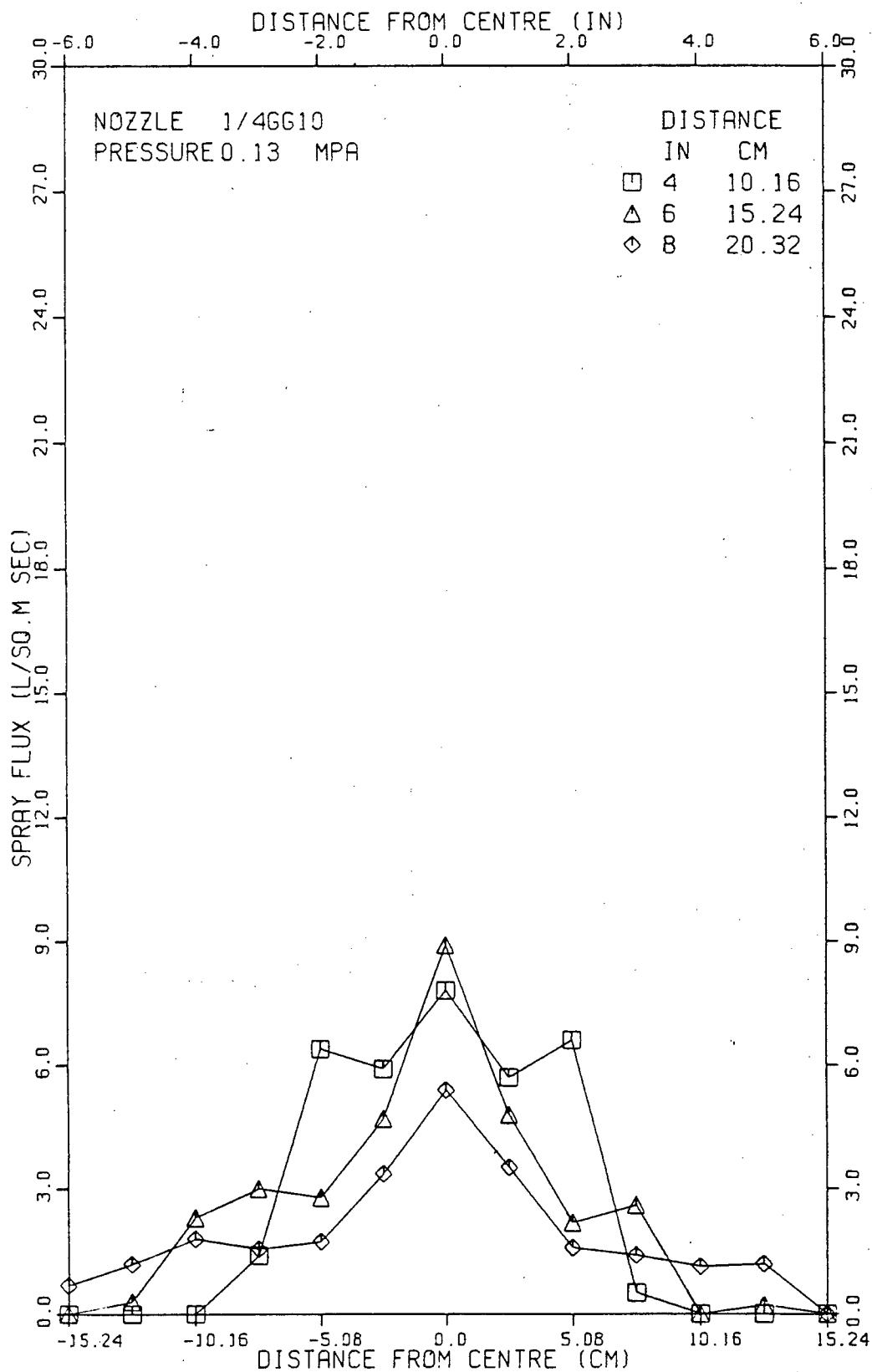


Figure 40 Effect of distance at constant pressure for a
14 GG 10 nozzle, for a spray pressure of 0.13 MPa.

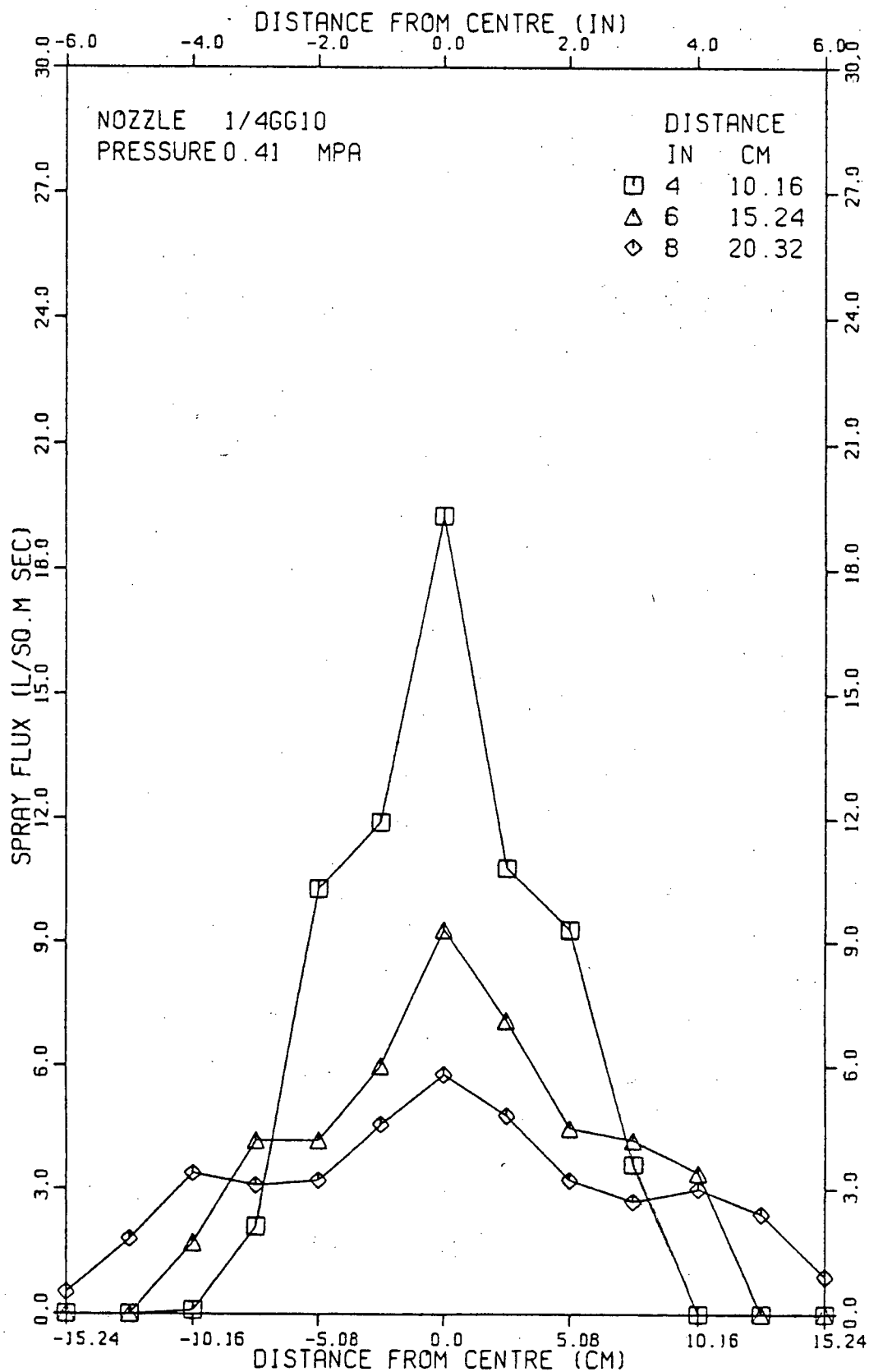


Figure 41 Effect of distance at constant pressure for a
1/4 GG 10 nozzle, for a spray pressure of 0.41 MPa.

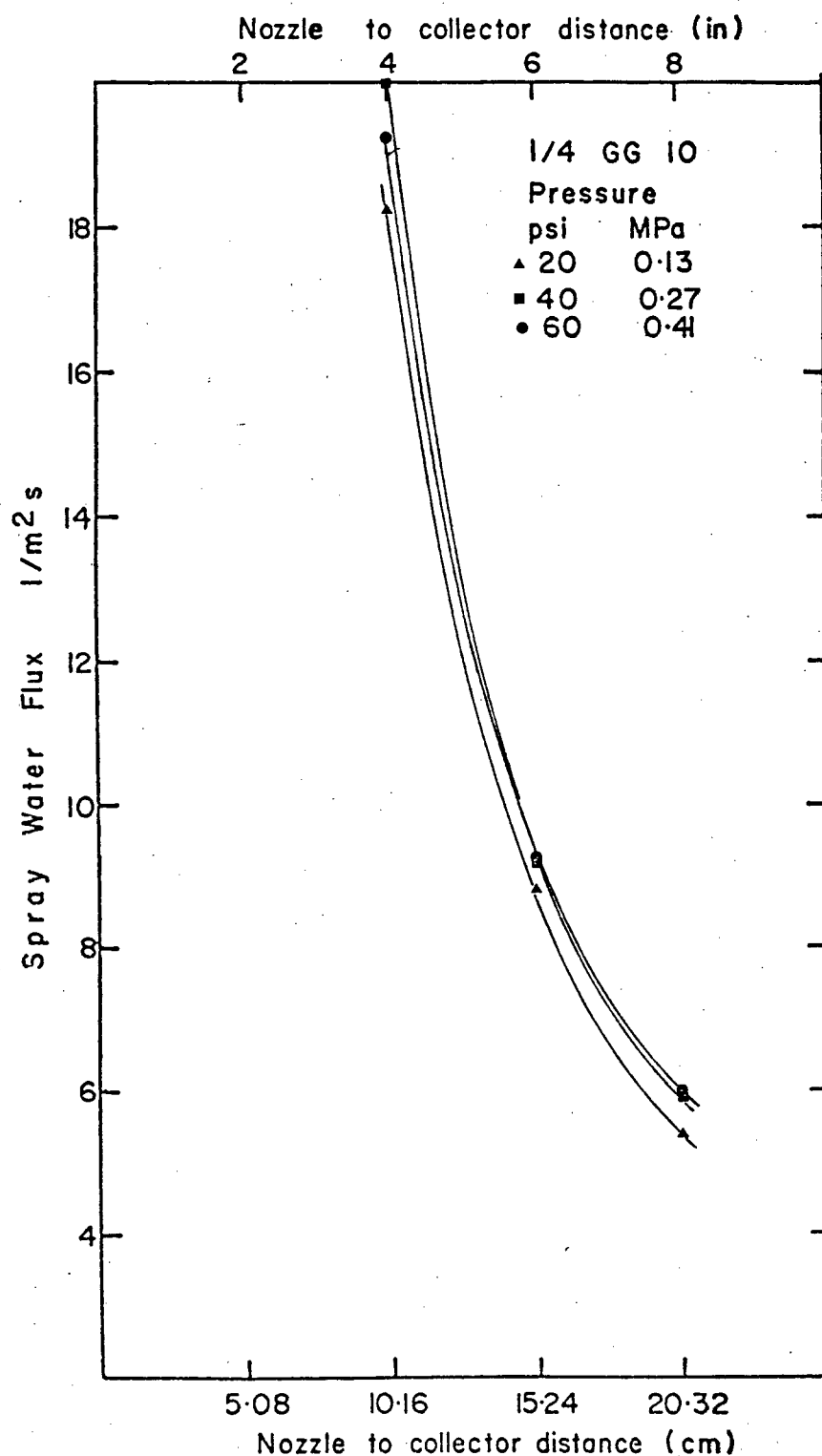


Figure 42 Variation of spray water flux with pressure and distance at the centre of the spray produced by a 1/4 GG 10 nozzle.

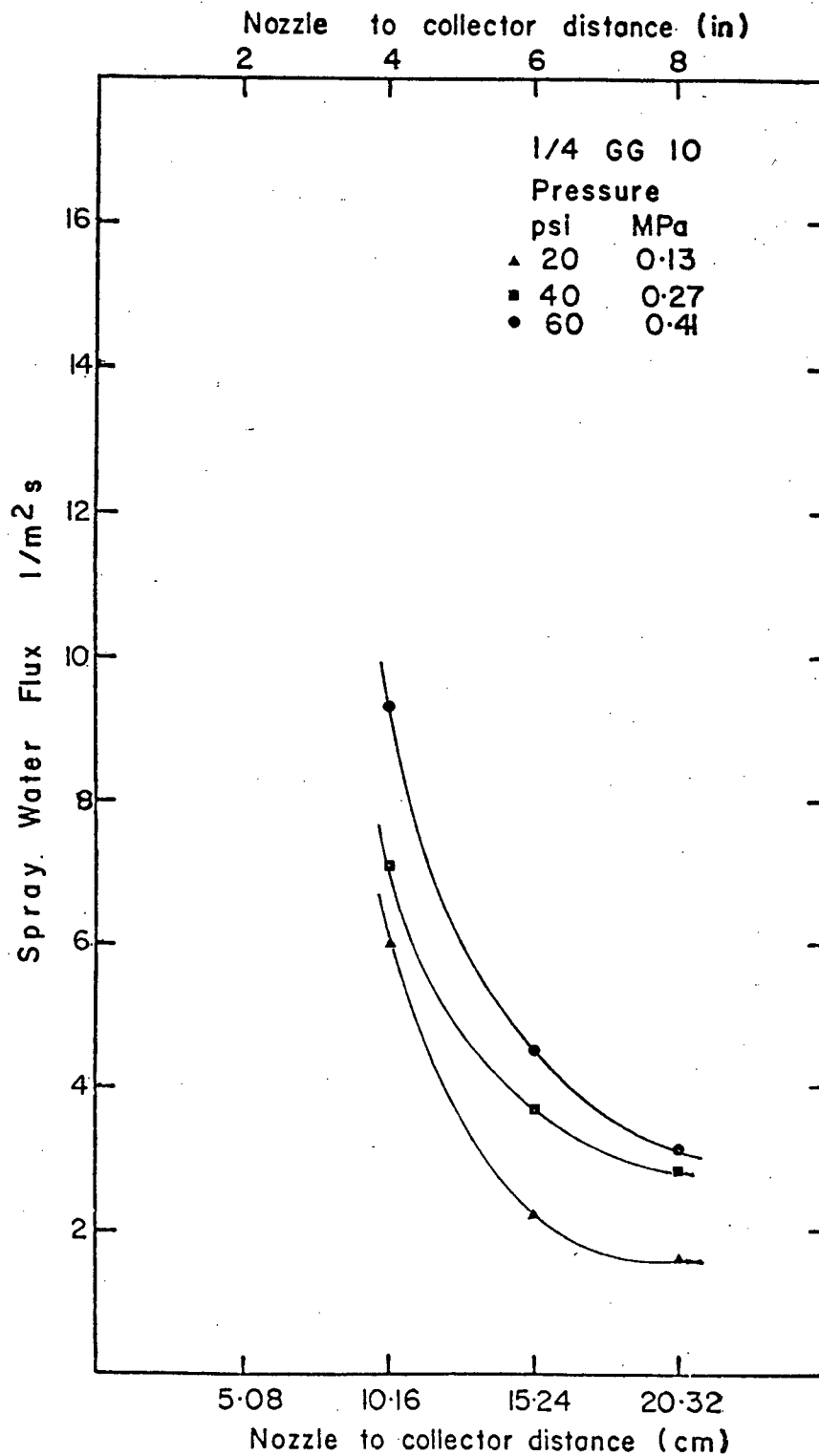


Figure 43 Variation of spray water flux with pressure and distance 5.08 cm from the centre of the spray produced by a 1/4 GG 10 nozzle.

of 2.54 cm (1 in) above and below the axis of the central collector tube. The results of these measurements have been tabulated in Appendix I. Contour maps and three-dimensional representations of the spray flux patterns are given in this section.

5.1.1.2.1 Water Fluxes Obtained with Type A Collectors

Spray flux contour maps for a constant spray pressure of 0.41 MPa (60 psi) and for nozzle distances of 10.16 cm, 15.24 cm, and 20.32 cm (4, 6 and 8 in) are shown in Figures 44, 45 and 46, respectively. The markings on the contours represent 10 times the spray flux in $l/m^2 s$. An increase in the spray coverage as the nozzle distance is increased can be observed from these Figures. In addition, it can be seen that the contours show a considerable amount of circular symmetry about the centreline of the spray. Contour maps of the spray fluxes for the other conditions under which the measurements were carried out are given in Appendix II. Three dimensional representations of the data have also been produced, and one such representation of the spray map for a nozzle distance of 15.24 cm (6 in) and a spray pressure of 0.27 MPa (40 psi) is shown in Figure 47. The sharp peak in the middle of the spray is evident in the Figure, as are the plateaus in the distributions at a distance approximately

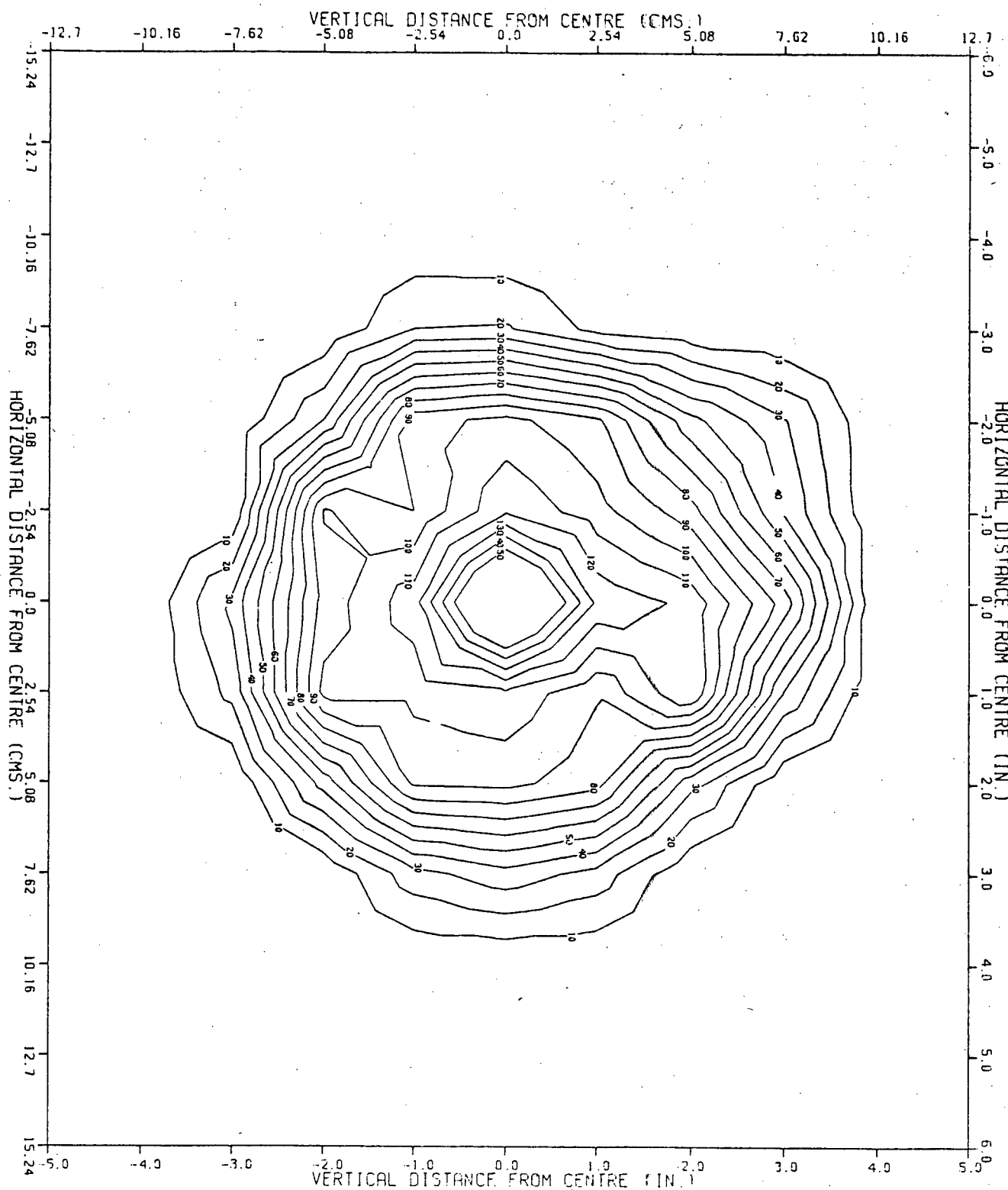


Figure 44 Spray flux contour maps for a 1/4 GG 10 nozzle for a nozzle distance of 10.16 cm and spray pressure of 0.41 MPa (Type A collectors).

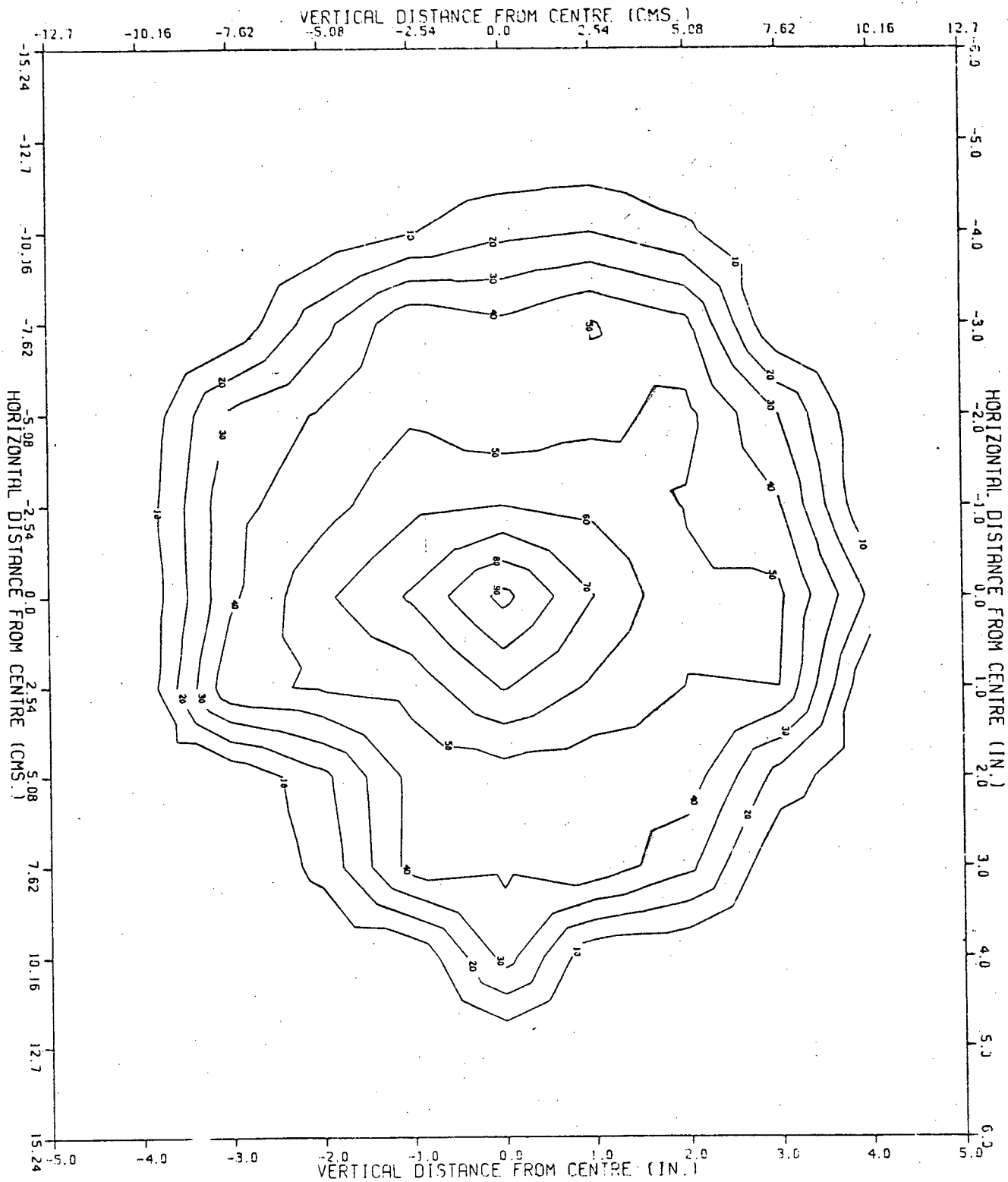


Figure 45 Spray flux contour maps for a 1/4 GG 10 nozzle for a nozzle distance of 15.24 cm and spray pressure of 0.41 MPa (Type A collectors).

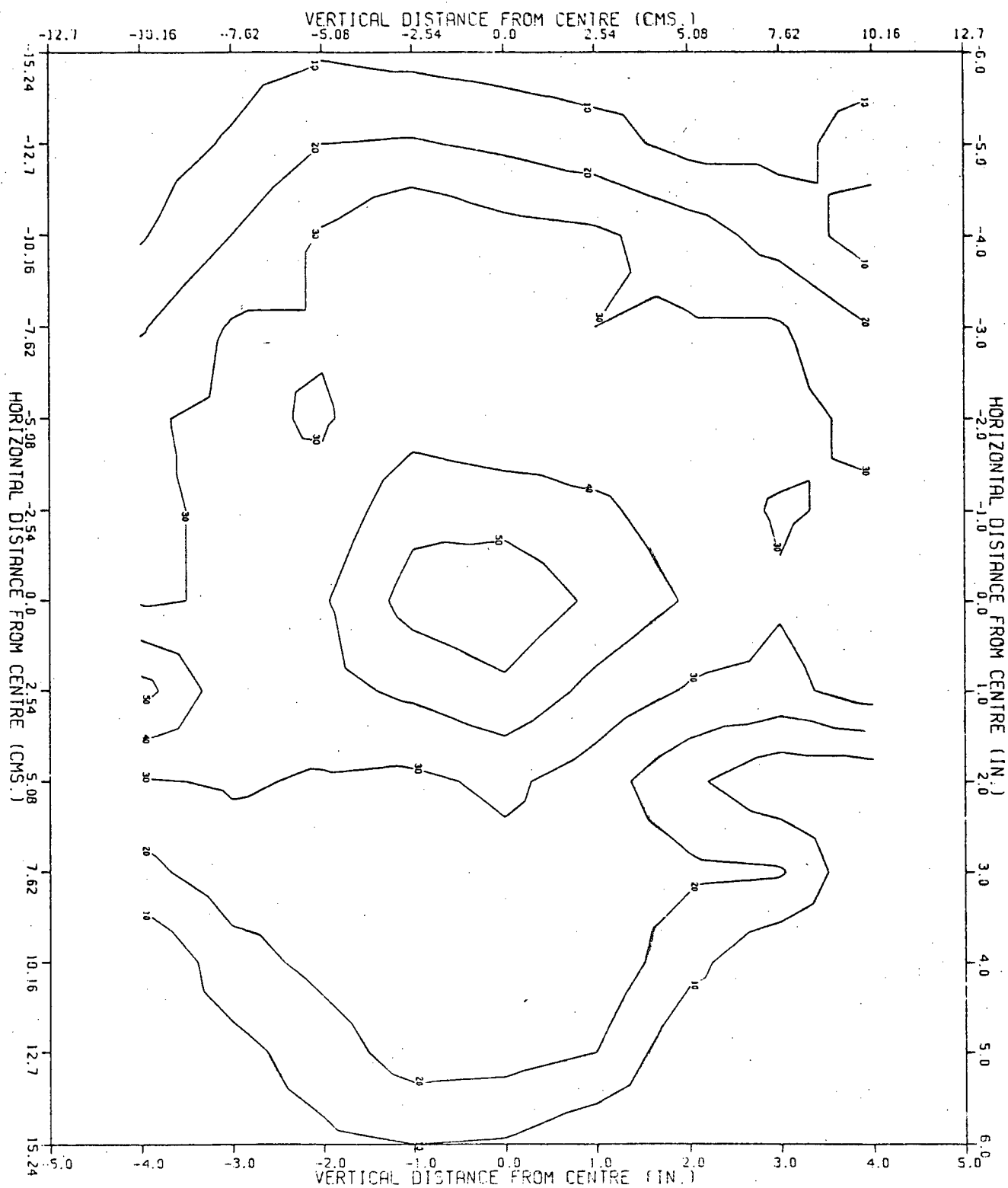


Figure 46 Spray flux contour maps for a 1/4 GG 10 nozzle for a nozzle distance of 20.32 cm and spray pressure of 0.41 MPa (Type A collectors).

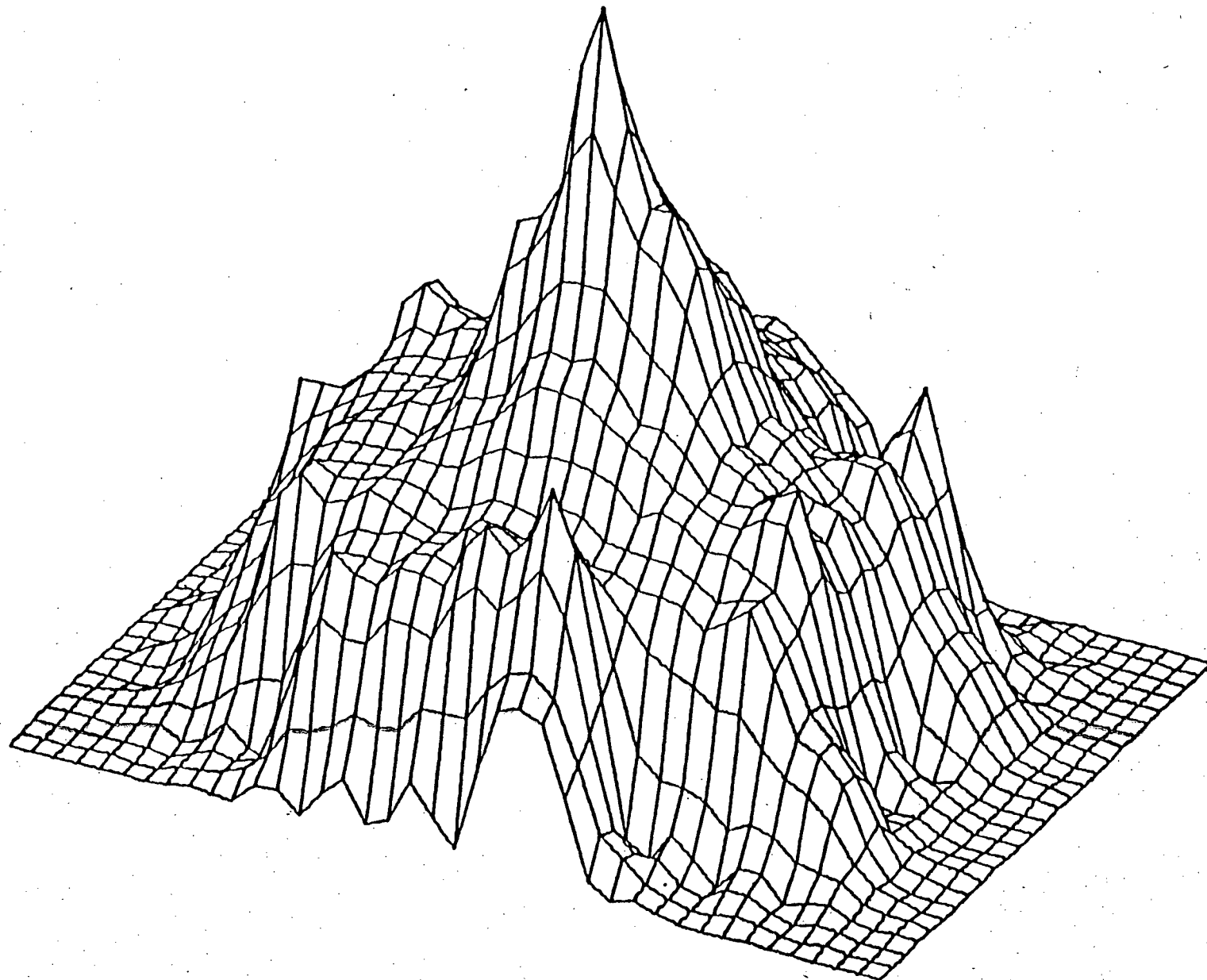


Figure 47 Three dimensional representation of the spray fluxes for the 1/4 GG 10 nozzle for a nozzle distance of 15.24 cm and spray pressure of 0.27 MPa.

halfway between the centre and the edge of the spray. Further on towards the edge of the spray, a sharp drop in the spray flux is observed. This Figure can be compared to Figure 31 effectively rotated about the central axis in the form of a cone. Spray flux representations similar to Figure 47 for other spray conditions are given in Appendix II.

5.1.1.2.2 Water Fluxes Obtained with Type B Collectors

From an examination of the Tables in Appendix I, it can be seen that there is considerably more water collected by the Type B collectors than with the Type A collectors, under identical spraying conditions. This is a direct result of the water flowing downward through the spray, adjacent to the sprayed face. In addition, a ring of water surrounds the sprayed area and flows downward just outside the area being directly sprayed. A contour map of the spray fluxes obtained for the 1/4 GG 10 nozzle for a spray pressure of 0.41 MPa (60 psi) and at a distance of 10.16 cm (4 in) is given in Figure 48. Comparing this Figure with Figure 44 shows that there is a higher water flux in the middle of the spray. Additionally, there are a large number of closely spaced contours near the top and the sides of the contour map. These correspond to the water flowing down outside

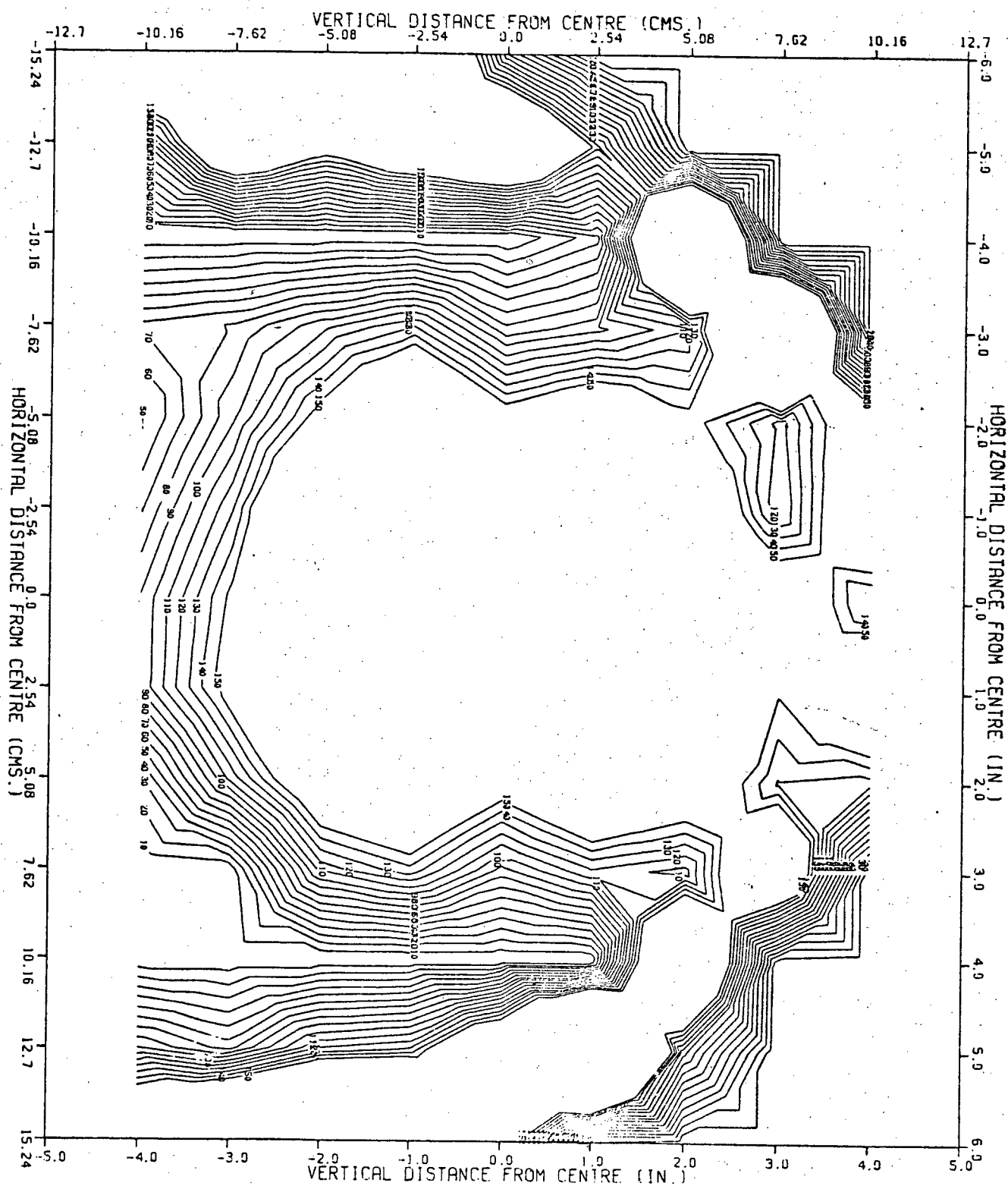


Figure 48 Spray flux contour map for a 1/4 GG 10 nozzle for a spray pressure of 0.41 MPa and nozzle distance of 10.16 cm (Type B collectors).

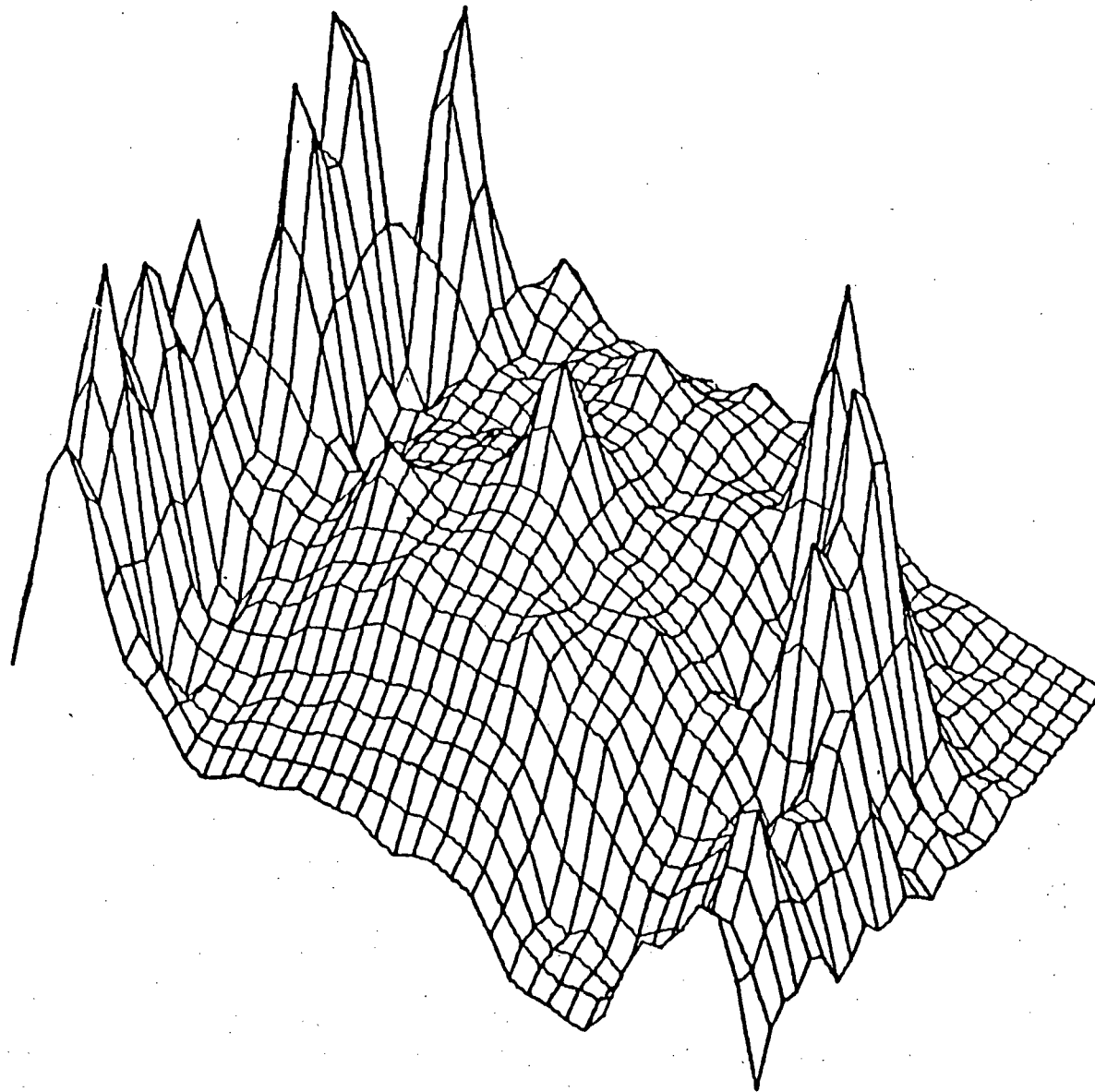


Figure 49 Three dimensional representation of the spray fluxes for a 1/4 GG 10 nozzle, for a spray pressure of 0.13 MPa and a nozzle distance of 10.16 cm (Type B collectors).

the sprayed area. This effect is graphically illustrated (Figure 49) by a three dimensional view of the spray flux map obtained for a spray pressure of 0.13 MPa (20 psi) at a distance of 10.16 cm (4 in) from the nozzle. The small peak in the centre corresponds to the peak in the sprayed cone discussed earlier. The much higher peaks toward the outside of the spray represent the regions of water flowing downward, surrounding the sprayed cone. Spray flux contour maps and three dimensional representations obtained for other spraying conditions are given in Appendix II.

5.1.2 Other Full Cone Nozzles - Spray Fluxes with Type A Collectors

Other full cone nozzles for which spray flux measurements were made include some with a higher capacity, and some with lower capacities than the 1/4 GG 10 nozzle for the same spray pressure. Nozzles with the lower capacities were the Spray Systems, Co. 1/8 GG 5, 1/8 GG 6 SQ and the 1/4 GG 6.5 nozzles, and for these nozzles, measurements were made at four different spray pressures. The horizontal centreline spray fluxes measured for the 1/8 GG 5 nozzle at spray distance of 10.16 and 15.24 cm (4 and 6 in) respectively are given in Figures 50 and 51. The distribution of the spray water flux exhibits a sharp peak in the centre, particularly at pressures up to 0.41 MPa (60 psi). In Figure 51, for a nozzle-collector distance of

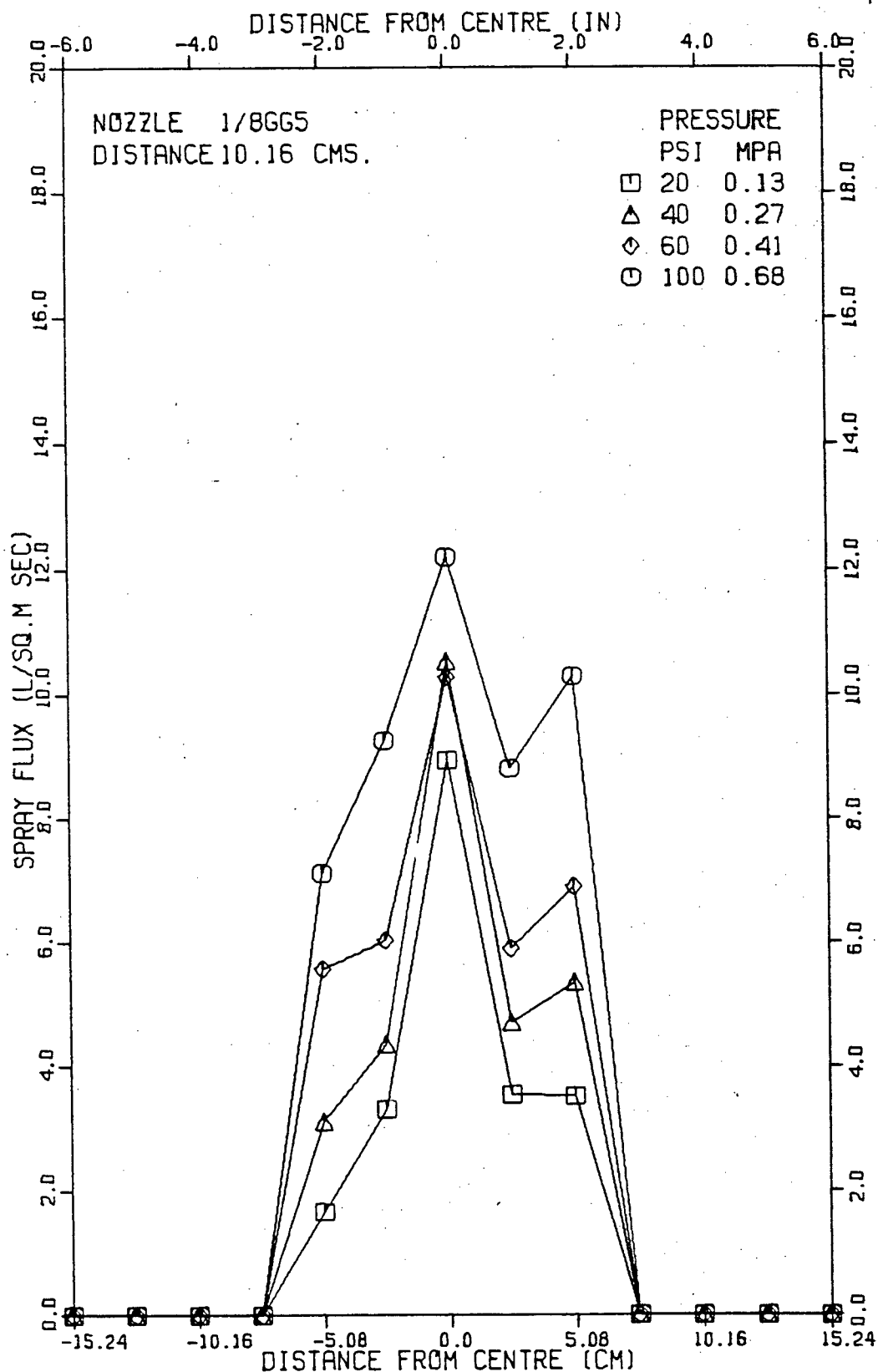


Figure 50 Horizontal centreline spray flux profiles for a 1/8 GG 5 nozzle, at a nozzle distance of 10.16 cm.

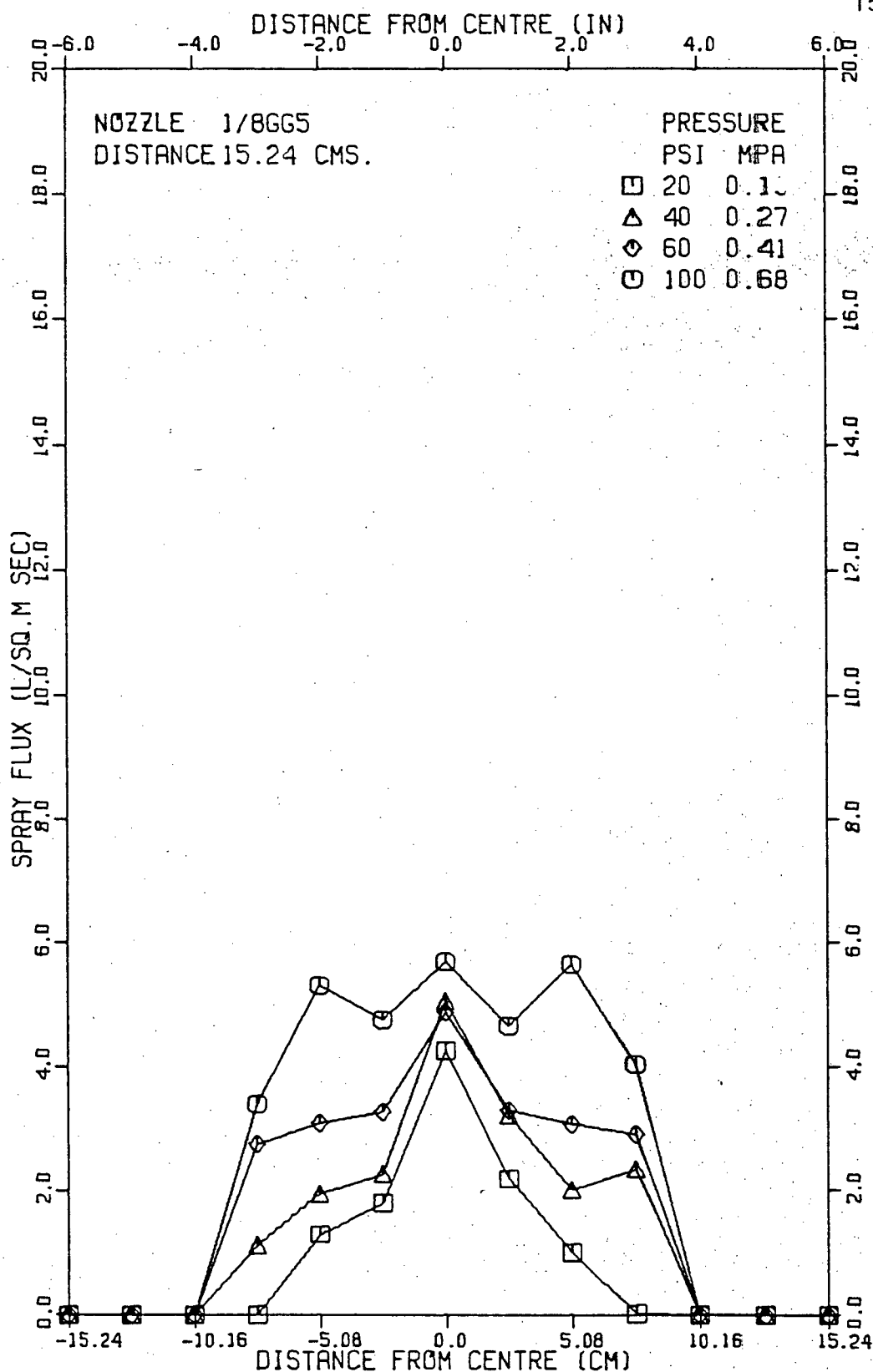


Figure 51 Horizontal centreline spray flux profiles for a 1/8 GG 5 nozzle, at a nozzle distance of 15.24 cm.

15.24 cm, the spray water flux is markedly lower. In the central portions of the spray, the spray flux tends to be more uniform for the higher pressures of 0.41 MPa and 0.68 MPa (60 and 100 psi).

The results of measurements made with the 1/4 GG 6.5 and 1/8 GG 6 SQ nozzles are given in Figures 52, 53 and 54. Peaks in the spray flux distributions are present in all three Figures. Plateaus appear in the distributions at the larger distances. Even at the nozzle distance of 15.24 cm (6 in), the distribution of the spray water is uneven in the central portion of the spray. The results obtained for the nozzles investigated with flow rates higher than those of the 1/4 GG 10 nozzle now follow.

Spray characteristics for the 1/4 GG 10 SQ and the 1/4 GG 12 SQ nozzles, which show characteristics essentially the same as those obtained for the 1/4 GG 10 nozzle, are tabulated in Appendix I. The horizontal centreline spray profiles obtained are given in Appendix II.

When higher capacity flow nozzles were being studied, the high flow rates involved caused large pressure drops in the water delivery system. As a consequence, the maximum available pressure at the nozzle was lowered, and the measurements were carried out only at low pressures. The

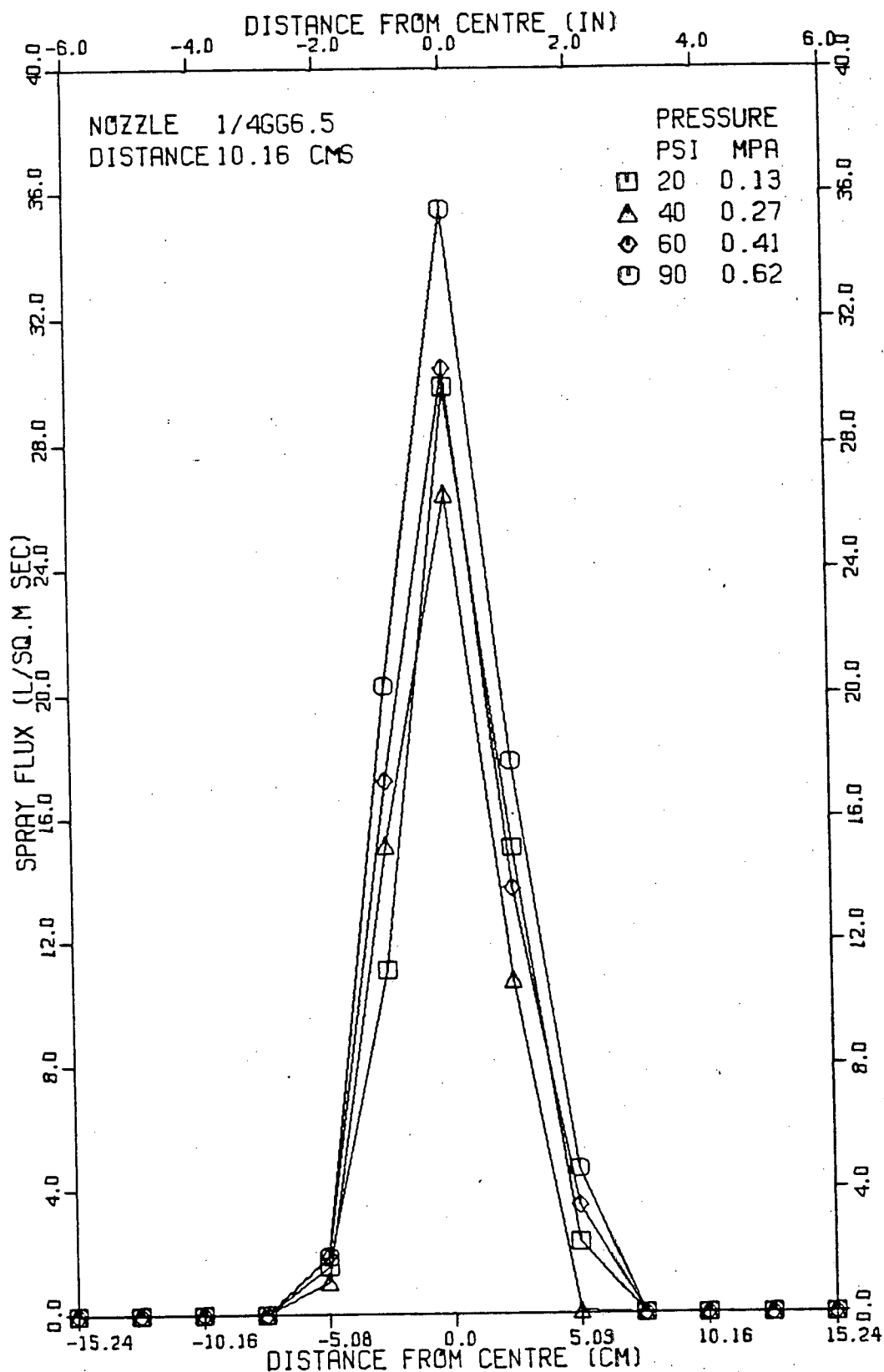


Figure 52 Horizontal centreline spray flux profiles for a 1/4 GG 6.5 nozzle, at a nozzle distance of 10.16 cm.

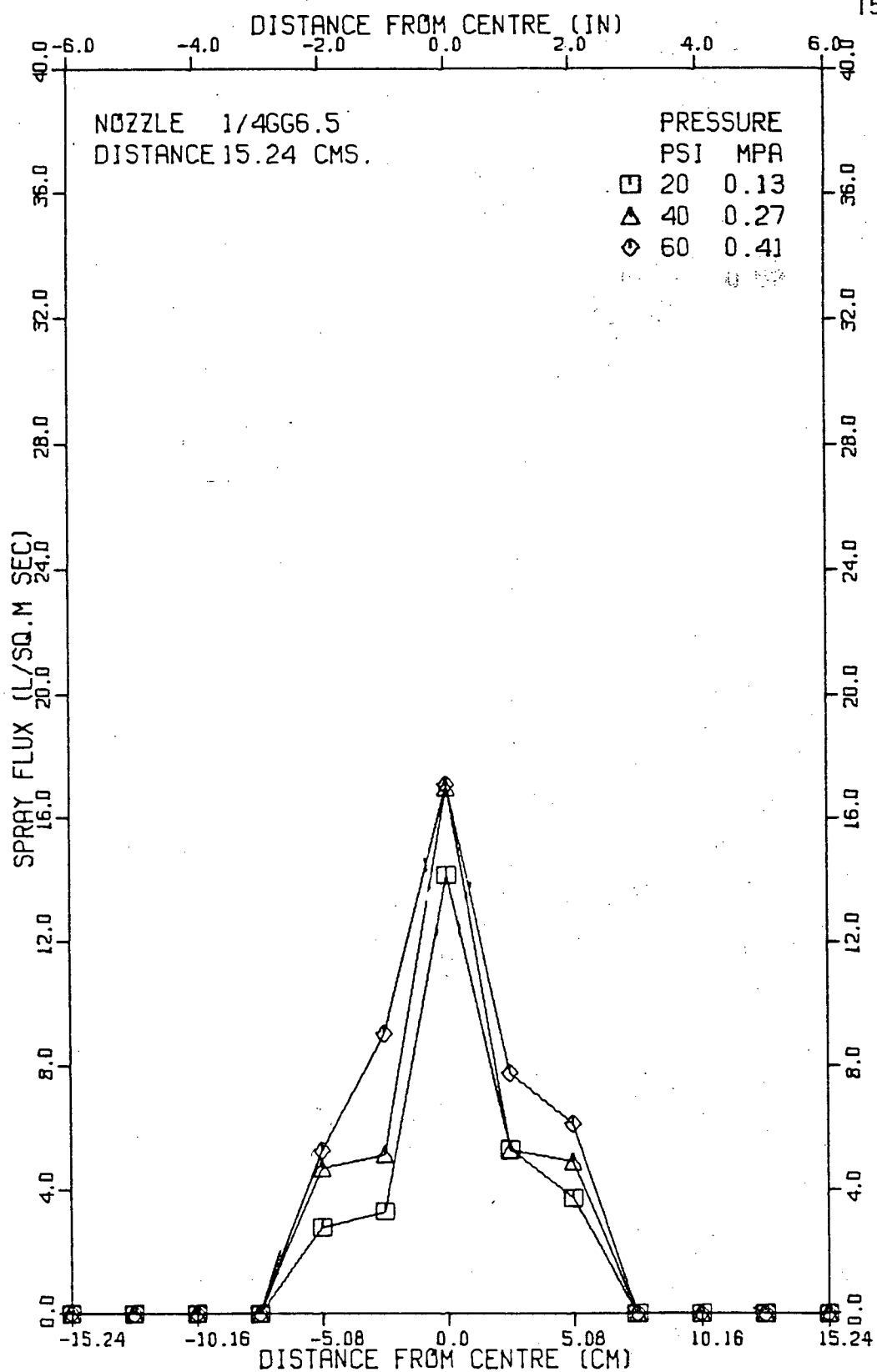


Figure 53 Horizontal centreline spray flux profiles for a 1/4 GG 6.5 nozzle, at a nozzle distance of 15.24 cm.

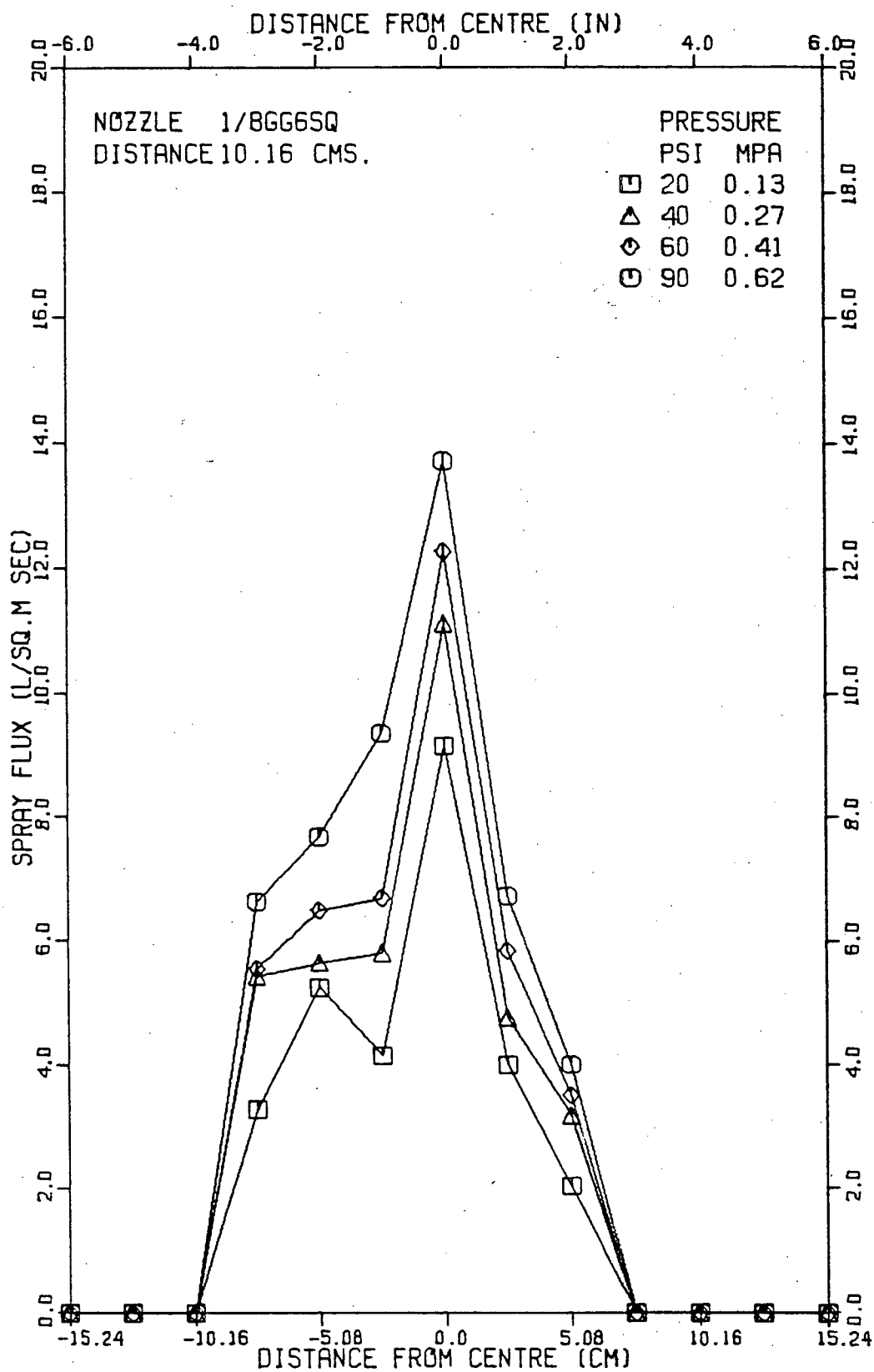


Figure 54 Horizontal centreline spray flux profiles for a 1/8 GG 6 SQ nozzle, at a nozzle distance of 10.16 cm.

results of measurements made on the 3/8 HH 18 SQ nozzle at 0.13 and 0.2 MPa (20 and 30 psi) are included in Appendices I and II. The spray characteristics of these nozzles are similar to those of the full cone nozzles discussed earlier. From measurements made on the 1/4 HH 14.5 SQ nozzles, as shown in Figures 55 and 56, it is observed that even at nozzle distances of only 15.24 cm (6 in), the majority of the sprayed area has an even distribution of the spray flux.

Uniform spray flux distributions can also be observed with wide angle nozzles, as evidenced by measurements made on the 1/4 GG 14 W nozzle, shown in Figure 57. At the lower pressure, the spray flux distribution becomes uneven, probably due to the lack of enough pressure driving force to break up the water flow into uniform droplets.

5.1.3 Vee-jet or Flat-jet Nozzles; Measurements Made with Type A Collectors

The nozzles provide a flat spray pattern (2 to 5 cm thick for the smaller nozzles) and are primarily used in slab casting applications. A few of these nozzles were investigated to determine their spray characteristics. Due to the high flow rates involved, measurements were made only at lower pressures. In most cases, fine spray droplets were not formed due to low operating pressures,

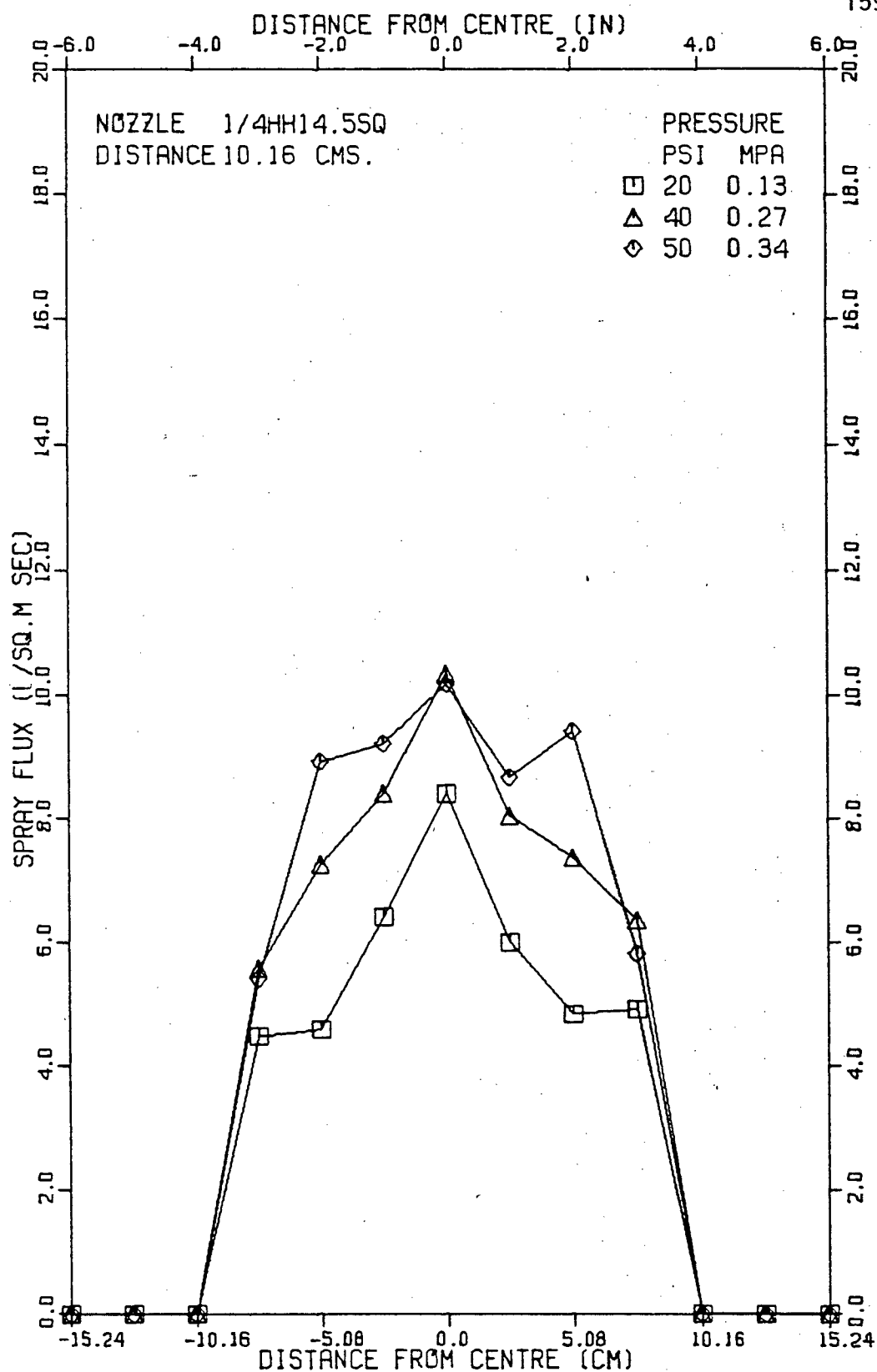


Figure 55 Horizontal centreline spray flux profiles for a 1/4 HH 14.5 SQ nozzle at a nozzle distance of 10.16 cm.

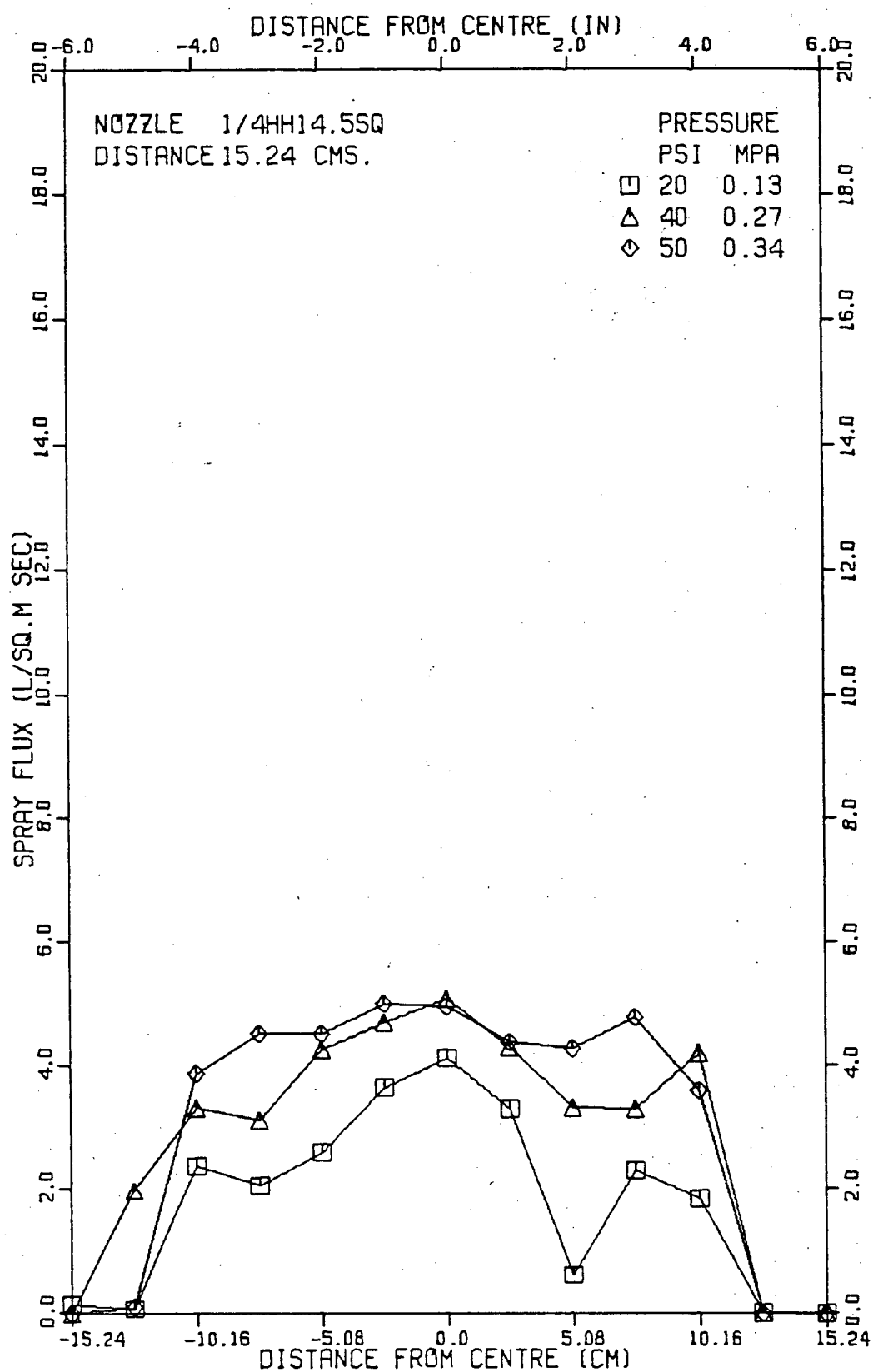


Figure 56 Horizontal centreline spray flux profiles for a
1/4 HH 14.5 SQ nozzle at a nozzle distance of 15.24 cm.

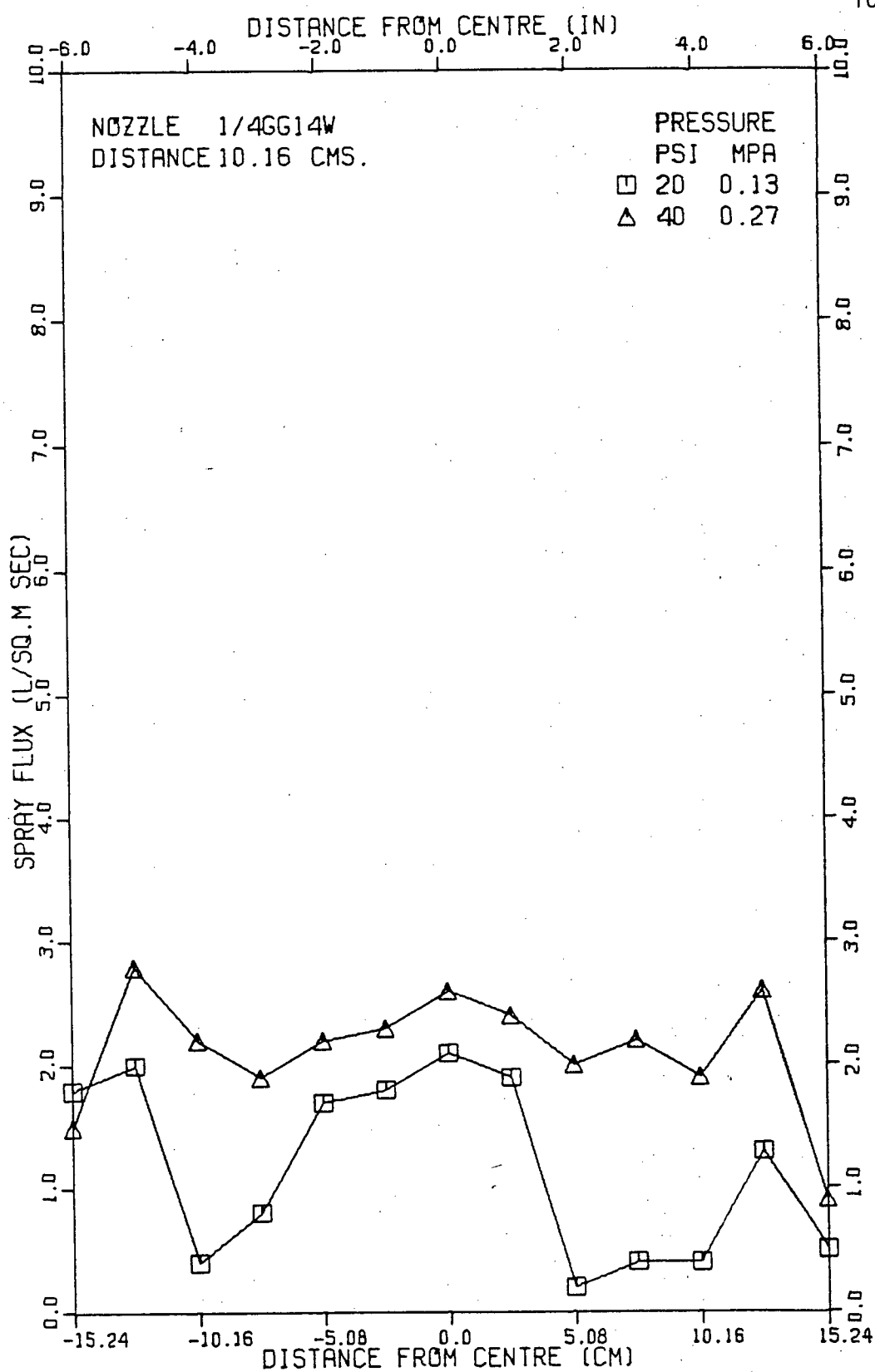


Figure 57 Horizontal centreline spray flux profiles for a 1/4 GG 14 W nozzle, at a nozzle distance of 10.16 cm.

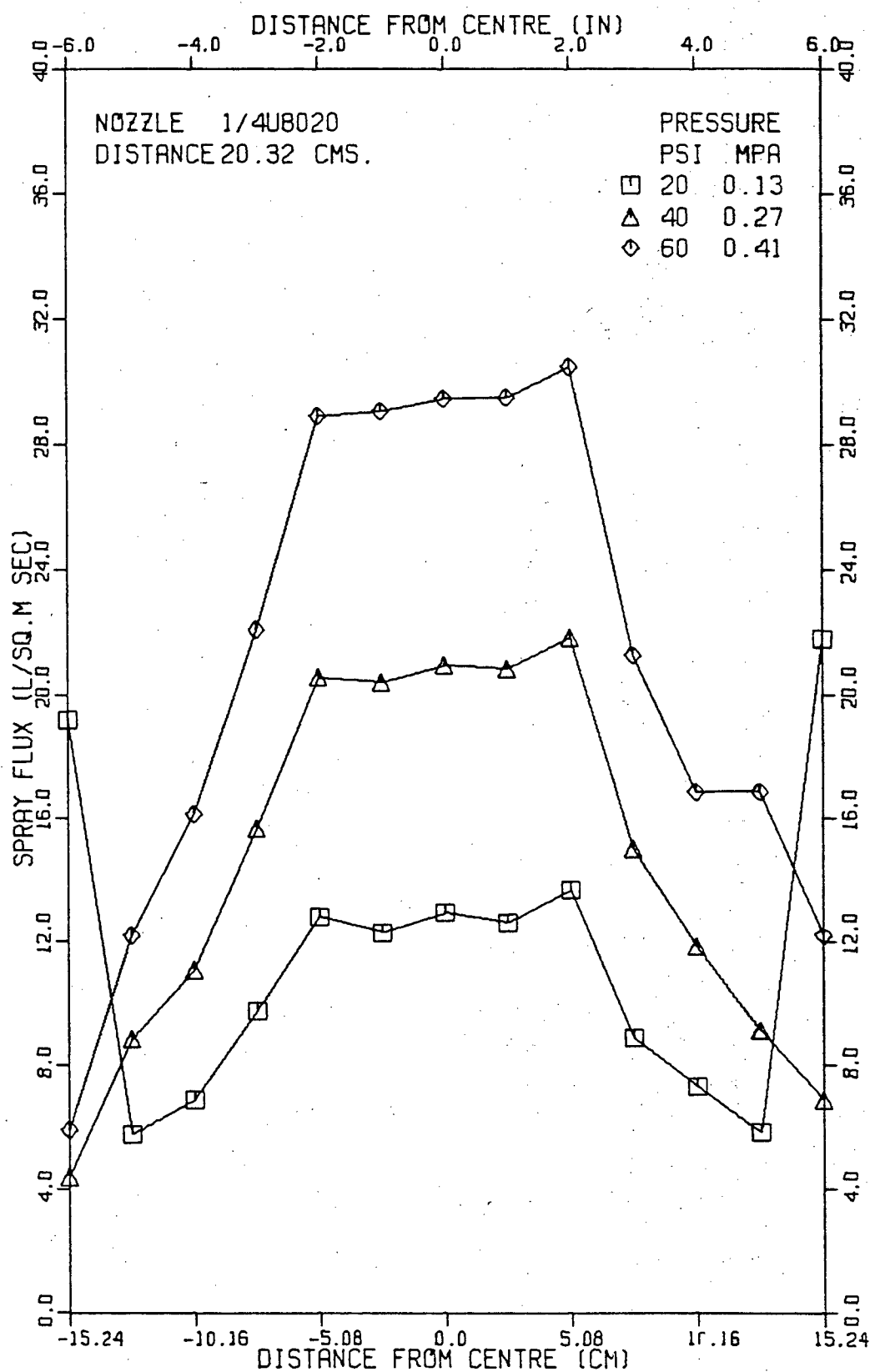


Figure 58

Horizontal centreline spray flux profiles for a
1/4 U8020 nozzle at a nozzle distance of 20.32 cm.

and therefore, no meaningful measurements could be obtained, particularly for the small nozzle to collector distances used in this work.

The horizontal centreline spray flux distributions obtained for the 1/4 U 8020 nozzle is given in Figure 58, for a nozzle to collector distance of 20.32 cm (8 in). It can be observed from this Figure that in the central region of the spray pattern, there is a fairly uniform distribution of the spray flux, tapering off towards the edges. This feature is useful when overlapping sprays are used to cool slabs of large widths.

5.2 Measurements of Heat-Transfer Coefficients

The heat-transfer coefficients reported in this section pertain to the heat transfer between water sprays discussed in the previous section and a heated AISI 304 stainless steel surface at temperatures in excess of 800° C. The majority of the results reported were measured during the cooling of the heated steel surface from an initial temperature of about 1100° C.

5.2.1 General Observations of the Cooling Process

Visual and aural observations of the cooled surface were made during the spray cooling and are discussed below.

In the early stages of cooling of the probe surface, when the "film boiling" regime was present, there was a low hissing noise emanating from the surface. Visual observations showed that the surface was dry and droplets could be seen bouncing away from it. On further cooling, when the transition point was reached, the hissing noise rose very sharply in intensity. Patches of liquid could be seen remaining on the surface and voluminous amounts of steam were produced. On cooling further, this stage was followed by a stage wherein the entire sprayed surface showed a wetted appearance and the amount of steam production decreased, with a corresponding lowering of the intensity of the hissing noise.

Under normal conditions, the wetting of the sprayed surface spread out from the region of the highest spray water flux in the central region of the spray, towards the edges of the spray cone in a symmetrical fashion. The presence of any semi-adherent scale or foreign matter on the surface caused a drastic change in the pattern. When the scale was not completely detached from the surface, the area immediately around it turned black and was wetted sooner than the other regions. Whenever such matter was present on the surface of the measuring probe, this change in colour was also reflected in high cooling rates being recorded by the thermocouples close to the cooled surface.

Such conditions were observed to have a higher frequency of occurrence when the measuring probe had undergone a number of heating - cooling cycles. When such occurrences were observed, the measuring probe was discarded (as were the results of that run and a few before it), and a new probe made and installed for subsequent measurements.

Initially, a new probe had a highly polished surface. However, after one heating and cooling cycle, the probe surface was covered by a thin, smooth, grayish oxide layer. Subsequent heating and cooling cycles slowly caused this layer to change colour to a blackish-gray in non-uniform patches. With a blackish-gray oxide covering, high cooling rates of the surface were observed when spray cooling from high temperatures. Wetting of the surface was also seen to occur earlier at these spots as compared with other regions. Such occurrences were considered sufficient cause to discard the probe.

These observations demonstrated that changes in the appearance of the probe surface resulted in variations in cooling rates under identical spraying conditions, and thus contributed to the scatter of the data. Gross variations in the heat-transfer coefficients (up to a factor of 10) were observed with large changes in the surface conditions of the measuring probe. Great care was therefore necessary in

the measurements to obtain data with small scatter.

5.2.2 Validation of the Experimental Technique Used

An important point to note when introducing a measuring sensor into a system to measure transients is that it could change the state of the system. The problem can arise in the system used in this investigation, where thermocouples are imbedded in a solid to measure the heat flow within it. If sufficient care is not taken to minimize the effect of the thermocouple installation on the heat flow, appreciable errors could develop in the measurements. For this reason, the thermocouple wire sizes and holes drilled for their installation were kept small.

In order to ensure that the imbedded thermocouples had no significant effect on the heat flow, a set of experiments was conducted in which four sets of thermocouple wires were installed in the heat transfer probe. The ends of these thermocouples were placed at distances of 1.02, 2.03, 3.05 and 19.05 mm (0.04, 0.08, 0.12 and 0.75 in) respectively from the sprayed face of the probe. The temperature transients obtained from the thermocouple closest to the sprayed face were then used to calculate the temperature-time relationship within the probe during cooling. The calculated values were then compared to the measured values of temperature at the positions of the thermocouples remote

from the surface as specified above. The results are shown in Figures 59 and 60, in which the calculated and measured values of temperature within the heat-transfer probe are plotted at different times from the start of cooling. Excellent agreement was obtained between the calculated and measured values. The average heat-transfer coefficients for these runs were $1.05 \text{ kW/m}^2\text{K}$ and $1.88 \text{ kW/m}^2\text{K}$ (0.025 and $0.045 \text{ cal/cm}^2 \text{ sec } ^\circ\text{C}$) respectively. These fall in the range of heat-transfer coefficients measured in this study.

The thermocouple closest to the sprayed face would be expected to influence the heat flow to the cooled surface the most as compared to the others. This would lead to a situation in which the volume of material ahead of this thermocouple would cool rapidly, causing the thermocouple to exhibit faster cooling than would be the case if there were no barrier to the heat flow. Using the cooling curve obtained from this thermocouple to calculate the thermal history of the probe would cause lower temperatures to be calculated at the other positions of the other thermocouples as well. Such is certainly not the case, as can be observed from Figures 59 and 60. This phenomenon of the disturbance of the heat flow by the measuring sensor could be expected to have larger effects as the heat-transfer coefficient at the surface increases i.e., with high heat fluxes. Therefore, when much higher heat fluxes are encountered,

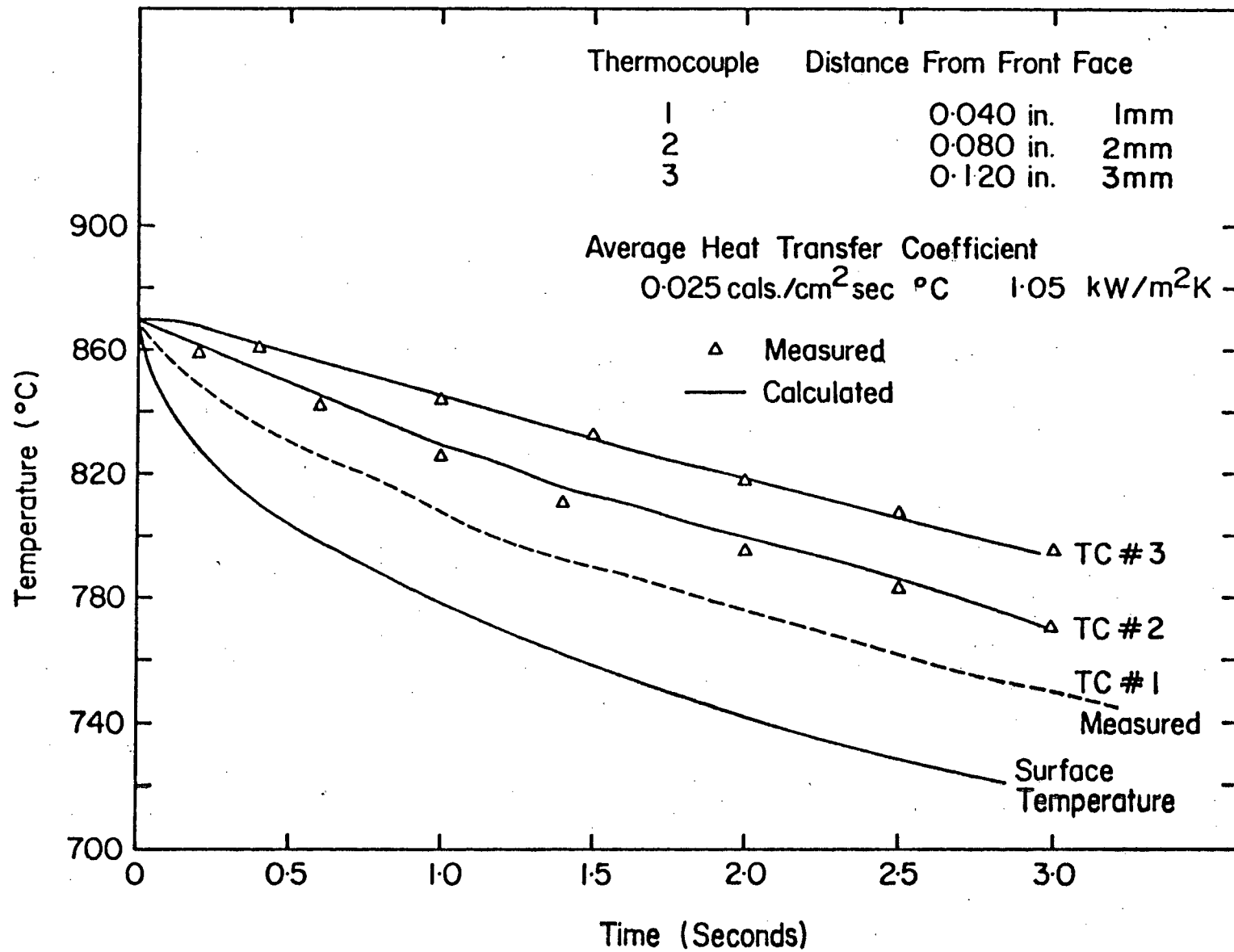


Figure 59 Comparison of calculated and measured temperatures, for an average heat-transfer coefficient of $1.05 \text{ kW/m}^2\text{K}$.

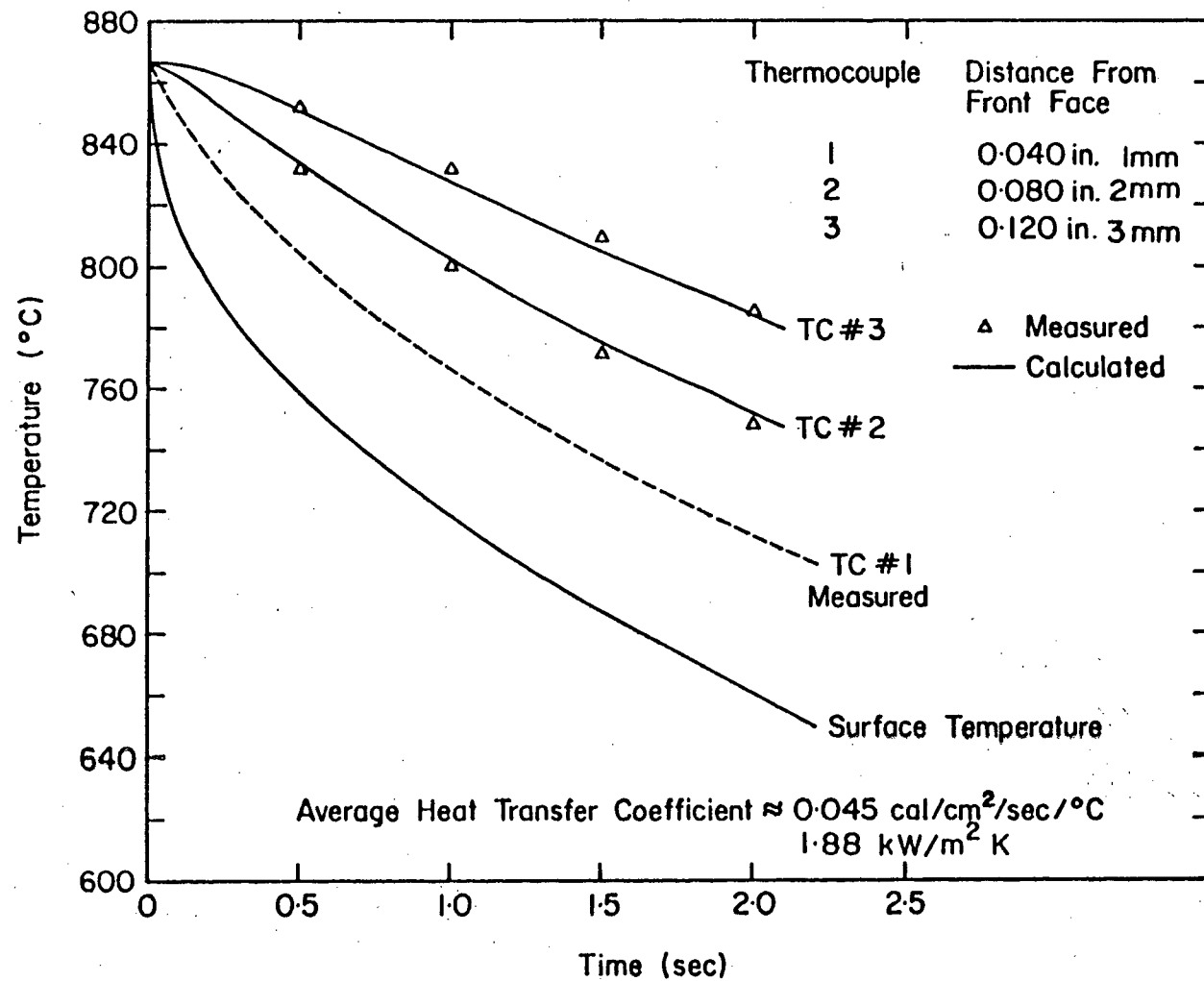


Figure 60 Comparison of calculated and measured temperatures, for an average heat-transfer coefficient of $1.88 \text{ kW/m}^2 \text{ K}$.

this method of measurement must be revalidated, as was done in this work.

5.2.3 Determination of the Initial Temperature Profiles

Temperature gradients of up to 10°C/cm (25°C/in) existed within the probe during heating, with the lower temperature at the sprayed face. These gradients were minimized prior to spray cooling by soaking the probe at temperatures with minimum heat input. However, since the temperatures within the probe were measured at different points by the embedded thermocouples, the temperature gradients within the probe could be incorporated into the mathematical analysis of the temperature transients as the initial condition. In the initial spray cooling runs, the temperature gradient in the sample was assumed to be linear along the probe axis. This caused anomalous heat-transfer coefficients to be determined for the first few time steps used in the calculations. This was attributed to the rearrangement of temperatures at various points within the probe in order to meet the requirements of the governing conduction equation. Subsequent measurements were then performed with four to five thermocouples inserted at various positions within the measuring probe to establish the initial conditions. These measurements showed that half of the magnitude of the temperature gradient was confined to the

first one-third of the length of the probe (towards the front face). Using this information to set up the initial temperatures within the probe as a function of the axial distance from the sprayed face reduced the anomalous bumps in the calculated heat-transfer coefficient vs. surface temperature relationship.

5.2.4 Results of Type I Experiments

The experimental results presented in this section were obtained with the sprayed steel surface mounted flush with the front of a vertical asbestos sheet. All the results presented in this section pertain to measurements made using a 1/4 GG 10 nozzle. The variation of the heat-transfer coefficients as a function of the spray water flux for the 1/4 GG 10 nozzle is presented in Figure 61 for a surface temperature of 850° C. These results are for measurements performed with operating spray pressures of 0.13, 0.27 and 0.41 MPa (20, 40 and 60 psi). In order to obtain different spray water fluxes at the probe surface, the nozzle was translated not only in a direction along the spray nozzle axis, but also in a direction perpendicular to it. This approach was taken in view of the fact that Mizikar⁷⁶ has reported that the angle of impingement of the spray droplets on the cooled surface had no effect on the heat-transfer coefficient for the same spray water flux. The results reported by Mizikar for this nozzle for two

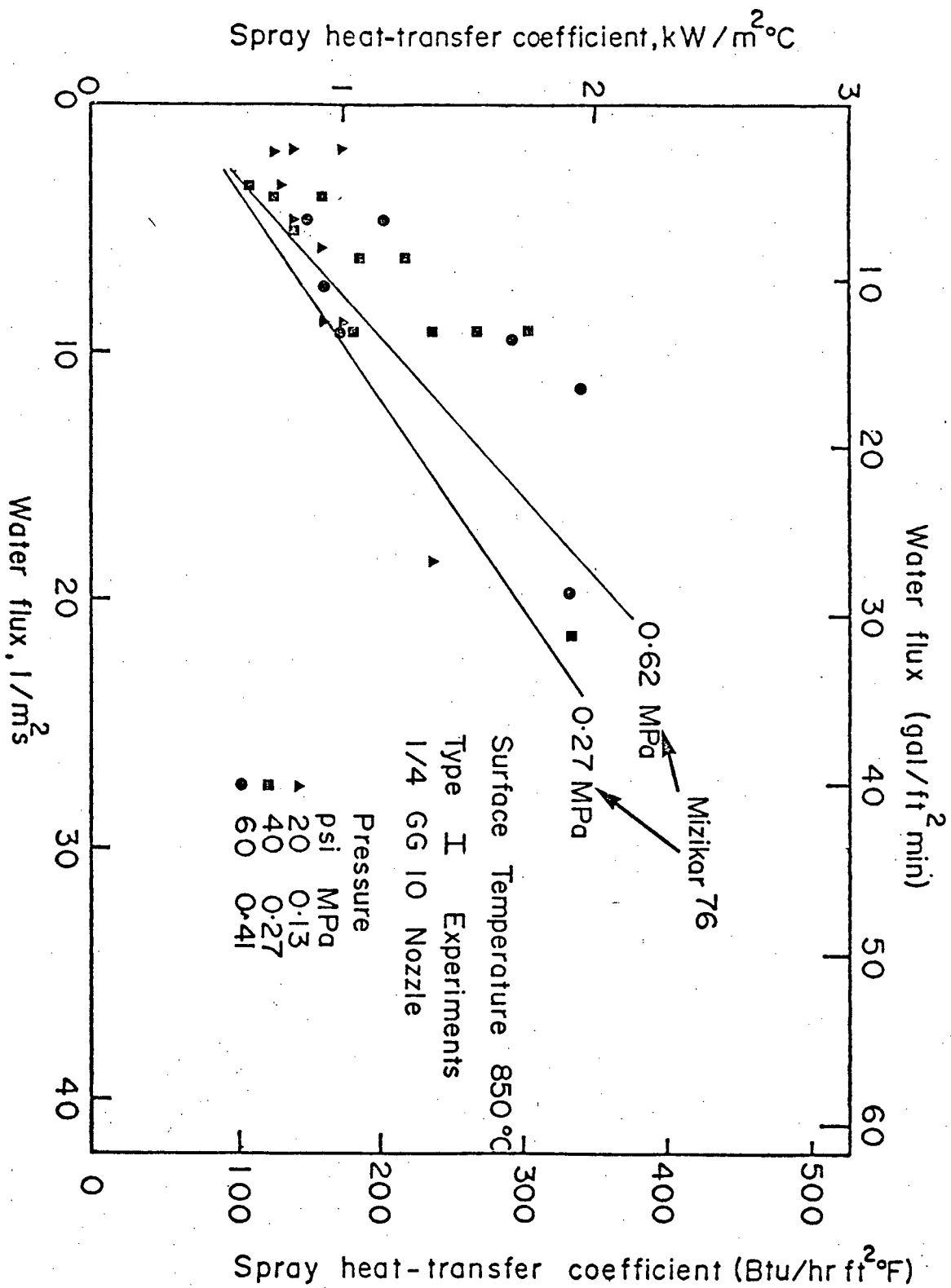


Figure 61 Variation of the heat-transfer coefficients with water flux for a surface temperature of 850°C (Type I Experiment).

different spray pressures of 0.27 and 0.62 MPa (40 and 90 psi) respectively are also plotted in Figure 61 as the two straight lines.

Whereas Mizikar⁷⁶ obtained a difference in the heat-transfer coefficients for the two spray pressures shown in this Figure, no such difference due to the effect of pressure is observed from the results of the present work. The present results give heat-transfer coefficients which are much higher, and have a much greater variability for the same spray flux than would be expected from the results of Mizikar.

Figure 62 presents results obtained for a surface temperature of 1000° C. The heat-transfer coefficient is again observed to be independent of the spray pressure. In addition, the heat-transfer coefficients for any given spray water flux are much higher than those reported by Mizikar for the highest spray pressure used in his work - 0.62 MPa (90 psi). A wide variability of the heat-transfer coefficients is again observed.

A comparison of the variation of the heat-transfer coefficients with surface temperatures for different spray fluxes is presented in Figure 63. From this Figure, it can be observed that the variation of the heat-transfer

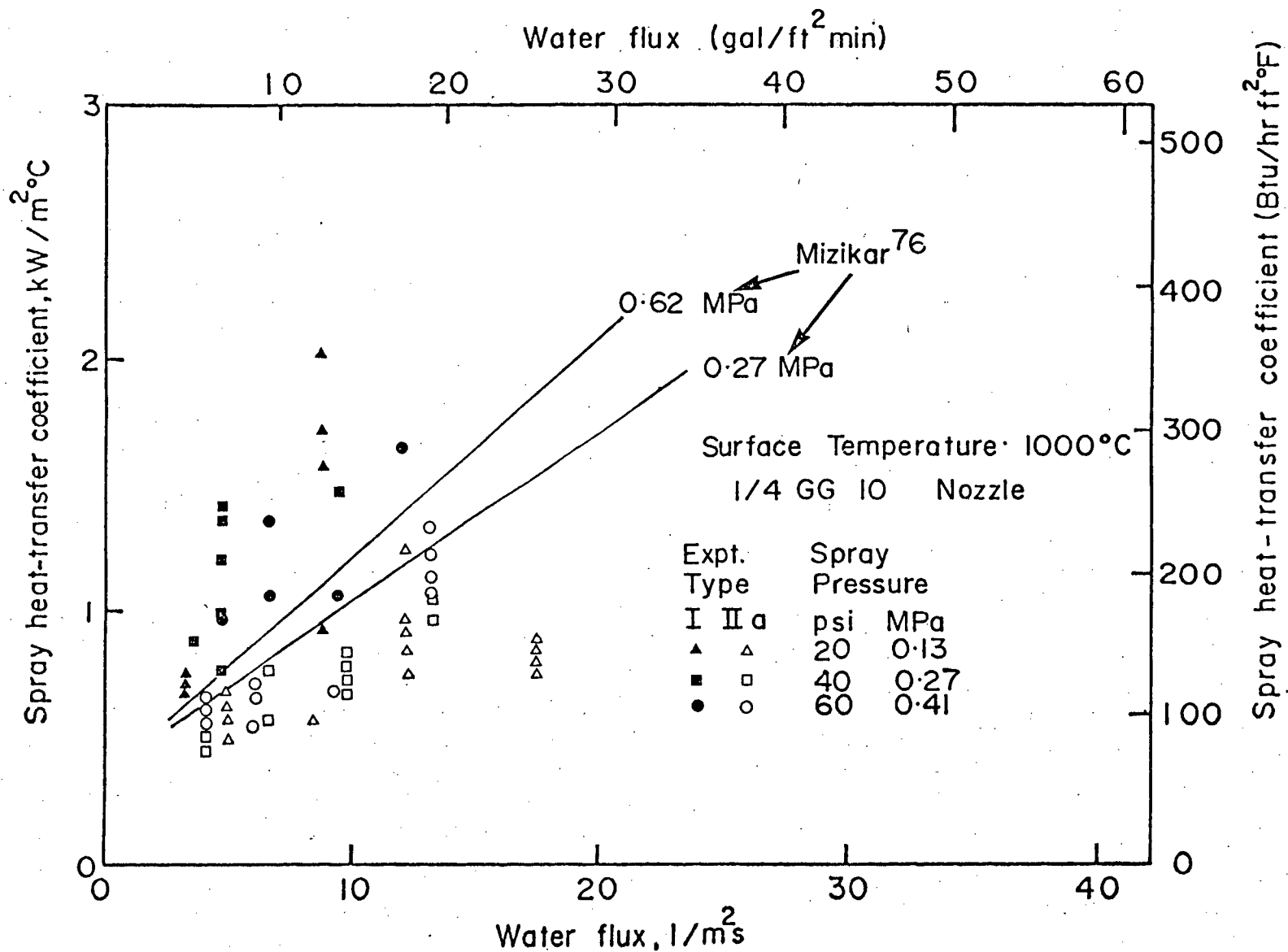


Figure 62 Variation of heat-transfer coefficients with water flux for a surface temperature of 1000°C (Type I and Type IIa Experiments).

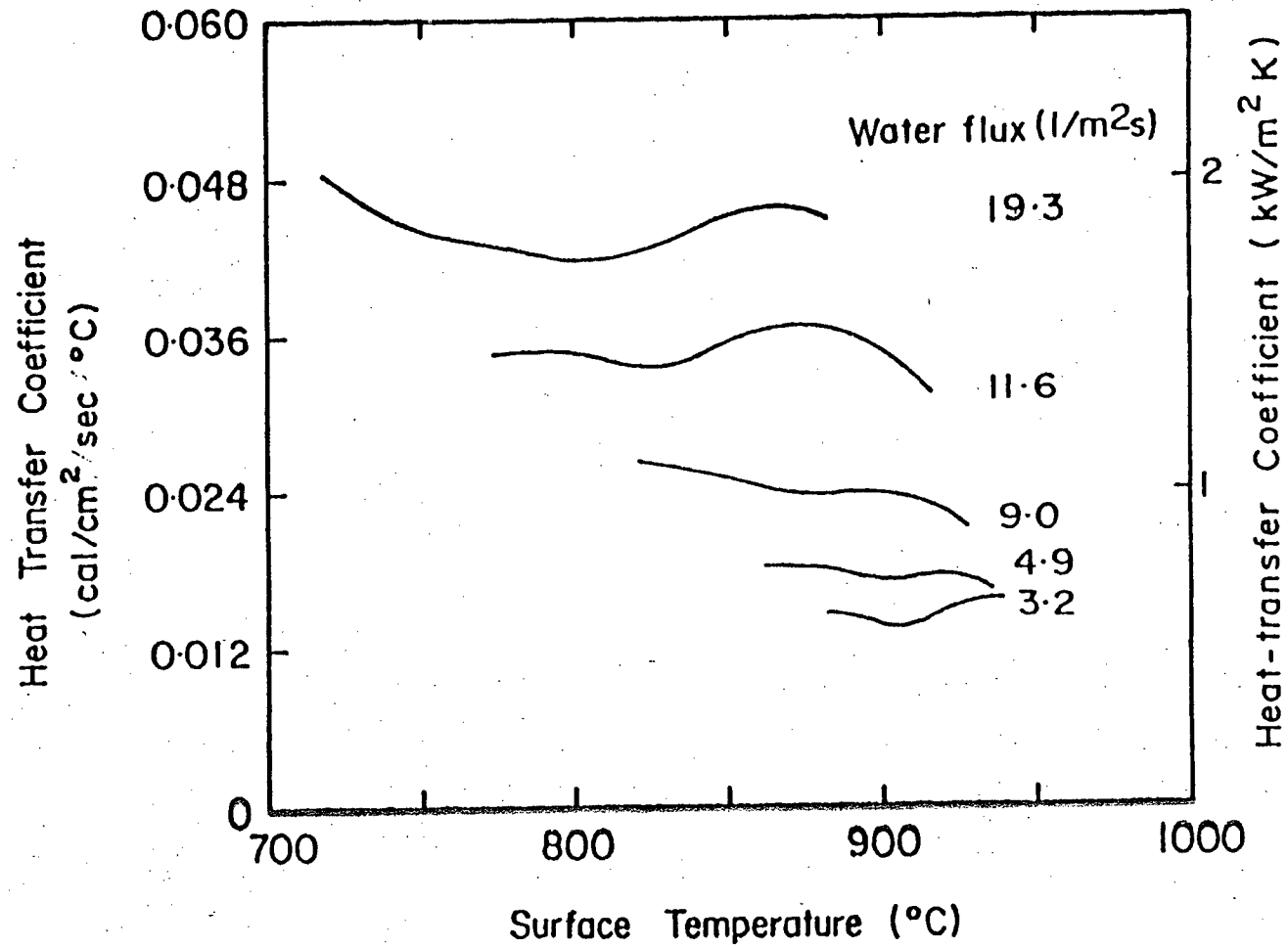


Figure 63 Variation of heat-transfer coefficients with surface temperature (Type I Experiments).

coefficients with temperature is small, but that at the higher spray flux of $19.3 \text{ l/m}^2\text{s}$, the heat-transfer coefficient increases slowly as the surface temperature drops below 850°C .

The relative insensitivity of the heat-transfer coefficients to the surface temperature at the lower water fluxes is in agreement with the results reported by Mizikar. The higher heat-transfer coefficients obtained in the present work are attributed to the presence of the "water curtain" flowing down the cold surface surrounding the heat-transfer probe. The presence of this "water curtain" has been observed in the previous measurement of spray fluxes as reported in a previous section.

5.2.5 Results of Type II Experiments

Further measurements were then conducted using the measuring probe imbedded in a steel plate. For these experiments, the face of the measuring probe was protected by a metallic shroud purged with nitrogen, during heating in a gas fired furnace.

In the first series of experiments, the surface of the measuring probe was flush with the surface of the stainless steel plate (Type IIa Experiment, Figure 23). These tests were done to confirm that the water

flowing down the cooled surface could cause an increase of the heat-transfer coefficients.

The results of this series of tests, plotted in Figure 62 show that there is a decrease in the scatter of results, as well as a general decrease in the heat-transfer coefficients for a given water flux, when compared to the Type I measurements presented in Figures 61 and 62. Since there is a large surface area capable of extracting heat from the impinging sprays in the Type II experiments, the quantity of water flowing downward adjacent to the sprayed surface would be drastically reduced, and thus would not interfere as much with the direct spray cooling of the measuring probe, when compared to the conditions obtained in the Type I experiments.

In these Type IIa experiments, the heat-transfer coefficients were found to be surface temperature sensitive. From the results presented in Figure 64, it can be observed that the heat-transfer coefficients decrease as the surface temperature increases. In addition, it can be seen that increase of the spray water flux shifts the curves upwards to higher heat-transfer coefficients. The effect of spray pressure on the heat-transfer coefficients could not be distinguished.

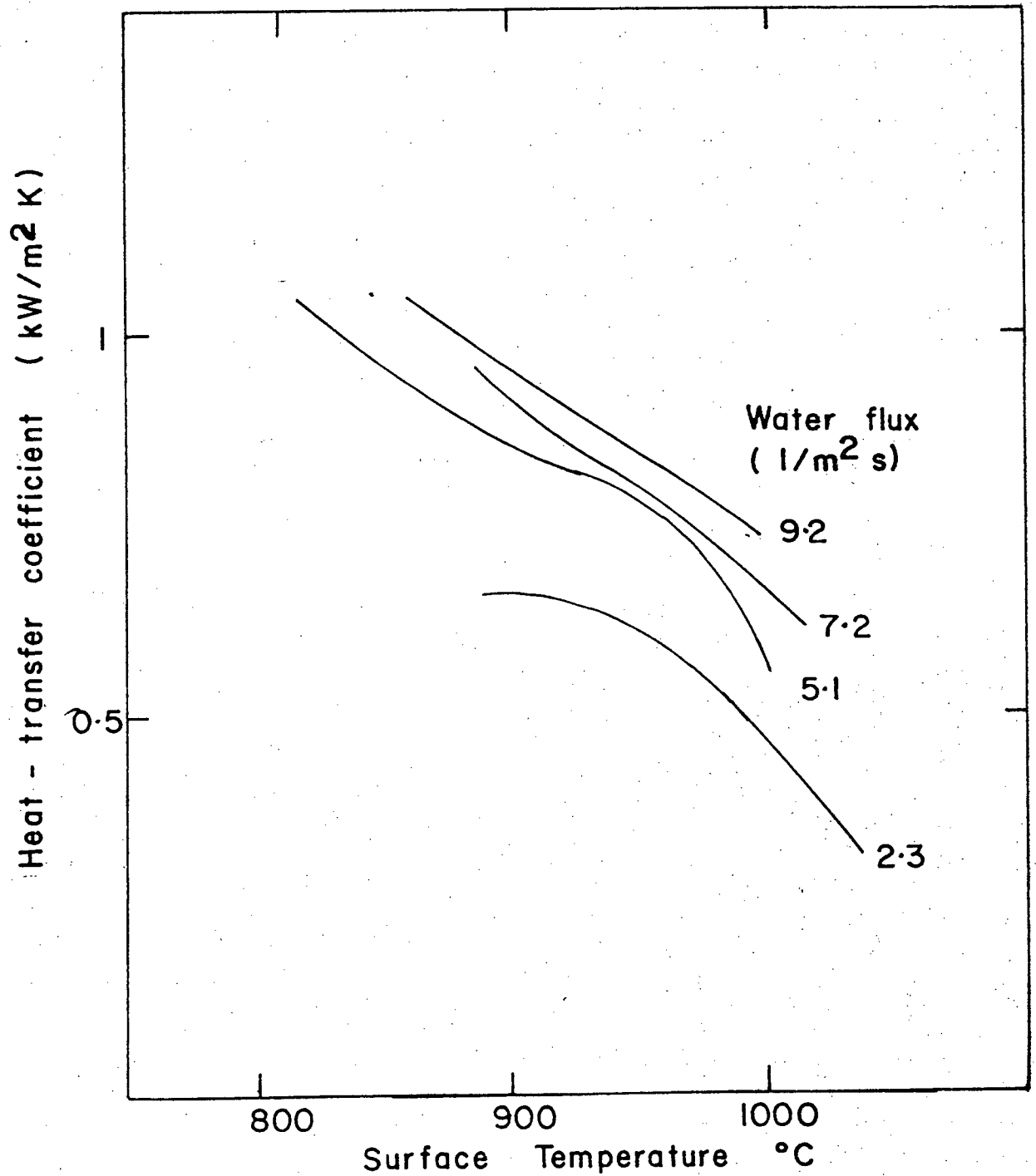


Figure 64 Variation of heat-transfer coefficients with surface temperature (Type IIa Experiments).

All further runs of the Type II experiments were carried out with heat-transfer probes of length 3.18 cm (1.25 in) fitted with a ring around the front of the probe so that only the water directly impinging on the probe surface from the spray nozzle would be used to cool the surface of the probe (Type IIb Experiments, Figure 25). Henceforth, spray water fluxes at the probe were varied only by movement of the nozzle along its axis, and by changing the spray pressure.

The variation of the heat-transfer coefficients with spray water flux at 1000° C for this set of experiments is presented in Figure 65. Spray pressures employed for this set of results were 0.14, 0.28, and 0.41 MPa (20, 40 and 60 psi). Similar results obtained for surface temperatures of 800, 850, 900, 950 and 1050° C are given in Figures 66 to 70. The heat-transfer coefficients plotted in these Figures do not include the radiation contribution. It can be observed from these Figures that as the temperature decreases, there is an increase both in the value and the variability of the heat-transfer coefficient. In general, the heat-transfer coefficients increase as the spray flux increases. Since it has been demonstrated that Type I experiments do not measure just the heat transfer from the impinging sprays, only the results of the Type II experiments have been used in further analyses. The results of the type IIa experiments fell within the limits of the variability of the data obtained from Type IIb experiments.

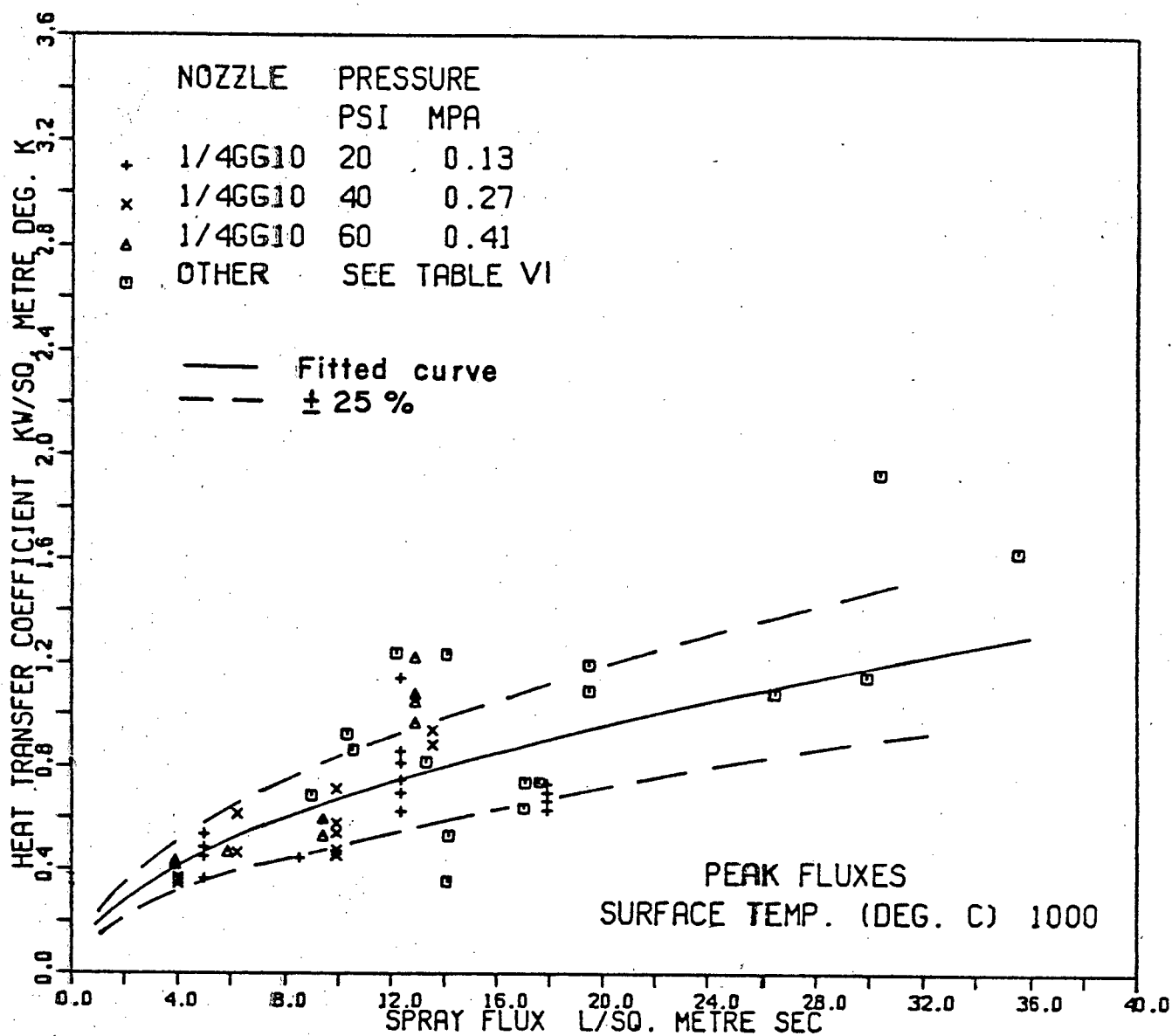


Figure 65 Variation of the measured heat-transfer coefficients with peak values water flux for a surface temperature of 1000°C.

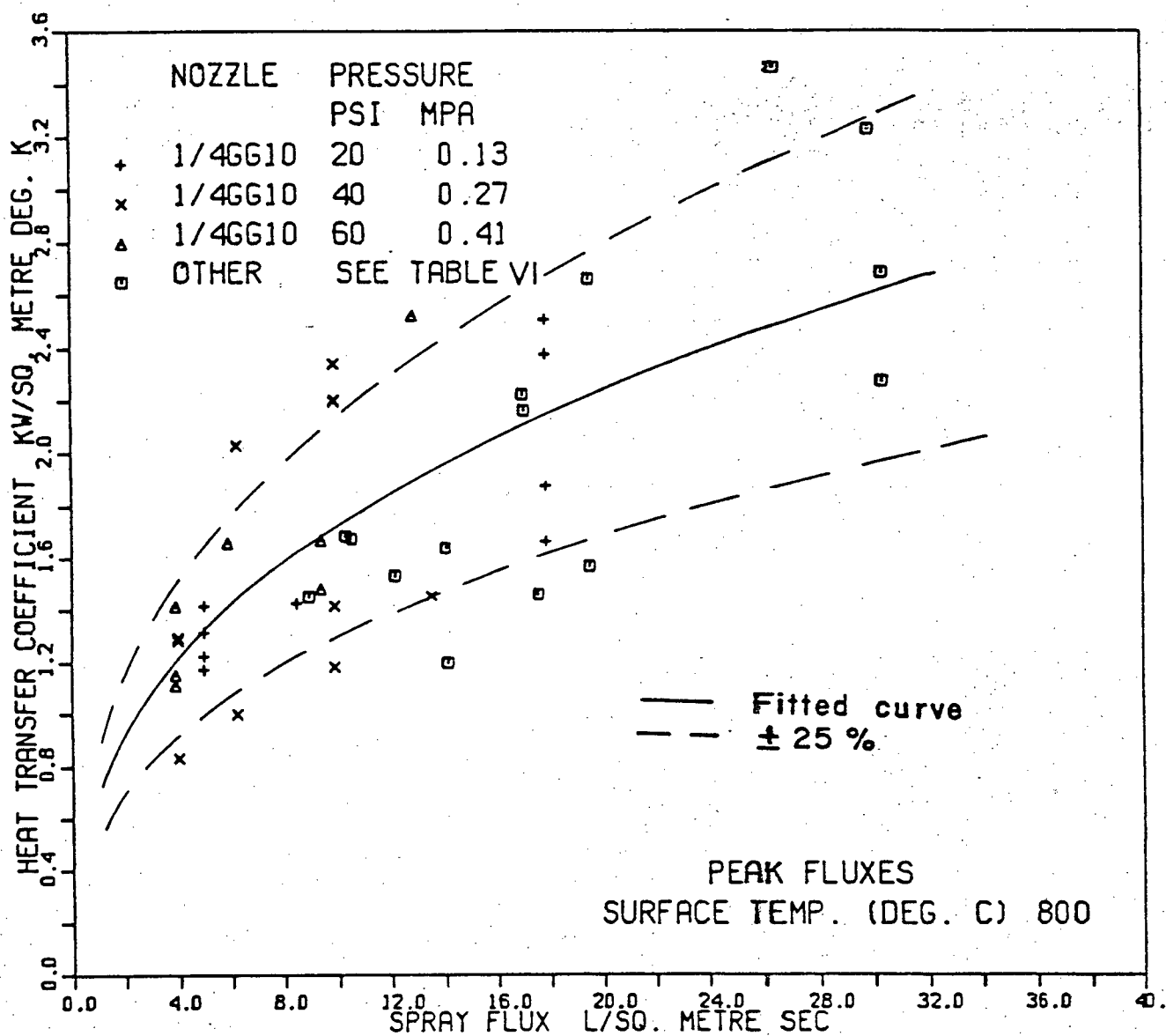


Figure 66 Variation of the measured heat-transfer coefficients with peak values water flux for a surface temperature of 800°C.

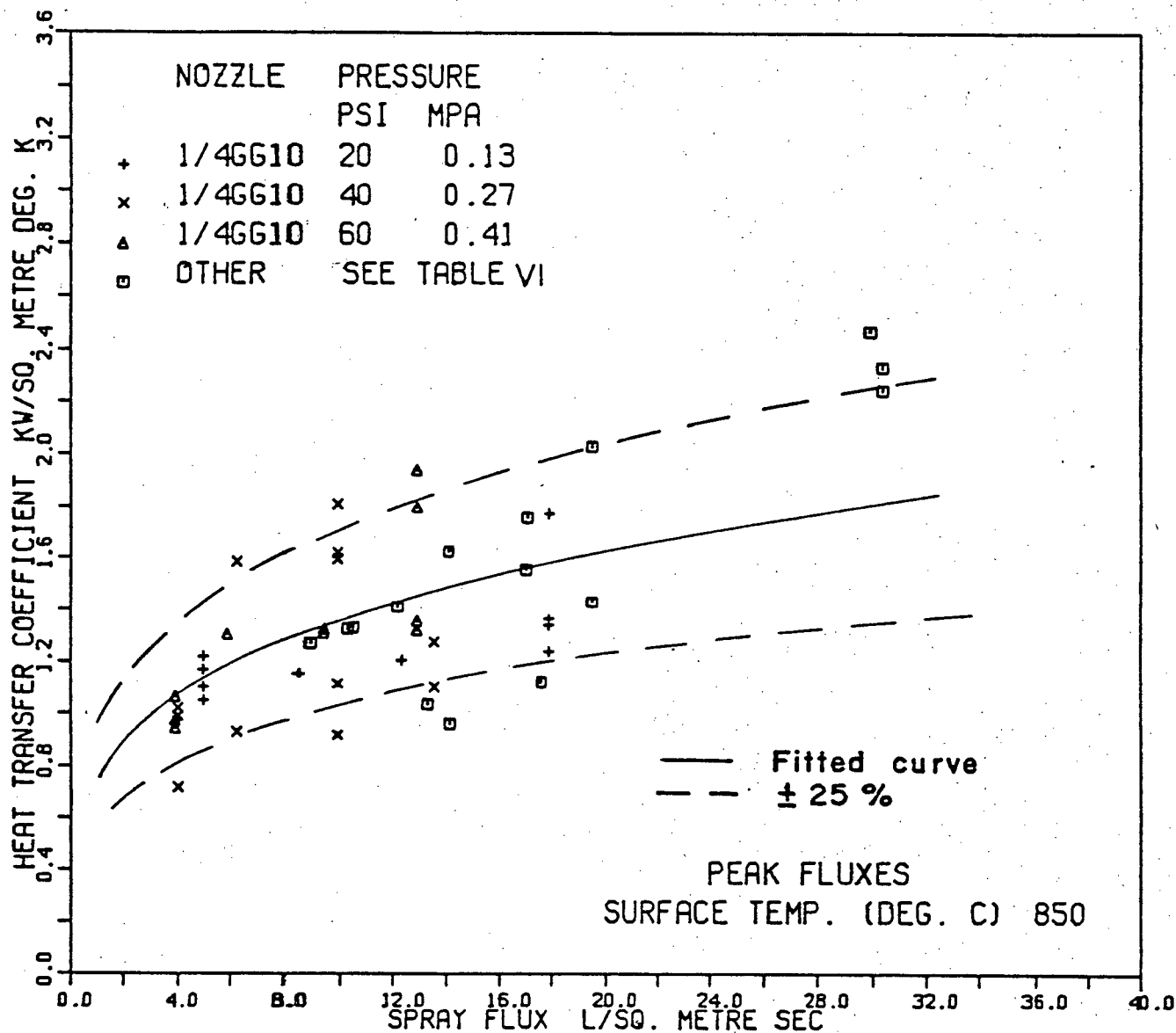


Figure 67 Variation of the measured heat-transfer coefficients with peak values water flux for a surface temperature of 850°C.

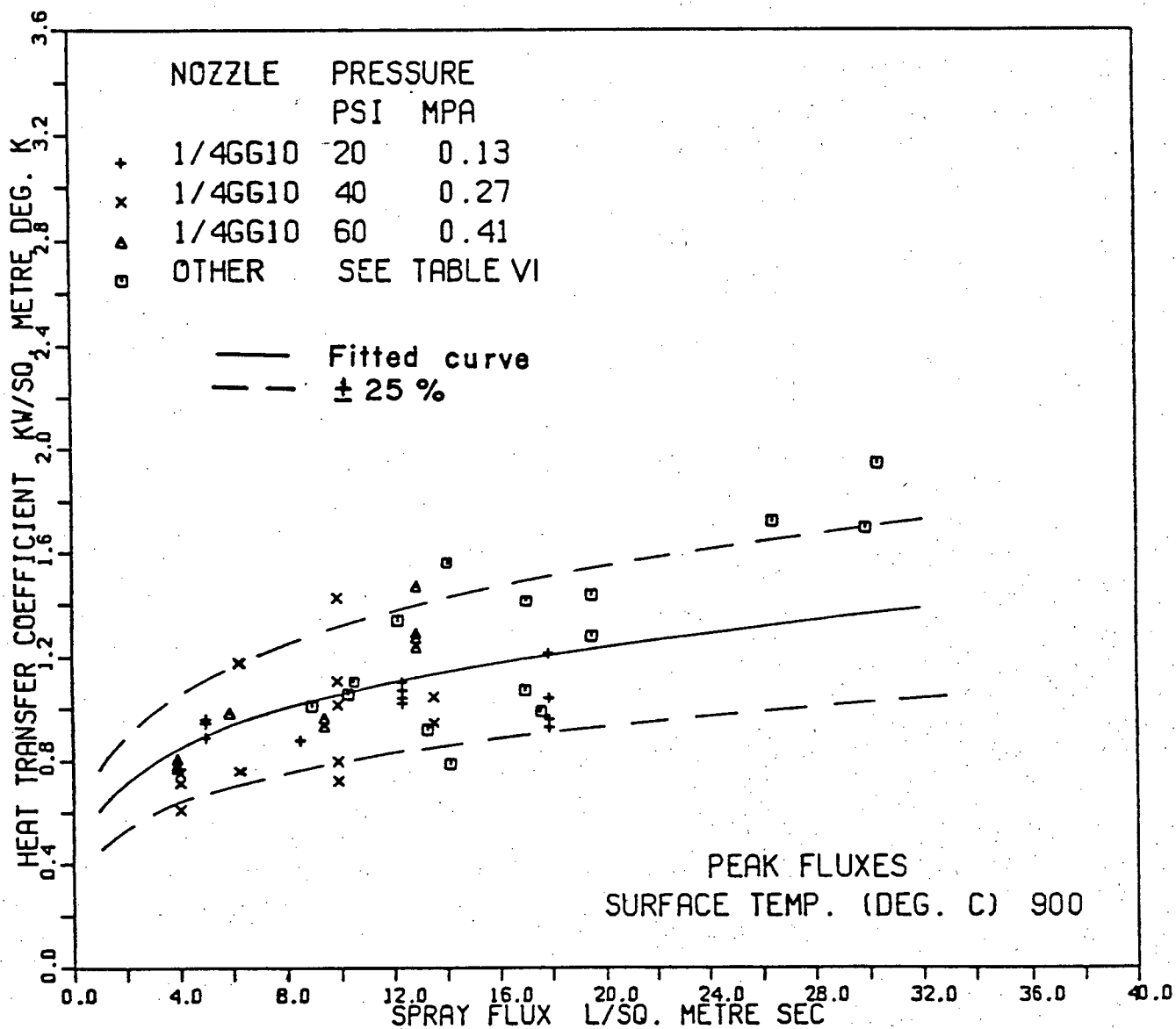


Figure 68 Variation of the measured heat-transfer coefficients with peak values water flux for a surface temperature of 900°C.

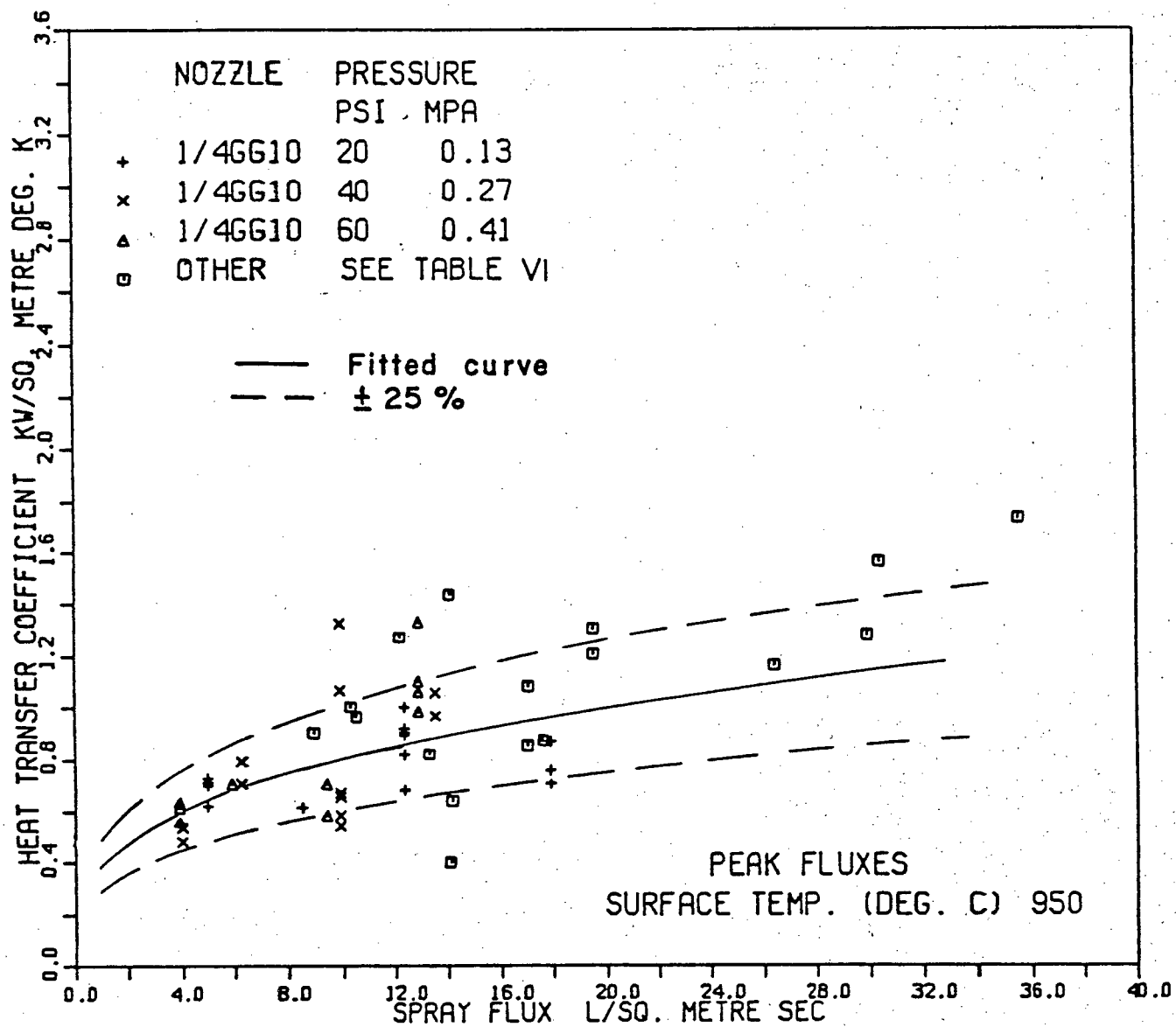


Figure 69 Variation of the measured heat-transfer coefficients with peak values water flux for a surface temperature of 950°C.

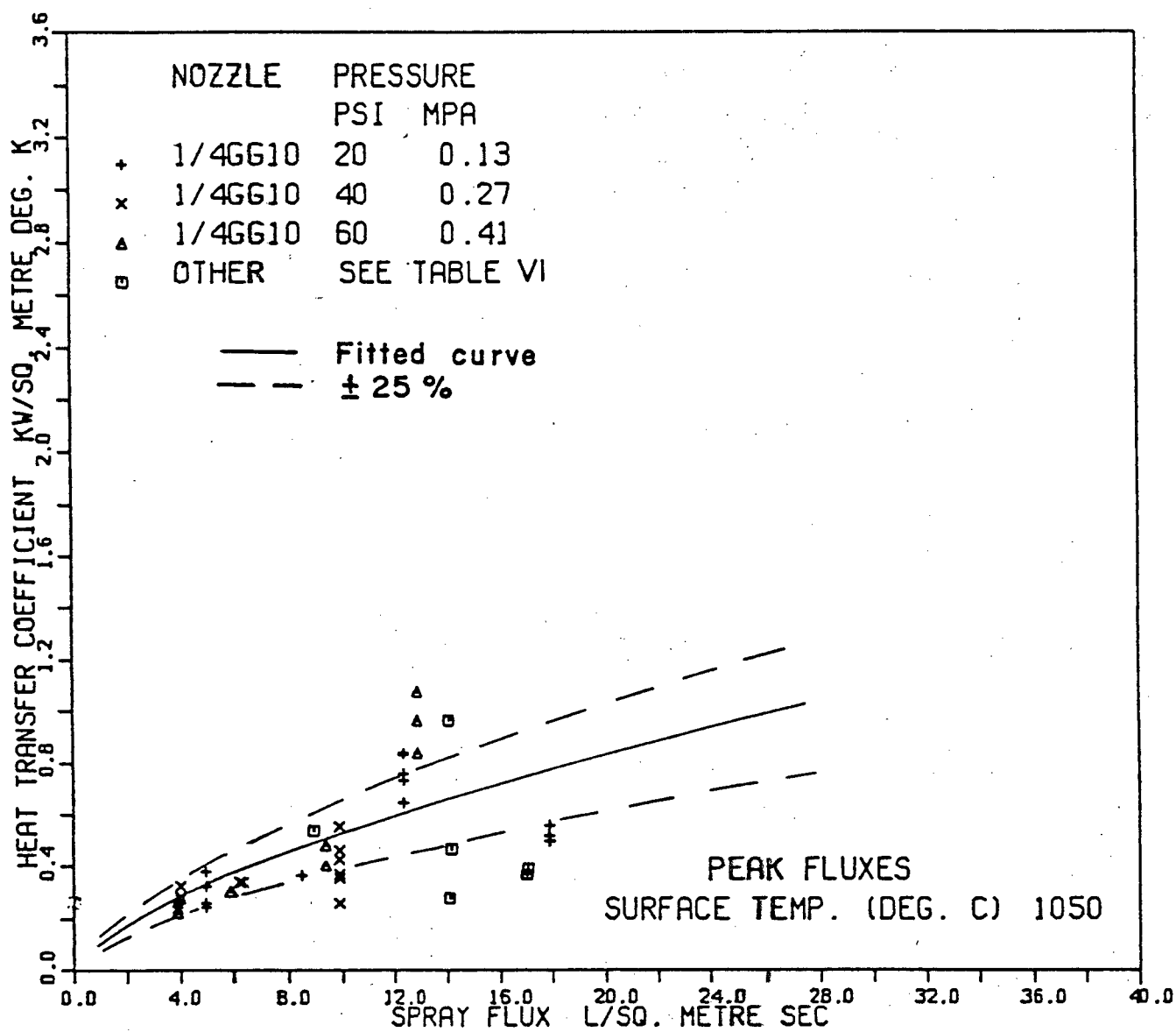


Figure 70 Variation of the measured heat-transfer coefficients with peak values water flux for a surface temperature of 1050°C.

Three types of curve fits were attempted to correlate the data. These were of the following forms:

$$\text{i)} \quad h = P(1) \dot{m} \quad \dots 5.1$$

$$\text{ii)} \quad h = P(1) \dot{m}^{P(2)} \quad \dots 5.2$$

$$\text{iii)} \quad h = P(1) + P(2) \dot{m} \quad \dots 5.3$$

where $P(1)$ and $P(2)$ are fitting parameters. The computer program used for the fitting utilized a derivative free nonlinear regression technique.¹¹⁷

The power fit (ii) was found to correlate the data best and the values of the parameters are given in Table IV. The water fluxes used for these fits and for Figures 65 to 70 are those measured by the central collectors in the spray flux measurement system using Type A collectors. The fitted curves to the data are drawn on the Figures and most of the data fall within 25% of these values. The fitted parameters are tabulated in Table IV.

5.2.5.1 Averaging of Spray Fluxes Over the Area of the Probe Face

Since the spray flux distributions show a sharp peak in the centre, average water fluxes over the 25.4 mm diameter probe surfaces were then calculated using the spray fluxes obtained at the three central collector tubes (Type A collectors, 25.4 mm apart) for the appropriate spraying conditions. This, in effect, lowers

TABLE IV Coefficients of the Fitted Power Curves Cor-
relating the Heat-Transfer Coefficients to the
Peak Values of Spray Water Flux at Different
Surface Temperatures.

Form of the curve $h = P(1) \dot{m}^{P(2)}$

Surface Temperature °C	Parameter Estimates		Standard Error of	
	P(1)	P(2)	P(1)	P(2)
800	0.73	0.38	0.14	0.08
850	0.76	0.25	0.16	0.09
900	0.61	0.23	0.12	0.08
950	0.40	0.31	0.08	0.08
1000	0.20	0.52	0.05	0.10
1050	0.12	0.65	0.04	0.15

the values of the spray flux at the probe for any given spraying condition, and yields a larger heat-transfer coefficient for a given spray flux when compared to values obtained using the peak fluxes. The variation of heat-transfer coefficients plotted as a function of the average spray flux for different temperatures is presented in Figures 71 to 76 for surface temperatures from 800 to 1050°C in 50°C increments. Again, power curves of the type discussed in the previous section were found to yield the best fits to the data. The values of the parameters obtained from the curve fitting routines are presented in Table V.

5.2.5.2 Comparison of Data for Peak and Averaged Fluxes

The heat-transfer coefficients measured in this study are seen to have a fairly wide variability as evidenced by an examination of the plots of heat-transfer coefficients vs. the spray water flux. The variability is seen to increase as the surface temperature decreases, and as the spray flux increases. The heat-transfer coefficients are also found to be surface temperature dependent, with their magnitudes increasing with decreasing surface temperature. As can be seen from Tables IV and V, in general, the exponents of the power curves increase from 0.25 to 0.99 as the surface temperature

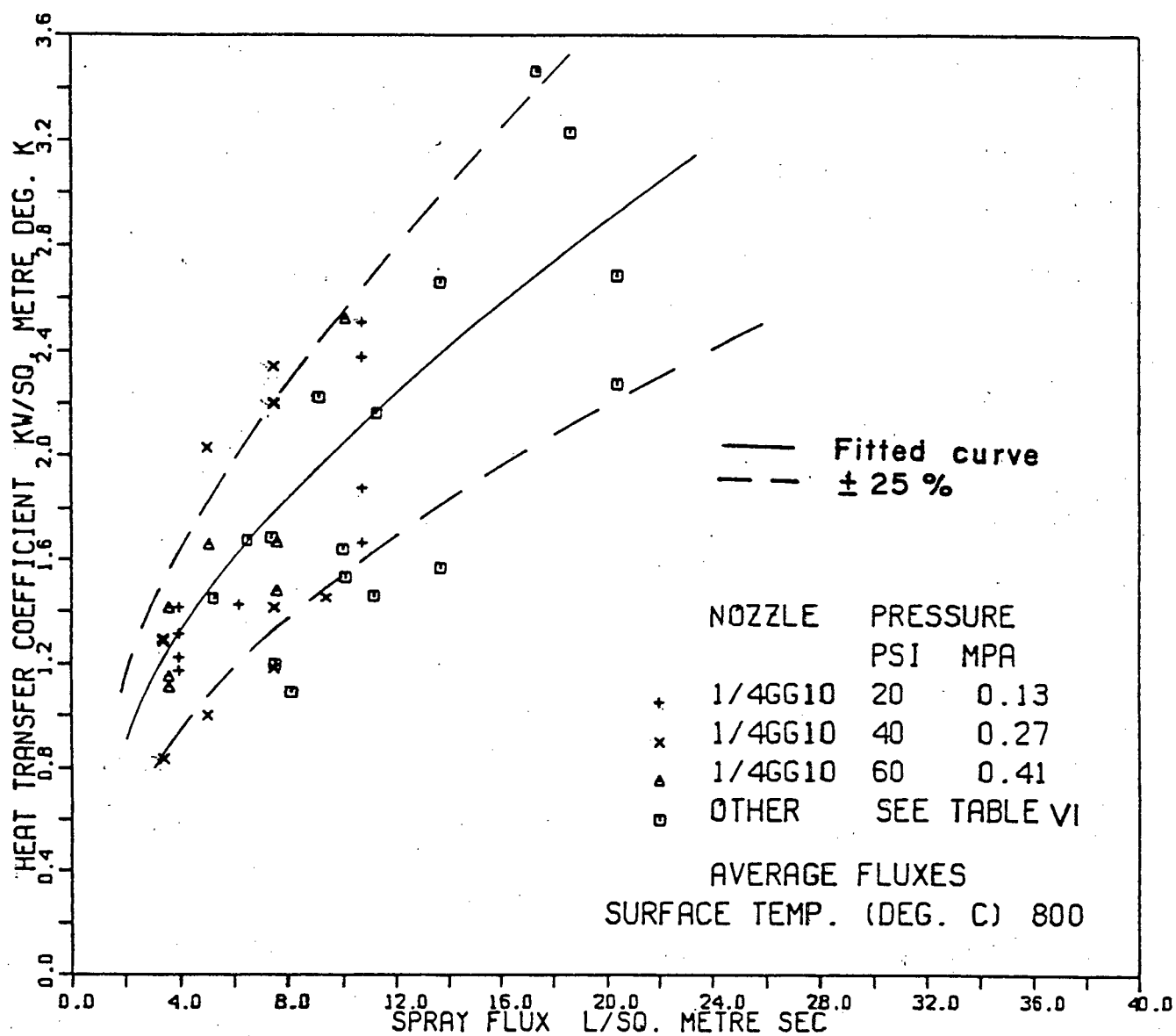


Figure 71 Variation of the measured heat-transfer coefficients with values of water flux averaged over the probe face, for a surface temperature of 800°C.

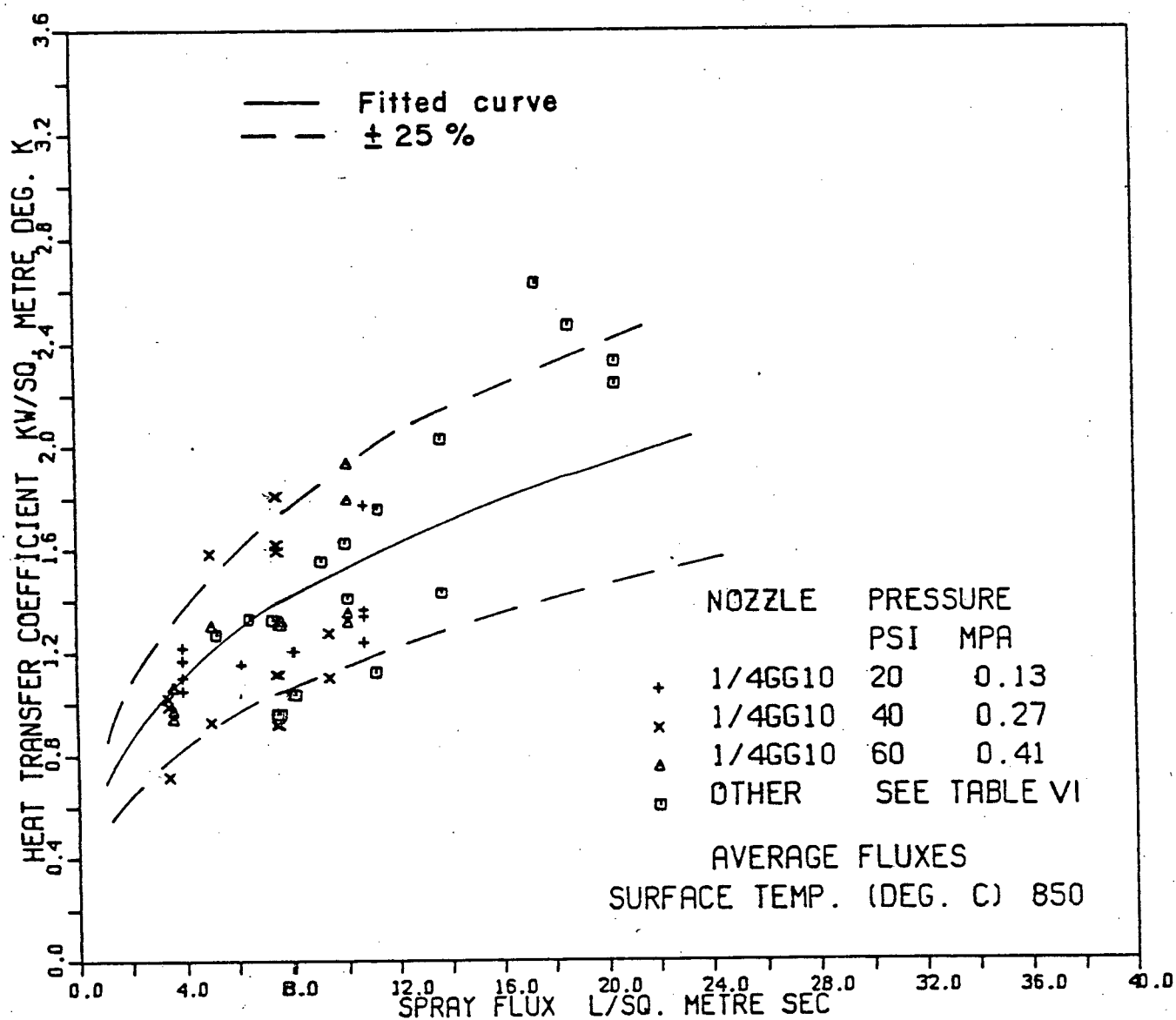


Figure 72 Variation of the measured heat-transfer coefficients with values of water flux averaged over the probe face, for a surface temperature of 850°C.

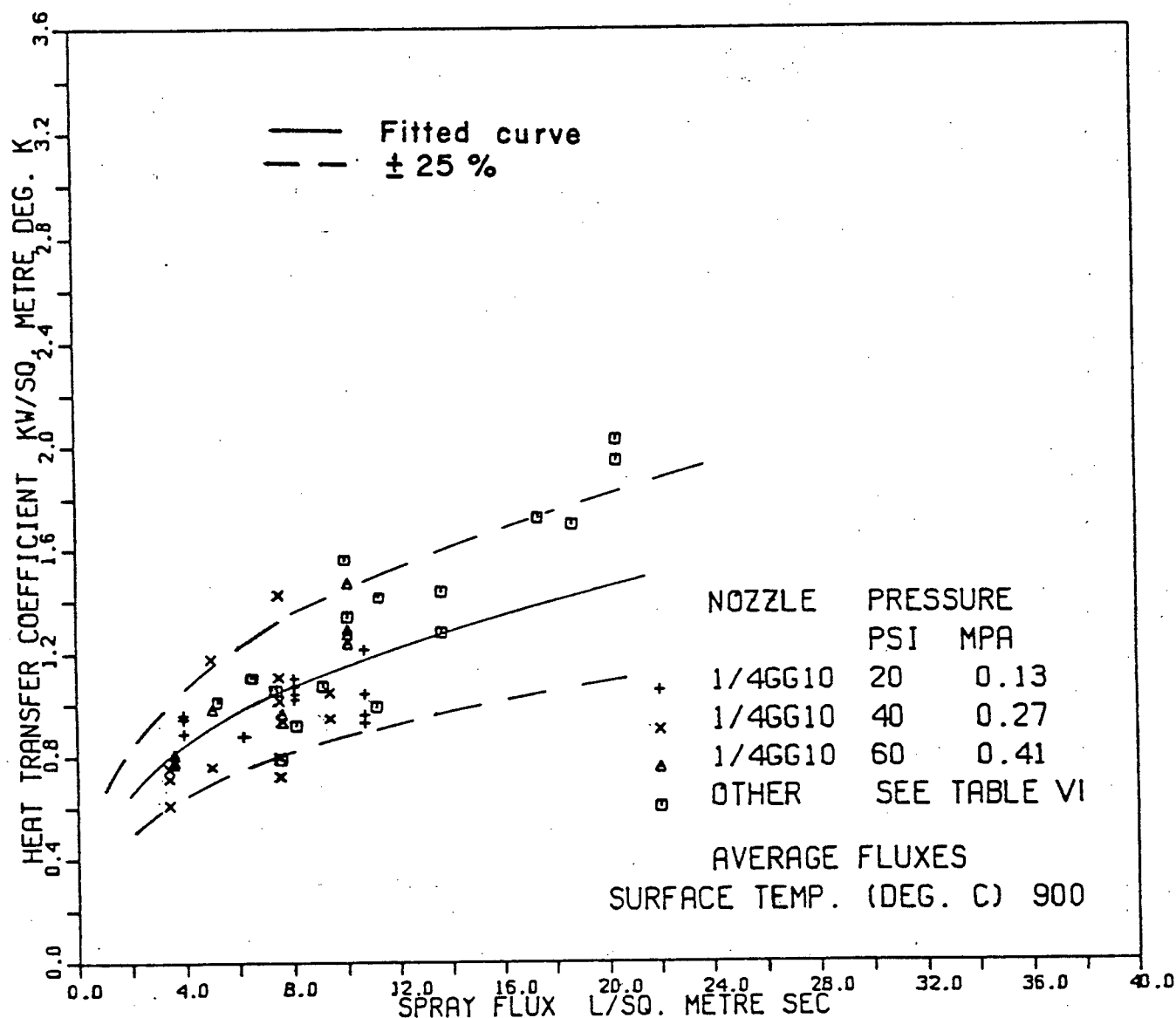


Figure 73 Variation of the measured heat-transfer coefficients with values of water flux averaged over the probe face, for a surface temperature of 900°C.

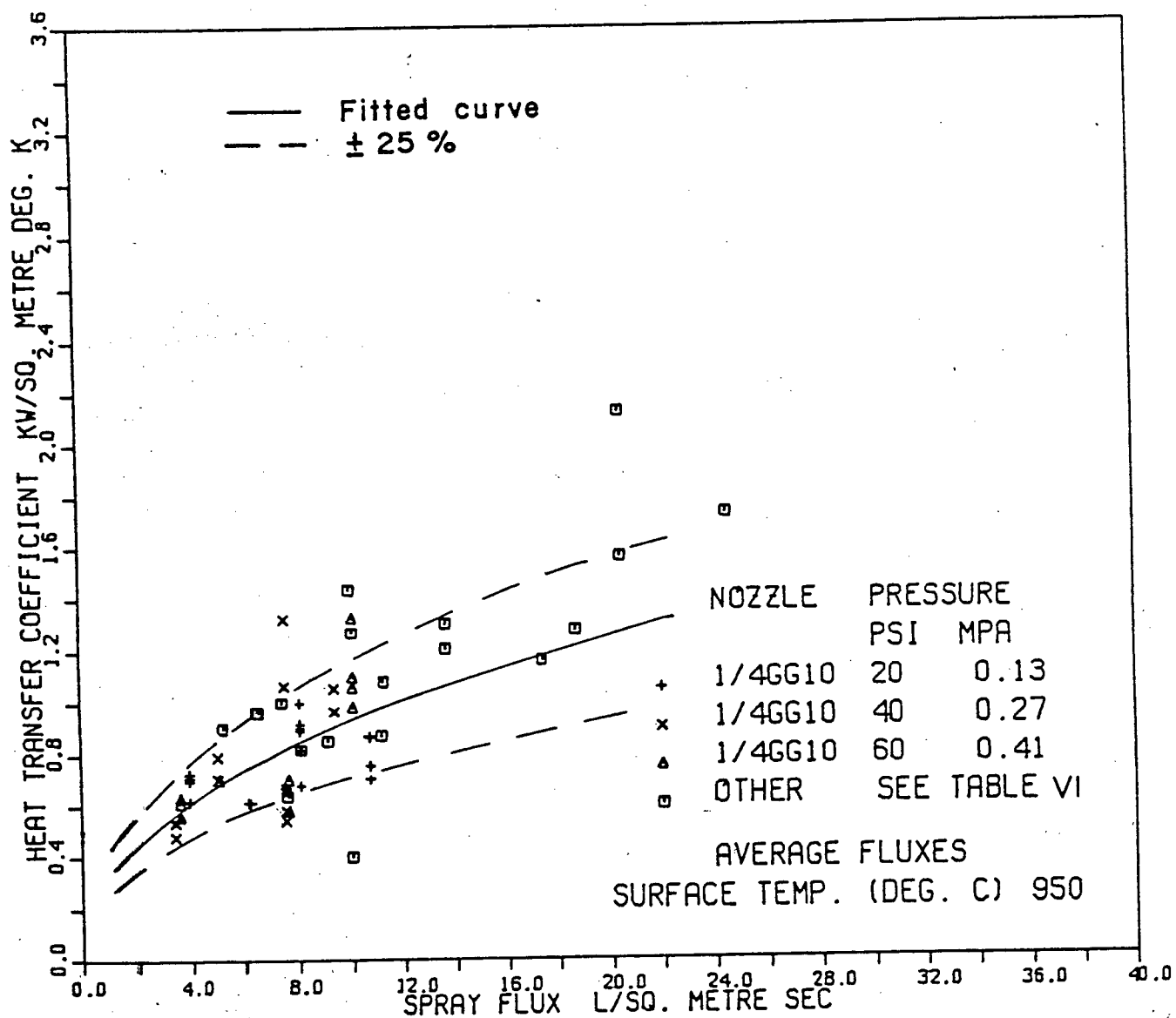


Figure 74 Variation of the measured heat-transfer coefficients with values of water flux averaged over the probe face, for a surface temperature of 950°C.

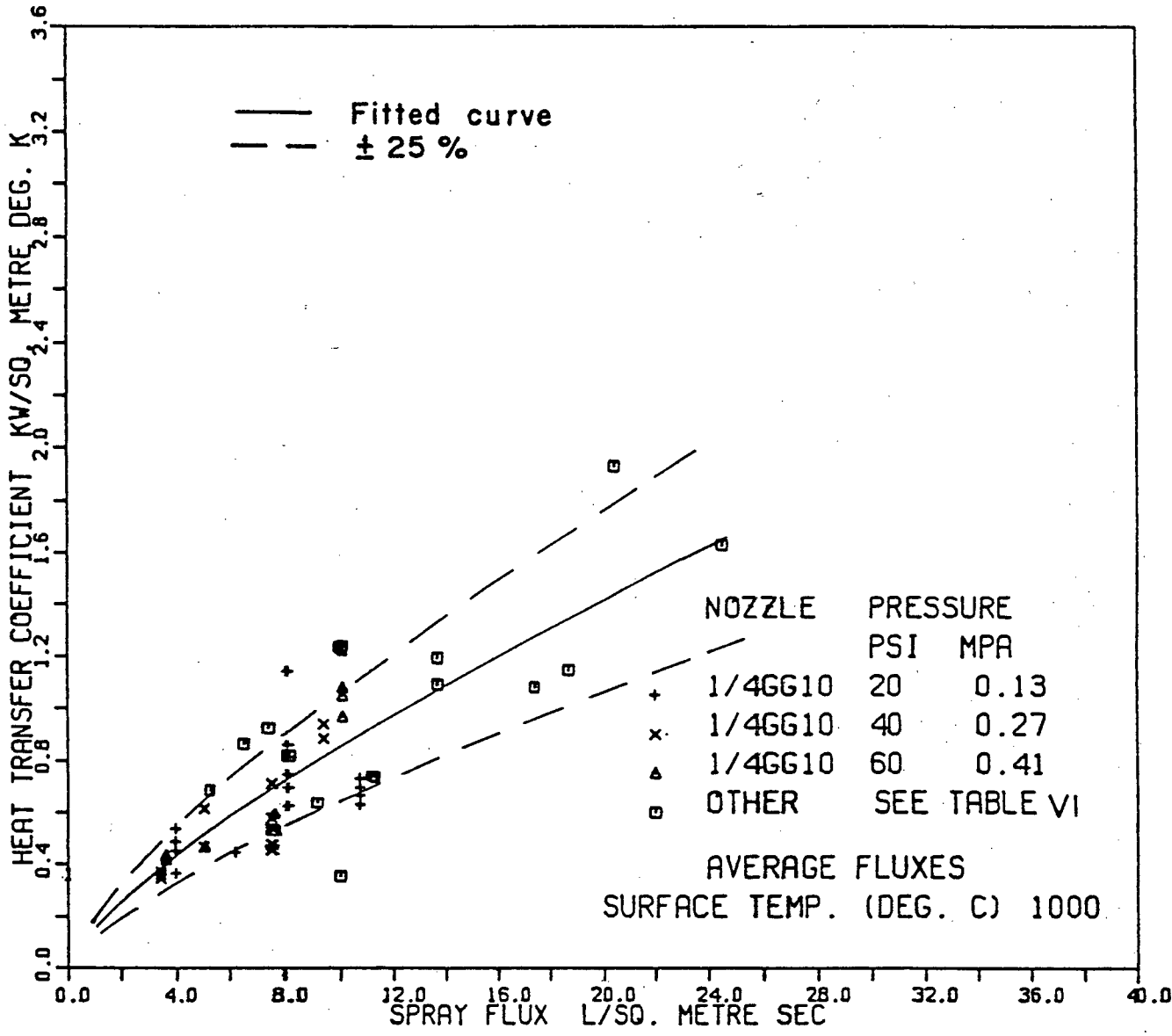


Figure 75 Variation of the measured heat-transfer coefficients with values of water flux averaged over the probe face, for a surface temperature of 1000°C.

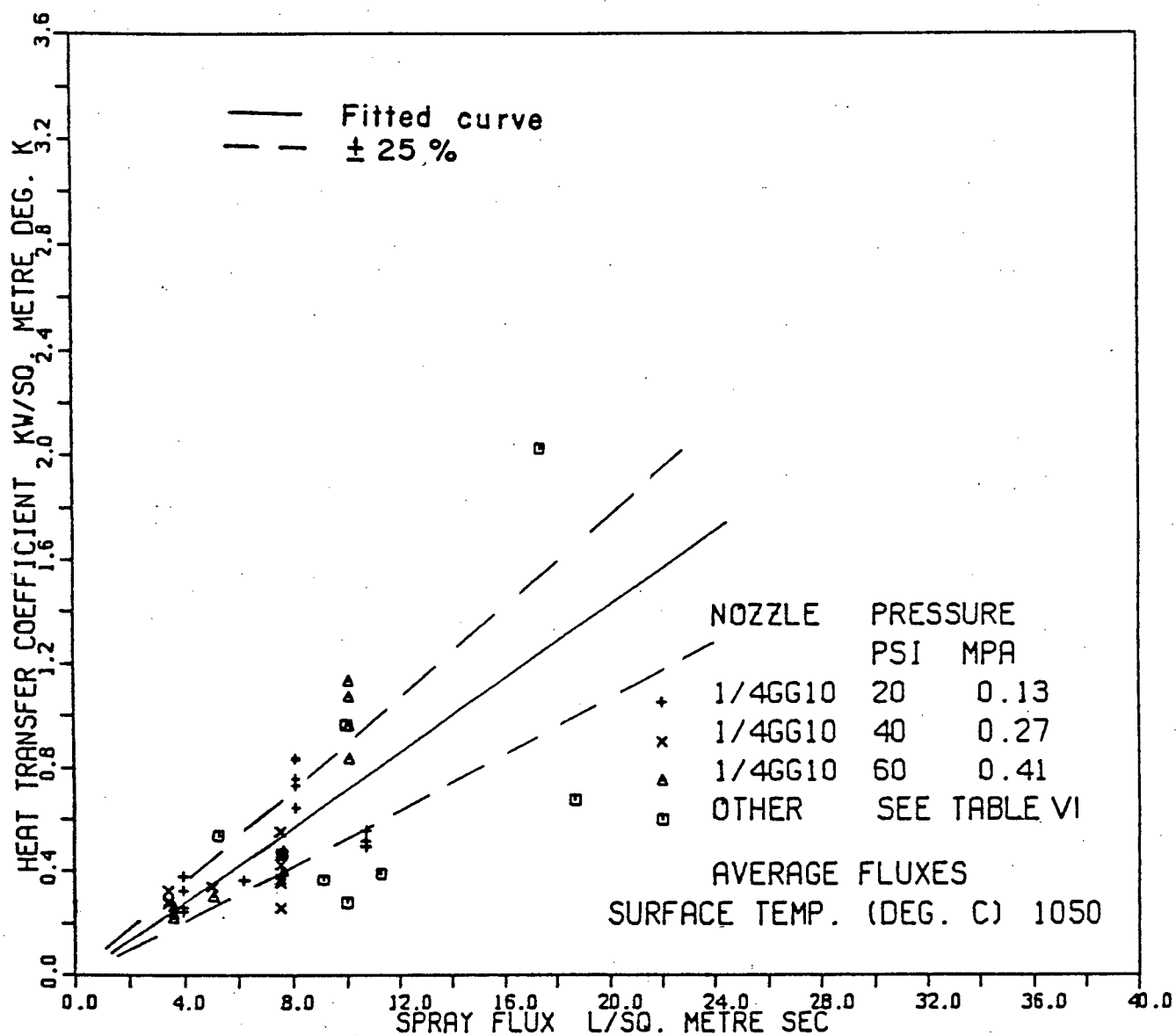


Figure 76 Variation of the measured heat-transfer coefficients with values of water flux averaged over the probe face, for a surface temperature of 1050°C.

TABLE V Coefficients of the Fitted Power Curves
Correlating the Heat-Transfer Coefficients
to Water Fluxes Averaged Over the Area of the
Probe Face, for Different Surface Temperatures.

Form of the curve $h = P(1) \cdot \dot{m}^{P(2)}$

Surface Temperature °C	Parameter Estimates		Standard Error of	
	P(1)	P(2)	P(1)	P(2)
800	0.64	0.50	0.13	0.10
850	0.68	0.34	0.16	0.11
900	0.55	0.33	0.11	0.10
950	0.34	0.43	0.07	0.10
1000	0.15	0.75	0.04	0.13
1050	0.07	0.99	0.03	0.19

increases. The fractional exponents indicate that the water flux has less than a proportional effect on the heat-transfer coefficient. The exponents are, as expected, higher in the cases where the heat-transfer coefficients have been related to the average water fluxes than when related to the peak water fluxes. The general trend of the increase in the exponent with increasing temperature does not hold when the surface temperature is 800°C , but this may be due to the large amount of scatter present in the results obtained for this temperature.

5.2.5.3 Results from Experiments Performed with Other Nozzles

In order to determine whether the sprays obtained from other full cone nozzles behaved in a similar manner, heat-transfer coefficients were measured for sprays produced by nozzles listed in Table VI. The operating conditions under which the measurements were made are also listed in this Table. The results are plotted in Figures 65 to 76 along with those of the 1/4 GG 10 nozzles. The heat transfer coefficients obtained for these nozzles are observed to be similar to that of the 1/4 GG 10 nozzle for the same water flux. Thus, the type of nozzle does not have a strong influence on the heat-transfer coefficient.

TABLE VI List of Nozzles Other Than 1/4 GG 10 and
Operating Spray Pressures Used in the
Measurement of Spray Heat-Transfer
Coefficients.

Nozzle Type	Spray Pressures	
	MPa	psi
3/8 HH 18 SQ	0.14,0.21	20,30
1/4 GG 12 SQ	0.14,0.28,0.41	20,40,60
1/4 GG 6.5	0.14,0.28,0.41,0.69	20,40,60,100
1/8 GG 5	0.14,0.28,0.41,0.69	20,40,60,100

5.3 Efficiency of Spray Cooling

Many authors^{53,65-67,76,81-84} have used the concept of spray cooling efficiency, n , which is defined as the ratio of the actual heat extracted by the impinging water, to the thermal power required to heat and vaporize all the impinging water.

$$n = \frac{h (T_s - T_w)}{\dot{m} [\Delta h_v + C_p (T_b - T_w)]} \quad \dots 5.4$$

Spray cooling efficiencies are calculated and the results are given for six surface temperatures in Figures 77 to 88 respectively, for the peak values and averaged values of water fluxes. Examination of the Figures shows that as the water flux increases, the spray cooling efficiency drops, until a limiting value is reached at about $16 \text{ l/m}^2\text{s}$. Beyond this value of the water flux, no appreciable decrease of the efficiency is observed. In addition, the magnitudes of the efficiencies increase as the surface temperature is lowered. This is considered to be a manifestation of the increase of the heat-transfer coefficient with decreasing surface temperature. Referring to Figure 88, for a surface temperature of 1050°C , it can also be observed that the spray cooling efficiency does not decrease as much with increasing water flux as compared to efficiencies at lower surface temperatures. This is reflected in the increase in the exponent in the power curves fitted to the heat-transfer

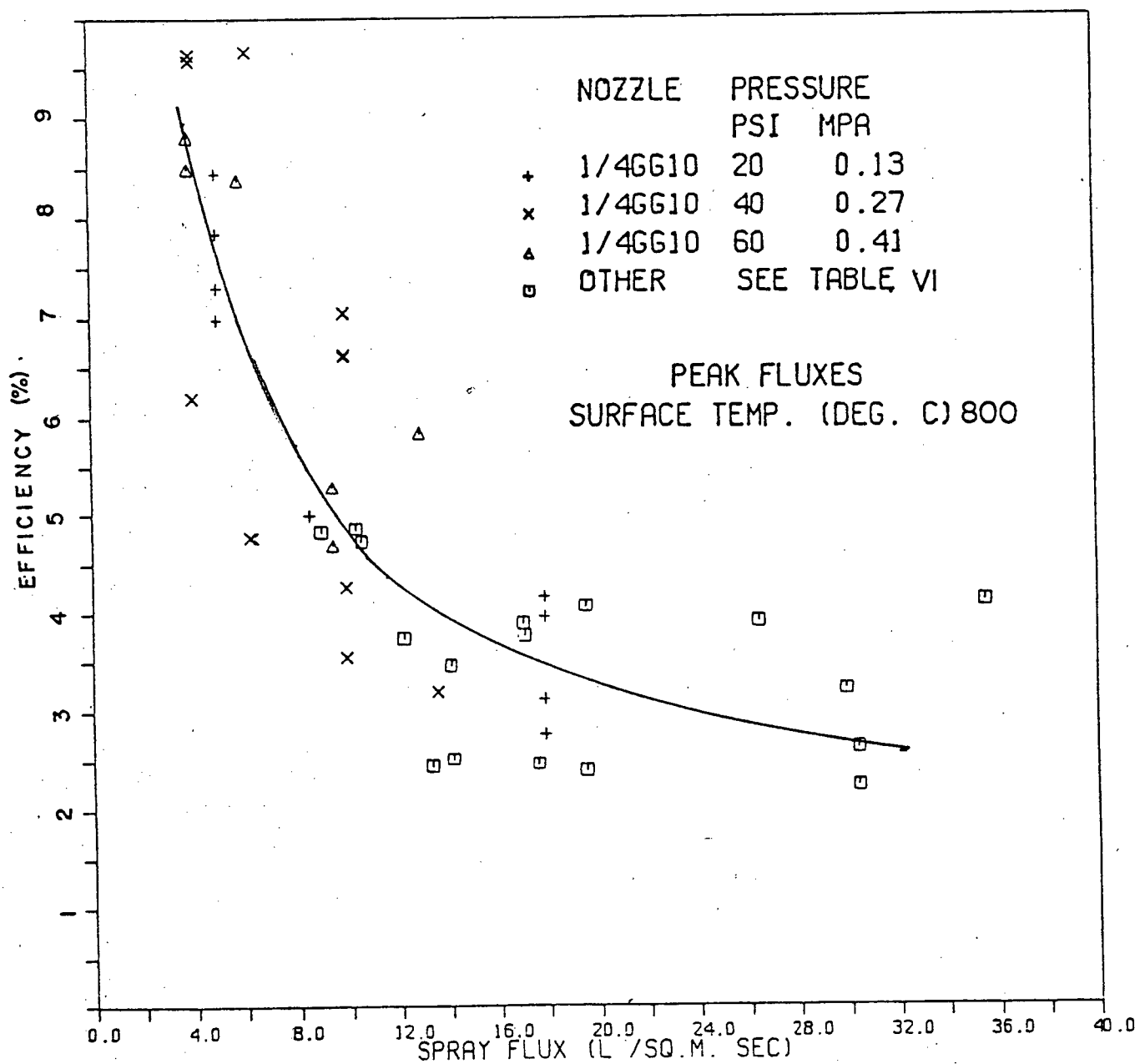


Figure 77 Variation of spray cooling efficiency with peak values of water flux, for a surface temperature of 800°C.

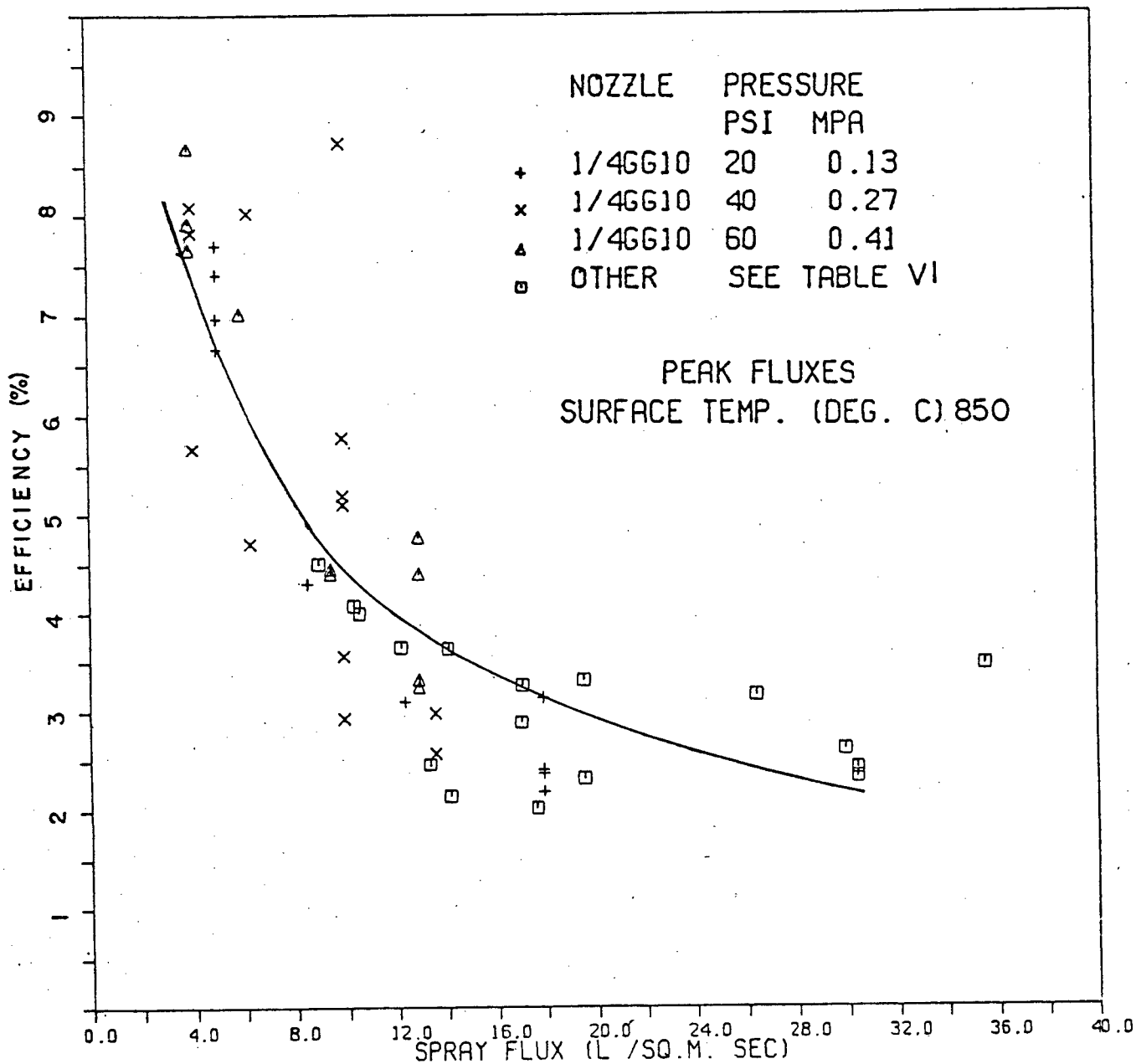


Figure 78 Variation of spray cooling efficiency with peak values of water flux, for a surface temperature of 850°C.

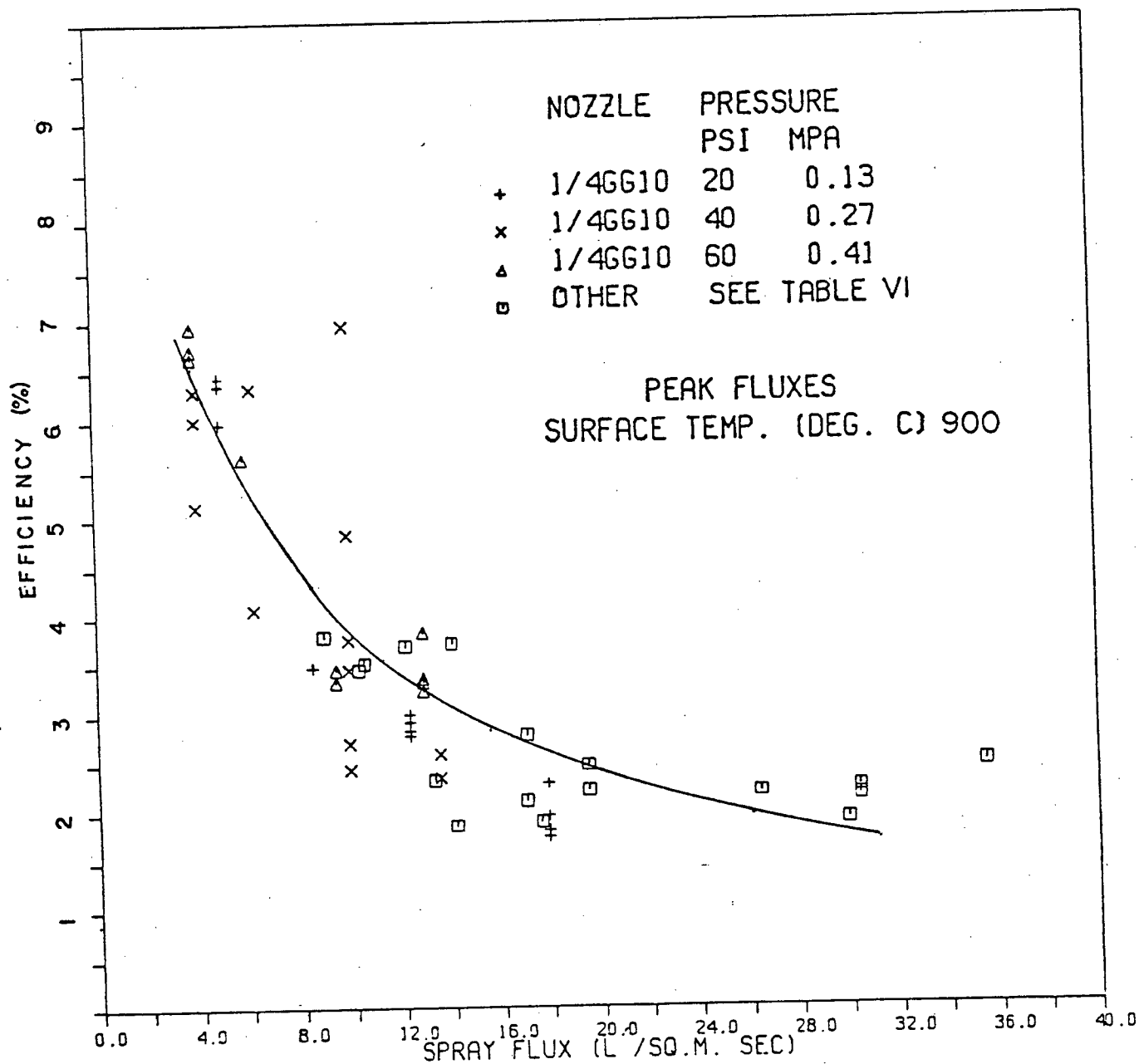


Figure 79 Variation of spray cooling efficiency with peak values of water flux, for a surface temperature of 900°C.

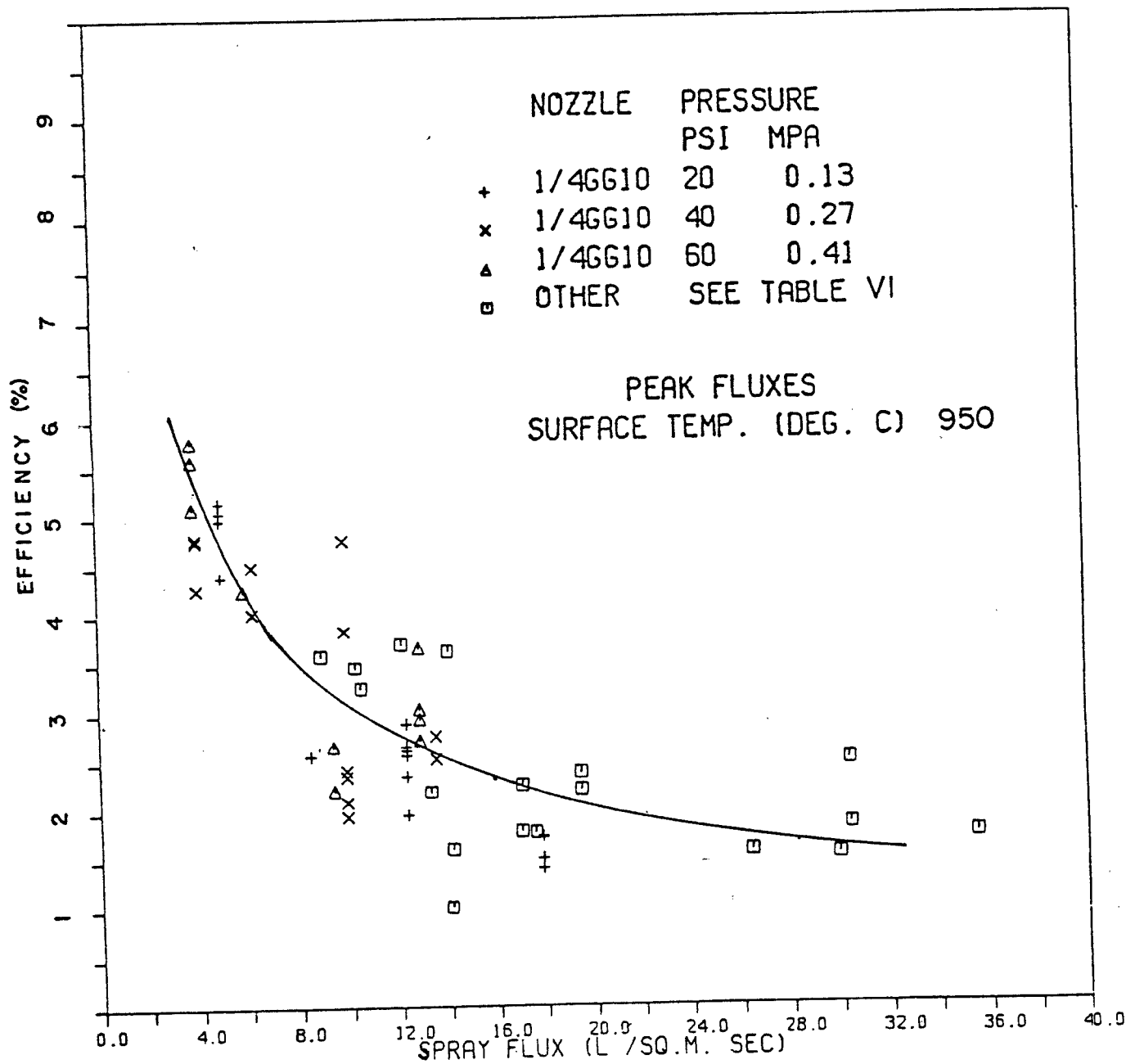


Figure 80 Variation of spray cooling efficiency with peak values of water flux, for a surface temperature of 950°C.

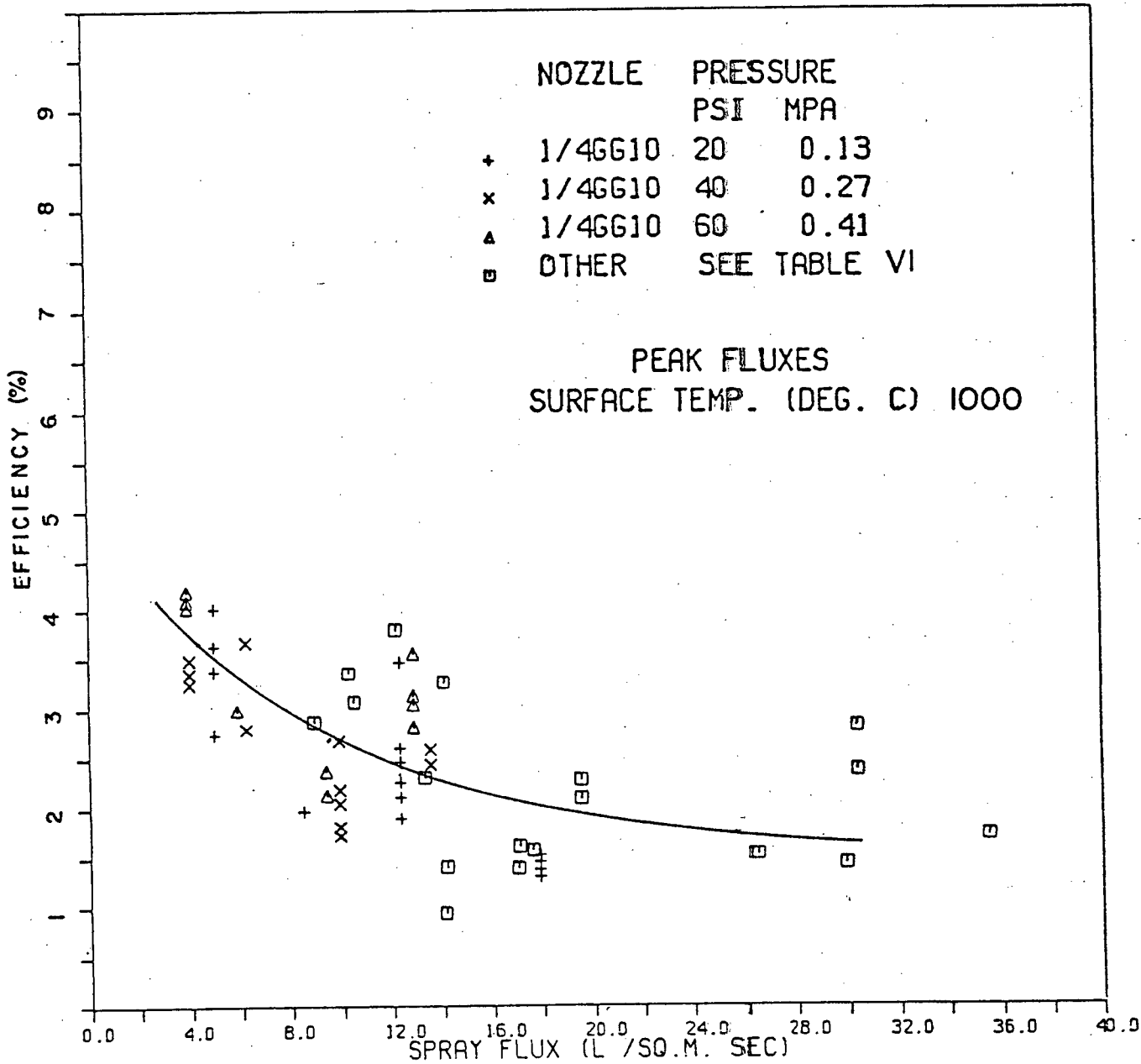


Figure 81 Variation of spray cooling efficiency with peak values of water flux, for a surface temperature of 1000°C.

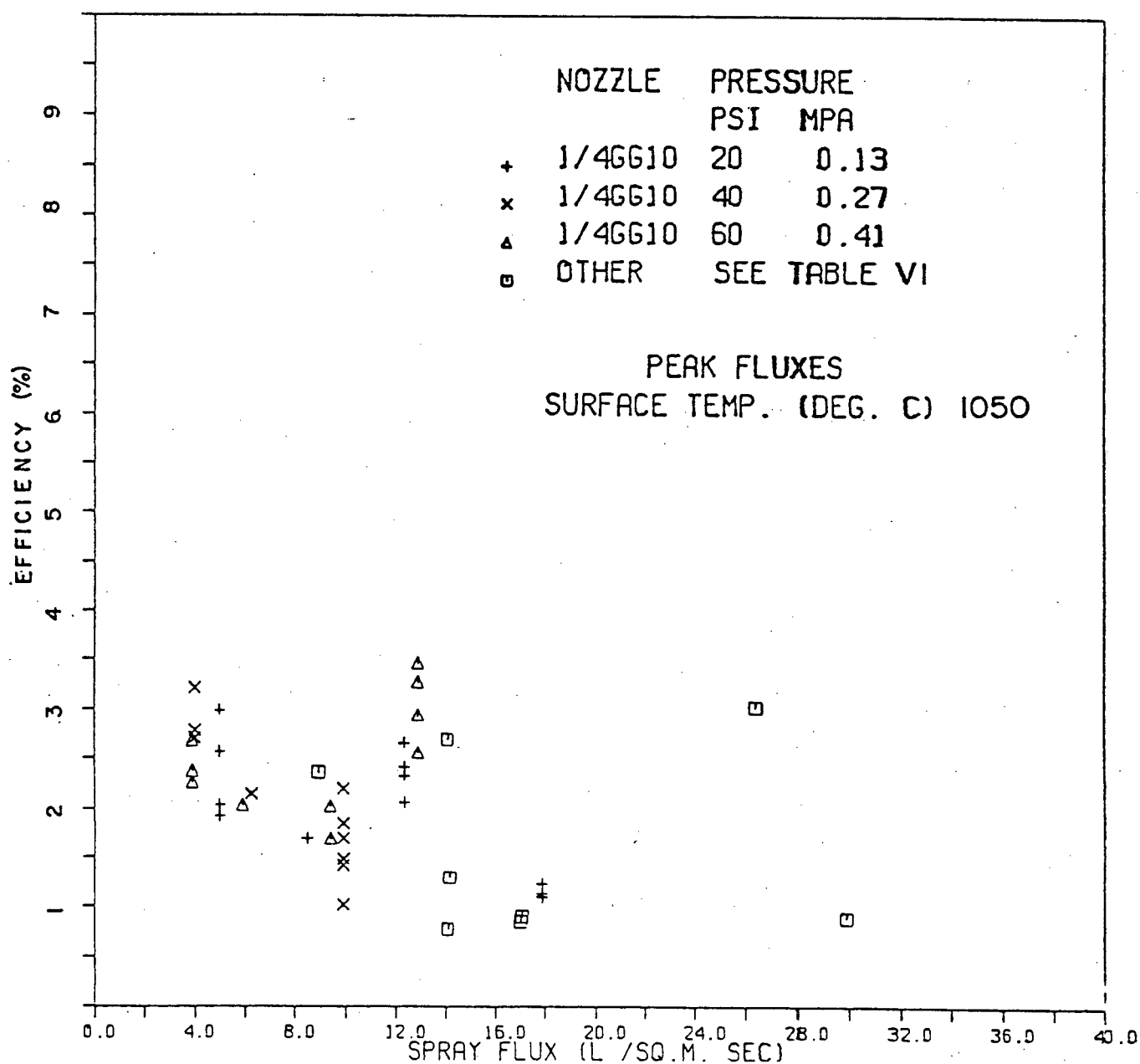


Figure 82 Variation of spray cooling efficiency with peak values of water flux, for a surface temperature of 1050°C.

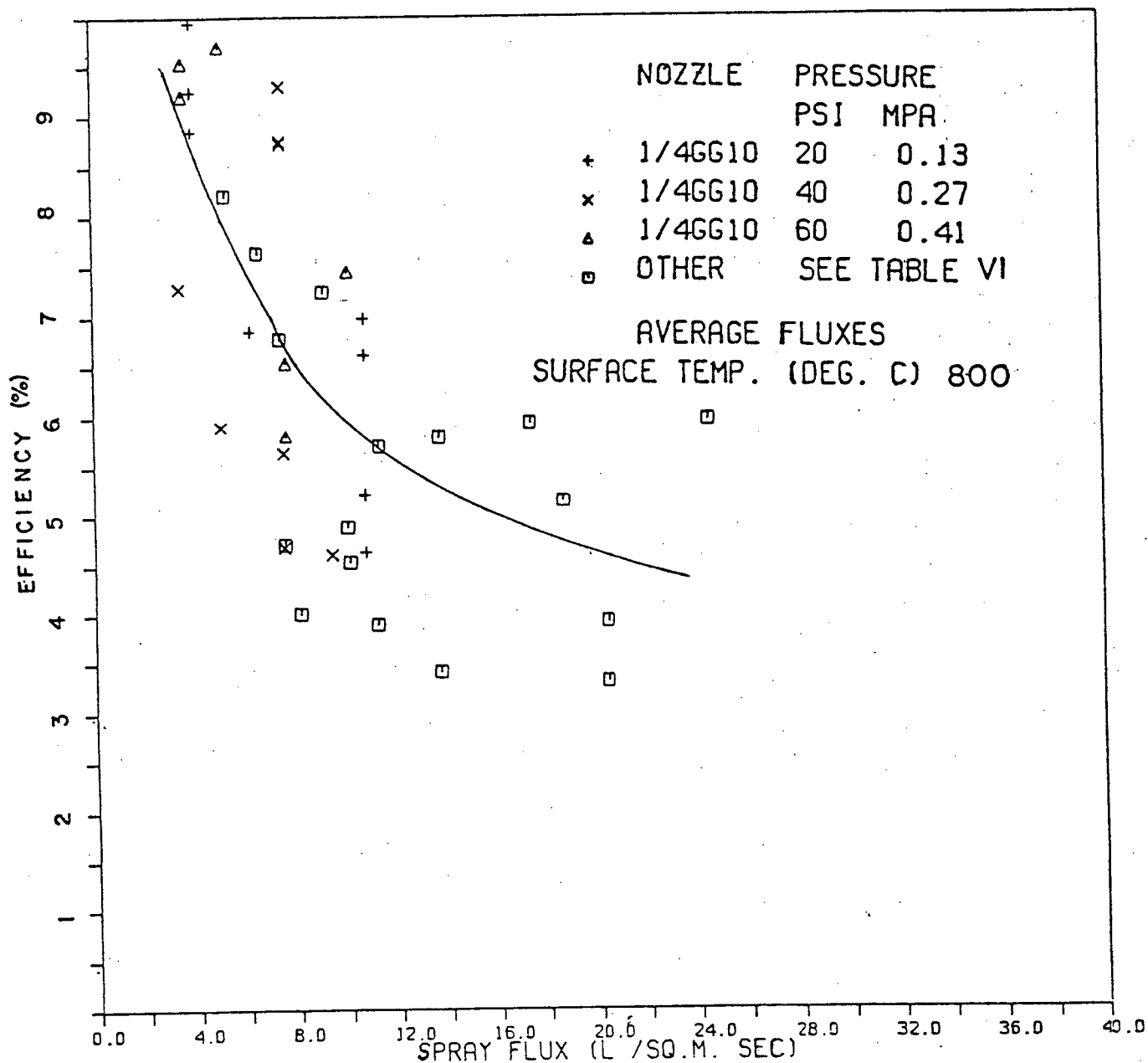


Figure 83 Variation of spray cooling efficiency with values of water flux averaged over the probe face, for a surface temperature of 800°C.

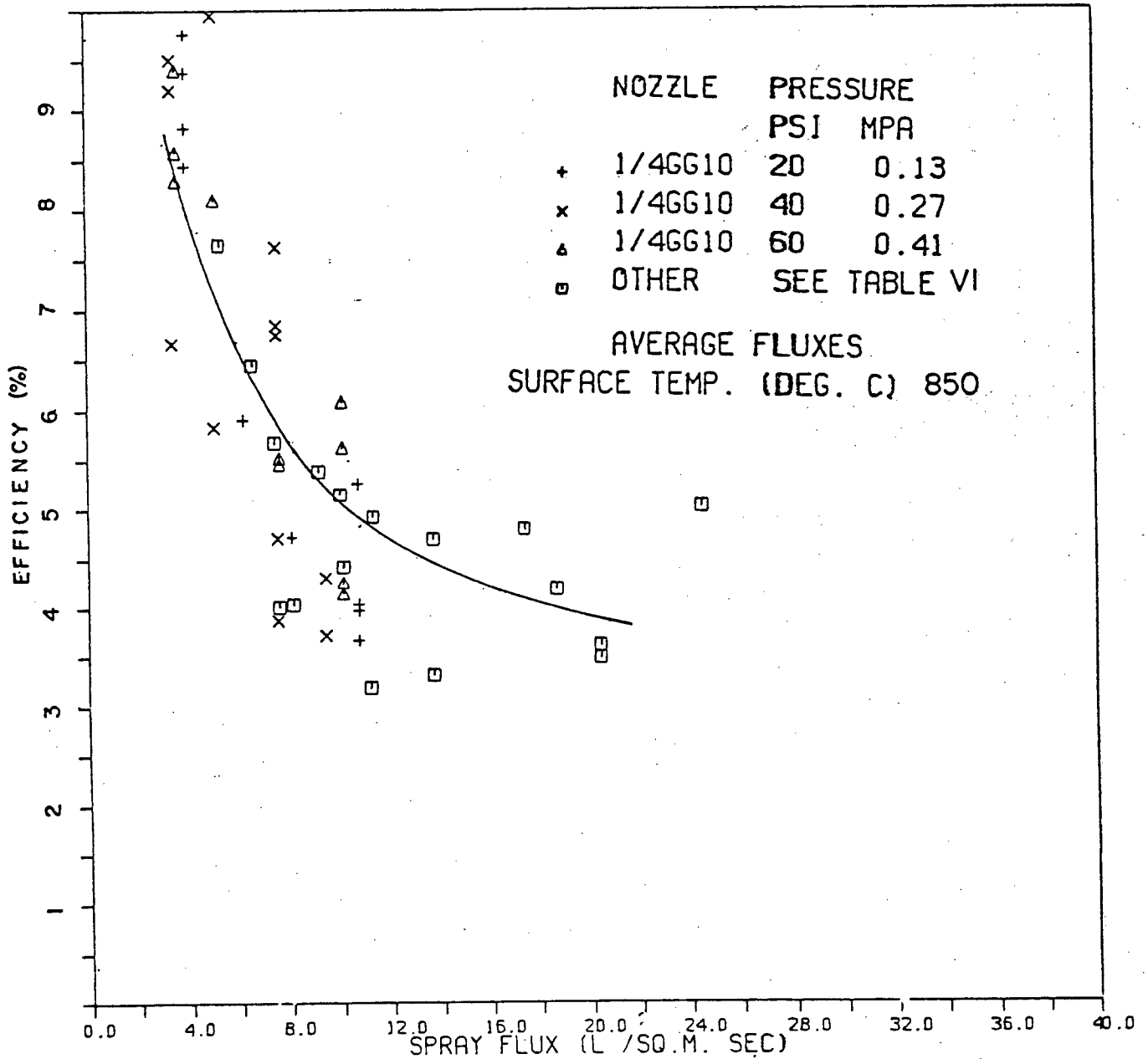


Figure 84 Variation of spray cooling efficiency with values of water flux averaged over the probe face, for a surface temperature of 850°C.

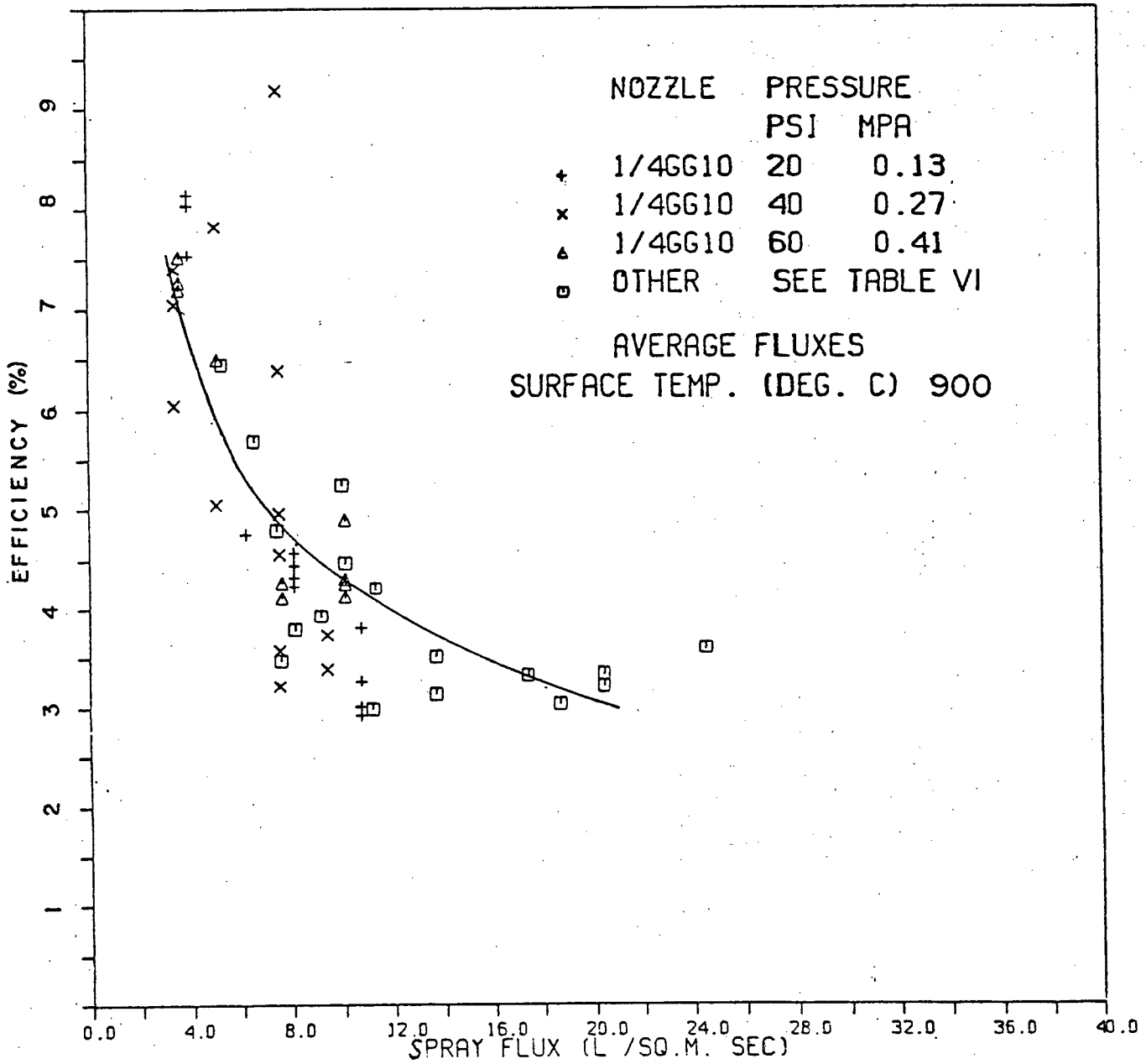


Figure 85 Variation of spray cooling efficiency with values of
water flux averaged over the probe face, for a
surface temperature of 900°C.

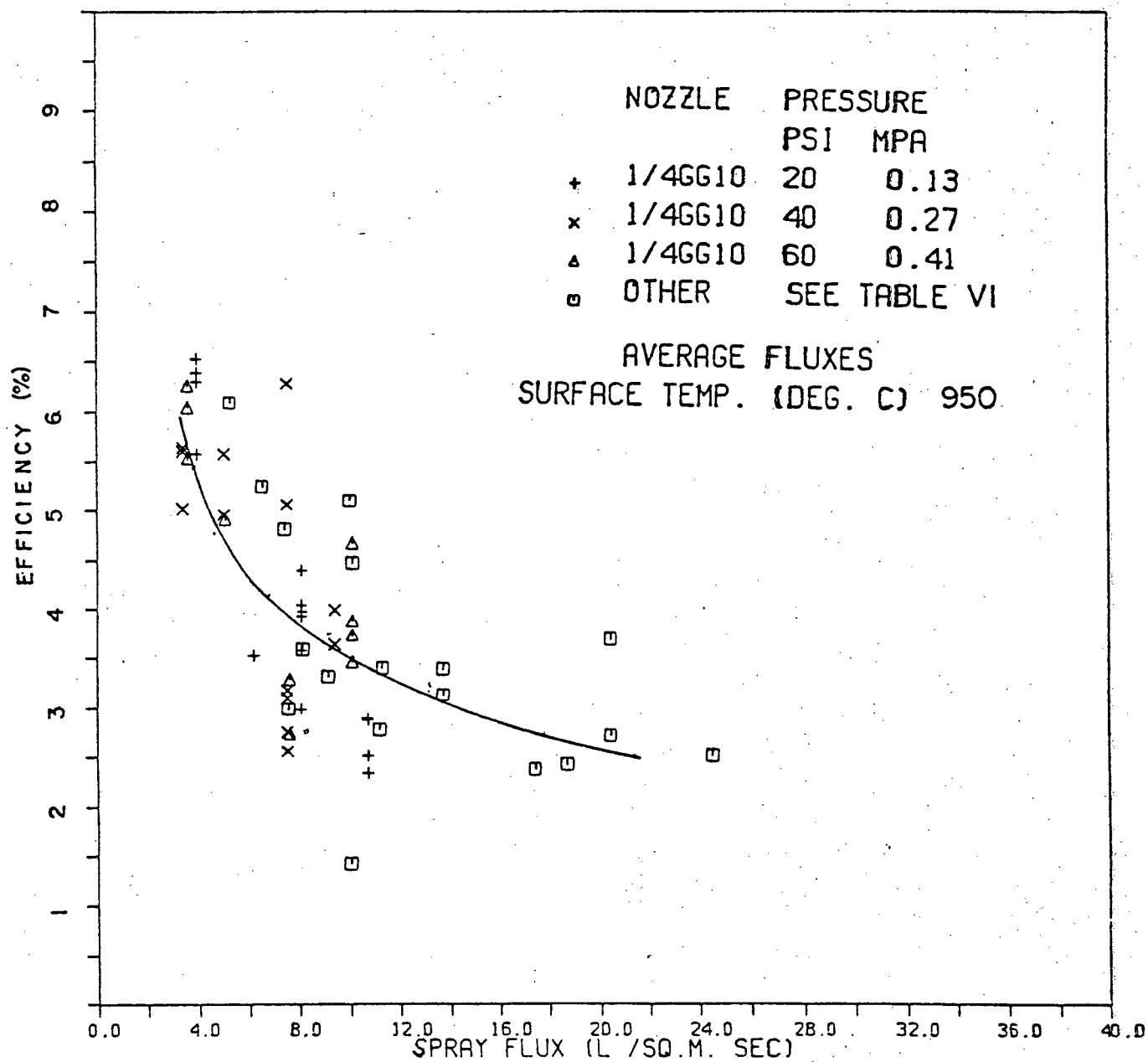


Figure 86 Variation of spray cooling efficiency with values of water flux averaged over the probe face, for a surface temperature of 950°C.

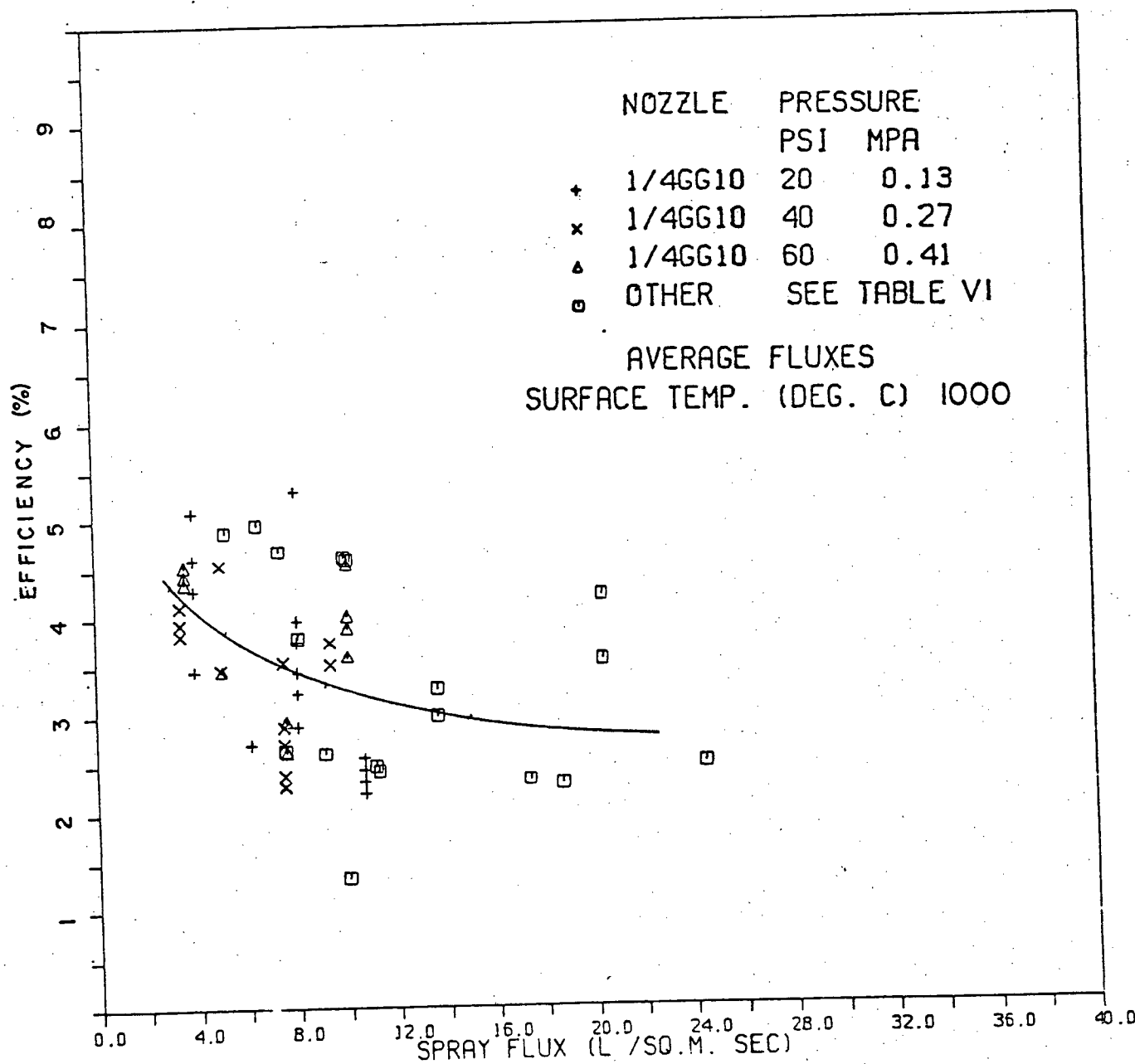


Figure 87 Variation of spray cooling efficiency with values of water flux averaged over the probe face, for a surface temperature of 1000°C.

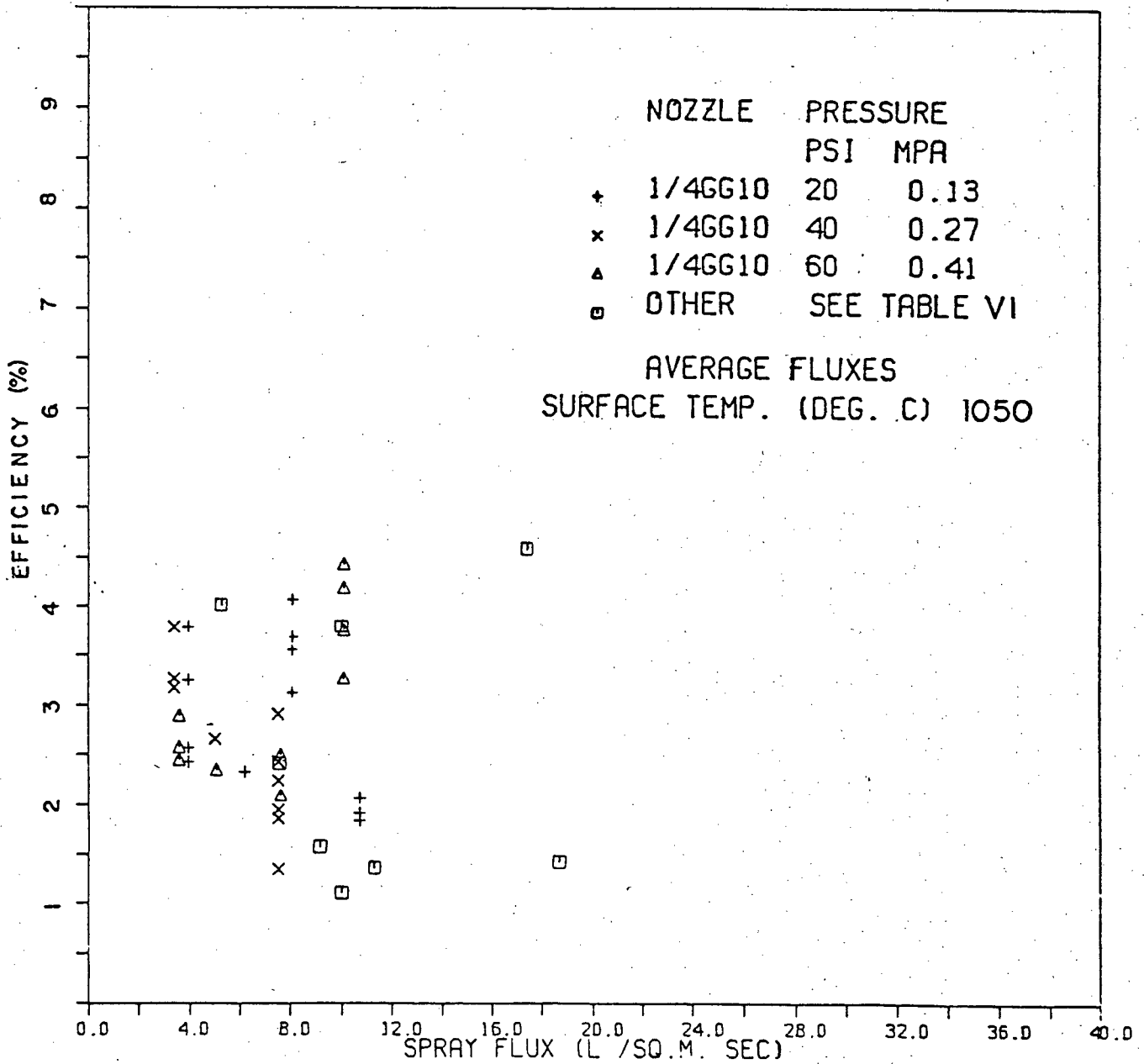


Figure 88 Variation of spray cooling efficiency with values of water flux averaged over the probe face, for a surface temperature of 1050°C.

TABLE VII Coefficients of the Curves Fitted to Correlate Spray Efficiency
to the Peak Value of the Spray Water Fluxes for Different Surface
Temperatures.

Form of the fitted curve:

$$\eta (\%) = P(1) + P(2) \dot{m}^{P(3)}$$

Surface Temperature °C	Parameter Estimates			Standard Error of		
	P(1)	P(2)	P(3)	P(1)	P(2)	P(3)
800	1.37	- 24.15	-0.83	1.60	7.36	0.34
850	0.29	19.61	-0.68	1.95	4.10	0.30
900	0.06	16.30	-0.66	1.51	2.74	0.26
950	0.43	12.50	-0.69	1.14	2.51	0.29
1000	1.26	7.06	-0.75	0.97	3.00	0.53

TABLE VIII Coefficients of the Curves Fitted to Correlate the Spray Efficiency
to the Value of Spray Water Flux Averaged Over the Area of the Probe
Face, for Different Surface Temperatures.

Form of the fitted curve:

$$\eta (\%) = P(1) + P(2) \dot{m}^{P(3)}$$

SURFACE TEMPERATURE °C	PARAMETER ESTIMATES			STANDARD ERROR OF		
	P(1)	P(2)	P(3)	P(1)	P(2)	P(3)
800	2.92	22.48	-0.89	2.35	8.75	0.52
850	2.02	20.32	-0.84	2.29	6.60	0.47
900	1.51	17.04	-0.82	1.72	4.52	0.39
950	1.51	12.43	-0.80	1.49	3.67	0.45
1000	2.54	5.89	-0.95	1.12	5.23	1.10

coefficient vs. spray water flux data (Tables IV and V). In Figure 76, the relationship between the heat-transfer coefficient and the spray water flux is almost linear, and as can be seen from Figure 88, the change in the efficiency with water flux is very small. Another point of note is that the data from other nozzles also falls within the variability for the 1/4 GG 10 nozzle. No effect of the spray pressure on the efficiency is observed.

The variation of efficiency with water flux for different surface temperatures were fitted to an equation of the form

$$\eta\% = P(1) + P(2) \dot{m}^{P(3)} \quad \dots 5.5$$

The coefficients $P(1)$, $P(2)$ and $P(3)$ for these fits using the peak and averaged values of water flux are given in Tables VII and VIII.

5.4 Calculation of Droplet Velocities and Droplet Momenta Within the Sprays

As a prelude to the comparison of the results from the present work to data reported in the literature, calculations of the droplet velocities at the nozzle exit and droplet momenta were made. Droplet sizes required for the calculation of droplet momenta were the median drop sizes published by the manufacturer of the nozzles.

Droplet velocity calculations were carried out using an energy balance approach suggested by Gaugler.⁵³ Negligible energy losses are assumed for the calculations. Upstream from the nozzle, the water has a velocity V_1 , pressure P_1 and flows through a pipe of area A_1 . Downstream, the flow consists of droplets of diameter d and velocity V_2 at atmospheric pressure P_2 . If the net rate of production of the droplets is considered to be \dot{N} , then the energy balance can be written as

$$\rho V_1 A_1 \left[\frac{V_1^2}{2g} + \frac{P_1}{\rho} \right] = \dot{N} \frac{\rho \pi d^3}{6} \left[\frac{V_2^2}{2g} + \frac{P_2}{\rho} \right] + \dot{N} \sigma \pi d^2 \quad \dots 5.6$$

Since the surface tension term accounts for less than 5% of the energy, it is neglected. Substituting

$$\dot{m} = \rho V_1 A_1 = \dot{N} \pi \frac{d^3}{6} \quad \dots 5.7$$

and simplifying yields

$$V_2^2 = V_1^2 + \frac{2g}{\rho} (P_2 - P_1) \quad \dots 5.8$$

Since $(P_2 - P_1)$ is the pressure gauge reading, knowledge of the mass flow rate through the nozzle yields a value for the droplet velocity V_2 . The results of the calculations are given in Table IX.

Examination of this Table shows that as the spray

TABLE IX

Calculated Droplet Velocities and Droplet
Momenta in the Sprays Produced by the Nozzles
Studied in this Investigation.

Nozzle Type	Spray psi	Pressure MPa	Droplet Velocity cm/sec	Mean Drop Diameter, microns	Droplet Momentum gm cm/sec
1/4 GG 10	20	0.14	1669	2420	12.39
	40	0.28	2359	2040	10.49
	60	0.41	2889	1730	7.83
1/4 GG 12 SQ	20	0.14	1672	2540	14.35
	40	0.28	2363	2120	11.79
	60	0.41	2894	1800	8.84
1/4 GG 6.5	20	0.14	1664	2120	8.30
	40	0.28	2354	1800	7.19
	60	0.41	2883	1520	5.30
	90	0.66	3627	1120	2.67
3/8 HH 18	20	0.14	1673	2820	19.65
	30	0.21	2049	2580	18.43
1/8 GG 5	20	0.14	1667	1900	5.99
	40	0.28	2357	1580	4.87
	60	0.41	2888	1360	3.80
	80	0.69	3728	970	1.78

pressure increases, there is a decrease in the droplet diameter. The calculated exit velocity of the droplets increases with the spray pressure. However, due to the rapid decrease of droplet diameter with increasing spray pressure, the droplet momentum decreases as the spray pressure increases, in the case of the nozzles investigated.

It should be noted that these calculations are approximate and that the actual velocity of the droplet would decrease as it moves away from the spray nozzle due to drag effects. The range of droplet velocities is seen to vary from about 16.5 to 30 m/s, and the droplet momentum from about 8 to 20 gm cm/s - a factor of 2 to 2.5, for the results presented in this thesis.

5.5 The Nature of the Boiling Process

Critical, or Liedenfrost temperatures for the onset of stable film boiling have been estimated from the results of other studies on spray cooling, and have been plotted in Figure 89 as a function of the spray water flux. It can be seen from this Figure that the critical point is moved to higher surface temperatures as the spray water flux is increased, thus extending the region of unstable film boiling to higher surface temperatures. It can also be observed that in the experiments of Mizikar⁷⁶, stable film boiling is present at surface temperatures

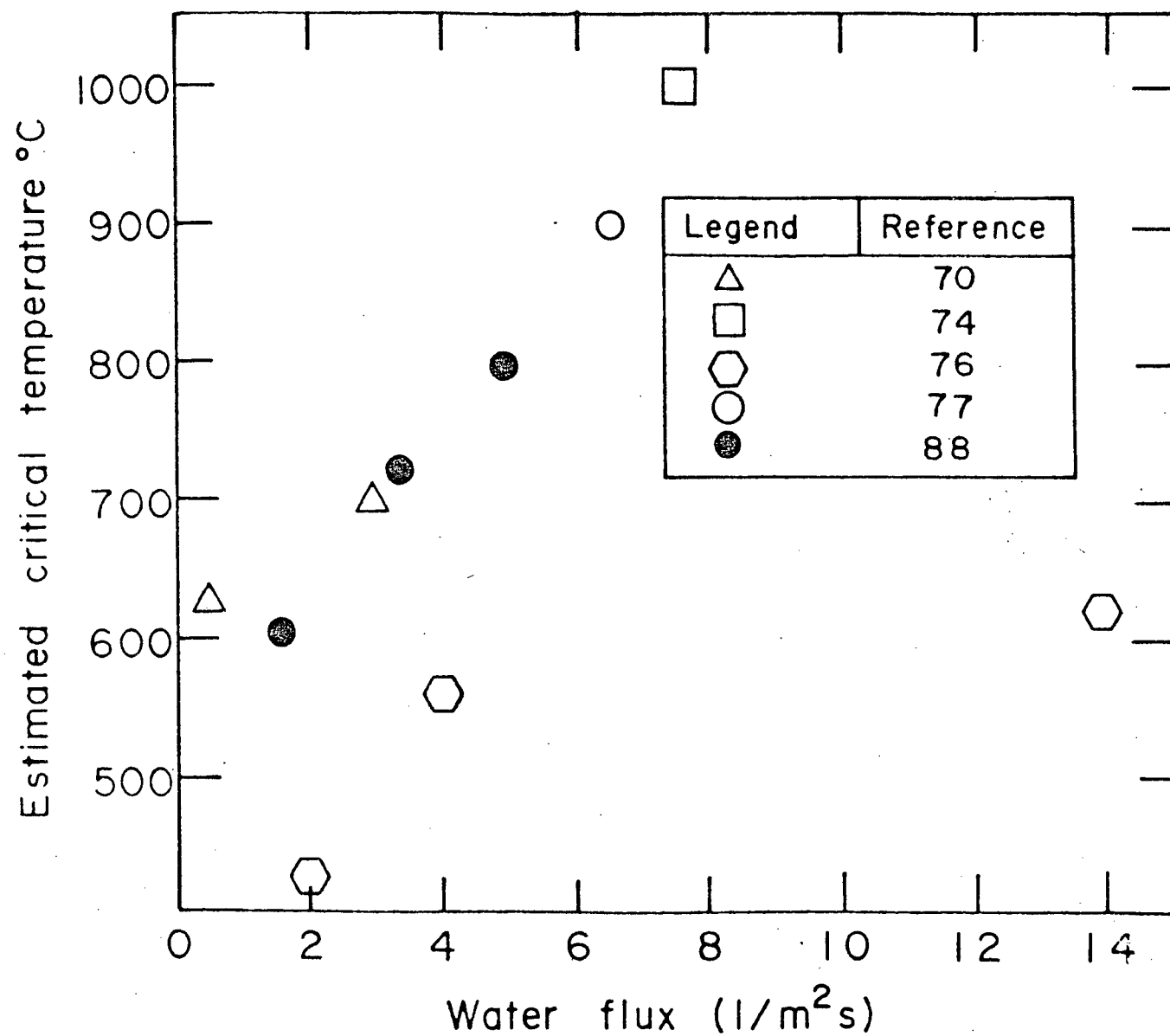


Figure 89: Variation of critical temperature with water flux

greater than 625°C even at water fluxes in excess of $10 \text{ l/m}^2\text{s}$. This is in contrast with other results presented in this Figure, in which the critical temperature exceeds 950°C when the water flux increases beyond $6 \text{ l/m}^2\text{s}$.

The variation of heat flux with surface temperature, as obtained from the present study for different water fluxes, is plotted in Figure 90. The results shown in this Figure have been calculated from the data shown in Table IV. The negative slopes of the curves in the temperature range studied indicate that the operating boiling mode is transition or unstable film boiling mode. This boiling mode has been obtained in this study even for the low water flux of $2 \text{ l/m}^2\text{s}$.

The magnitude of the heat fluxes presented in Figure 90 is in reasonable agreement with that in the high temperature end (just below the critical point) of the unstable film boiling region shown in Figure 3. It must be noted in comparing these Figures that the data in Figure 3 has been obtained from pool boiling studies of heat transfer from a hot wire immersed in water at its saturation temperature.

The existence of unstable film boiling serves to explain the observation that the heat-transfer coefficients

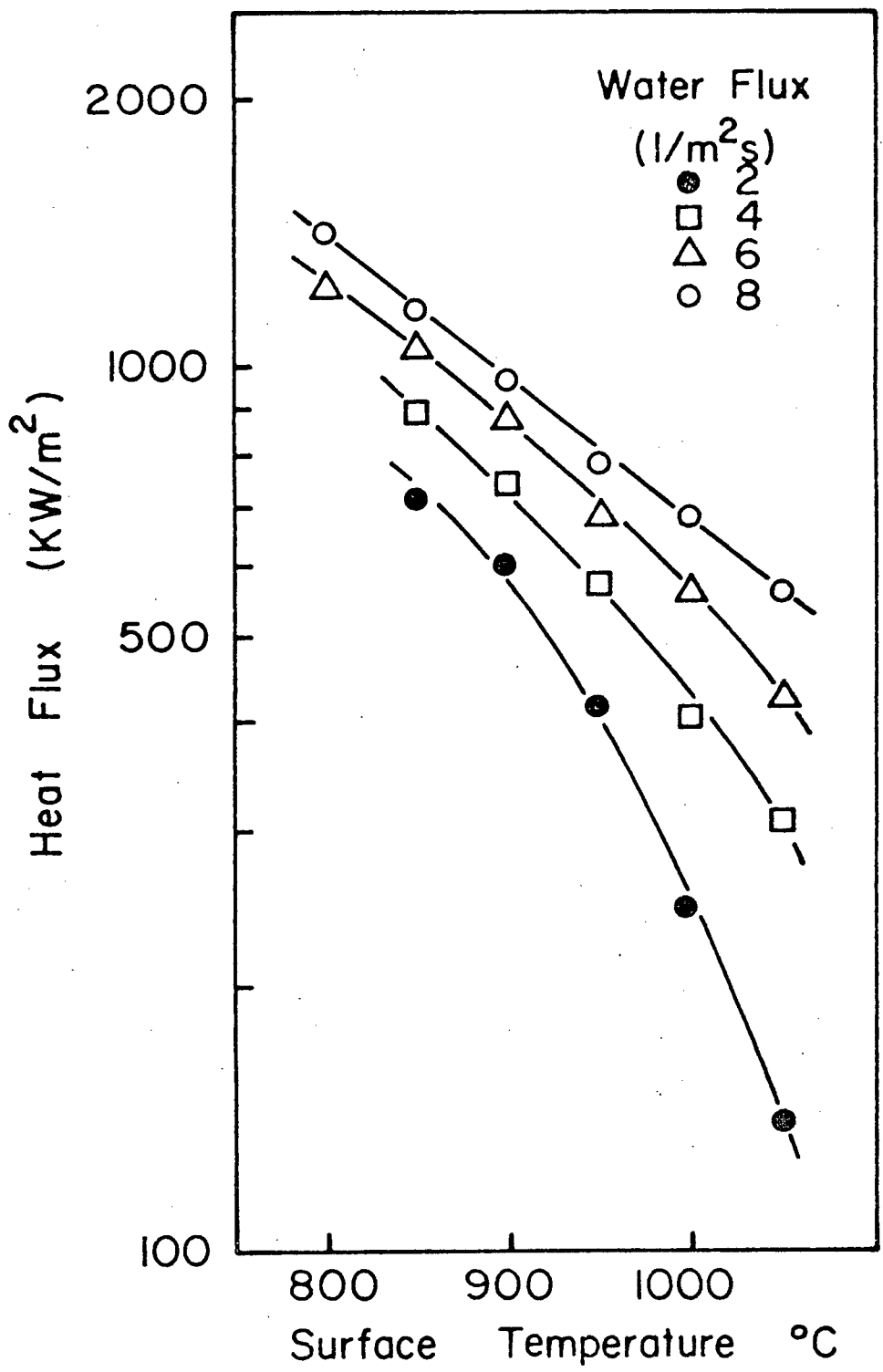


Figure 90: Variation of the heat flux with surface temperature for different water fluxes.

that were measured were influenced by the surface condition of the heat-transfer probe. The extent of scatter due to the presence of adherent scale on the surface is, however, limited to that reported in Figures 65-76. This is in view of the fact that whenever the cooling of the probe was affected by the presence of semidetached scale, (section 5.2.1), the data from such runs was not used in the calculation of the heat-transfer coefficients.

In Figure 12, it can be observed that only the results of Sugitani ⁷⁴ show any significant temperature dependence of the heat-transfer coefficients for surface temperatures greater than 700°C. His spray cooling studies employed a transient method for the determination of the heat-transfer coefficients. The other results plotted in Figure 12 were obtained using steady-state measurement techniques. The results of Muller and Jeschar ⁸¹, obtained from steady-state measurements, also did not indicate any significant temperature dependence of the heat-transfer coefficients for surface temperatures between 700 and 1200°C. In contrast with these results, recent spray cooling studies, utilising transient measurements ^{14, 74, 75, 77-79} have shown that the heat-transfer coefficients decrease as the surface temperature increases between 700 and 1000°C. In summary, these findings indicate that, while for the steady-state measurements stable film boiling is achieved above a surface temperature of

600°C, unstable film boiling is the operating boiling phenomenon in transient type studies, even at surface temperatures much in excess of 600°C, (except in the case of Mizikar's study).

5.6 Temperature Dependence of the Heat-Transfer Coefficients

$$\text{Curves of the type: } h = P(1) \left(\frac{T_s}{1000} \right)^{P(2)} \dots 5.9$$

were fitted to the heat-transfer data obtained for the ¼ GG 10 nozzle using a multiple regression technique¹¹⁷.

The results of the regression are presented in Table X. Thus large values of P(3) can be seen which shows the significant temperature dependence of h, as reported in the previous section. These values for P(3) are much higher than the value of 1.2 reported by Sasaki⁷⁷. The values of P(2) fall within the range reported in other spray cooling studies.

5.7 Comparison with the Results of Other Workers

Since laboratory investigations on spray heat transfer have been carried out using a variety of experimental methods and conditions (Table II), there is a large variation in the published spray-heat transfer data, as can be seen in Figure 11. In many cases, all the relevant experimental details are not published, which makes comparison between the results of different workers uncertain. The basis on which the spray water fluxes have been calculated is by far the most important factor, because this has been found to be the variable that plays the largest role in the

TABLE X Multiple Regression Coefficients for the Water Flux and Temperature
Dependence of the Heat-Transfer Coefficients

$$\text{Form of the Fit: } h = P(1) m^{P(2)} \left(\frac{T_s}{1000} \right)^{P(3)}$$

(¼ GG10 nozzle)

Surface Temperature: 800 to 1050°C

Waterflux	Parameter Estimates			Standard Error of		Multiple R Squared
	P(1)	P(2)	P(3)	P(2)	P(3)	
Peak	0.239	0.417	-4.736	0.034	0.190	0.7834
Averaged Over 25mm Diameter	0.214	0.537	-4.733	0.041	0.185	0.7961
Averaged Over Sprayed Area	0.403	0.323	-4.807	0.031	0.203	0.7546

variation in the heat-transfer coefficients. A summary of the different ways in which the spray fluxes have been obtained is given in Table XI. It can be observed from this Table that a number of workers have used average values of spray water flux. These have been calculated either from data on water flow rates through the spray nozzle and the spray angle, or, in the case of in-plant measurements, from the water flows in different spray zones in the caster. In addition, where local water fluxes have been measured, different cross-sectional areas of the collectors have been used. It becomes evident from the results of the measurements made on the full cone nozzles in the present work, that when peaks are present in the spray water flux distributions, the value of the average water flux would change by a substantial amount depending on the area used for the calculations. This, as has been shown in a previous section (5.2.5.2), changes the relationship between the heat-transfer coefficients and the spray water flux. As mentioned earlier, use of averaged water fluxes (when peaked flux distributions are present) would yield higher heat-transfer coefficients for the same value of water flux, when compared with those calculated using peak fluxes. Thus, a consistent approach to the calculation of the spray water fluxes becomes mandatory if the heat-transfer coefficient vs. spray flux correlations obtained by different workers are to be interpreted in a meaningful fashion. Since most workers have not reported any

Table XI Basis for the Method Used for the Determination
of Water Fluxes by Different Investigators of
Spray Heat Extraction

Investigator	Basis for the Calculation of Water Fluxes
Mitsutsuka ^{71,72}	Average, over the sprayed area.
Ishiguro ⁷³	Average, over the sprayed area.
Etienne et al. ⁷⁵	Average, depending on nozzle position, for veejet nozzles.
Auman ⁶⁸	Average, over the sprayed area.
Nozaki ³⁵	Average, in-plant measurements
Akimenko et al. ⁸⁵⁻⁸⁷	Average, in-plant measurements
Alberny et al. ^{88,89}	Average, in-plant measurements
Hoogendoorn and den Hond ⁷⁰	Peak water fluxes, unknown collector area.
Mizikar ⁷⁶	Peak water fluxes, 6 mm dia. collectors.
Sugitani et al. ^{74,78}	Peak water fluxes, 6 mm dia. collectors.
Junk ⁸⁰	Peak water fluxes, unknown collector area.
Muller and Jeschar ⁸¹	Peak water fluxes, 120 mm ² to 600 mm ² collector area.
Bolle and Moreau ⁸²⁻⁸⁴	Peak water fluxes, 40 mm x 20 mm collectors.

data regarding the distribution of water fluxes in the sprays produced by the nozzles employed in their measurements, it becomes impossible to reconstruct the values of the local water fluxes in the sprays for which the measurements of heat-transfer coefficients have been reported.

To aid in the comparison of the heat transfer results obtained in this study with those of other investigators, the power curves fitted to the data (Tables IV and V) have been plotted in Figures 91 and 92. Peak values of water flux have been used for Figure 91 and water fluxes averaged over the cooled surface of the heat transfer probe have been used in Figure 92. The range of water fluxes for which the fitted curves are valid representations of the data are shown in the Figures.

The present results can be compared most readily to those reported by Mizikar,⁷⁶ since the nozzles and experimental conditions employed by him are similar to those used in the present investigation. Comparison of Mizikar's results (Figure 11a) and the results in Figure 91 show that for the higher surface temperatures ($>900^{\circ}\text{C}$) the present results are lower than the heat-transfer coefficients reported by him for \dot{m} greater than 2 to 14 $\text{g/m}^2\text{s}$, with the agreement being better for a larger range of water fluxes as the surface temperature decreases. While he has found

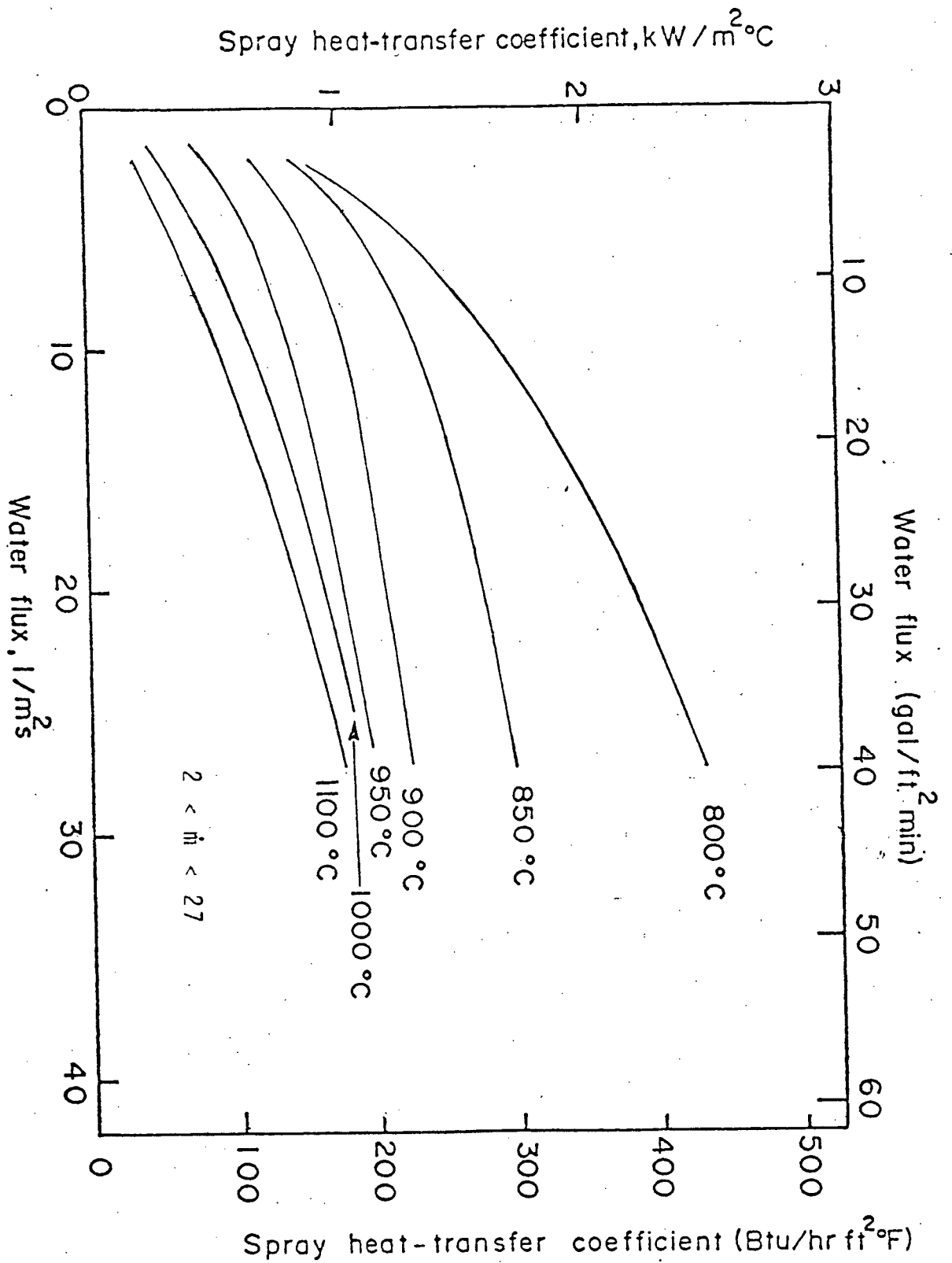


Figure 91 Curves fitted to the measured variation of htc with peak values of water flux.

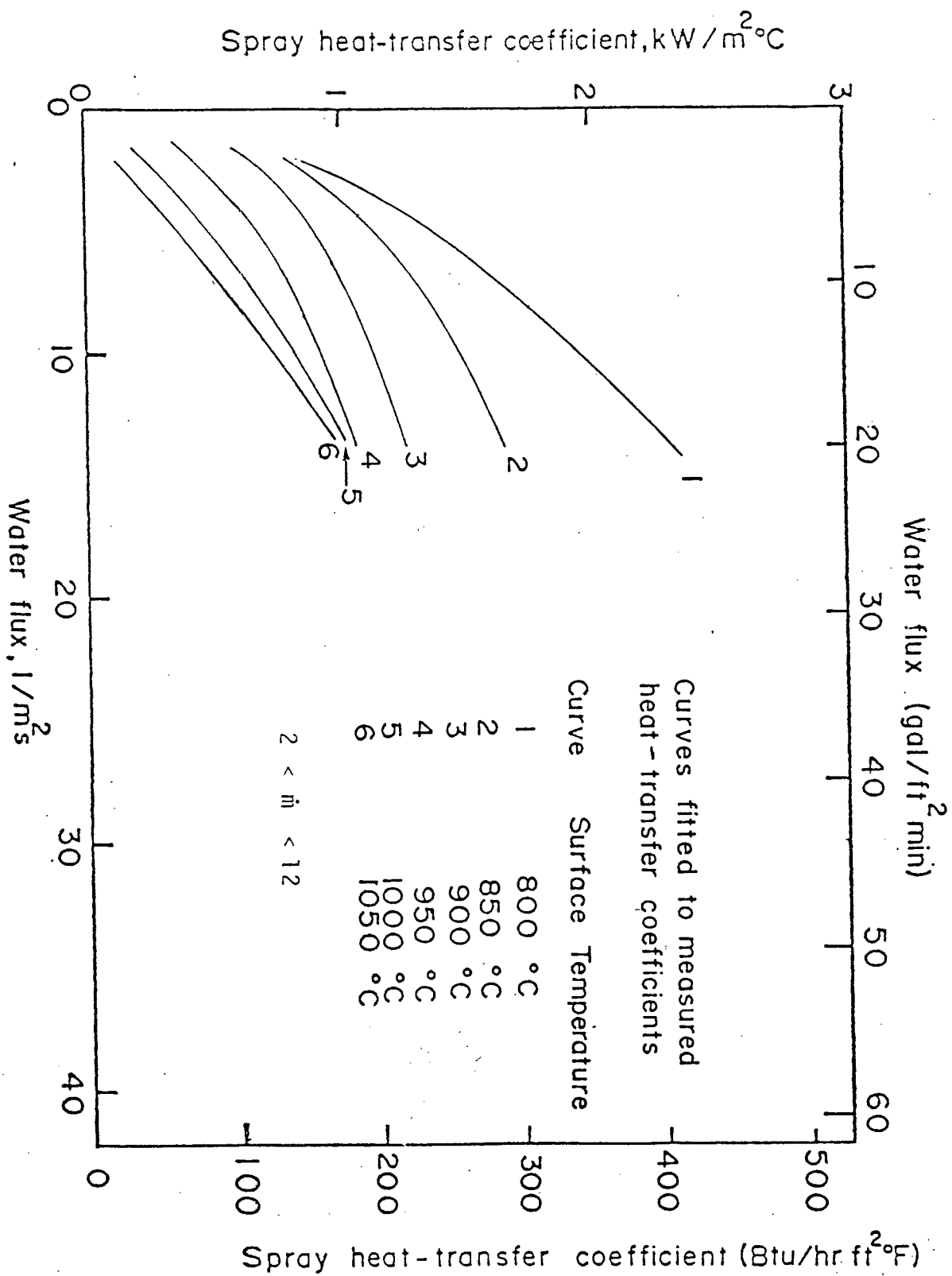


Figure 92 Curves fitted to the measured variation of htc with values of water flux averaged over the probe face.

that the heat-transfer coefficients are fairly independent of surface temperature when the surface temperatures are in excess of about 600 to 700°C, the present results indicate that these coefficients are temperature sensitive even when the surface temperatures are in excess of 800°C. In contrast with the results of the present study, very little scatter is evident in Mizikar's work. This is surprising in view of the fact that even with the great care used to perform the experiments reported in this thesis under similar conditions, a considerable amount of scatter in the data was obtained.

There was also no evidence of pressure on the heat-transfer coefficients as was reported in his work. Comparison of the results shown in Figure 92 with those reported by him (Figure 11a) show that for surface temperatures in excess of 950°C, the agreement between the two sets of results is fairly good for $\dot{m} < 15 \text{ g/m}^2\text{s}$. Although there is no mention of average water fluxes in his work, the fact that the present results are closer to his results when average fluxes are used may be due to the lower water fluxes used by him for the $\frac{1}{4}$ GG 10 nozzle.

Examination of Figures 11, 91 and 92 show that the present investigation yields the lowest heat-transfer

coefficients for any given water flux, when compared to other laboratory heat transfer measurements for surface temperatures of 1000 and 1050° C. While this could be attributed to the different methods used for the calculation of the water flux by various investigators, it must be noted that the experimental technique used also appears to strongly affect the measured heat-transfer coefficients. In general, the heat-transfer coefficients measured by spraying vertically downward upon a horizontal heated plate are higher than those obtained by spray cooling a vertical plate. This can be seen by comparing the results of Bolle and Moreau⁸²⁻⁸⁴ and Muller and Jeschar.⁸¹ Bolle and Moreau, spraying downward onto a horizontal plate, found that their steady-state experiments yielded heat-transfer coefficients that were 20% higher than those obtained by Muller and Jeschar, who used vertical plates. For the range of water fluxes used in these two sets of investigations (up to 12 $\text{g/m}^2\text{s}$), it is seen from Figure 11 that both show the highest heat-transfer coefficients (except for the results of Ishiguro⁷³).

Spraying downward onto horizontal heated surfaces would be expected to raise the heat-transfer coefficients because of either of the following reasons:

- i) Spray droplets impinging on the surface and rebounding from it after impact would fall

back onto the surface, thus effectively increasing the actual water flux on the sprayed surface and increasing the efficiency of spray cooling.

- ii) A horizontal layer of water held up by a vapour cushion could exist above the surface, and be forced against the surface by the impinging spray. This again would have the effect of increasing the spray cooling efficiency, with a corresponding increase in the heat-transfer coefficient.

The results reported by Muller and Jeschar⁸¹ show that the velocity of the impinging droplets exerts an influence on the heat-transfer coefficients (Eq. 2.17), which increase with increasing droplet velocity. For a water flux of $10 \text{ kg/m}^2\text{s}$, an increase in the droplet velocity from 15 to 30 m/s (a factor of 2) causes a 25% increase in the heat-transfer coefficients. Increases of the heat-transfer coefficients have also been linked to increasing droplet momenta. Due to the scatter of the results in this study, no effects due to the dynamic droplet properties could be discerned.

The very high heat-transfer coefficients reported by Mitsutsuka^{71,72} are probably due to a combination of a number of effects. Plain carbon steels were used in

his experiments, and these steels tend to scale easily. The horizontal, 28 mm thick, heated plates were sprayed both from the bottom and top simultaneously, and the transient temperatures at distances between 5 and 23 mm from the top surface of the plate were monitored. These temperatures were then used to calculate the surface temperatures and heat-transfer coefficients. It has been mentioned in Chapter 3 that increasing the distance of the point of measurement below the surface could lead to gross errors in the calculated heat-transfer coefficients. In addition, the heat-transfer coefficients have been estimated for specific temperature differences at the surface. Since it has been shown from the present results that the heat-transfer coefficients increase rapidly with decreasing surface temperatures, the average values of the calculated heat-transfer coefficients would be expected to have higher values than those obtained for higher surface temperatures. Another point to note is that even though full cone nozzles were employed in his work, the spray water fluxes used in his correlations were averaged over the plate area, thus effectively yielding higher heat-transfer coefficients for the same value of water flux, when compared to local water fluxes.

Among the investigators reporting the dependence of heat-transfer coefficients on surface temperature, only

the results of Sugitani,⁷⁴ Sasaki et al.⁷⁷ and Etienne et al.⁷⁵ show any significant dependence in the high temperature range above 700° C. Sasaki et al.⁷⁷ obtained their heat-transfer coefficients using optical pyrometric measurements of the heated plate surface during spray cooling. Since no mention is made of the use of two colour pyrometers in their work, it would appear that the presence of water in the sighting path could lead to errors in the calculated heat-transfer coefficients. The correlation of Sasaki (Eq. 2.15) predicts a 13% difference (as against a 11% difference from the results of the present study) in the heat-transfer coefficients as the surface temperature falls from 1000° C to 900° C for a water flux of 10 $\text{kg/m}^2\text{s}$. The fact that surface conditions could affect the heat-transfer conditions is mentioned in his work.

When comparing the heat transfer correlation obtained by Etienne et al.,⁷⁵ for a surface temperature of 900° C, with the present results, it is found that the present results are lower than the predictions for their correlations above \dot{m} of about 10 $\text{kg/m}^2\text{s}$. Even though platinum rods with a high resistance to scaling have been employed in their experiments, they have found that a fair amount of scatter was present in their measurements, and that the scatter increased at lower surface temperatures. The difference between the results of the present study and their results

could be attributed partially to the different surface conditions of their measuring probe, and partially to the fact that the measurements were made while spraying downward onto the probe surface.

As a final step in the comparison of the present results with those of other workers, water fluxes were averaged over the whole sprayed area (for the 1/4 GG 10 nozzle) and power curves of the form given in Equation 5.2 were then fitted to the variation of the heat-transfer coefficients with the averaged water fluxes. The coefficients of the fitted curve are given in Table XII and are valid for \dot{m} between 1 and 10 g/m²s. These fitted curves are plotted in Figure 93. Comparison of this Figure with Figure 11 shows that for surface temperatures in excess of 900°C, the present results fall within the range of heat-transfer coefficients reported by other investigators. This, again reinforces the necessity of using a consistent basis for the calculation of water fluxes, so that meaningful interpretations of the data can be made.

The form of the power curves fitted to the variation of heat-transfer coefficients with water flux is in agreement with those proposed from several of the studies on spray heat extraction (Table II). Several of the investigators have also reported that the exponent of the

Table XII Coefficients of Power Curves Fitted to the
Variation of Heat-Transfer Coefficients with
Water Fluxes Averaged over the Whole Sprayed
Area, for Different Surface Temperatures.

Form of the curve: $h = P(1) \dot{m}^{P(2)}$

Surface Temperature °C	Parameter Estimates		Standard Error of	
	P(1)	P(2)	P(1)	P(2)
800	1.22	0.27	0.13	0.08
850	1.14	0.13	0.12	0.08
900	0.86	0.15	0.08	0.07
950	0.59	0.25	0.05	0.06
1000	0.36	0.49	0.04	0.07
1050	0.18	0.75	0.04	0.12

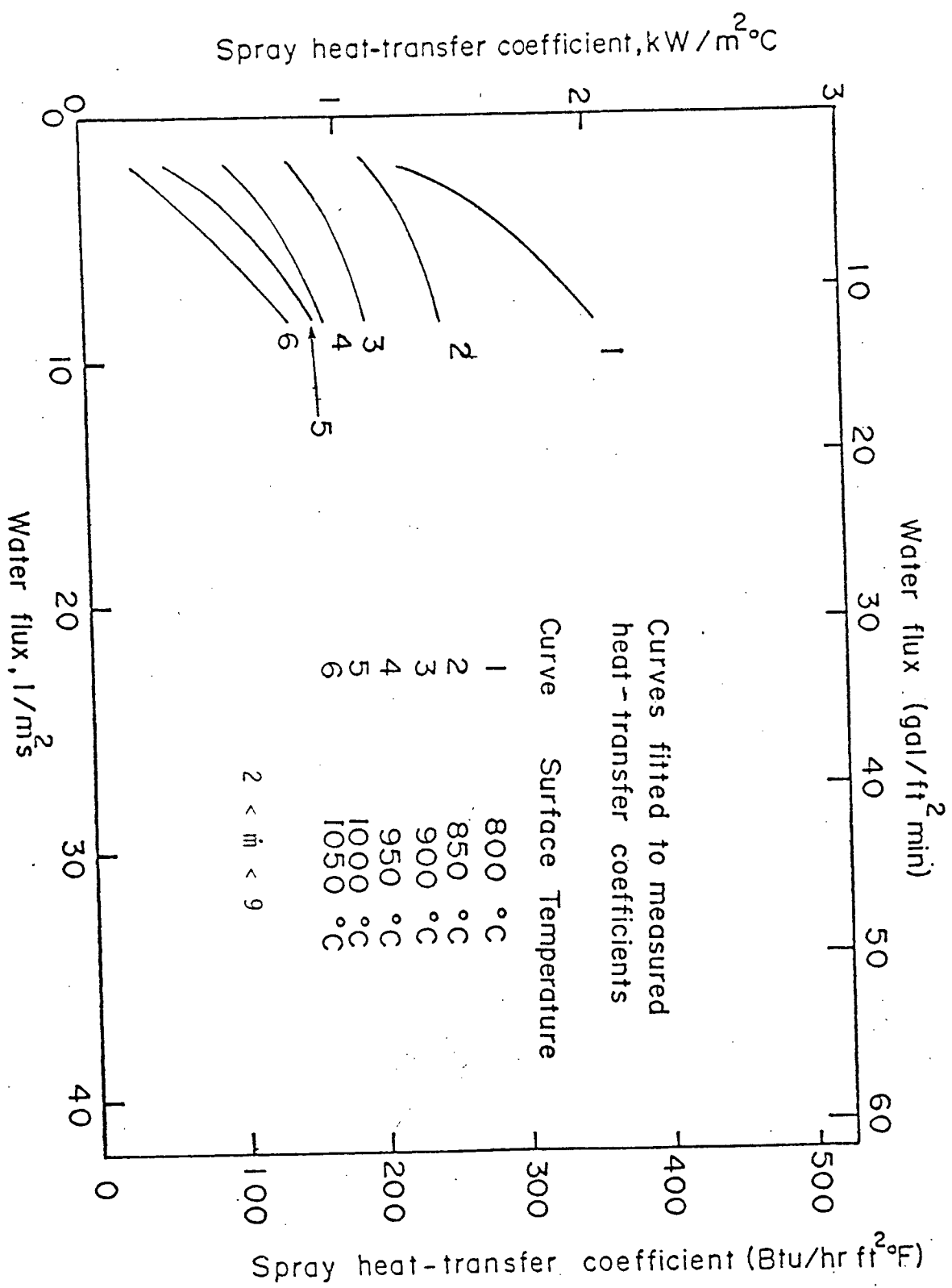


Figure 93 Curves fitted to the measured variation of htc with values of water flux averaged over the whole sprayed area.

power curve changes with the surface temperature.^{72,75} The fractional values of the exponent in the curves is linked to the reduction in the efficiency of spray cooling as the water flux increases. The decrease in the efficiency can be attributed to the interactions between the droplets propelled towards the cooled surface and those rebounding away from it.

5.8 Problems Limiting the Measurements

Of the many problems encountered in the course of the measurements of heat-transfer coefficients, the most troublesome were the problems of failure of the measurement systems and non-reproducibility of cooling rates under similar spraying conditions.

The high temperatures and repeated thermal cycling of the measuring probe were the main contributors to the problems with the measuring systems. The thermocouples in the measuring probe were being operated at temperatures close to their maximum operating range. In addition, the thermocouple wires were welded in the bottom of blind holes and therefore, as mentioned earlier, examination of these welds before starting the measurements was impracticable. These factors, including thermal cycling, were very detrimental to the useful life of the probe under service conditions, and led to frequent failures of the temperature

measurement system. In the initial experiments, the welds between the thermocouple wire and the AISI 304 stainless steel of the heat transfer probe were, in most instances, the site of failure. Careful control of the welding procedure tended to reduce the incidence of such failures, but did not eliminate the problem. The thermocouple wires subsequently failed at other locations as well. The useful lifetime of the probes could not be estimated - the probes might last anywhere from 1 to 15 thermal cycles. The only remedy found to prevent such occurrences was to use lower operating temperatures, and to use slow heating and cooling rates. Since the cooling rates were the parameters being measured, and thus not amenable to control, slow heating rates were employed to even out the temperature gradients associated thermal stresses which could contribute to the failures of the thermocouples.

Non-reproducibility of the cooling rates under similar external cooling conditions was another persistent problem, and could occur due to a variety of reasons, the most important of which was the surface condition of the probe. Due to this problem, the probe surfaces to be sprayed were initially polished. However, repeated heating and blasting with water soon marred the surface finish. Oxidation of the probe surface was minimized by the choice of a scale resistant steel, but the harsh conditions imposed on

the probe changed the probe surface condition, and changed the cooling rates. Therefore, many repeated measurements were made for each spraying condition, and the presence of any factor that could adversely affect the measurements was reason for disregarding the results of that particular run. Only the cooling curves from reproducible runs were used for the analysis and calculation of heat-transfer coefficients. Tests were repeated at frequent intervals with similar spraying conditions to determine that reproducibility was being maintained. These two problems made the acquisition of data with small scatter a long and arduous task.

Electrical noise reaching the recording equipment was a problem more easily dealt with, by installing filter capacitors at the terminals of the signal conditioning experiments. The use of amplifiers with noise suppression circuits would be a great asset in performing the measurements of the fast transient signals. These were not available in the course of the present investigation.

5.9 Application of the Data for Spray Chamber Design

Since, in an actual casting operation, especially for the casting of carbon steels, areas of semidetached scale, may exist on the strand surface, the heat-transfer coefficients between the spray and the strand surface could be much higher than those reported in this thesis. As such,

the surface temperature of the strand would be lower than that calculated using the results of this laboratory study. Evaluation of the effect of this scale on the heat-transfer coefficients would therefore have to be done with the aid of in-plant measurements of the strand surface temperature using optical pyrometric devices.

Chapter 6

SUMMARY AND CONCLUSIONS

Measurements have been carried out to characterize the water distribution in the sprays produced by several commercial spray nozzles as a function of the spray pressure and distance from the nozzle. It has been found that, when spraying onto a vertical, cold surface, there is a substantial amount of water flowing downward adjacent to the sprayed surface, designated as the 'water curtain'. Therefore, two types of measurements have been made to determine:

- i) The amount of water arriving at any point in the spray directly from the spray nozzle.
- ii) The combined volume of water arriving at this point in the spray directly from the spray nozzle, as well as that flowing downward adjacent to the sprayed surface under the influence of gravity.

The measurements indicated that there is a fair degree of variability in the sprays produced by similar nozzles, yielding a variation in the water flux of about 30% under similar operating conditions. Spray flux 'maps' and contours over the whole sprayed area show that, for the full cone nozzles, there is a reasonable amount of

circular symmetry of the spray fluxes about the spray axis. The horizontal centreline spray flux profiles for the sprays from full cone nozzles show that sharp peaks are present in the spray flux distributions at the centre of the sprays. Reduction in the spray pressures and increasing the distance from the spray nozzles tend to yield more even distributions in the spray fluxes at the centre of the sprayed cone.

Heat-transfer coefficients have been measured for these sprays impinging on heated, vertical surfaces of stainless steel "heat transfer probes". Measurement of temperature transients within the probe during spray cooling (with the aid of thermocouples embedded in them), and analysis of these transients yielded the required heat-transfer coefficients and heat fluxes as a function of the temperature of the cooled surface. The temperature-time transients were analyzed using a solution to the "Inverse Boundary Value Problem". The results of the measurements show that:

- i) The most important variable affecting the heat-transfer coefficients is the magnitude of the local water flux at the probe surface.
- ii) The heat-transfer coefficients are surface temperature dependent even at temperatures in excess of 800°C . The operating boiling

phenomenon is unstable film boiling up to the maximum surface temperature (1050°C) that was used.

- iii) The nozzle type does not strongly affect the measured heat-transfer coefficients for the same local water flux.
- iv) The spray pressure (within the range used in the measurements) does not have a strong influence on the heat-transfer coefficients.
- v) The presence of the "water curtain" was found to increase the heat-transfer coefficients.
- vi) The spray cooling efficiency decreases with increasing water flux and increasing surface temperature.

Correlations have been obtained linking the spray heat-transfer coefficients and water fluxes, and are of the form:

$$h = P(1) \dot{m}^{P(2)} \left(\frac{T_s}{1000} \right)^{P(3)} \dots \quad 6.1$$

The value of the exponent $P(2)$ is fractional, and indicates that increase of the water flux has less than a proportional effect on the heat-transfer coefficients.

It has been determined that a consistent method must be used as the basis for the determination of the water flux at the cooled surface, in order to be able to make meaningful comparison with the results obtained by different workers.

BIBLIOGRAPHY

1. Kurzinski, E.F., "Continuous Casting Cooling Water Flow Control", Iron and Steel Engineer, October 1979, pp. 57-59.
2. Taylor, C.R., "Continuous Casting Update", Met. Trans. B, Vol. 6B, 1975, pp. 359-375.
3. Mori, H., "Causes and Prevention of Defects in Continuous Casting, Part I", Tetsu-to-Hagané, Vol. 58, 1972, pp. 1511-1534, [HB Transl. No. 9000-I & II].
4. Brimacombe, J.K. and Sorimachi, K., "Crack Formation in the Continuous Casting of Steel", Met. Trans. B, Vol. 8B, 1977, pp. 489-505.
5. Ushijima, K., "Continuous Casting of Steel", ISI Special Report No.89, 1965.
6. Ushijima, K., "Mechanism of Internal Crack Formation in Continuously Cast Steel Billets", Tetsu-to-Hagané, Vol. 47, No. 2, 1961, pp. 116-124. [HB Transl. No. 5220].
7. Mori, H., "Causes and Prevention of Defects in Continuous Casting, Part II", Tetsu-to-Hagané, Vol. 60, 1974, pp. 784-806. [HB Transl. No. 9355-I & II].
8. Definitions and Causes of Continuous Casting Defects ISI Pub. 106, 1967.
9. Brimacombe, J.K., Agarwal, P.K., Baptista, L.A., Hibbins, S., and Prabhakar, B., "Spray Cooling in the Continuous Casting of Steel", Paper presented at the NOH-BOS Conference, Washington, 1980.
10. Adams, C.J., "Hot Ductility and Strength of Strand Cast Steels up to their Melting Points" Open Hearth Proc., TMS-AIME, Vol. 54, 1971, pp. 290-302.
11. Wray, P.J. and Holmes, M.F., "Plastic Deformation of Austenitic Iron at Intermediate Strain Rates", Met. Trans. A, Vol. 6A, No. 6, 1975, pp. 1189-1196.
12. Fuchs, A., "Untersuchung der Hochtemperaturzähigkeit von Stählen mit der Gleeble-apparatur", ESTEL-Berichte aus Forschung und Entwicklung Unserer Werke, No. 3, 1975, pp. 127-135.

13. Nadai, A. and Manjoine, M.J., "High Speed Tension Tests at Elevated Temperatures", J. Appl. Mech. Vol. 63, No. 6, 1941, pp. A77-91.
14. Nilles, P., Dauby, P., Etienne, A., Mairy, B. and Palmaers, A., "Quality Improvements of Continuously Cast Products", Proc. Open Hearth Conf., Chicago, ISS-AIME, Vol. 61, 1978, pp. 399-410.
15. Weinberg, F., "The Ductility of Continuously Cast Steel Near the Melting Point - Hot Tearing", Met. Trans. B, Vol. 10B, 1979, pp. 219-227.
16. Vom Ende, H. and Vogt, G., "Comparison of the Influence of Straight and Curved Mould Continuous Casting Machines on Product Quality", J. Iron Steel Inst., Vol. 210, No. 12, 1972, pp. 889-894.
17. Van Drunen, G., Brimacombe, J.K. and Weinberg, F., "Internal Cracks in Strand-cast Billets", Ironmaking Steelmaking, Vol. 2, No. 2, 1975, pp. 125-133.
18. Backer, L. and Gosselin, P., "Continuous Casting: Its Metallurgical Aspects Relative to High-Grade Alloy and Carbon Steels", Open Hearth Proc., TMS-AIME, Vol. 53, 1970, pp. 145-156.
19. Miller, C.I. Jr., "Metallurgical Process Control Yields Consistent Strand Cast Billet Quality", Open Hearth Proc., TMS-AIME, Vol. 54, 1971, pp. 316-321.
20. Donaldson, J.W., "Quality Control of Continuously Cast Steel Billets", J. Metals, Vol. 17, No. 12, 1965, pp. 1338-1343.
21. Brimacombe, J.K., "Design of Continuous-Casting Machines Based on a Heat Flow Analysis: A State-of-the-Art Review", Can. Met. Quart., Vol. 15, No. 2, 1976, pp. 163-175.
22. Agarwal, P.K., "Case Study of Spray Design for a Continuous Billet Caster", M.A.Sc. Thesis, University of British Columbia, 1979.
23. Schmidt, L. and Fredriksson, H., "Formation of Macro-Segregation and Centre-Line Cracks in Continuously Cast Steel", Ironmaking Steelmaking, Vol. 2, No. 1, 1975, pp. 61-67.
24. Brovman, M. Ya. Stal in English, Vol. 1, 1967, p. 26.

25. Ozeki, R.K. and Duke, J.D., "The Casting of High Quality Plate Steel Slabs at Texas Works", Proc. Int. Conf. on Continuous Casting of Steel, Biarritz, France, 1976, The Metals Society/IRSID, pp. 292-299.
26. Lankford, W.T., "Some Considerations of Strength and Ductility in the Continuous Casting Process", Met. Trans., Vol. 3, No. 6, 1972, pp. 1331-1357.
27. Myoshi, S., "Influence of Operating Conditions and Mechanical Factors on Centre Segregation of Slabs", Proc. Int. Conf. on Continuous Casting of Steel, Biarritz, France, June 1976, The Metals Society/IRSID, pp. 286-291.
28. Asano, K., Hiromoto, T. and Ohashi, T., "Centre Segregation in Continuously Cast Steel Slabs-Parts I and II", Tetsu-to-Hagané, Vol. 59, No. 4, 1973, pp. S82-S83 [HB Transl. No. 9099].
29. Asano, K., Hiromoto, T. and Ohashi, T., "Study of Centre Segregation in Continuously Cast Slabs - Parts III, IV and V", Tetsu-to-Hagané, Vol. 60, No. 4, 1974, pp. S63-S64, and S65 [HB Transl. No. 9320].
30. Abe, Y., Koike, A., Shibutani, A., and Shinoda, K., "Segregation in Continuously Cast High Carbon Steel Blooms", Tetsu-to-Hagané, Vol. 59, No. 4, Lecture 82, 1973, p. S84 [HB Transl. No. 9108].
31. Nashiwa, H., Yasumoto, K., Tokuda, M. and Hirakawa, K., "Effect of Roll Alignment on the Centre Segregation in Continuously Cast Slabs", Tetsu-to-Hagané, Vol. 60, No. 4, Lecture 96, 1974, p. S96 [HB Transl. No. 9374].
32. Irving, W.R. and Perkins, A., "Basic Parameters Affecting the Quality of Continuously Cast Slabs", Proc. Int. Conf. on Continuous Casting of Steel, Biarritz, France, 1976, The Metals Society/IRSID, pp. 107-115.
33. Brimacombe, J.K., Weinberg, F. and Hawbolt, E.B., "Formation of Longitudinal, Midface Cracks in Continuously Cast Slabs", Met. Trans. B, Vol. 10B, 1979, pp. 279-292.
34. Schmidt, L. and Josefsson, A., "On the Formation and Avoidance of Transverse Cracks in Continuously Cast Slabs from Curved Mould Machines", Scandinavian Journal of Metallurgy, Vol. 3, No. 5, 1974, pp. 193-199.

35. Nozaki, T., Matsuno, J., Murata, K., Ooi, H. and Kodama, M., "A Secondary Cooling Pattern for Preventing Surface Cracks of Continuous Casting Slab", Trans. ISIJ, Vol. 18, 1978, pp. 330-338.
36. Fisher, K., Litterscheidt, H., Rudacks, W., Simon, R.W. and Weber, R.A., "Industrial Experience with the Production of Continuously Cast Slabs", Proc. Int. Conf. on the Continuous Casting of Steel, Biarritz, France, 1976, The Metals Society/IRSID, pp. 280-285.
37. Eto, B., Onozawa, M., Abe, M. and Aoyagi, T., "Internal Cracks in Continuously Cast Blooms", Tetsu-to-Hagané, Vol. 58, No. 4, Lecture 111, 1972, p. S111 [HB Transl. No. 8830].
38. Sakamoto, E., Miyashita, Y., Yano, K. and Ansai, T., "Avoidance of Surface Defects in Continuously Cast Slabs for Plate", Tetsu-to-Hagané, Vol. 60, No. 4, Lectures 37-39, 1974, pp. S37-S39. [HB Transl. No. 9321].
39. Fujii, H., Ohashi, T. and Hiromoto, T., "On the Formation of Internal Cracks in Continuously Cast Slabs", Trans. ISIJ, Vol. 18, 1978, pp. 510-518.
40. Gray, R.J., Perkins, A. and Walker, B., "Quality of Continuously Cast Slabs", Proc. Int. Conf. on Solidification and Casting of Metals, Sheffield, England, 1977, The Metals Society, pp. 300-305.
41. Grill, A., "Cooling System to Prevent Centre-Line Cracks in Continuously Cast Steel Billets", Ironmaking Steelmaking, No. 2, 1979, pp. 62-67.
42. Baptista, L.A., "Control of Spray Cooling in the Continuous Casting of Steel", M.A.Sc. Thesis, University of British Columbia, 1979.
43. Foussal, J., "Model Pratique de Gestion et de Commande du Refroidissement Secondaire en Calculateur à la Coulee Continue de Solmer à Fos-Sur-Mer", Rev. de Met., Vol. 75, 1978, pp. 403-414.
44. Etienne, A., "Method of Controlling Continuous Casting of a Metal", U.S. Patent No. 4,073,332, 1978.
45. Adams, R.V., "Method of Continuously Casting Steel", U.S. Patent 3,478,808, November 18, 1969.
46. Fekete, K. and Bruderer, W., "Method of Controlling the Secondary Cooling of a Continuously Cast Strand", U.S. Patent No. 3,915,216, 1975.

47. Tiskus, J.R., "Method and Apparatus for Controlling the Rate of Heat Transfer to or From an Elongated Object", British Patent No. 1,302,040, 1973.
48. Tiskus, J.R., "Automation for High Tonnage Continuous Casting", Iron and Steelmaking Automation Conference, Vol. 1B, 1976, p. 4.2.2.
49. Etienne, A., Mairy, B. and Dauby, P., "Metallurgical Control and Automation for Continuous Casting Operation", Iron and Steelmaking Automation Conference, Vol. 1B, 1976, p. 4.2.3.
50. Etienne, A., "Reflexions sur le Controle du Refroidissement Secondaire des Installations de Coulee Continue", Circulaire d'Information-techniques, Vol. 34, No. 9, 1977, pp. 1929 - 1942.
51. Dewar, W.A.G. and Patrick, B., "Computer Control of Secondary Spray Cooling on an Eight-Strand Continuous Bloom Casting Machine", Iron and Steelmaking Automation Conference, Vol. 1B, 1976, p. 4.2.1.
52. Kreith, F. and Black, W.Z., "Basic Heat Transfer", Harper and Row Publishers, 1980.
53. Gaugler, R.E., "An Experimental Study of Spray Cooling of High Temperature Surfaces", Ph.D. Thesis, Department of Mechanical Engineering, Carnegie Institute of Technology, 1966.
54. Heymann, F.J., "High Speed Impact Between a Liquid Drop and a Solid Surface", Journal of Applied Physics, Vol. 40, No. 13, 1969, pp. 5113-5122.
55. Heymann, F.J., "On the shock Wave Velocity and Impact Pressure in High Speed Liquid-Solid Impact", Trans. ASME, Journal of Basic Engineering, Paper No. 68-FE-B, 1968, pp. 1-3.
56. Savic, P. and Boulton, G.T., "The Fluid Flow Associated with the Impact of Liquid Drops with Solid Surfaces", Report MT-26, 1955, National Research Council of Canada, Ottawa.
57. Gottfried, B.S., "The Evaporation of Small Drops on a Flat Plate in the Film Boiling Range", Ph.D. Thesis, Case Institute of Technology, 1962.

58. Wachters, L.H., Bonne, H. and van Nouhis, H.J., "The Heat Transfer From a Hot Horizontal Plate to Sessile Water Drops in the Spheroidal State", Chem. Eng. Sci., Vol. 21, 1966, pp. 923-926.
59. Moriyama, A., "Heat Transfer From a Hot Steel Surface to a Water Droplet", Trans. ISIJ, Vol. 14, 1974, pp. 285-289.
60. Moriyama, A., "Evaporation Rate of a Single Water Droplet on a Hot Surface", Trans. ISIJ, Vol. 14, 1974, pp. 290-295.
61. Wachters, L.H., Smulders, L., Vermeulen, J.R. and Kleiweg, H.C., "The Heat Transfer From a Hot Wall to Impinging Mist Droplets in the Spheroidal State", Chem. Eng. Sci., Vol. 21, 1966, pp. 1231-1238.
62. Wachters, L.H. and Westerling, N.A., "The Heat Transfer From a Hot Wall to Impinging Water Drops in the Spheroidal State", Chem. Eng. Sci., Vol. 21, 1966, pp. 1047-1056.
63. McGinnis, F.K. and Holman, J.P., "Individual Droplet Heat Transfer Rates for Splattering on Hot Surfaces", Int. J. Heat Mass Transfer, Vol. 12, 1969, pp. 95-108.
64. Holman, J.P., Jenkins, P.E. and Sullivan, F.G., "Experiments on Individual Droplet Heat Transfer Rates", Int. J. Heat Mass Transfer, Vol. 15, 1972, pp. 1489-1495.
65. Pedersen, C.O., "An Experimental Study of the Dynamic Behaviour and Heat-Transfer Characteristics of Water Droplets Impinging Upon a Heated Surface", Int. J. Heat Mass Transfer, Vol. 13, 1970, pp. 369-381.
66. Pedersen, C.O., "The Dynamics and Heat-Transfer Characteristics of Water Droplets Impinging on a Heated Surface", Department of Mechanical Engineering, Carnegie Mellon University, 1967.
67. Corman, J.C., "Water Cooling of a Moving, High Temperature Metal Strip", Ph.D. Thesis, Department of Mechanical Engineering, Carnegie Institute of Technology, 1966.
68. Auman, P.M., Griffiths, D.K. and Hill, D.R., "Hot Strip Mill Runout Table Temperature Control", Iron and Steel Engineer, September 1967, pp. 174-181.

69. Lambert, N. and Economopoulos, M., "Measurement of the Heat-Transfer Coefficients in Metallurgical Processes", Journal of the Iron and Steel Institute, Vol. 10, 1970, pp. 917-928.
70. Hoogendoorn, C.J. and den Hond, R., "Liedenfrost Temperature and Heat-Transfer Coefficients for Water Sprays Impinging on a Hot Surface", Paper B3.12, Fifth International Heat Transfer Conference, Tokyo, 1974, pp. 135-138.
71. Shimada, M. and Mitsutsuka, M., "On Heat Transfer Coefficient by Forced Water Cooling to Carbon Steel", Tetsu-to-Hagané, Vol. 52, 1966, p. 1643.
72. Mitsutsuka, M., "Study on the Water Cooling of Steel Plate at High Temperature", Tetsu-to-Hagané, Vol. 54, 1968, pp. 1457-1471.
73. Ishiguro, M., Ichihara, T., et. al., "Secondary Spray Cooling in Continuous Casting", Tetsu-to-Hagané, Vol. 60, No. 11, Lectures 126 and 127, 1974, pp. S464-S465 [HB Transl. No. 8735].
74. Sugitani, Y., Takashima, K. and Kawasaki, S., "Study of Secondary Cooling in Continuous Casting", Tetsu-to-Hagané, Vol. 59, No. 11, Lectures 12 and 13, 1973, pp. S388-S389 [HB Transl. No. 9236].
75. Etienne, A. and Mairy, B., "Heat Transfer in Continuously Cast Strands", C.N.R.M. Report 55, November 1979, pp. 3-13.
76. Mizikar, E.A., "Spray Cooling Investigation for Continuous Casting of Billets and Blooms", Iron and Steel Engineer, Vol. 47, No. 6, 1970, pp. 53-60.
77. Sasaki, K., Sugitani, Y. and Kawasaki, M., "Heat Transfer in Spray Cooling on Hot Surface", Tetsu-to-Hagané, Vol. 65, 1979, pp. 90-96.
78. Sugitani, Y., "Heat-Transfer Coefficient in Spray Cooling", Tetsu-to-Hagané, Vol. 61, No. 12, 1975, p. S513.
79. Bamberger, M., Jeschar, R. and Prinz, B., "Untersuchung des Wärmeübergangs beim Kühlen von Nichteisenmetallen durch Wasser", Zeits. Metallkunde, Vol. 70, No. 9, 1979, pp. 553-560.

80. Junk, J., "Heat Transfer Investigations in a Simulated Secondary Cooling Zone for the Continuous Casting of Steel", Neue Hutte, Vol. 17, No. 1, 1972, pp. 13-18 [HB Transl. No. 8740].
81. Müller, H. and Jeschar, R., "Untersuchung des Wärmeübergangs an einer simulierten Sekundärkühlzone beim Stranggiessverfahren", Arch. Eisenhüttenwes., Vol. 44, 1973, pp. 589-594.
82. Bolle, L. and Moureau, J.C., "Spray Cooling of Hot Surfaces: A Description of the Dispersed Phase and a Parametric Study of Heat Transfer Results", Proc. of Two Phase Flows and Heat Transfer, Vol. III, NATO Advanced Study Institute, 1976, pp. 1327-1346.
83. Bolle, L. and Moureau, J.C., "Experimental Study of Heat Transfer by Spray Cooling", Int. Conf. on Heat and Mass Transfer Metallurgical Processes, Dubrovnik, Yugoslavia, 1979.
84. Bolle, L. and Moreau, J.C., Universite Catholique de Louvain, Belgium, Unpublished work.
85. Akimenko, A.D., Korotkov, K.P., Maiorov, N.P., Skvortsov, A.A. and Shenderov, L.B., "Continuous Casting of Steel", BISITS Translation No. BISI 2380, 1962, Iron and Steel Institute, London.
86. Akimenko, A.D., Kazanovich, L.B., Skvortsov, A.A. and Slutskii, B.I., "Investigating Heat Transfer in the Secondary Cooling Zone in a Continuous Casting Plant", Steel in the USSR, 1972, pp. 448-449.
87. Akimenko, A.D. and Skvortsov, A.A., "Heat Transfer in Zone of Secondary Cooling of Continuous Steel Casting Installations", Nauchn. Doklady Vyssh. Shkoly-Metallurgiya, April - June 1959, No. 2, pp. 123-130 [HB Transl. No. 4796].
88. Alberny, R., "Heat Transfer and Solidification in Continuous Casting", Info. Symp. on Casting and Solidification of Steel, Vol. 1, Committee of European Communities, Luxembourg, 1977, IPC Science and Technology Press, pp. 278-335.
89. Alberny, R., Leclercq, A. and Basilis, J., "Thermal Study of Secondary Cooling of a Continuous Casting Machine", Circulaire d'Informatio-techniques, Vol. 3(315), 1973, pp. 763-776.

90. Industrial Catalog 26, Spraying Systems Co., Wheaton, Illinois 60187.
91. Otter, A.J., "Thermocouples and Surface Temperature Measurement", AECL Report 3062, March 1968, Chalk River, Ontario.
92. Benedict, R.P., Chapter 12, "Fundamentals of Temperature, Pressure and Flow Measurement", 2nd Edition, Pub. J. Wiley and Sons, pp. 238-264.
93. Sparrow, E.M., "Error Estimates in Temperature Measurement", Measurement Techniques in Heat Transfer, Eds. Eckert, E.R.G. and Goldstein, R.J., Pub. Technivision Services, Slough, England, 1st. Edition, 1970, pp. 13-32.
94. Beck, J.V., "Thermocouple Temperature Disturbances in Low Conductivity Materials", Trans. ASME, Journal of Heat Transfer, May 1962, pp. 124-132.
95. Beck, J.V. and Hurwicz, H., "Effect of Thermocouple Cavity on Heat Sink Temperature", Trans. ASME, Journal of Heat Transfer, February 1960, pp. 27-36.
96. Masters, J.I. and Stein, S., "Effect of an Axial Cavity on the Temperature History of a Surface Heated Slab", The Review of Scientific Instruments, Vol. 27, No. 12, 1956, pp. 1065-1069.
97. Economopoulos, M., "New Calculation Method of the Heat Transfer Coefficients in Steel Making Processes", C.N.R.M. Report No. 14, 1968, pp. 45-58.
98. Gat, U., Kammer, D.S. and Hahn, O.J., "The Effect of Temperature Dependent Properties of Transients Measurements with Intrinsic Thermocouple", Int. J. Heat Mass Transfer, Vol. 18, 1975, pp. 1337-1342.
99. Henning, C.D. and Parker, R., "Transient Response of an Intrinsic Thermocouple", Trans. ASME, Journal of Heat Transfer, May 1967, pp. 146-154.
100. Shumakov, N.V., "A Method for the Experimental Study of the Process of Heating of a Solid Body", Soviet Physics, Technical Physics, Vol. 2, 1957, pp. 771-781.
101. Paschkis, V. and Stoltz, G., "Quenching as a Heat Transfer Problem", Journal of Metals, August 1956, pp. 1074-1075.
102. Paschkis, V. and Stoltz, G., "How Measurements Lead to Effective Quenching", The Iron Age, November 22, 1956, pp. 95-97.

103. Mirsepassi, T., "Graphical evaluation of a Convolution Integral", Mathematics of Computation, Vol. 13-14, 1959-60, pp. 202-212.
104. Stoltz, Jr. G., "Numerical Solutions to an Inverse Problem of Heat Conduction for Simple Shapes", Trans. ASME, Journal of Heat Transfer, February 1960, pp. 20-26.
105. Sparrow, E.M., Haji-Sheik, A. and Lundgren, T.S., "The Inverse Problem in Transient Heat Conduction", Trans. ASME, Journal of Applied Mechanics, September 1964, pp. 369-375.
106. Kolp, A. Ya. and Lebedev, V.V., "Comparison of Solutions of the Inverse Transient Heat Conduction by the Methods of Tikhonov and Sparrow", Teplofizika Vysokikh Temperatur, Vol. 11, No. 2, 1973, pp. 369-374.
107. Alifanov, O.M., "Regularisation of Solutions of Inverse Problems of Heat Conduction", Heat Transfer, Soviet Research, Vol. 5, No. 4, 1973, pp. 163-169.
108. Makhin, V.A. and Shmukin, A.A., "Inverse Problems of Unsteady Heat Conduction", Heat Transfer, Soviet Research, Vol. 5, No. 2, 1973, pp. 160-165.
109. Frank, I., "An Application of Least Squares Method to the Solution of the Inverse Problem of Heat Conduction", Trans. ASME, Journal of Heat Transfer, September 1963, pp. 378-379.
110. Lambert, N. and Greday, T., "Determination of the Heat-Transfer Coefficient", C.N.R.M. Report No. 44, 1975, pp. 13-27.
111. Thaler, R.H., "An Inverse Finite Difference Method for the Determination of Thermal Conductivity", Paper Cu 2.8, Proceedings of the 5th International Heat Transfer Conference, Tokyo, 1974, pp. 202-204.
112. Imber, M., "The Two Dimensional Inverse Problem in Heat Conduction", Paper Cu 2.2, Proceedings of the 5th International Heat Transfer Conference, Tokyo, 1974, pp. 174-178.
113. Carnahan, B., Luther, H.A. and Wilkes, J.O., "Applied Numerical Methods", John Wiley and Sons, Publishers, 1969.

114. Price, P.H. and Slack, M.R., "Stability and Accuracy of Numerical Solutions of the Heat Flow Equation", British Journal of Applied Physics, Vol. 3, 1952, pp. 379-384.
115. Douglas, J., "A Survey of Numerical Methods for Parabolic Differential Equations", Advances in Computers, Vol. 2, 1962, pp. 1-54.
116. Barakat, H.Z. and Clark, J.A., "On the Solution of the Diffusion Equations by Numerical Methods", Trans. ASME, Journal of Heat Transfer, Vol. 88, November 1966, pp. 421-427.
117. Biomedical Computer Programs, P Series, Ed. W.J. Dixon, 1977, University of California Press, pp.484-498.
118. Mairy, B. and Ramelot, D., "Sensor for Measuring the Surface Temperature of the Strand in a Continuous Casting Machine", C.N.R.M. Report No. 46, March 1976, pp. 23-28.

APPENDIX I

Measured spray fluxes for the various
nozzles used in this investigation.

TABLE I - 1

NOZZLE TYPE 1/4 CG 10

PRESSURE 20. PSI 0.14 MPA

DISTANCE 10.16 CM

COLLECTOR TYPE A

	DISTANCE FROM CENTRE (CM)												
	-15.24	-12.70	-10.16	-7.62	-5.08	-2.54	0.0	2.54	5.08	7.62	10.16	12.70	15.24
-10.16	0.0	0.0	0.0	0.0	0.0	0.0	0.0	0.0	0.0	0.0	0.0	0.0	0.0
-7.62	0.0	0.0	0.0	0.0	0.0	0.0	0.0	0.0	0.0	0.0	0.0	0.0	0.0
-5.08	0.0	0.0	0.0	1.60	2.80	4.70	6.60	6.00	0.0	0.0	0.0	0.0	0.0
-2.54	0.0	0.0	8.60	0.70	4.80	5.20	8.00	5.20	5.60	0.0	0.0	0.0	0.0
0.0	0.0	0.0	0.0	1.45	5.50	6.40	18.25	6.80	6.00	2.00	0.0	0.0	0.0
2.54	0.0	0.0	0.0	1.40	6.30	5.90	7.80	5.70	6.60	0.50	0.0	0.0	0.0
5.08	0.0	0.0	0.0	0.70	2.60	5.60	5.70	6.70	2.60	0.10	0.0	0.0	0.0
7.62	0.0	0.0	0.0	0.0	0.0	0.0	0.0	0.0	0.0	0.0	0.0	0.0	0.0
10.16	0.0	0.0	0.0	0.0	0.0	0.0	0.0	0.0	0.0	0.0	0.0	0.0	0.0

TABLE I - 2

NOZZLE TYPE 1/4 G0 10

PRESSURE 20. PSI 0.14 MPA

DISTANCE 15.24 CM

COLLECTOR TYPE A

DISTANCE FROM CENTRE (CM)

DISTANCE FROM CENTRE (CM)														
	-15.24	-12.70	-10.16	-7.62	-5.08	-2.54	0.0	2.54	5.08	7.62	10.16	12.70	15.24	
-10.16	0.10	0.10	0.0	0.30	1.50	1.80	3.20	2.00	0.0	0.0	0.0	0.0	0.0	
-7.62	0.10	0.10	0.30	0.80	2.20	2.70	3.10	2.50	0.0	0.0	0.0	0.0	0.0	
-5.08	0.10	0.50	0.60	2.30	2.00	2.30	2.70	2.40	0.10	1.50	0.0	0.0	0.0	
-2.54	0.10	0.10	1.70	3.70	2.00	2.60	5.00	4.40	2.20	3.20	0.0	0.0	0.0	
0.0	0.0	0.30	2.30	3.00	2.00	4.70	0.90	4.80	2.20	2.60	0.0	0.20	0.0	
2.54	0.0	0.0	1.40	2.70	2.00	3.70	4.10	2.80	2.70	3.60	0.0	0.0	0.0	
5.08	0.40	0.0	0.90	3.00	3.10	2.60	2.70	2.60	2.90	2.20	0.0	0.0	0.0	
7.62	0.20	0.10	0.0	0.40	2.10	2.40	3.00	3.80	1.00	0.0	0.0	0.0	0.0	
10.16	0.10	0.0	0.0	0.0	0.60	0.50	1.70	1.20	0.0	0.0	0.0	0.0	0.0	

TABLE I - 3

NOZZLE TYPE 1/4 GG 10

PRESSURE 20. PSI 0.14 MPA

DISTANCE 20.32 CM

COLLECTOR TYPE A

		DISTANCE FROM CENTRE (CM)												
		-15.24	-12.70	-10.16	-7.62	-5.08	-2.54	0.0	2.54	5.08	7.62	10.16	12.70	15.24
DISTANCE FROM CENTRE (CM)	-10.16	0.10	0.30	0.80	1.30	1.40	1.60	2.00	2.00	0.30	0.80	0.0	0.0	0.10
	-7.62	0.20	0.50	1.10	1.50	1.40	1.50	1.90	1.80	0.40	1.00	0.0	0.0	0.0
	-5.08	0.40	0.50	1.30	1.70	1.60	1.70	2.30	1.80	0.0	1.00	0.0	0.0	0.0
	-2.54	1.00	0.50	1.40	1.40	1.80	3.10	3.90	2.20	0.40	0.90	0.10	0.30	0.30
	0.0	0.70	1.20	1.80	1.55	1.75	3.35	5.40	3.50	1.60	1.40	1.40	1.15	1.20
	2.54	0.40	1.20	2.00	1.60	1.70	2.50	3.70	2.90	1.60	1.30	0.80	1.10	0.60
	5.08	0.40	1.00	1.90	1.90	1.60	1.70	1.90	1.90	1.40	1.60	0.90	0.60	0.50
	7.62	0.30	0.60	1.30	1.80	1.70	1.60	1.50	1.40	1.00	1.70	0.40	0.30	0.40
	10.16	0.30	0.50	0.60	1.00	1.40	1.60	1.50	1.60	1.40	1.50	0.0	0.20	0.30

TABLE I - 4

NOZZLE TYPE 1/4 00 10
 PRESSURE 20. PSI 0.14 MPA
 DISTANCE 10.16 CM
 COLLECTOR TYPE B

		DISTANCE FROM CENTRE (CM)												
		-15.24	-12.70	-10.16	-7.62	-5.08	-2.54	0.0	2.54	5.08	7.62	10.16	12.70	15.24
DISTANCE FROM CENTRE (CM)	-10.16	0.0	0.0	0.0	0.0	0.0	0.0	0.0	0.0	0.0	0.0	0.0	0.0	0.0
	-7.62	0.0	0.0	0.0	0.0	12.50	9.30	9.80	11.80	11.70	0.0	0.0	0.0	0.0
	-5.08	0.0	0.0	0.0	31.80	9.30	11.60	15.40	13.10	10.20	27.90	0.0	0.0	0.0
	-2.54	0.0	0.0	34.40	4.20	10.40	9.30	13.00	11.20	13.30	6.00	29.40	0.0	0.0
	0.0	0.30	0.30	31.10	5.20	11.70	13.80	22.80	12.10	11.30	4.60	20.60	1.50	0.0
	2.54	0.0	22.80	8.40	8.10	15.10	12.70	15.00	12.10	13.50	9.20	2.60	16.50	0.0
	5.08	0.0	24.80	0.50	6.20	10.20	13.50	13.20	14.90	10.80	4.20	7.70	13.00	0.0
	7.62	0.0	27.40	0.10	2.50	5.10	7.10	8.30	8.70	0.40	0.0	2.50	17.40	4.50
	10.16	0.0	19.20	5.50	1.20	3.20	4.60	3.70	4.90	0.0	0.0	8.80	14.00	0.0

TABLE I - 5

NOZZLE TYPE 1/4 CC 10

PRESSURE 40. PSI 0.28 MPa

DISTANCE 10.16 CM

COLLECTOR TYPE A

		DISTANCE FROM CENTRE (CM)												
		-15.24	-12.70	-10.16	-7.62	-5.08	-2.54	0.0	2.54	5.08	7.62	10.16	12.70	15.24
DISTANCE FROM CENTRE (CM)	-10.16	0.0	0.0	0.0	0.0	0.0	0.0	0.0	0.0	0.0	0.0	0.0	0.0	0.0
	-7.62	0.0	0.0	0.0	0.80	2.30	2.70	4.60	2.20	0.0	0.0	0.0	0.0	0.0
	-5.08	0.0	0.0	0.0	2.00	4.30	6.30	9.40	10.00	4.00	0.0	0.0	0.0	0.0
	-2.54	0.0	0.0	0.0	1.70	7.50	7.30	10.50	7.00	7.30	2.10	0.0	0.0	0.0
	0.0	0.0	0.0	0.0	2.60	6.70	8.20	20.20	9.50	7.10	3.90	0.0	0.0	0.0
	2.54	0.0	0.20	0.0	2.60	8.80	7.40	9.10	7.60	7.50	2.80	0.0	0.30	0.0
	5.08	0.0	0.0	0.0	0.70	3.50	6.50	6.10	5.90	4.10	0.0	0.0	0.0	0.0
	7.62	0.0	0.0	0.0	0.0	1.90	2.00	3.40	2.40	0.0	0.0	0.0	0.0	0.0
	10.16	0.0	0.0	0.0	0.0	0.0	0.0	0.0	0.0	0.0	0.0	0.0	0.0	0.0

TABLE I - 6

NOZZLE TYPE 1/4 CG 10

PRESSURE 40. PSI 0.28 MPA

DISTANCE 15.24 CM

COLLECTOR TYPE A

		DISTANCE FROM CENTRE (CM)												
		-15.24	-12.70	-10.16	-7.62	-5.08	-2.54	0.0	2.54	5.08	7.62	10.16	12.70	15.24
DISTANCE FROM CENTRE (CM)	-10.16	0.0	0.10	0.0	0.40	1.90	2.10	3.10	2.30	0.0	0.0	0.0	0.0	0.0
	-7.62	0.0	0.0	0.40	1.80	3.40	3.10	3.40	3.10	0.10	0.0	0.0	0.0	0.0
	-5.08	0.0	0.0	1.00	3.00	3.60	3.40	4.40	3.40	2.10	3.90	0.0	0.0	0.0
	-2.54	0.0	0.0	2.10	4.40	4.00	4.80	6.50	5.40	3.30	3.50	1.30	0.0	0.0
	0.0	0.0	0.0	3.30	3.60	3.70	6.20	9.20	6.70	3.70	3.30	0.0	0.0	0.0
	2.54	0.0	0.0	2.10	3.40	3.40	4.10	4.90	4.30	3.60	4.10	0.10	0.0	0.0
	5.08	0.0	0.0	1.00	3.50	3.40	3.00	3.20	3.10	3.00	3.20	1.50	0.0	0.0
	7.62	0.0	0.0	0.0	0.0	3.00	3.10	3.70	4.60	0.0	0.0	0.0	0.0	0.0
	10.16	0.0	0.0	0.0	0.0	0.0	0.0	0.0	2.20	0.0	0.0	0.0	0.0	0.0

TABLE I - 7

NOZZLE TYPE 1/4 CC 10

PRESSURE 40. PSI 0.28 MPA

DISTANCE 20.32 CM

COLLECTION TYPE A

		DISTANCE FROM CENTRE (CM)													
		-15.24	-12.70	-10.16	-7.62	-5.08	-2.54	0.0	2.54	5.08	7.62	10.16	12.70	15.24	
DISTANCE FROM CENTRE (CM)	-10.16	0.40	0.70	1.10	1.60	1.60	1.90	2.40	2.50	1.70	2.10	0.0	0.10	0.0	
	-7.62	1.60	0.60	1.50	1.80	1.70	2.00	2.60	2.50	1.50	2.40	0.30	0.10	0.20	
	-5.08	0.70	0.90	2.20	2.30	2.20	2.60	3.00	2.30	0.70	1.70	0.70	0.20	0.0	
	-2.54	0.50	1.50	2.40	2.00	2.40	3.50	4.50	3.30	1.60	2.00	1.40	1.60	0.50	
	0.0	0.50	1.60	2.20	2.10	2.40	4.00	5.90	4.60	2.70	2.00	2.10	2.10	0.90	
	2.54	0.60	1.60	2.30	2.00	2.10	3.00	4.30	3.80	2.50	1.60	1.90	1.90	1.10	
	5.08	0.80	1.90	2.60	2.30	2.20	2.40	2.70	2.80	2.20	1.90	1.80	1.40	0.60	
	7.62	0.90	1.30	2.10	2.60	2.30	2.20	2.20	2.50	2.30	2.10	1.40	0.70	0.60	
10.16	0.30	0.50	1.00	1.60	2.00	1.90	1.80	2.00	1.90	1.60	0.0	0.50	0.40		

TABLE I - 8

NOZZLE TYPE 1/4 GO 10

PRESSURE 40 PSI 0.28 MPA

DISTANCE 10.16 CM

COLLECTOR TYPE B

		DISTANCE FROM CENTRE (CM)												
		-15.24	-12.70	-10.16	-7.62	-5.08	-2.54	0.0	2.54	5.08	7.62	10.16	12.70	15.24
DISTANCE FROM CENTRE (CM)	-10.16	0.0	0.0	0.0	0.0	1.70	11.60	8.00	15.00	0.0	0.0	0.0	0.0	0.0
	-7.62	0.0	0.0	0.0	34.20	11.40	9.40	15.40	11.40	13.10	29.90	0.0	0.0	0.0
	-5.08	0.0	0.0	37.50	8.60	12.90	16.10	19.30	17.60	16.10	9.40	32.60	0.0	0.0
	-2.54	0.10	1.50	18.30	6.50	13.30	12.30	18.50	15.40	18.20	10.60	10.10	11.20	0.10
	0.0	0.0	16.80	0.0	6.40	12.20	13.10	25.50	15.50	11.90	9.10	0.0	32.60	0.60
	2.54	10.60	14.10	3.00	10.70	17.00	14.80	18.10	15.70	17.40	11.00	0.0	18.30	30.10
	5.08	27.10	20.90	0.0	8.10	12.90	17.30	17.00	19.30	15.10	8.30	0.0	12.50	45.00
	7.62	33.40	15.30	2.00	6.10	7.90	10.40	12.30	12.00	8.00	0.50	0.0	6.10	43.60
	10.16	23.20	0.93	0.0	0.0	0.80	3.70	4.50	4.90	0.0	0.0	0.0	10.10	26.70

TABLE I - 9

NOZZLE TYPE 1/4 CG 10
 PRESSURE 60. PSI 0.41 HPA
 DISTANCE 15.24 CM
 COLLECTOR TYPE A

	DISTANCE FROM CENTRE (CM)															
	-15.24	-12.70	-10.16	-7.62	-5.08	-2.54	0.0	2.54	5.08	7.62	10.16	12.70	15.24			
-10.16	0.0	0.0	0.0	0.0	0.0	0.0	1.80	0.0	0.0	0.0	0.0	0.0	0.0			
-7.62	0.0	0.0	0.0	0.0	0.0	3.00	4.10	5.20	5.00	1.60	0.0	0.0	0.0			
-5.08	0.0	0.0	1.17	4.23	5.27	4.93	5.20	4.97	4.57	3.27	0.0	0.0	0.0			
-2.54	0.0	0.0	2.00	5.07	4.70	5.77	7.02	5.83	4.33	4.73	0.10	0.0	0.0			
0.0	0.0	0.0	1.70	4.20	4.20	6.00	9.30	7.10	4.50	4.20	3.40	0.0	0.0			
2.54	0.0	0.0	0.93	4.80	4.87	5.73	7.13	5.37	4.33	4.43	0.10	0.0	0.0			
5.08	0.0	0.0	0.0	2.60	4.10	4.60	5.80	5.10	1.70	1.30	0.0	0.0	0.0			
7.62	0.0	0.0	0.0	0.10	3.20	3.70	3.80	4.80	0.10	0.0	0.0	0.0	0.0			
10.16	0.0	0.0	0.0	0.0	0.10	0.30	0.0	0.10	0.0	0.0	0.0	0.0	0.0			

DISTANCE FROM CENTRE (CM)

DISTANCE FROM CENTRE (CM)

TABLE I - 10

NOZZLE TYPE 1/4 CG 10

PRESSURE 60 PSI 0.41 MPA

DISTANCE 20.32 CM

COLLECTOR TYPE A

DISTANCE FROM CENTRE (CM)														
	-15.24	-12.70	-10.16	-7.62	-5.08	-2.54	0.0	2.54	5.08	7.62	10.16	12.70	15.24	
-10.16	0.60	1.40	0.50	2.00	2.70	3.20	3.70	3.50	0.20	0.0	0.0	0.0	0.0	
-7.62	0.60	0.70	1.60	3.10	3.40	2.90	3.10	2.70	0.20	2.10	0.10	0.10	0.0	
-5.08	0.60	0.70	2.50	3.10	3.30	3.50	3.90	2.90	1.20	2.20	1.30	0.20	0.10	
-2.54	0.40	1.40	3.20	3.00	3.30	4.20	4.80	3.70	2.50	2.60	2.80	2.00	0.20	
0.0	0.50	1.80	3.40	3.10	3.20	4.60	5.80	4.80	3.20	2.70	3.00	2.40	0.90	
2.54	0.70	2.10	4.00	3.50	3.60	4.70	5.40	4.20	2.80	2.30	2.90	2.50	1.00	
5.08	0.90	2.00	3.10	3.10	2.90	3.30	3.90	3.70	2.90	2.60	2.30	1.50	0.80	
7.62	0.60	1.10	2.00	3.10	3.20	3.10	3.10	3.30	3.10	2.60	1.60	0.70	0.50	
10.16	0.20	0.50	0.90	1.90	2.90	2.90	2.90	3.40	2.90	1.70	0.0	0.40	0.30	

TABLE I - 11

NOZZLE TYPE 1/4 G0 10

PRESSURE 60. PSI 0.41 MPA

DISTANCE 10.16 CM

COLLECTOR TYPE A

	DISTANCE FROM CENTRE (CM)													
	-15.24	-12.70	-10.16	-7.62	-5.08	-2.54	0.0	2.54	5.08	7.62	10.16	12.70	15.24	
-10.16	0.0	0.0	0.0	0.0	0.0	0.0	0.0	0.0	0.0	0.0	0.0	0.0	0.0	
-7.62	0.0	0.0	0.0	0.0	3.10	3.90	7.60	3.90	0.0	0.0	0.0	0.0	0.0	
-5.08	0.0	0.0	0.50	0.20	5.30	8.40	11.70	12.00	3.30	0.0	0.0	0.0	0.0	
-2.54	0.0	0.0	0.0	0.70	9.20	10.40	12.80	9.10	8.40	2.60	0.0	0.0	0.0	
0.0	0.0	0.0	0.10	2.10	10.30	11.90	14.30	10.80	9.30	3.60	0.0	0.0	0.0	
2.54	0.0	0.0	0.20	2.00	9.60	9.00	11.60	10.30	9.20	2.60	0.0	0.0	0.0	
5.08	0.0	0.0	0.0	0.10	3.00	10.10	9.40	10.30	4.40	0.0	0.0	0.0	0.0	
7.62	0.0	0.0	0.0	0.0	0.0	0.10	3.30	2.30	0.0	0.0	0.0	0.0	0.0	
10.16	0.0	0.0	0.0	0.0	0.0	0.0	0.0	0.0	0.0	0.0	0.0	0.0	0.0	

TABLE I - 12

NOZZLE TYPE 1/4 CO 10

PRESSURE 60. PSI 0.41 MPA

DISTANCE 10.16 CM

COLLECTOR TYPE B

		DISTANCE FROM CENTRE (CM)													
		-15.24	-12.70	-10.16	-7.62	-5.08	-2.54	0.0	2.54	5.08	7.62	10.16	12.70	15.24	
DISTANCE FROM CENTRE (CM)	-10.16	0.0	0.0	0.0	0.0	18.60	19.90	12.30	20.70	12.40	0.0	0.0	0.0	0.0	
	-7.62	0.0	0.0	0.0	37.50	11.60	11.00	18.80	19.10	12.90	22.60	0.30	0.0	0.0	
	-5.08	0.0	0.0	37.40	10.80	15.70	21.10	27.00	25.20	10.40	10.50	29.30	10.40	0.0	
	-2.54	0.0	14.20	2.60	8.70	17.70	18.40	22.50	18.20	21.40	11.00	0.0	48.00	0.0	
	0.0	8.00	26.80	0.0	7.20	16.60	10.20	26.40	17.30	16.80	8.60	0.0	22.50	18.60	
	2.54	27.70	22.40	0.0	13.10	23.80	21.40	20.10	19.70	21.40	13.70	0.0	13.10	38.40	
	5.08	26.90	17.20	0.0	10.70	16.20	23.90	23.60	25.10	19.00	11.40	0.0	12.10	35.50	
	7.62	26.40	23.50	0.0	8.10	9.00	12.90	15.40	16.30	11.30	0.50	0.0	6.50	31.70	
	10.16	25.80	9.10	0.0	7.20	4.70	6.90	9.10	9.20	2.80	0.0	0.0	9.00	23.80	

TABLE I - 13

HORIZONTAL CENTRELINE SPRAY WATER FLUXES (L / SQ. M. S)

1/8 GG 5

NOZZLE

SPRAY PRESSURE		SPRAY DIST. (CM)	DISTANCE FROM CENTRE (CM)												
			-15.24	-12.70	-10.16	-7.62	-5.08	-2.54	0.0	2.54	5.08	7.62	10.16	12.70	15.24
PSI	MPA														
20	0.14	10.16	0.0	0.0	0.0	0.0	1.67	3.32	8.94	3.54	3.53	0.0	0.0	0.0	0.0
40	0.28	10.16	0.0	0.0	0.0	0.0	3.13	4.37	10.54	4.70	5.37	0.0	0.0	0.0	0.0
60	0.41	10.16	0.0	0.0	0.0	0.0	5.59	6.04	10.27	5.90	6.90	0.0	0.0	0.0	0.0
100	0.69	10.16	0.0	0.0	0.0	0.0	7.13	9.26	12.20	8.80	10.29	0.0	0.0	0.0	0.0
20	0.14	15.24	0.0	0.0	0.0	0.0	1.29	1.80	4.26	2.21	1.00	0.01	0.0	0.0	0.0
40	0.28	15.24	0.0	0.0	0.0	1.12	1.96	2.29	5.06	3.22	2.02	2.37	0.0	0.0	0.0
60	0.41	15.24	0.0	0.0	0.0	2.75	3.11	3.29	4.88	3.30	3.08	2.93	0.0	0.0	0.0
100	0.69	15.24	0.0	0.0	0.0	3.40	5.32	4.77	5.71	4.66	5.67	4.04	0.0	0.0	0.0

TABLE I - 14

HORIZONTAL CENTRELINE SPRAY WATER FLUXES (L / SQ. M. S)

1/8 G9 6 S9

NOZZLE

SPRAY PRESSURE		SPRAY DIST. (CM)	DISTANCE FROM CENTRE (CM)												
			-15.24	-12.70	-10.16	-7.62	-5.08	-2.54	0.0	2.54	5.08	7.62	10.16	12.70	15.24
PSI	MPA														
20	0.14	10.16	0.0	0.0	0.0	3.28	5.27	4.17	9.16	4.00	2.05	0.0	0.0	0.0	0.0
40	0.28	10.16	0.0	0.0	0.0	5.44	5.66	5.83	11.15	4.77	3.18	0.0	0.0	0.0	0.0
60	0.41	10.16	0.0	0.0	0.0	5.57	6.51	6.70	12.29	5.85	3.51	0.0	0.0	0.0	0.0
90	0.62	10.16	0.0	0.0	0.0	6.64	7.68	9.36	13.72	6.72	4.00	0.0	0.0	0.0	0.0

TABLE I - 15

HORIZONTAL CENTRELINE SPRAY WATER FLUXES (L / SQ. M. S)

1/4 CG 6.5

NOZZLE

SPRAY PRESSURE		SPRAY DIST. (CM)	DISTANCE FROM CENTRE (CM)												
			-15.24	-12.70	-10.16	-7.62	-5.08	-2.54	0.0	2.54	5.08	7.62	10.16	12.70	15.24
PSI	MPA														
20	0.14	10.16	0.0	0.0	0.0	0.0	1.52	11.13	29.86	15.06	2.29	0.0	0.0	0.0	0.0
40	0.28	10.16	0.0	0.0	0.0	0.0	1.03	15.11	26.41	10.77	0.06	0.0	0.0	0.0	0.0
60	0.41	10.16	0.0	0.0	0.0	0.0	1.84	17.21	30.39	13.71	3.49	0.0	0.0	0.0	0.0
90	0.62	10.16	0.0	0.0	0.0	0.0	1.85	20.29	35.47	17.84	4.69	0.0	0.0	0.0	0.0
20	0.14	15.24	0.0	0.0	0.0	0.0	2.76	3.29	14.17	5.31	3.73	0.0	0.0	0.0	0.0
40	0.28	15.24	0.0	0.0	0.0	0.0	4.71	5.15	17.01	5.28	4.91	0.0	0.0	0.0	0.0
60	0.41	15.24	0.0	0.0	0.0	0.0	5.29	9.04	17.08	7.77	6.13	0.0	0.0	0.0	0.0
90	0.62	15.24	0.0	0.0	0.0	0.0	6.32	10.59	19.26	9.91	7.57	0.91	0.0	0.0	0.0
20	0.14	20.32	0.0	0.0	0.0	0.0	0.15	2.20	10.31	5.07	0.17	0.0	0.0	0.0	0.0
40	0.28	20.32	0.0	0.0	0.0	1.63	2.64	5.08	10.91	4.49	2.68	2.48	0.0	0.0	0.0
60	0.41	20.32	0.0	0.0	0.0	0.96	3.31	5.45	10.95	5.37	3.53	2.97	0.0	0.0	0.0
90	0.62	20.32	0.0	0.0	0.0	3.33	3.87	6.26	12.20	6.54	4.19	4.55	0.0	0.0	0.0

TABLE I - 16

HORIZONTAL CENTRELINE SPRAY WATER FLUXES (L / SQ. M. S)

1/4 CG 12 SQ NOZZLE

SPRAY PRESSURE		SPRAY DIST	DISTANCE FROM CENTRE (CM)												
PSI	MPA	(CM)	-15.24	-12.70	-10.16	-7.62	-5.08	-2.54	0.0	2.54	5.08	7.62	10.16	12.70	15.24
20	0.14	10.16	0.0	0.0	0.0	2.05	5.15	5.50	13.30	5.55	4.45	4.10	0.0	0.0	0.0
40	0.28	10.16	0.0	0.0	0.0	3.45	6.55	8.80	17.55	8.50	6.60	5.20	0.0	0.0	0.0
60	0.41	10.16	0.0	0.0	0.0	4.00	8.15	10.85	19.50	10.65	8.30	5.95	0.0	0.0	0.0
20	0.14	15.24	0.0	0.0	0.90	2.55	2.30	4.10	6.65	3.60	1.40	2.20	2.50	0.0	0.0
40	0.28	15.24	0.0	0.0	2.70	3.10	3.50	6.00	8.35	5.20	3.00	2.95	3.10	0.0	0.0
60	0.41	15.24	0.0	0.0	3.00	3.95	4.50	7.05	10.20	6.45	4.00	3.80	3.55	0.0	0.0
20	0.14	20.32	0.0	0.0	0.70	0.80	1.50	2.65	5.25	3.65	0.85	0.0	0.0	0.0	0.0
40	0.28	20.32	0.0	0.50	1.80	1.60	2.60	3.90	6.20	4.80	2.70	1.50	0.70	1.20	0.0
60	0.41	20.32	0.0	0.70	2.10	1.95	2.85	4.45	6.50	5.30	3.15	1.95	1.30	1.65	0.15

TABLE I - 17

HORIZONTAL CENTRELINE SPRAY WATER FLUXES (L / SQ. M. S)

1/4 HH 14.5 SQ NOZZLE

SPRAY PRESSURE		SPRAY DIST. (CM)	DISTANCE FROM CENTRE (CM)												
			-15.24	-12.70	-10.16	-7.62	-5.08	-2.54	0.0	2.54	5.08	7.62	10.16	12.70	15.24
20	0.14	10.16	0.0	0.0	0.0	4.48	4.61	6.42	8.41	6.00	4.84	4.92	0.0	0.0	0.0
40	0.28	10.16	0.0	0.0	0.0	5.58	7.26	8.41	10.35	8.04	7.36	6.36	0.0	0.0	0.0
50	0.34	10.16	0.0	0.0	0.0	5.43	8.93	9.23	10.17	8.67	9.43	5.83	0.0	0.0	0.0
20	0.14	15.24	0.15	0.07	2.38	2.06	2.61	3.64	4.12	3.31	0.61	2.30	1.84	0.0	0.0
40	0.28	15.24	0.0	1.97	3.32	3.12	4.26	4.70	5.09	4.30	3.33	3.30	4.20	0.0	0.0
50	0.34	15.24	0.0	0.09	3.88	4.53	4.53	5.01	4.96	4.39	4.29	4.78	3.60	0.0	0.0

TABLE I - 18

HORIZONTAL CENTRELINE SPRAY WATER FLUXES (L / SQ. M. S)

1/4 G0 14 W NOZZLE

SPRAY PRESSURE		SPRAY DIST. (CM)	DISTANCE FROM CENTRE (CM)												
			-15.24	-12.70	-10.16	-7.62	-5.08	-2.54	0.0	2.54	5.08	7.62	10.16	12.70	15.24
PSI	MPA	(CM)													
20	0.14	10.16	1.80	2.00	0.40	0.00	1.70	1.80	2.10	1.90	0.20	0.40	0.40	1.30	0.50
40	0.28	10.16	1.50	2.80	2.20	1.90	2.20	2.30	2.60	2.40	2.00	2.20	1.90	2.60	0.90

TABLE I - 19

HORIZONTAL CENTRELINE SPRAY WATER FLUXES (L / SQ.M. S)

1/4 U 8020

NOZZLE

SPRAY PRESSURE		SPRAY DIST. (CM)	DISTANCE FROM CENTRE (CM)												
PSI	MPA		-15.24	-12.70	-10.16	-7.62	-5.08	-2.54	0.0	2.54	5.08	7.62	10.16	12.70	15.24
20	0.14	15.24	0.0	0.0	8.66	10.08	15.91	19.37	19.66	19.81	19.10	13.10	10.40	0.0	0.0
40	0.28	15.24	3.37	6.76	11.79	16.63	24.73	26.93	28.80	28.88	25.13	18.91	11.63	20.12	0.0
60	0.41	15.24	3.30	7.13	18.24	25.40	39.07	43.27	45.75	45.97	41.16	28.55	19.24	16.88	0.20
20	0.14	20.32	19.20	5.75	6.89	9.75	12.81	12.30	12.91	12.59	13.68	8.68	7.31	5.86	21.80
40	0.28	20.32	4.42	8.84	11.07	15.63	20.55	20.39	20.98	20.83	21.65	15.01	11.85	9.12	6.89
60	0.41	20.32	5.94	12.21	16.11	22.08	28.93	29.09	29.50	29.52	30.49	21.27	16.85	16.85	12.18

TABLE I - 20

HORIZONTAL CENTRELINE SPRAY WATER FLUXES (L / SQ. M. S)

3/8 U 5060

NOZZLE

SPRAY PRESSURE		SPRAY DIST. (CM)	DISTANCE FROM CENTRE (CM)												
			-15.24	-12.70	-10.16	-7.62	-5.08	-2.54	0.0	2.54	5.08	7.62	10.16	12.70	15.24
PSI	MPA														
10	0.07	17.78	0.0	0.0	0.0	14.90	56.95	84.70	106.90	96.40	63.45	17.75	0.0	0.0	0.0
5	0.03	17.78	0.0	0.0	0.0	9.80	87.45	46.90	86.95	69.55	104.75	0.0	0.0	0.0	0.0

APPENDIX II

Horizontal centreline spray flux profiles,
spray flux contour maps and three dimensional
representations of spray fluxes.

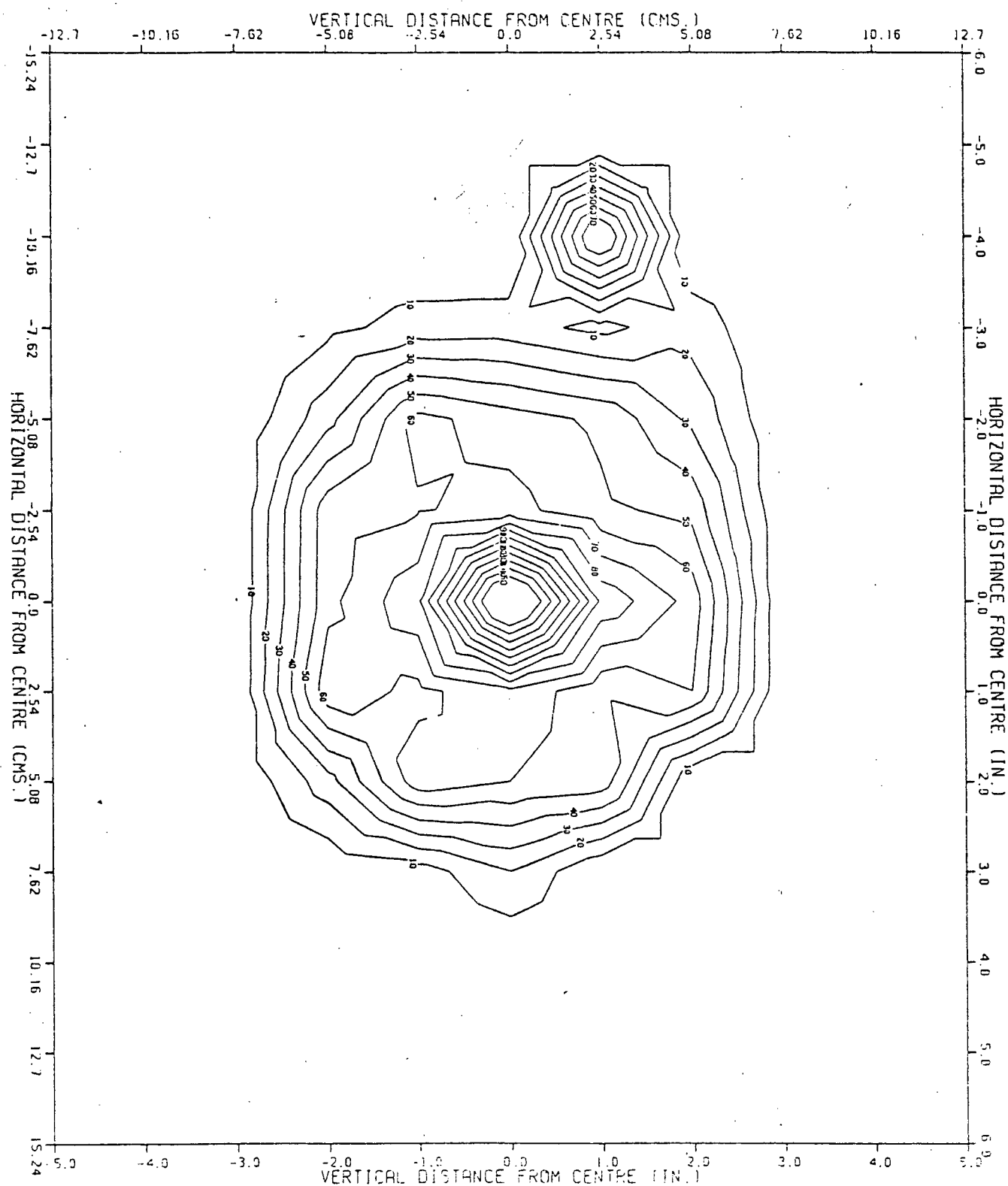


Figure II-1 Spray flux contour map for a 1/4 GG 10 nozzle, for a spray pressure of 0.13 MPa at a nozzle distance of 10.16 cm (Type A collectors).

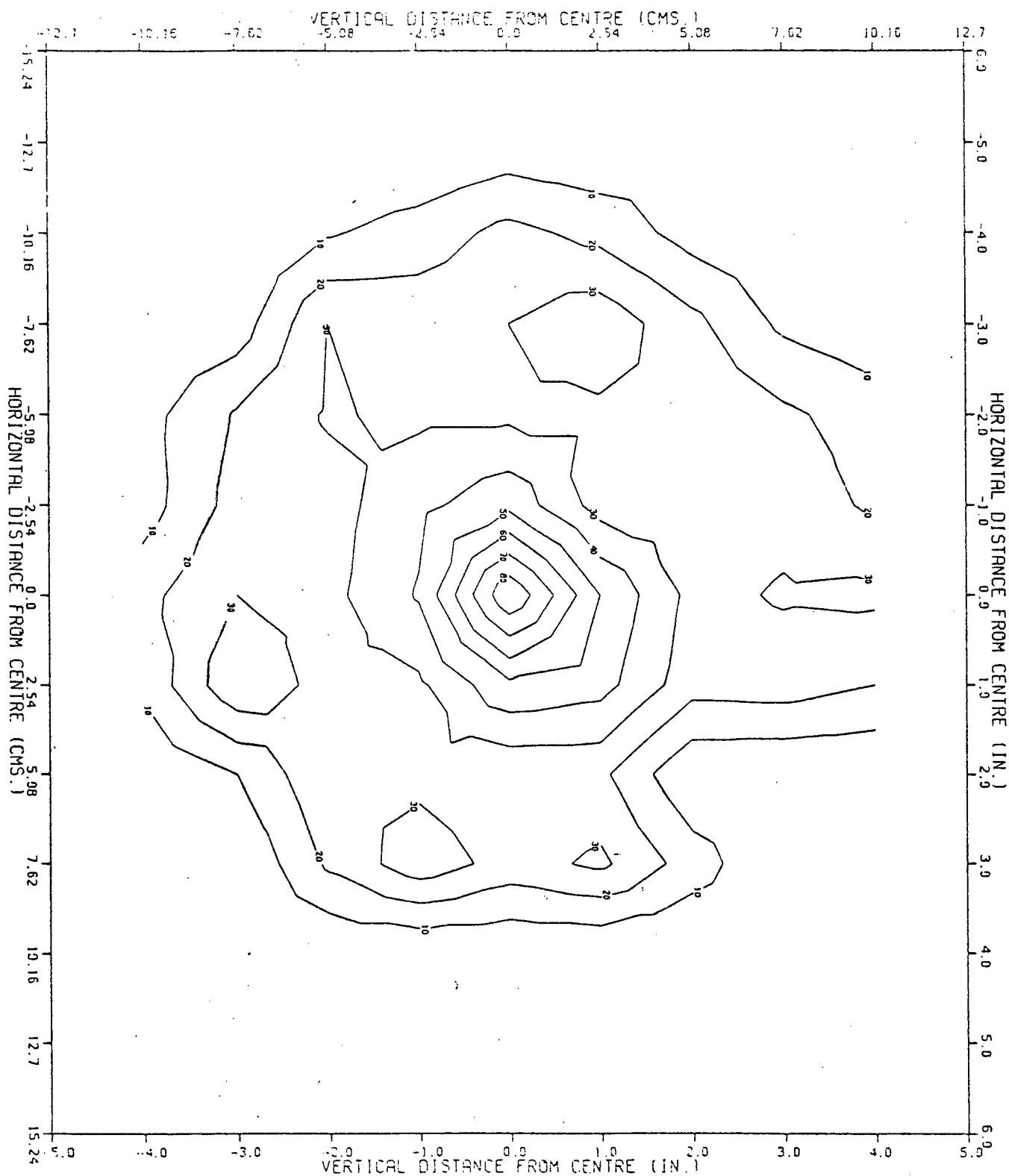


Figure II-2 Spray flux contour map for a 1/4 GG 10 nozzle, for a spray pressure of 0.13 MPa at a nozzle distance of 15.24 cm (Type A collectors).

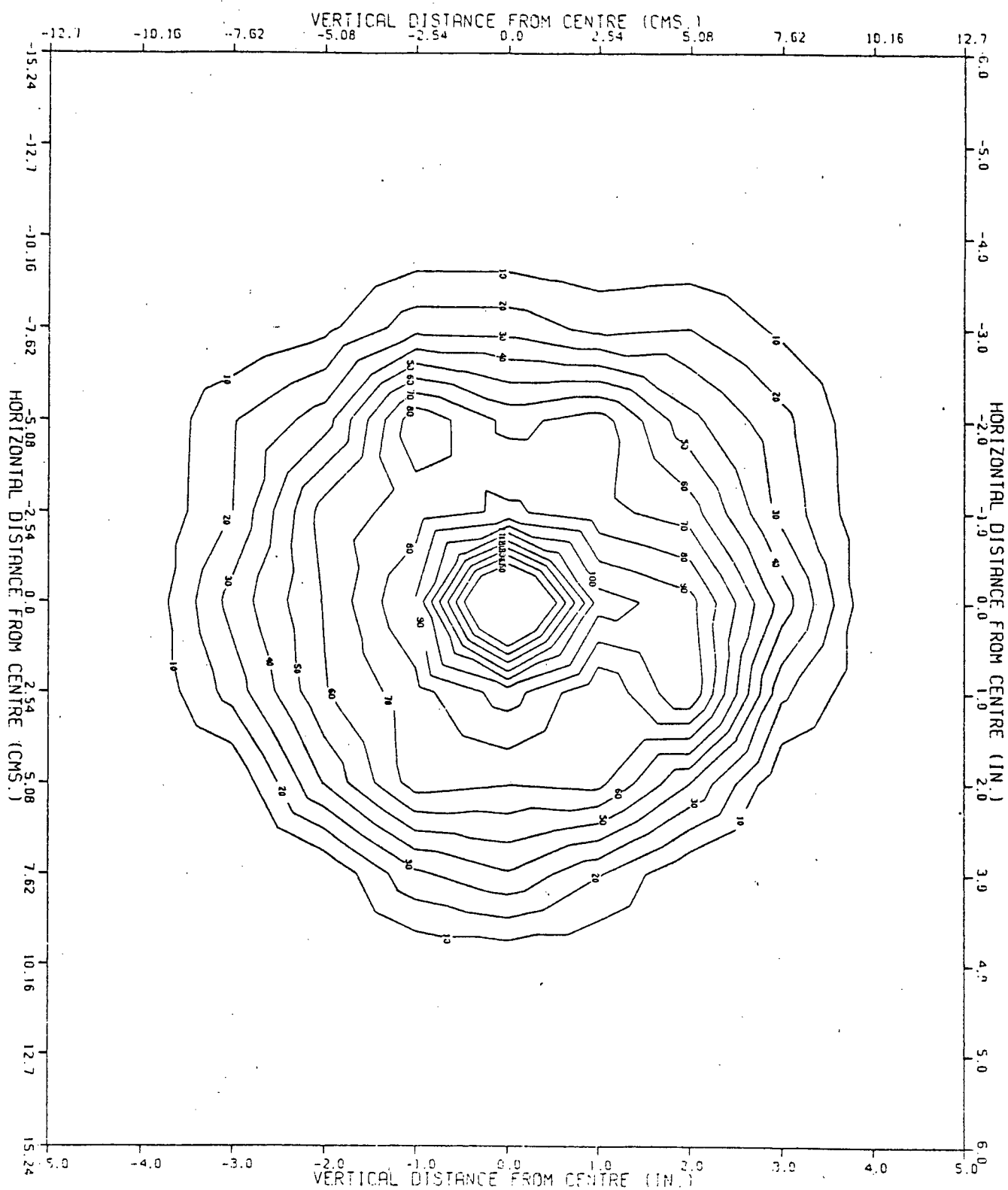


Figure II-3 Spray flux contour map for a 1/4 GG 10 nozzle, for a spray pressure of 0.27 MPa at a nozzle distance of 10.16 cm (Type A collectors).

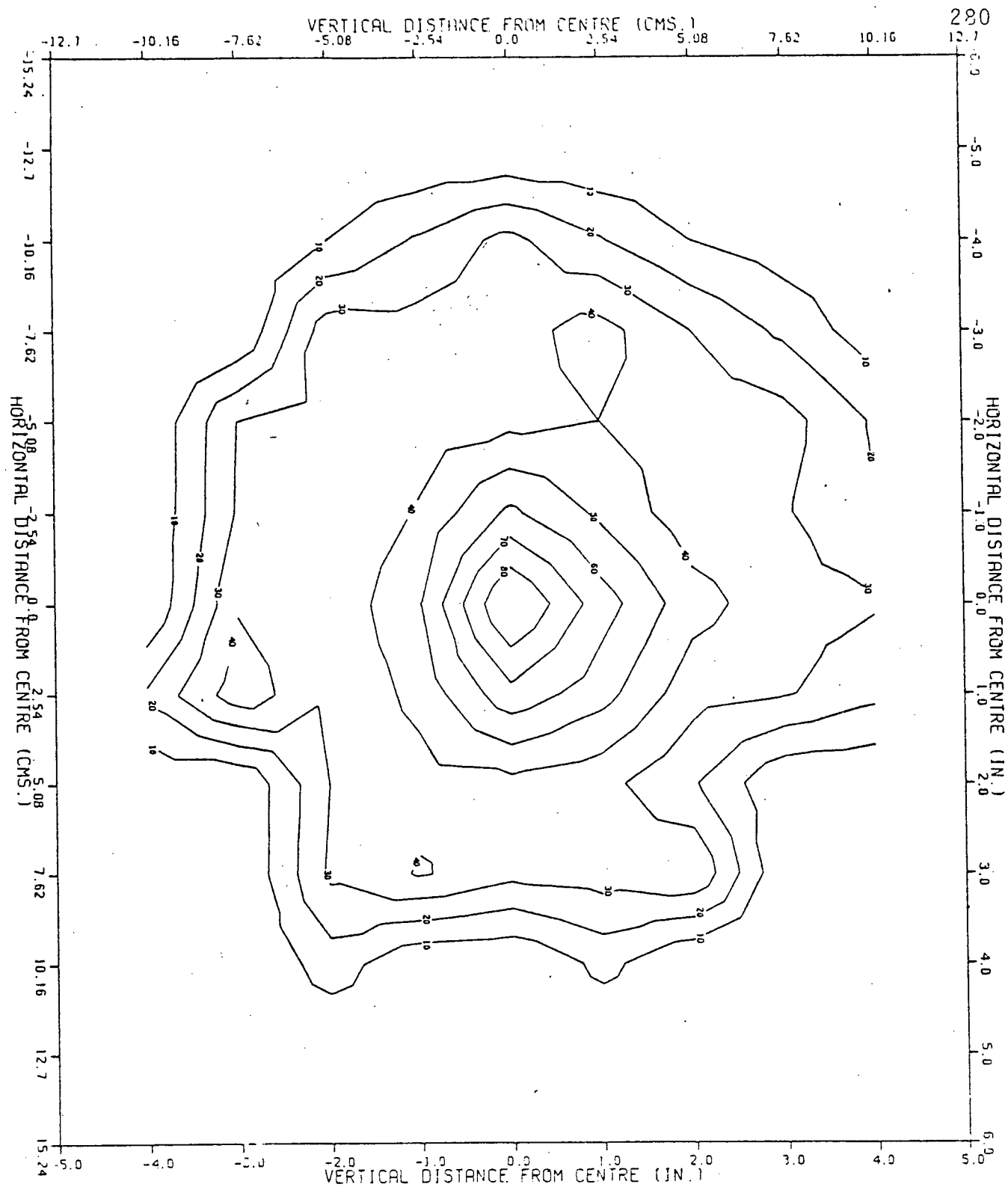


Figure II-4 Spray flux contour map for a 1/4 GG 10 nozzle, for a spray pressure of 0.27 MPa at a nozzle distance of 10.16 cm (Type A collectors).

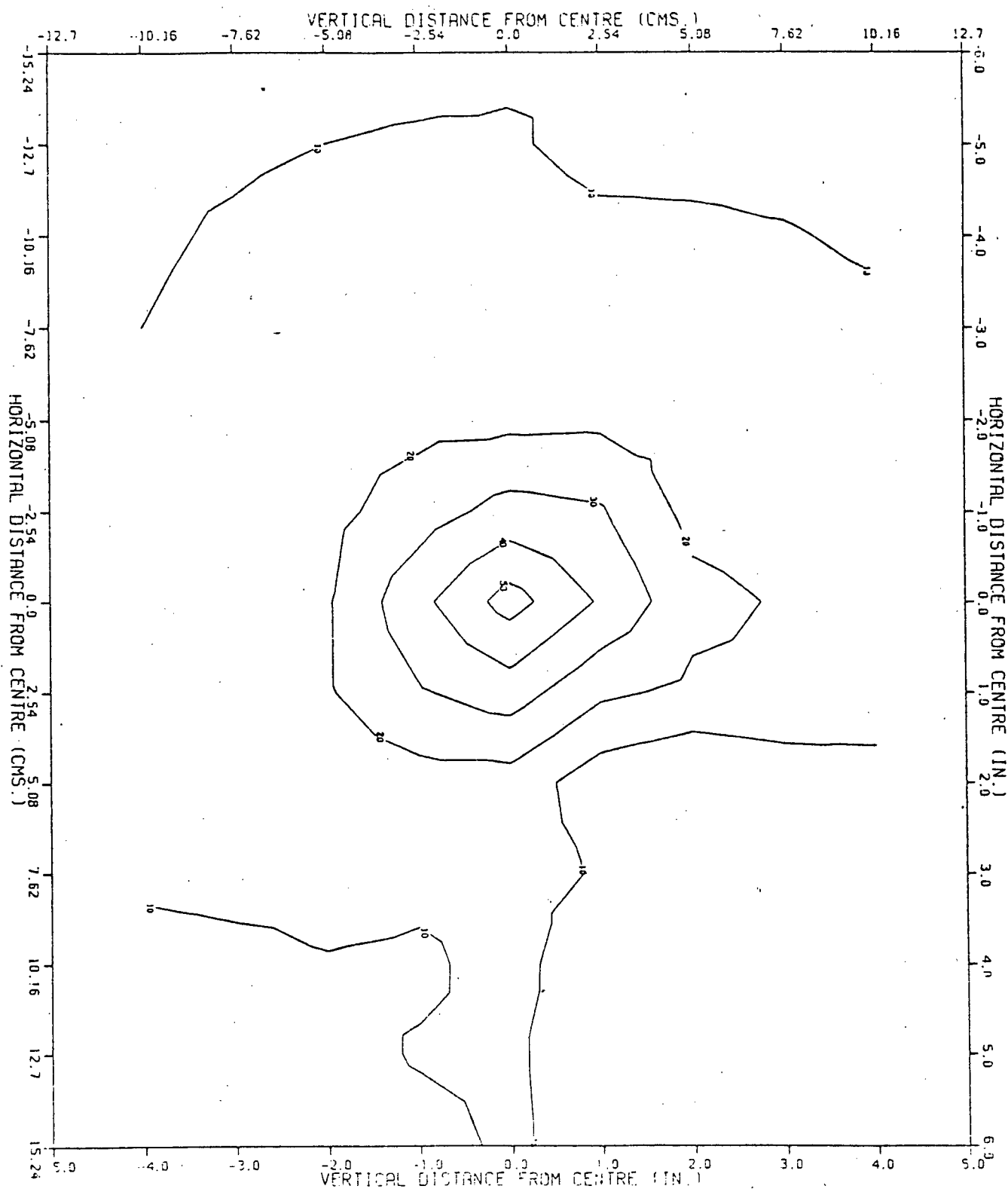


Figure II-5 Spray flux contour map for a 1/4 BB 10 nozzle, for a spray pressure of 0.13 MPa at a nozzle distance of 20.32 cm (Type A collectors).

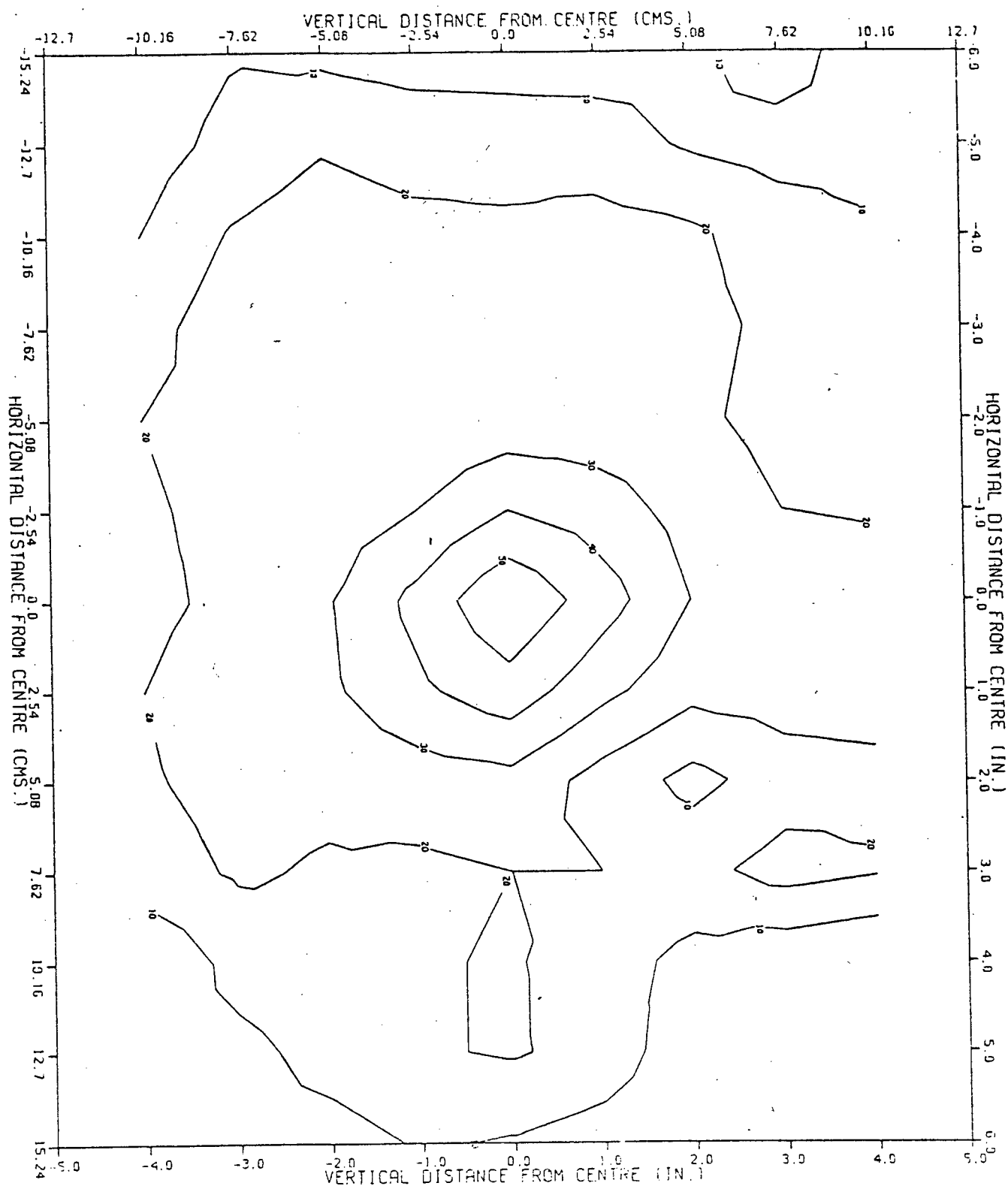


Figure II-6 Spray flux contour map for a 1/4 GG 10 nozzle, for a spray pressure of 0.27 MPa at a nozzle distance of 20.32 cm (Type A collectors).

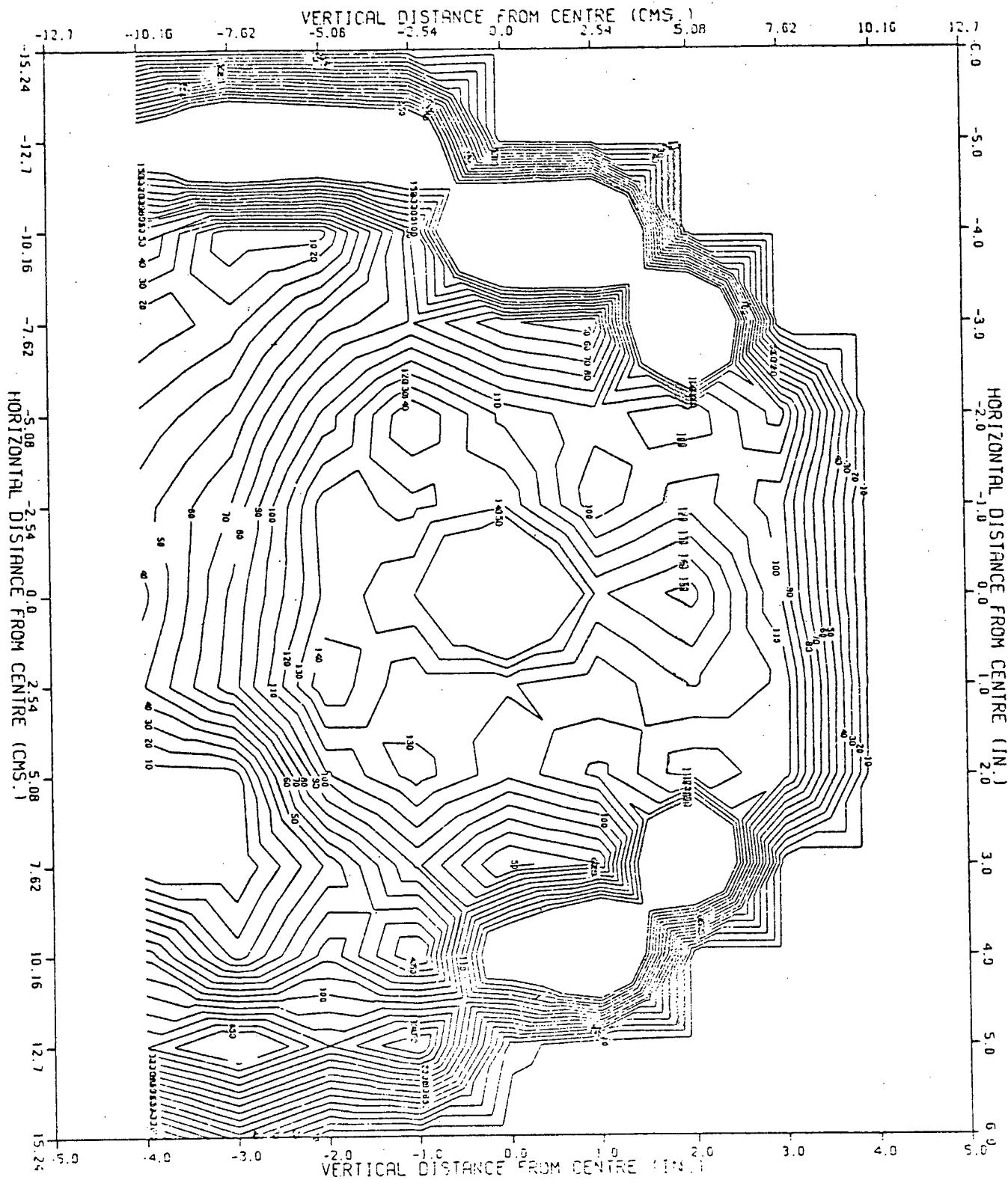


Figure II-7 Spray flux contour map for a 1/4 GG 10 nozzle, for a spray pressure of 0.13 MPa at a nozzle distance of 10.16 cm and Type B collectors.

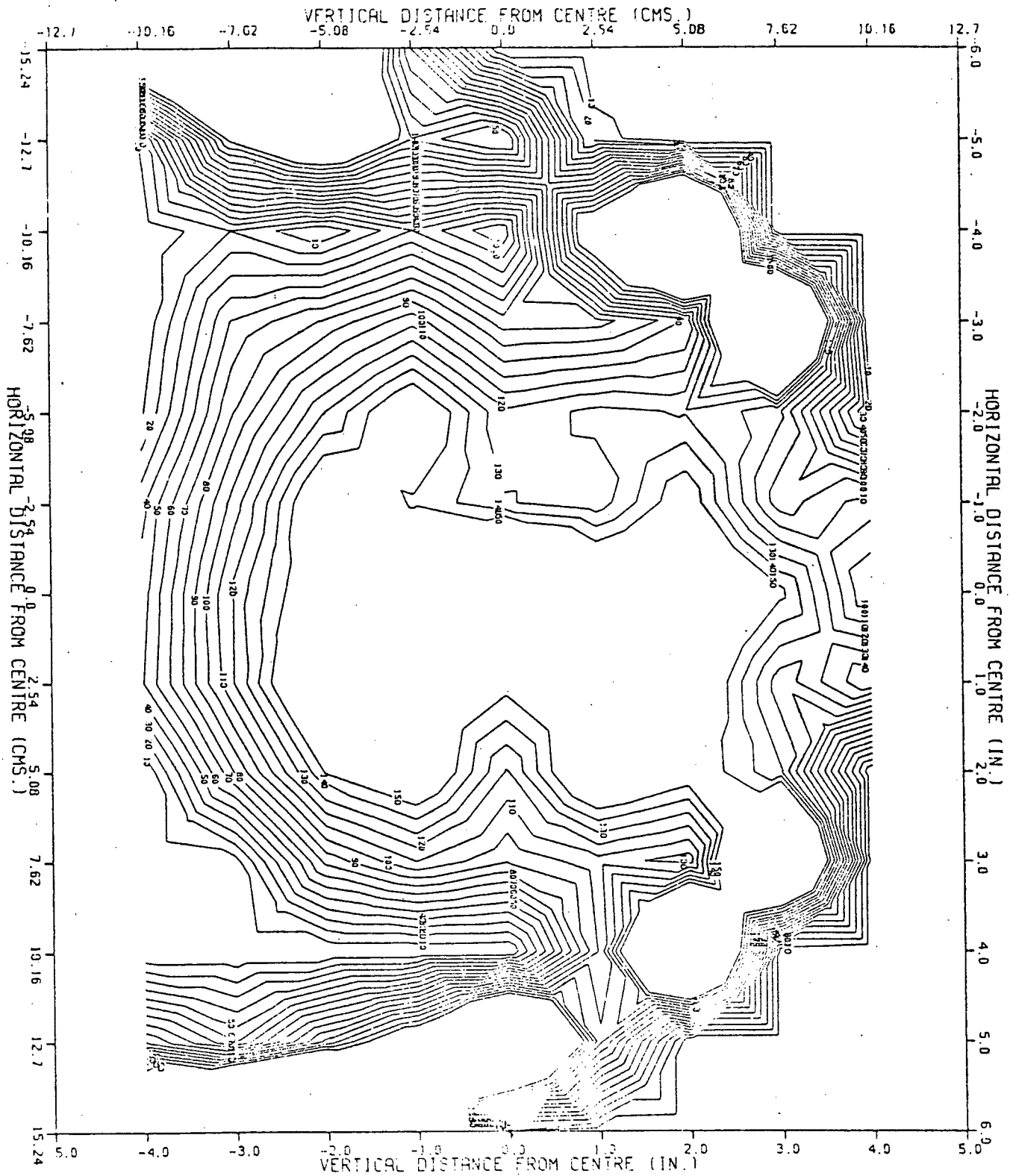


Figure II-8 Spray flux contour map for a 1/4 GG 10 nozzle, for a spray pressure of 0.27 MPa at a nozzle distance of 10.16 cm Type B collectors.

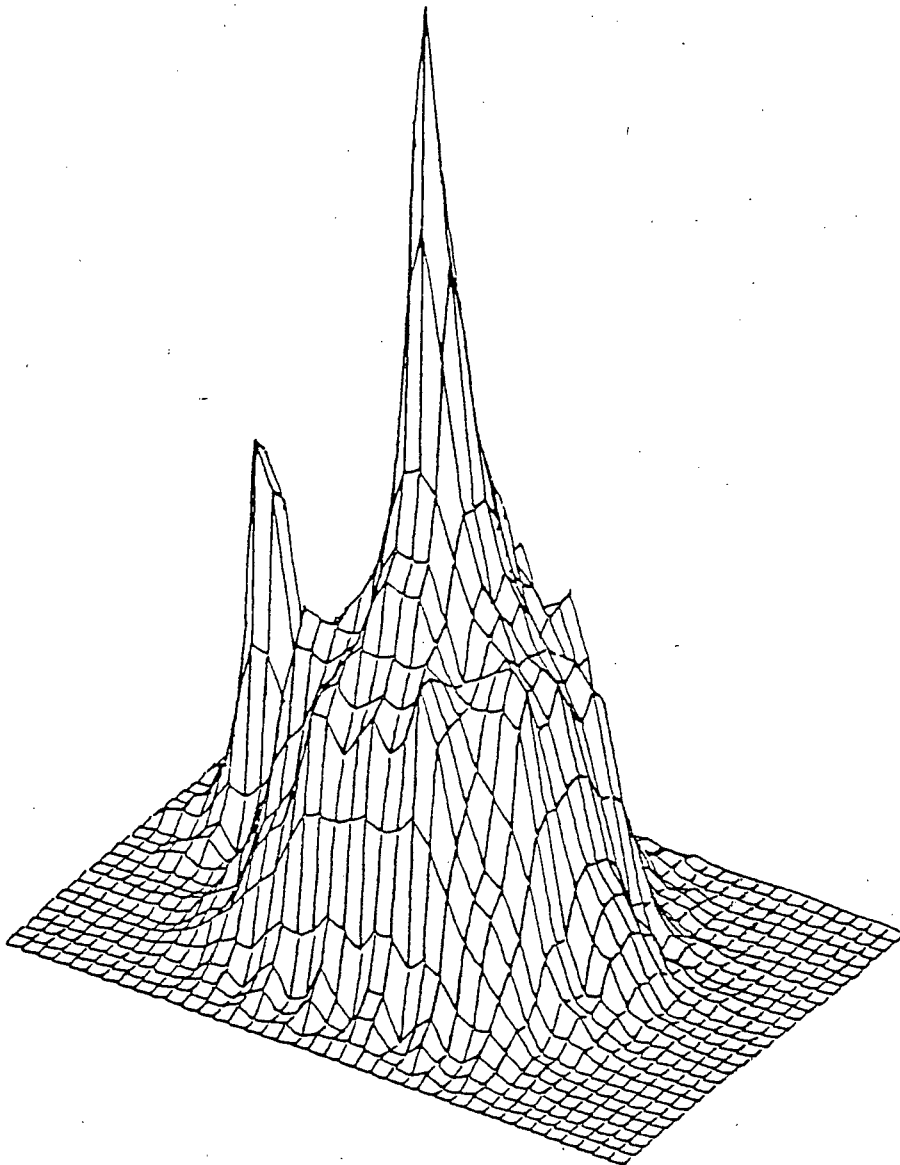


Figure II-9 Three dimensional representation of the spray flux distribution for a 1/4 GG 10 nozzle, for a spray pressure of 0.13 MPa and a nozzle distance of 10.16 cm (Type A collectors).

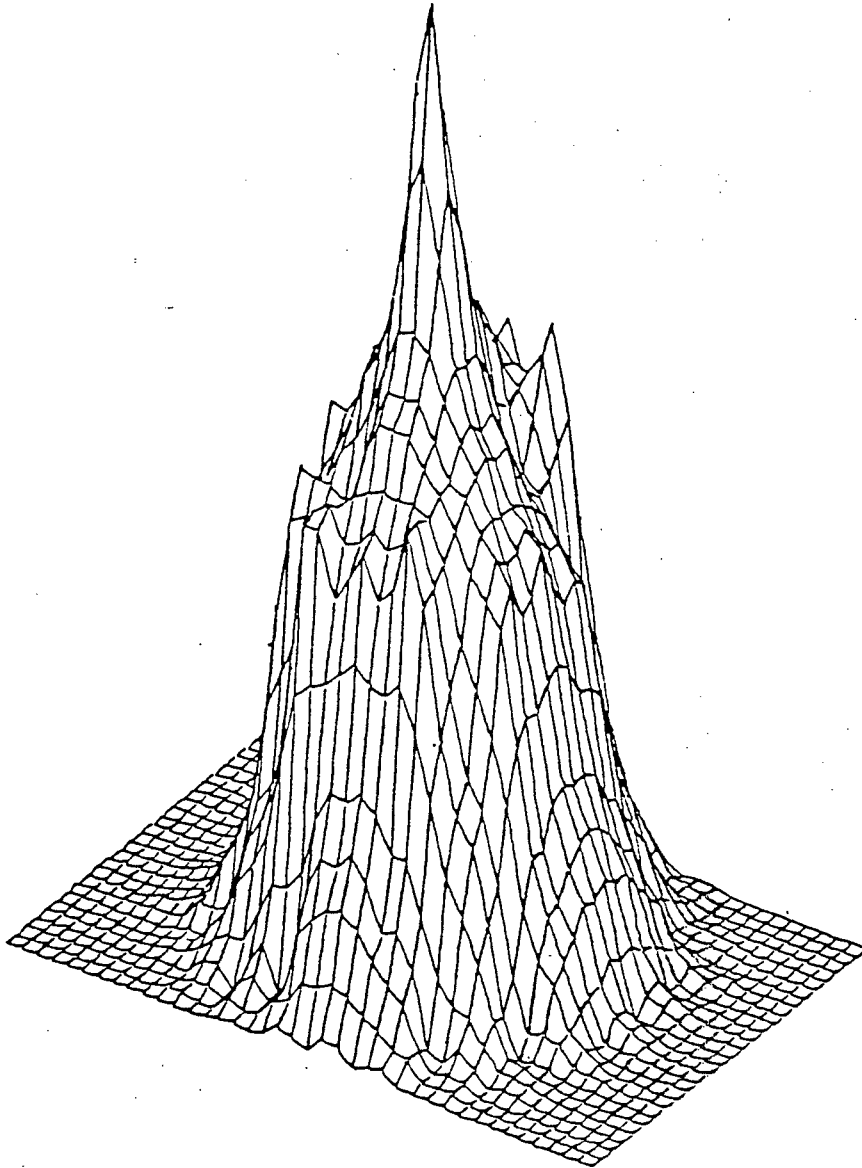


Figure II-10 Three dimensional representation of the spray flux
distribution for a 1/4 GG 10 nozzle, for a spray
pressure of 0.27 MPa and a nozzle distance of
10.16 cm (Type A collectors).

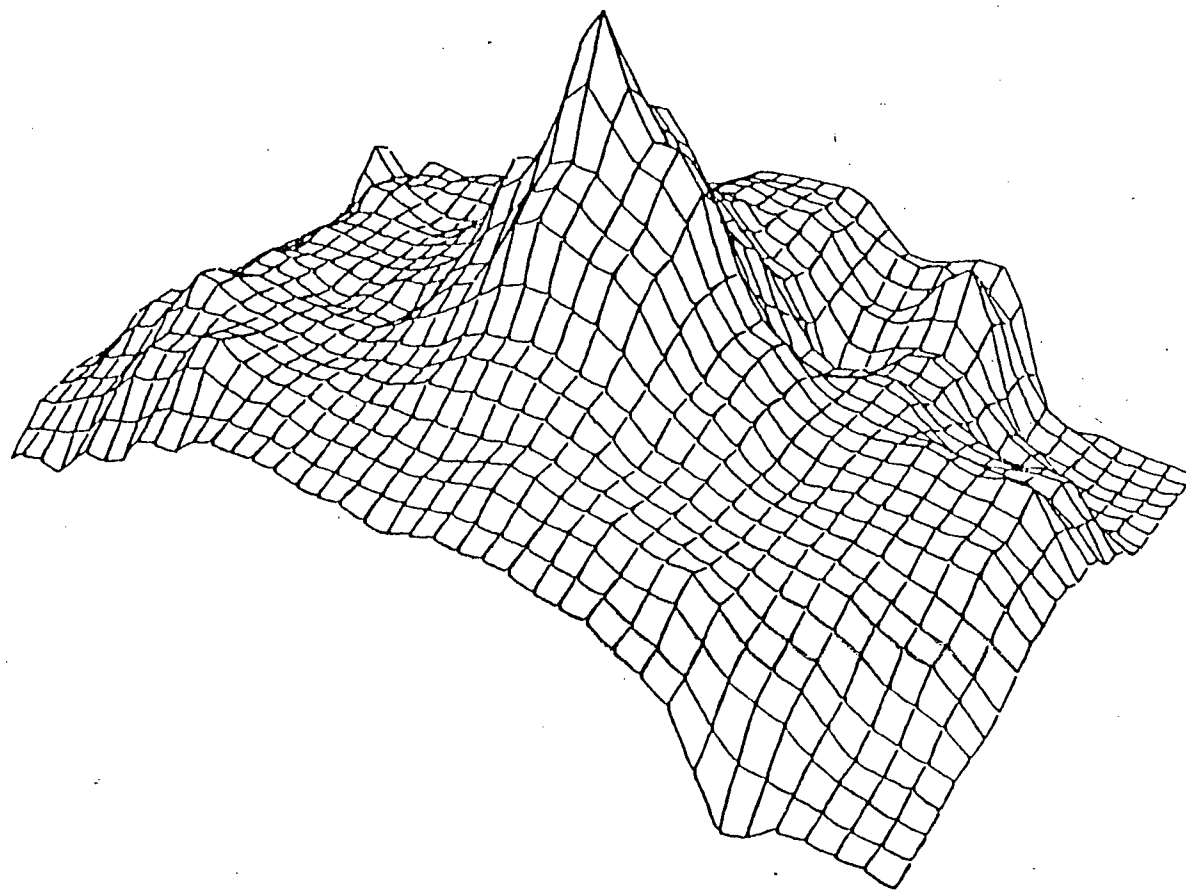


Figure II-11 Three dimensional representation of the spray flux distribution for a
1/4 GG 10 nozzle, for a spray pressure of 0.13 MPa and a nozzle
distance of 15.32 cm (Type A Collectors)

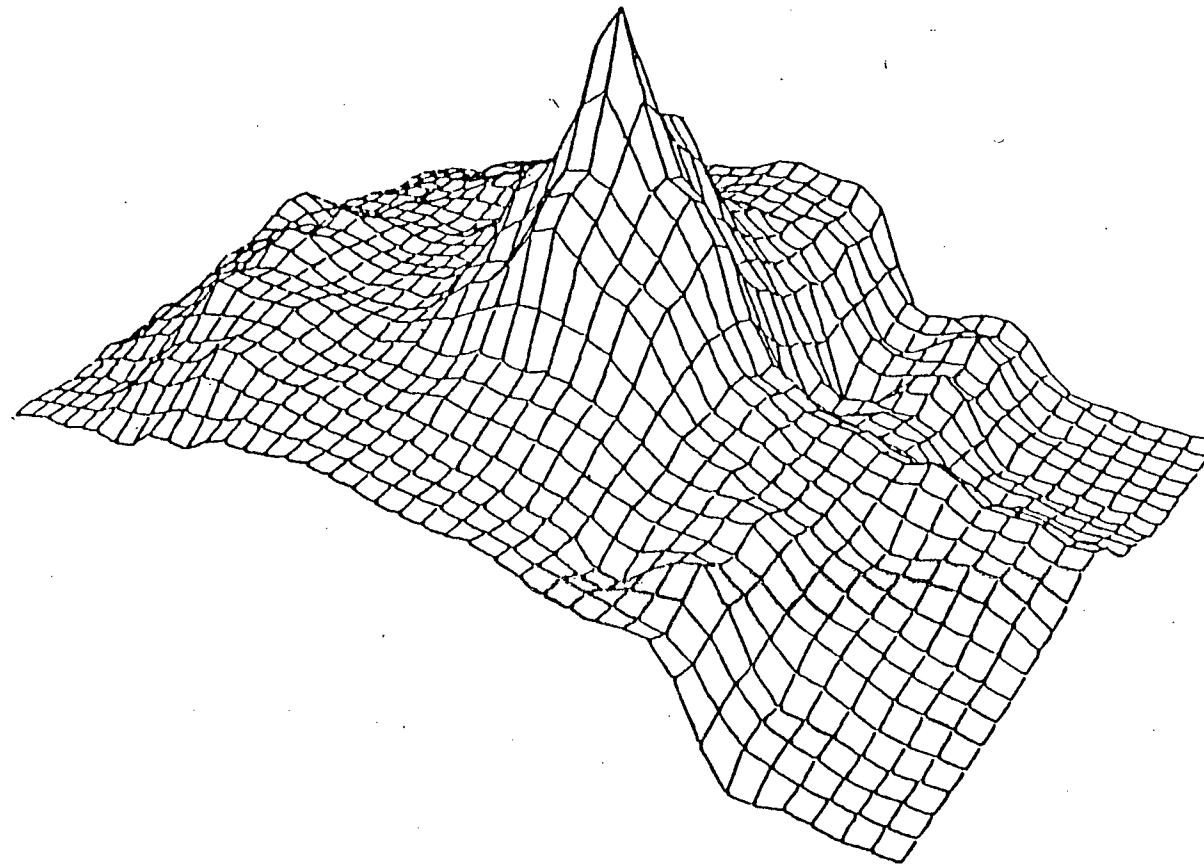


Figure II-12 Three dimensional representation of the spray flux distribution for a spray pressure of 0.13 MPa and a nozzle distance of 20.32 cm (Type A Collectors).

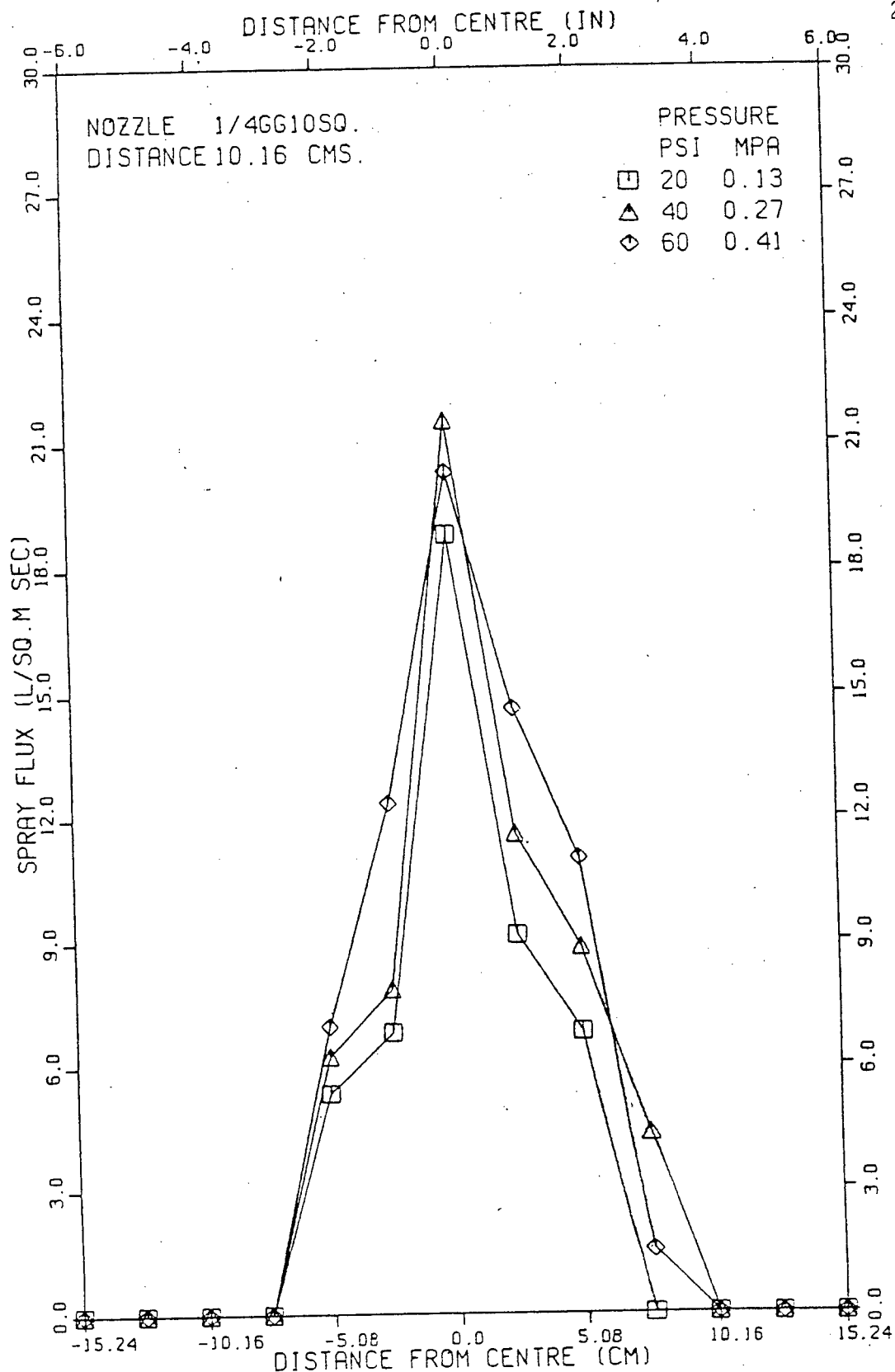


Figure II-13 Horizontal centreline spray flux profiles for a 1/4 GG 10 SQ nozzle at a nozzle distance of 10.16 cm.

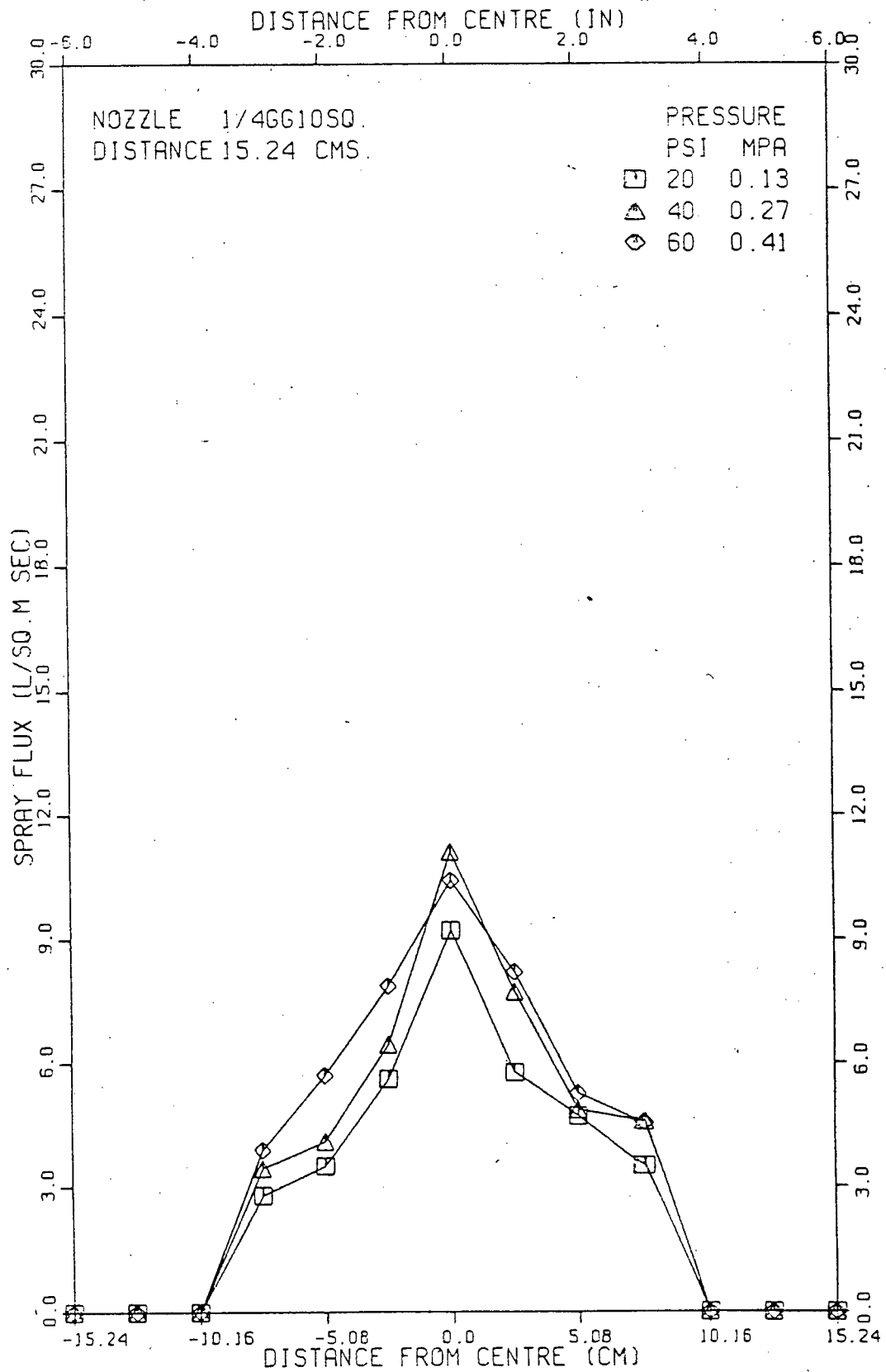


Figure II-14 Horizontal centreline spray flux profiles for a
1/4 GG 10 SQ nozzle at a nozzle distance of 15.24 cm.

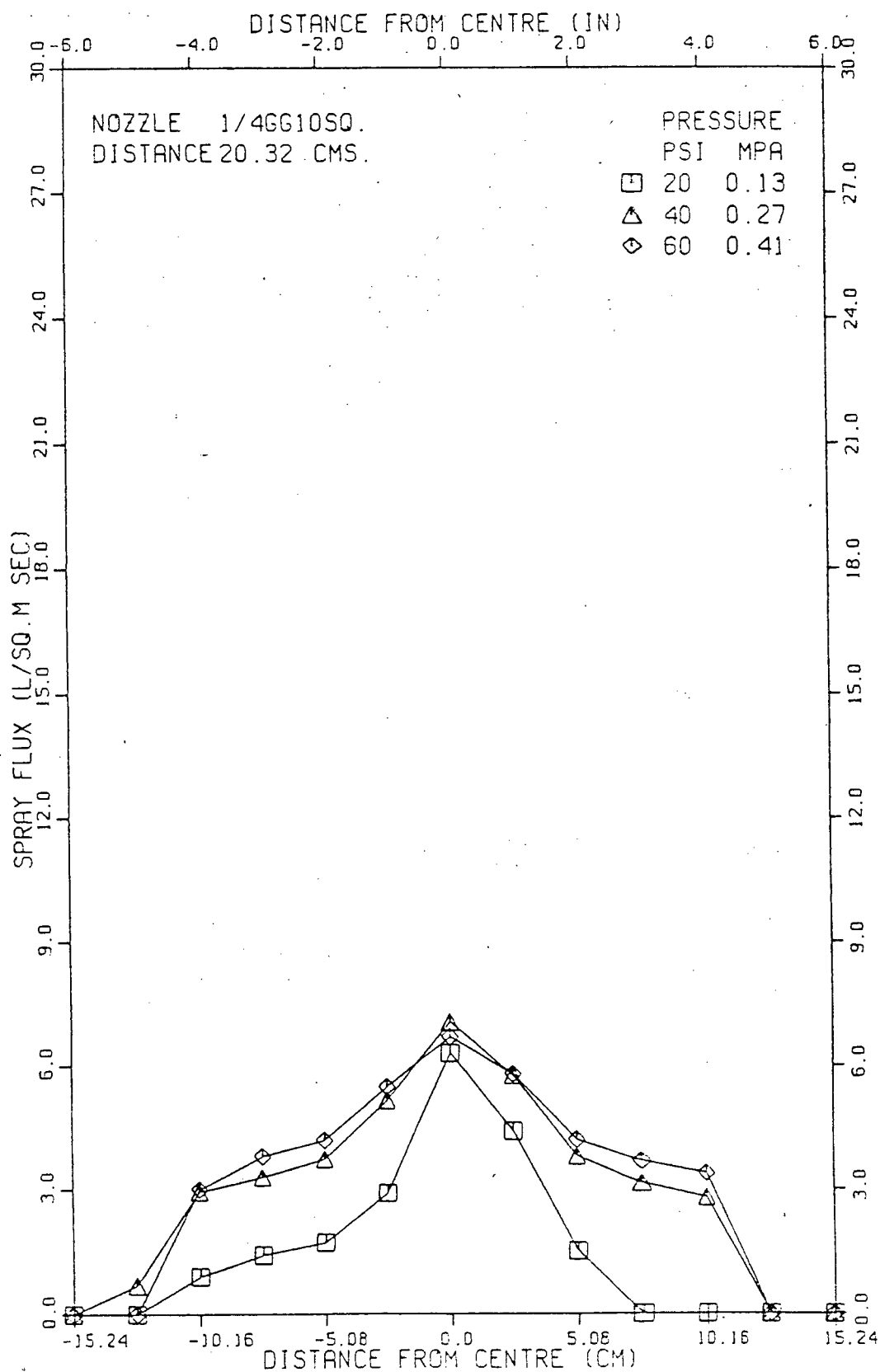


Figure II-15 Horizontal centreline spray flux profiles for a 1/4 GG 10 SQ nozzle at a nozzle distance of 20.32 cm.

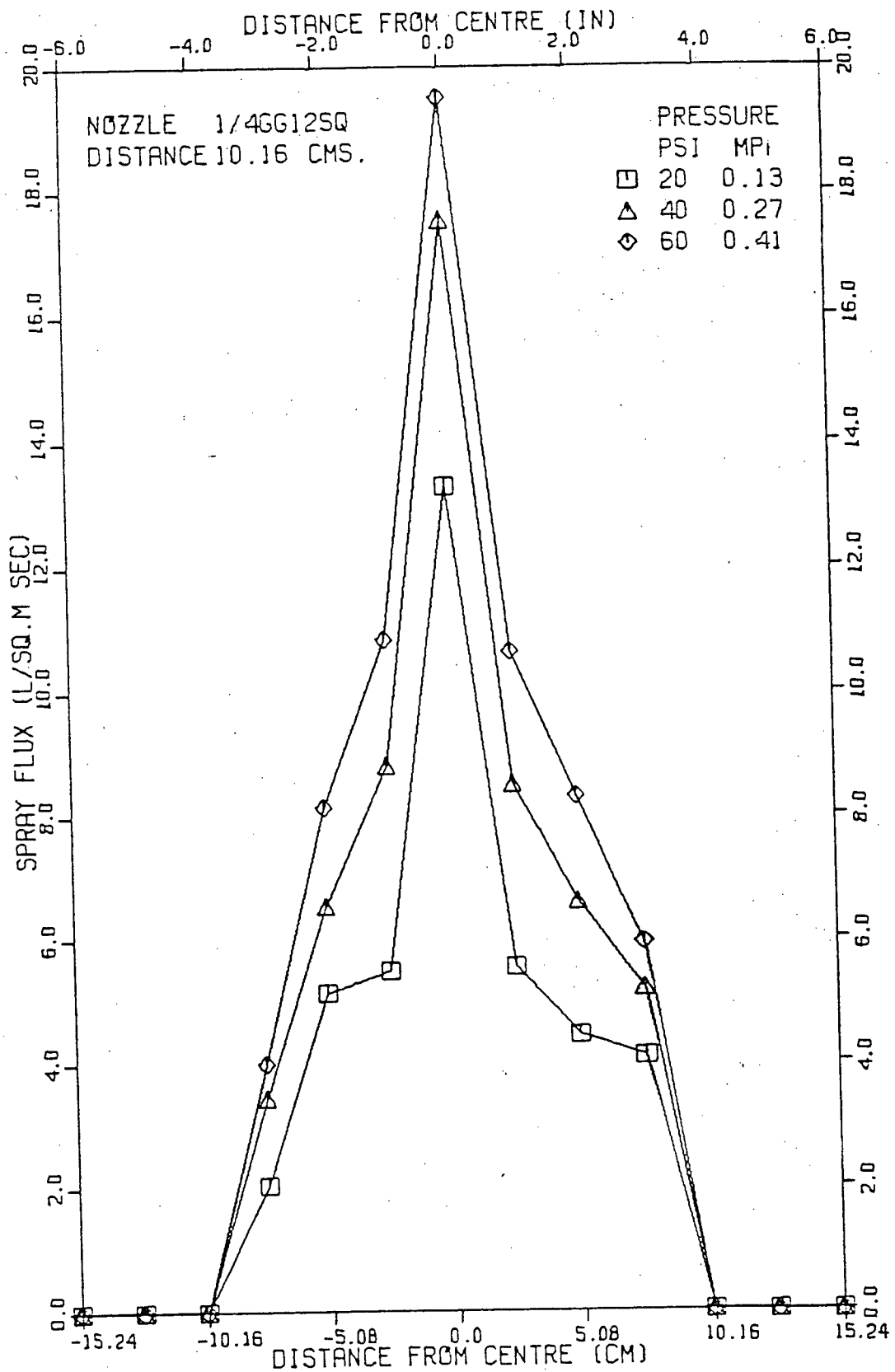


Figure II-16 Horizontal centreline spray flux profiles for a 1/4 GG 12 SQ nozzle at a nozzle distance of 10.16 cm.

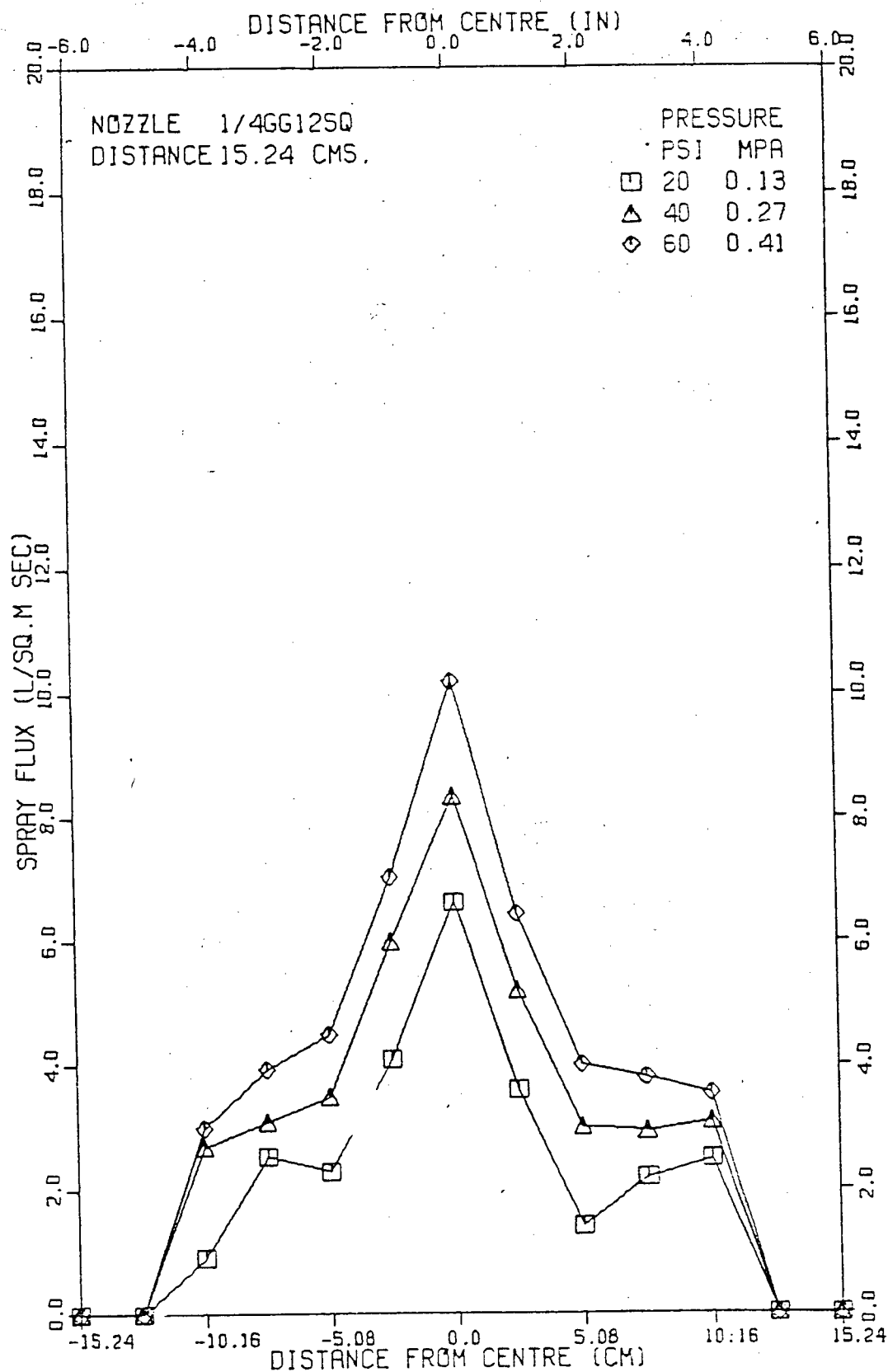


Figure II-18 Horizontal centreline spray flux profiles for a
1/4 GG 12 SQ nozzle at a nozzle distance of 20.32 cm.

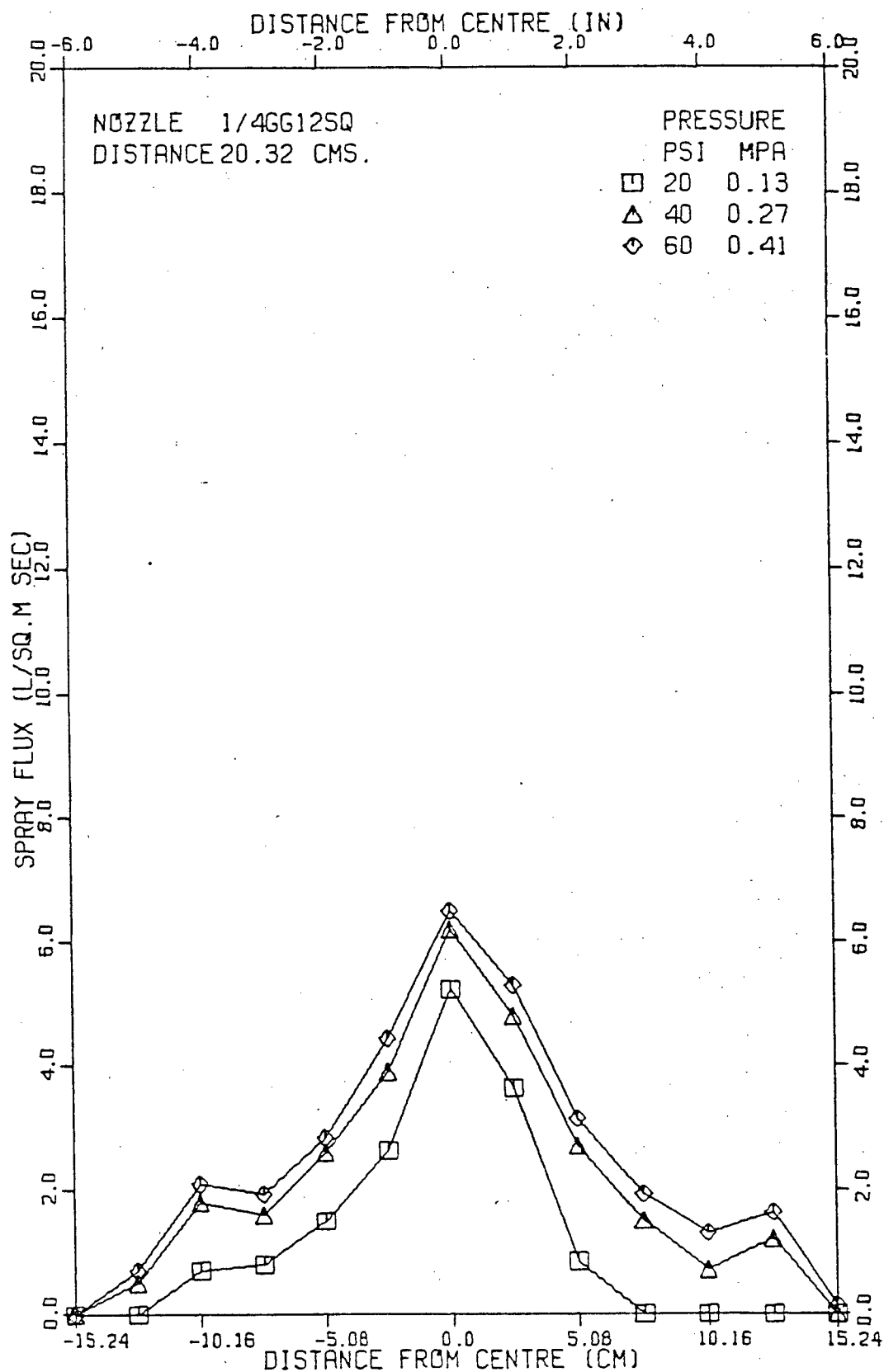


Figure II-18 Horizontal centreline spray flux profiles for a
1/4 GG 12 SQ nozzle at a nozzle distance of 20.32 cm.

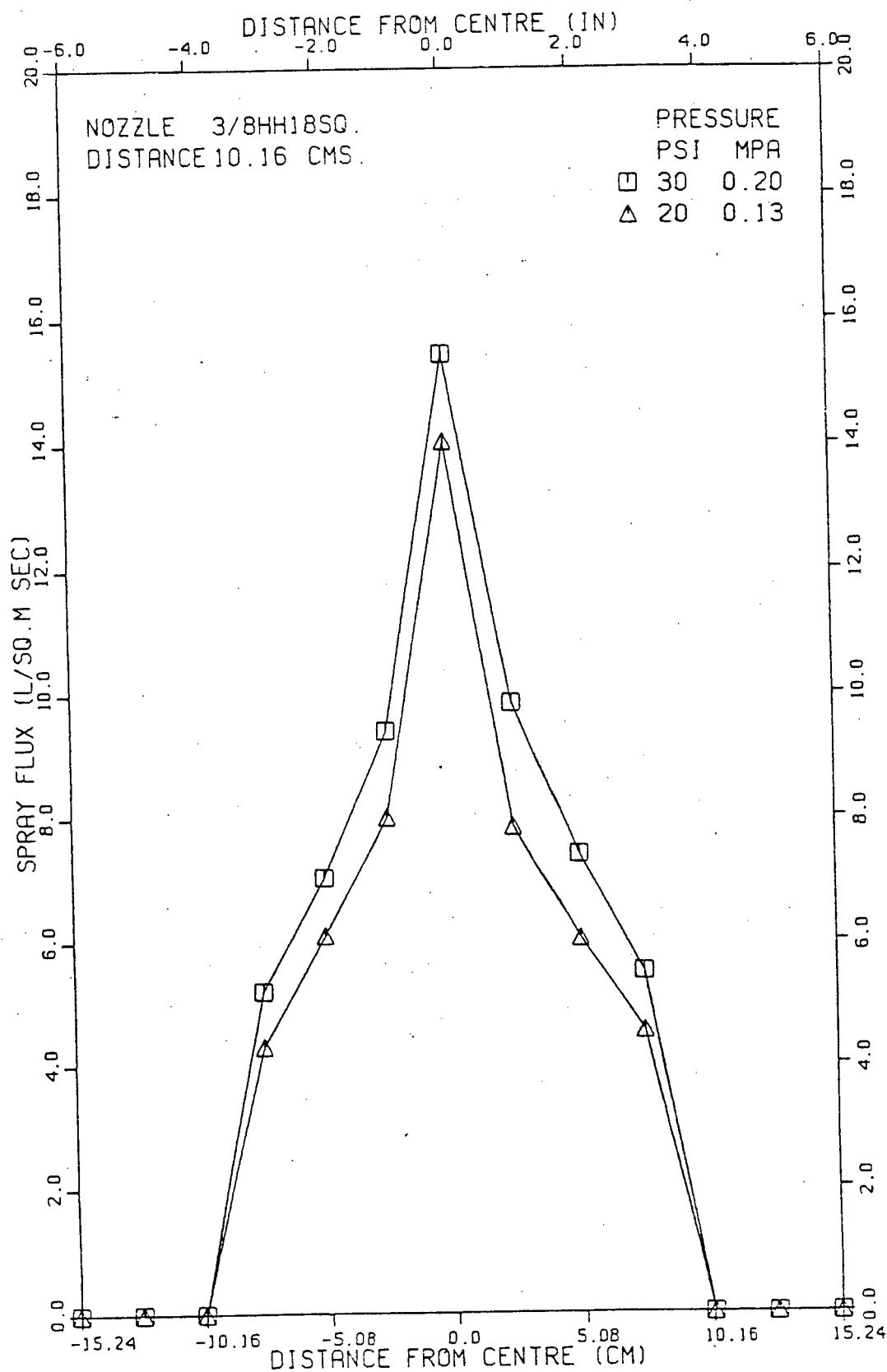


Figure II-19 Horizontal centreline spray flux profiles for a 3/8 HH 18 SQ nozzle at a nozzle distance of 10.16 cm.

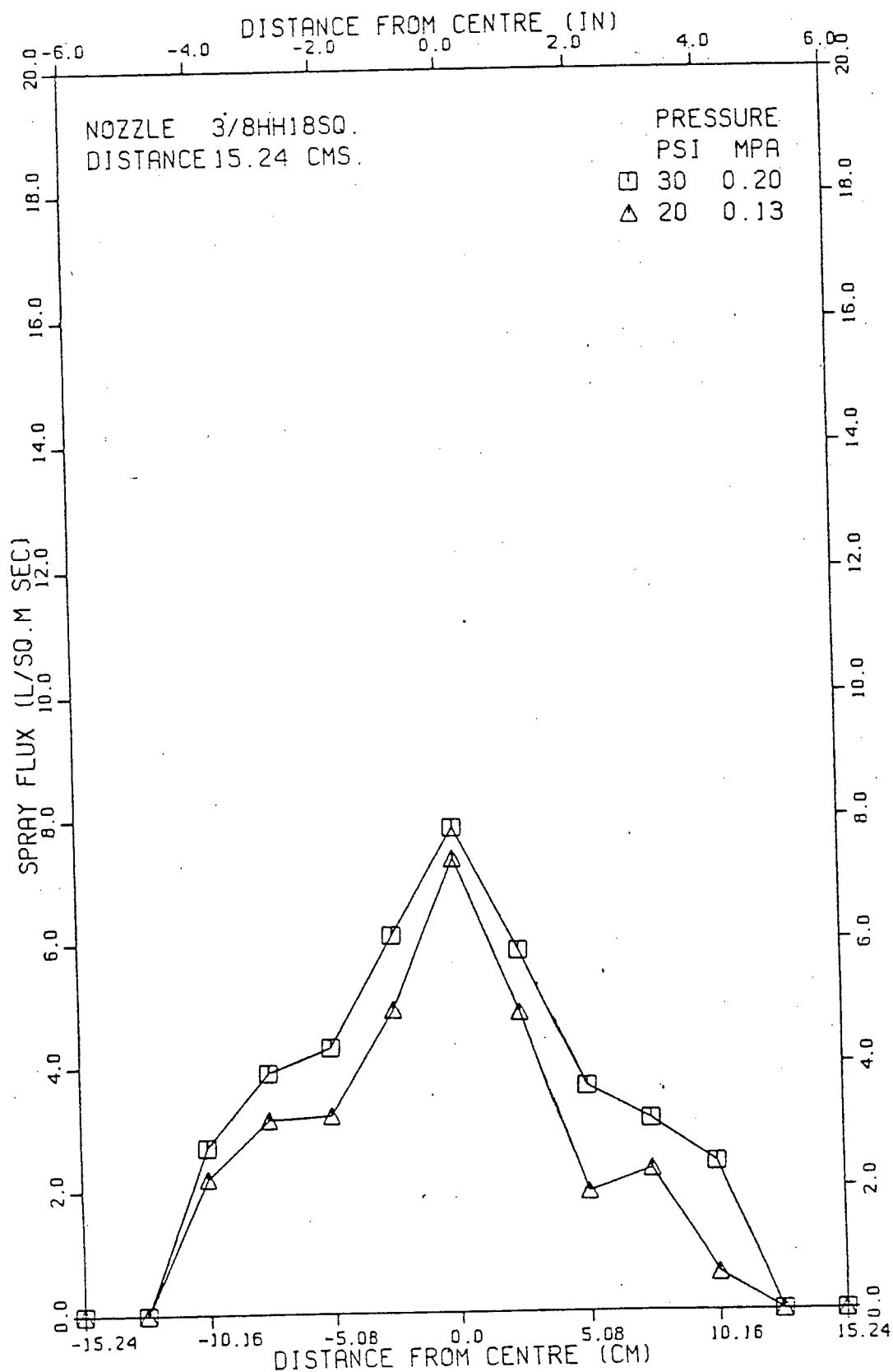


Figure II-20 Horizontal centreline spray flux profiles for a 3/8 HH 18 SQ nozzle at a nozzle distance of 15.24 cm.

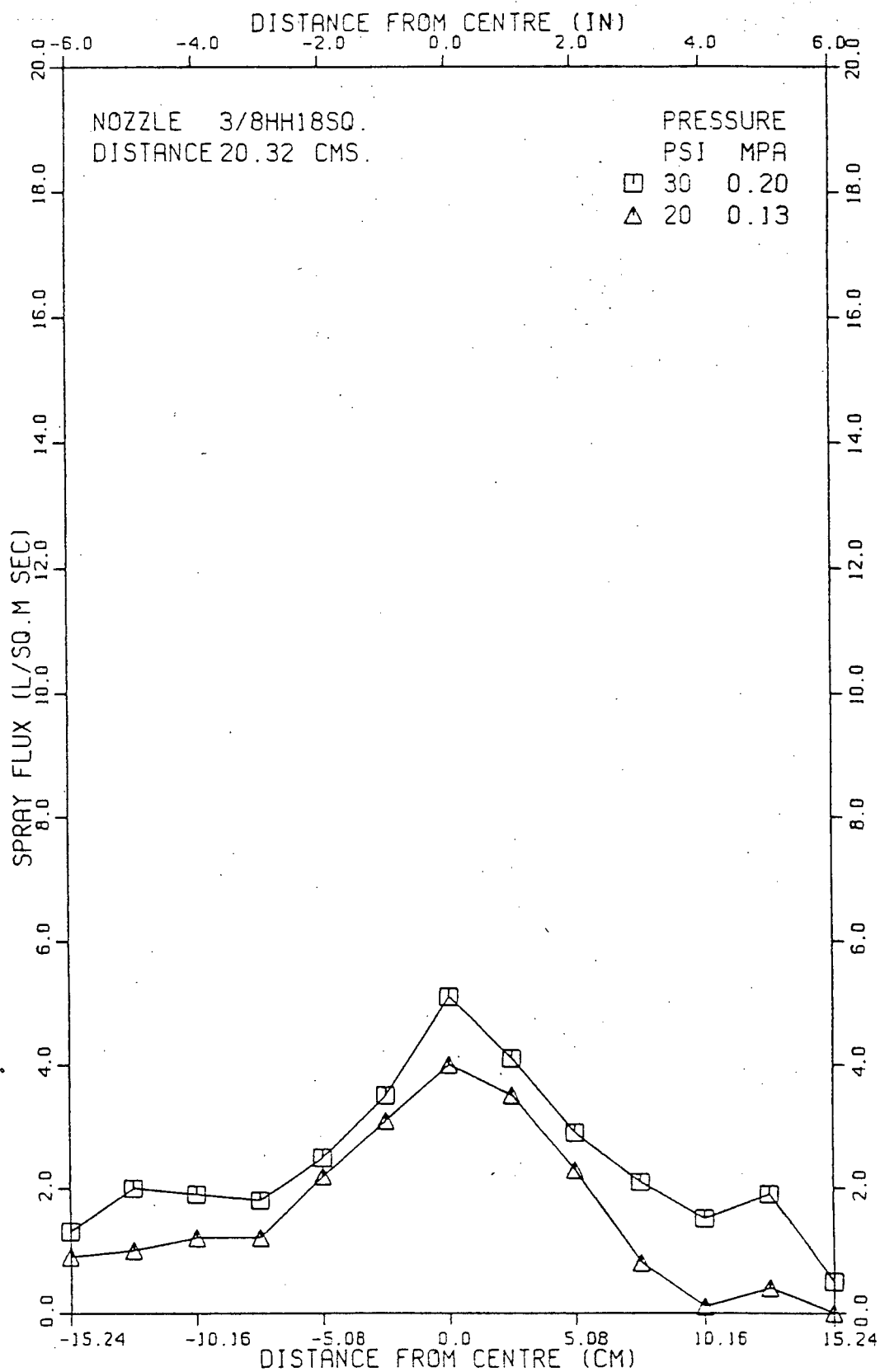


Figure II-21 Horizontal centreline spray flux profiles for a
3/8 HH 18 SQ nozzle at a nozzle distance of 20.32 cm.

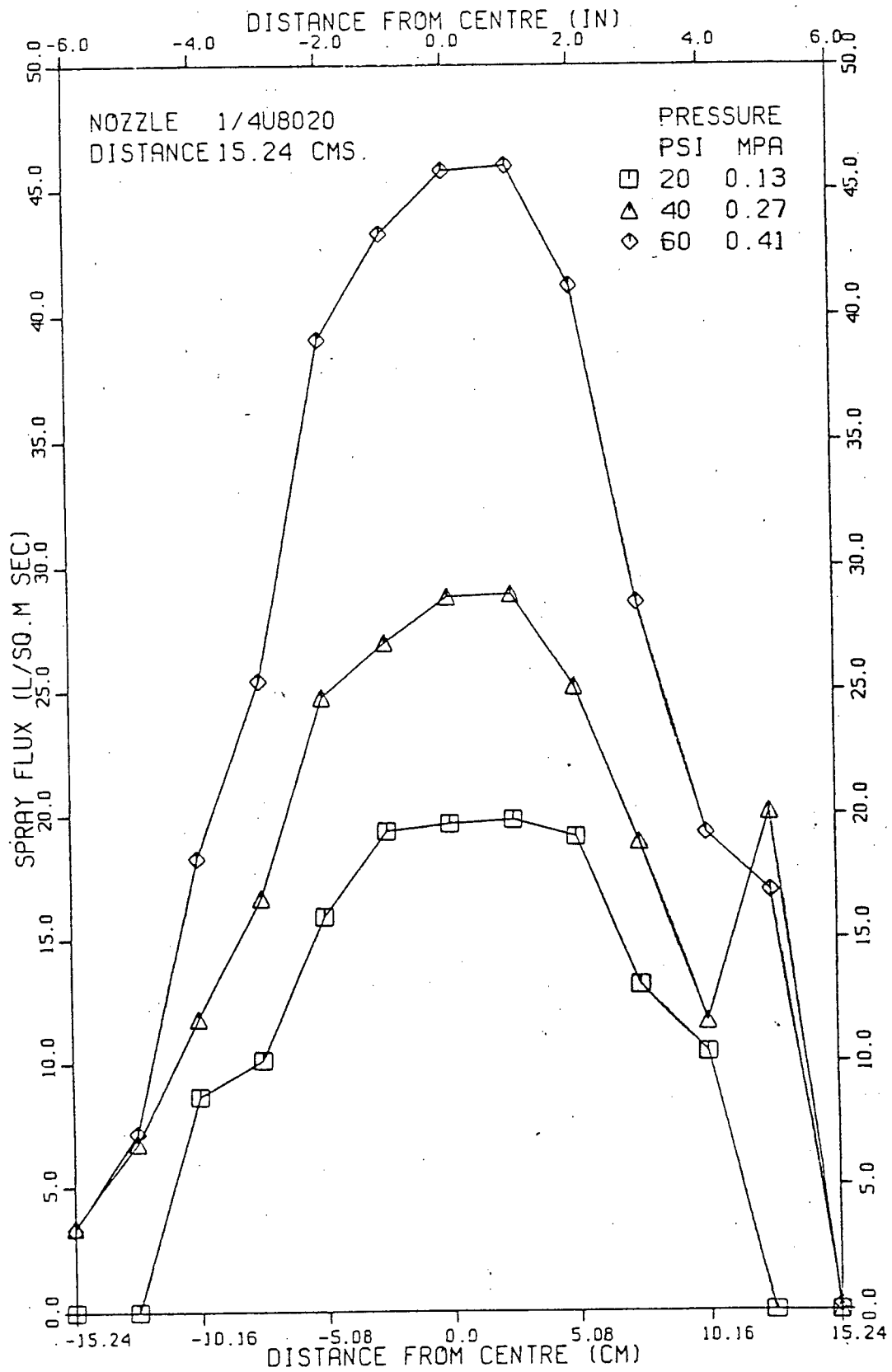


Figure II-22 Horizontal centreline spray flux profiles for a
1/4 U8020 nozzle, at a nozzle distance of 15.24 cm.

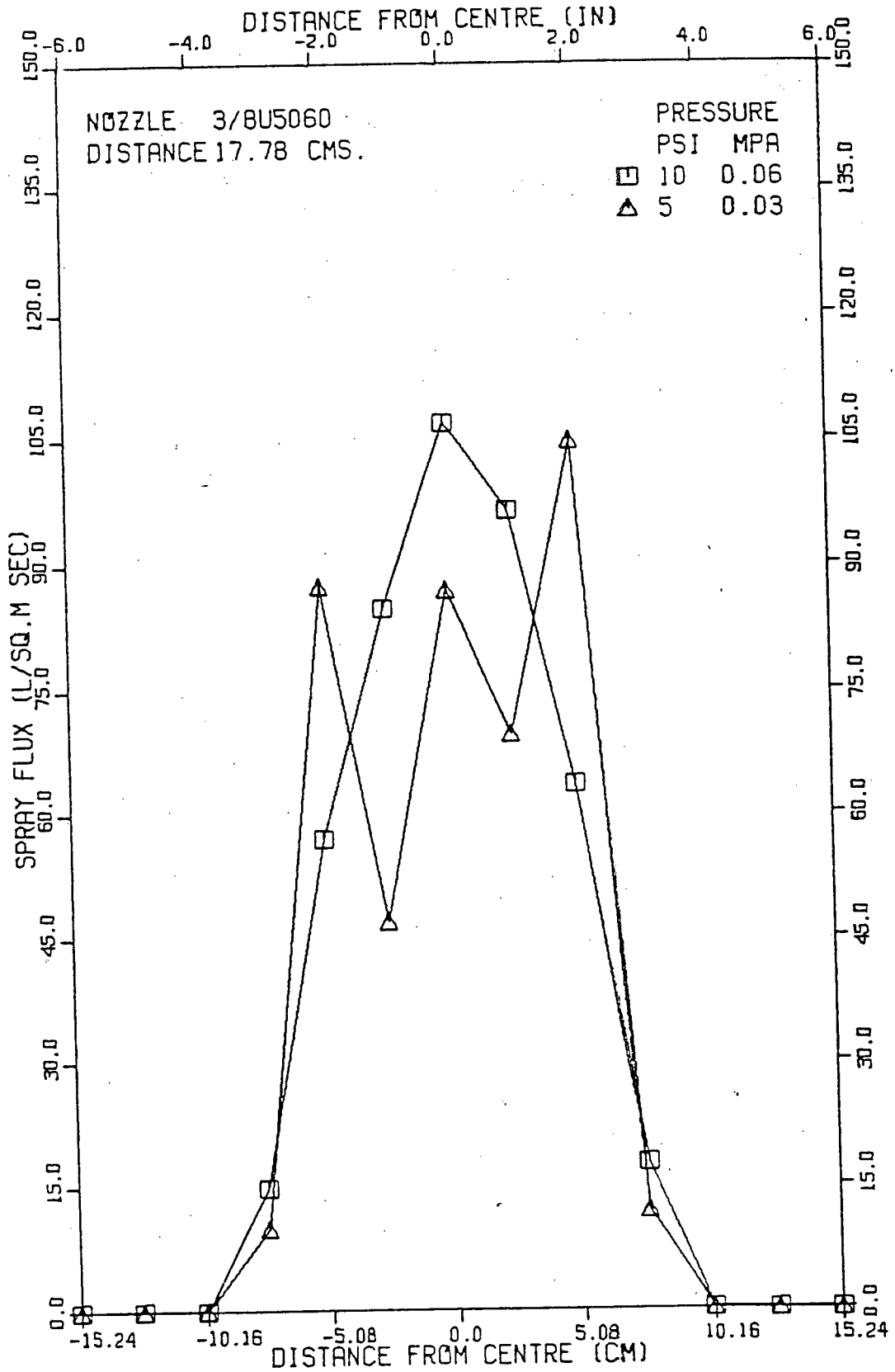


Figure II-23 Horizontal centreline spray flux profiles for a 3/8 U5060 nozzle at a nozzle distance of 17.78 cm.